N64 13013 *
CODE-1
(NASA CR-55075)
OTS:

454p.

OTS PRICE

XEROX $ 23.50 ph.

MICROFILM $ 13.82 mf.

9431008

Westinghouse

ELECTRIC CORPORATION

Baltimore, Md. Air Arm Div.

PART II - ANALYTICAL SOLUTION [Final Report]

Study and Analysis of

ADVANCED SPACEBORNE DETECTION, TRACKING,

AND NAVIGATION SYSTEM.

(NASA Contract NASw 460)

(Unclassified Title)

(NASA CR - - - - -) OTS:

0 auth April 1963 refs

Submitted to:

NASA Headquarters

Office of Advanced Research & Technology

Code RE

Washington 25, D.C.

This page intentionally left blank

TABLE OF CONTENTS

Para.		Page
Abstract		xvi
Problem Status		xvii
Authorization		xvii
Scope		xviii
Analytical Solution		
1.0	Introduction	1-1
2.0	Summary	2-1
3.0	Earth Launch to Injection, Manned	3-1
3.1	Introduction	3-1
3.2	Approach	3-1
3.3	Summary of Results	3-2
4.0	Manned Lunar Midcourse Guidance	4-1
4.1	Introduction	4-1
4.2	Background and Problem Approach	4-1
4.2.1	Geometry and Physics of Midcourse Problem	4-2
4.2.2	System Constraints and Assumptions	4-4
4.2.3	Problem Approach	4-5
4.3.	Problem Definition	4-6
4.3.1	Mission	4-7
4.3.2	Astronomical Model	4-7
4.3.3	Trajectory	4-7
4.3.4	Observables	4-9
4.3.5	Data-Handling	4-10

TABLE OF CONTENTS (Continued)

Para.		Page
4.3.6	Guidance Logic	4-10
4.3.7	Vehicle	4-11
4.3.8	Assumptions on Corrections and Observations	4-11
4.3.9	Independence of System	4-11
4.4	Description of Analysis	4-11
4.4.1	Introduction	4-11
4.4.2	Onboard System Model	4-12
4.4.3	Development of Statistical Information for Parametric Analysis	4-15
4.4.4	Geometric Considerations	4-17
4.5	Digital Program	4-21
4.5.1	General Description of Inputs, Outputs	4-21
4.5.2	Development of Computer Program	4-22
4.5.3	Operation of the Computer Program	4-23
4.6	Program Results	4-28
4.6.1	Preliminary Runs	4-28
4.6.2	Improvement of Schedules	4-35
4.6.3	Variation of Parameters	4-43
4.6.4	Increased Number of Measurements	4-48
4.6.5	Comparison with 2-Angle Measurements	4-48
4.7	Summary of Computer Results and Discussion	4-49
4.7.1	Summary of Computer Results	4-49
4.7.2	Discussion of Results	4-50
4.7.3	Determination of Sensor Requirements	4-52
4.8	Sensor Requirements	4-52
4.9	Recommendations	4-52

TABLE OF CONTENTS (Continued)

Para.		Page
5.0	Lunar Parking and Descent Orbits, Manned	5-1
5.1	Introduction	5-2
5.2	Background and Approach	5-10
5.3	Problem Description	5-12
5.3.1	Ground Rules and Assumptions	5-12
5.3.2	Quantitative Inputs to Analysis	5-14
5.3.2.1	Nominal Trajectory Geometry	5-14
5.3.2.2	Navigation Parameters	5-15
5.3.2.3	Astronomical Constants	5-16
5.3.2.4	Input Error Statistics	5-17
5.4	Summary of Analytical Techniques	5-18
5.4.1	Acquisition of Results	5-18
5.4.2	Summary of Notation	5-18
5.4.3	Determination of Nominal Orbits	5-21
5.4.4	On-Board Navigation Technique	5-22
5.4.5	On-Board Linear Prediction	5-22
5.4.6	Linearized Dynamic Equations	5-22
5.4.7	Typical Input Errors	5-23
5.5	Digital Program	5-23
5.6	Summary of Digital Computation	5-27
5.7	Numerical Results	5-30
5.8	Sensor Requirements	5-39
5.9	Recommendations	5-39

TABLE OF CONTENTS (Continued)

Page	Para.
6.0 Lunar Descent Trajectory, Manned	6-1
6.1 Introduction.	6-1
6.2 Background and Approach	6-1
6.3 Preliminary Analysis.	6-5
6.3.1 Guidance Law.	6-8
6.3.2 Reference Trajectory.	6-15
6.3.3 Observables	6-19
6.4 Analytical Techniques Description	6-28
6.4.1 Discussion of Available Analytical Techniques	6-28
6.4.2 Analysis.	6-30
6.4.2.1 Propagation of Observation Errors	6-30
6.4.2.2 Propagation of Thrust Errors.	6-35
6.5 Digital Program	6-43
6.5.1 Qualitative Program Description	6-43
6.5.2 Program Flexibility	6-44
6.5.3 Program Mechanization Difficulties.	6-45
6.6 Program Results	6-45
6.7 Discussion and Interpretation of Results.	6-47
6.7.1 Presentation of Results, and Example.	6-47
6.7.2 Discussion	6-59
6.7.2.1 Effects of Over-Control	6-59
6.7.2.2 Effect of Changing Time Interval.	6-60
6.7.2.3 Validity	6-62
6.7.2.4 Bias Error Effects.	6-63

TABLE OF CONTENTS (Continued)

Para.		Page
6.7.2.5	Remarks Concerning Generalization of the Analysis	6-64
6.7.2.6	Sensor Mechanization	6-65
6.7.2.7	The Role of the Pilot	6-65
6.8	Sensor Requirements	6-65
6.9	Recommendations	6-66
7.0	Lunar Landing, Hover-to-Touchdown, Manned	7-1
7.1	Introduction	7-1
7.2	Summary	7-1
8.0	Lunar Ascent Trajectory; Manned	8-1
8.1	Introduction	8-1
8.2	Background and Approach	8-2
8.3	Preliminary Analysis and Problem Definition	8-3
8.3.1	Trajectory Determination	8-3
8.3.1.1	Introductory Discussion	8-3
8.3.1.2	Definition and Comparison of Parking and Direct Ascent	8-6
8.3.1.3	Ascent Trajectory Selection and Division Into Sub-Phases	8-9
8.3.2	Selection of Boost Sensors and Observables	8-9
8.4	Analytical Description	8-13
8.4.1	Restrictions	8-13
8.4.2	Analytical Trajectory Definition	8-14
8.4.2.1	Target Definition	8-14
8.4.2.2	Orbital Transfer Trajectory	8-15
8.4.2.3	Parking Orbit Trajectory	8-19
8.4.2.4	Boost Trajectory	8-19
8.4.2.5	Launch-Site Definition	8-26

TABLE OF CONTENTS (Continued)

Para.		Page
8.4.3	Error Analysis	8-28
8.4.3.1	Introductory Discussion	8-28
8.4.3.2	Parking Orbit Error Sensitivity	8-28
8.4.3.3	Boost Error Analysis	8-29
8.4.3.4	Pre-Launch Uncertainties	8-33
8.5	Results	8-37
8.6	Interpretation of Results	8-50
8.7	Sensor Requirements	8-55
8.8	Recommendations	8-56
9.0	Lunar Rendezvous, Manned	9-1
9.1	Introduction	9-1
9.2	Background and Approach	9-1
9.3	Problem Definition	9-6
9.3.1	Injection Conditions	9-6
9.3.2	Active Rendezvous	9-8
9.3.3	Propellant Consumption	9-8
9.4	Analytical Description	9-9
9.4.1	Vertical Control	9-13
9.4.2	Lateral Control	9-17
9.4.3	Horizontal Control	9-17
9.4.4	Data Processing	9-18
9.5	Digital Program	9-22
9.6	Program Results	9-23
9.6.1	Transfer Angle	9-23

TABLE OF CONTENTS (Continued)

Para.		Page
9.6.2	Injection Errors	9-24
9.6.2.1	Effects on Miss Distance	9-24
9.6.2.2	Effects on Propellant Consumption	9-28
9.6.2.3	Effects on Accuracy	9-31
9.6.3	Rendezvous Sensor Errors	9-31
9.7	Discussion and Interpretation of Results	9-32
9.7.1	Injection Sensors	9-32
9.7.2	Rendezvous Sensors	9-42
9.8	Sensor Requirements	9-44
9.8.1	Injection Sensor Requirements	9-44
9.8.2	Rendezvous Sensor Requirements	9-45
9.9	Recommendations	
10.0	Midcourse Return, Manned	10-1
10.1	Introduction	10-1
10.2	Discussion	10-1
11.0	Rendezvous With Orbiting Space Station	11-1
11.1	Introduction	11-1
11.2	Background and Approach	11-1
11.3	Problem Definition	11-2
11.4	Analytical Description	11-2
11.4.1	Vertical Control	11-6
11.4.2	Lateral Control	11-8
11.4.3	Longitudinal Control	11-8
11.4.4	Data Processing	11-10

TABLE OF CONTENTS (Continued)

Para.		Page
11.5	Digital Program	11-10
11.6	Program Results	11-13
11.6.1	Nominal Trajectory	11-13
11.6.2	Injection Errors	11-13
11.6.2.1	Effects on Miss Distance	11-13
11.6.2.2	Effects on Propellant Consumption	11-17
11.6.2.3	Effects on Accuracy	11-17
11.6.3	Rendezvous Sensor Errors	11-17
11.7	Discussion and Interpretation of Results	11-18
11.7.1	Injection Sensors	11-18
11.7.2	Rendezvous Sensors	11-27
11.8	Sensor Requirements	11-27
11.8.1	Injection Sensor Requirements	11-28
11.8.2	Rendezvous Sensor Requirements	11-29
11.9	Recommendations	11-30
12.0	Unmanned Midcourse	12-1
12.1	Analysis	12-1
12.2	Sensor Requirements	12-4
13.0	Parking Orbit, Unmanned	13-1
14.0	Lunar Descent Trajectory, Unmanned	14-1
14.1	Introduction	14-1
14.2	Problem Approach and Results	14-1
14.3	Recommendations	14-1
15.0	Lunar Landing Trajectory	15-1

TABLE OF CONTENTS (Continued)

Para.		Page
16.0	Integration Between Phases	16-1
17.0	Conclusions	17-1
18.0	Approach to Part III	18-1
19.0	Appendix I: Lunar Midcourse Trajectory	19-1
19.1	Appendix I-A: Analytical Development	19-1
19.2	Appendix I-B: Computation of Statistical Information	19-15
19.3	Appendix I-C: Literature Survey	19-20
20.0	Appendix II: Lunary Parking and Descent Orbits	20-1
20.1	Determination of Nominal Orbits	20-1
20.2	On-Board Navigation Technique	20-6
20.3	On-Board Linear Prediction	20-9
20.3.1	Linearized State Transition	20-9
20.3.2	Statistical Filter Equations	20-10
20.3.3	Data Conditioning	20-11
20.4	Linearized Dynamic Equations	20-14
20.4.1	The Guidance Law	20-14
20.4.2	Computation of Extrapolated Covariance Matrices	20-16
20.5	Typical Input Error Magnitudes	20-18
20.5.1	Thrust Tolerances	20-18
20.5.2	Measurement Errors	20-20
20.5.3	Initial Conditions	20-21
21.0	Appendix III: Lunar Descent Trajectory	21-1
21.1	Appendix III-A: Guidance Law Derivation	21-1
21.2	Appendix III-B: Equations Relating Observables to Dynamic State Variables	21-12

TABLE OF CONTENTS (Continued)

Para.		Page
21.3	Appendix III-C: Computer Program	21-20
22.0	Appendix IV: Computer Simulation of Rendezvous Techniques . .	22-1
22.1	Initial Positioning of Target and Chaser.	22-1
22.2	General Flow of the Program	22-2
22.3	Firing Laws	22-
22.4	Corrections to Chaser Orbit for Firing.	22-9
22.5	Noise Generation and Smoothing.	22-9
22.6	Corrections to Smoother Input for Firing.	22-11
22.7	Transformations Between Geocentric Coordinates and Orbital Elements	22-12
22.8	Modifications for Simulation of Earth Rendezvous	22-20
23.0	Appendix V:	23-1
23.1	Velocity Requirements for Minimum Fuel Trajectories	23-1
23.2	Determination of Thrust Acceleration Components	23-9
23.3	Error Sensitivity for Near-Circular Orbit	23-10
23.4	Error Analysis for Space-Stabilized Inertial System	23-10
23.5	Development of a computer Program for Evaluating Differential Error Equation	23-23
24.0	References and Bibliography	24-1

List of Figures

Fig. No.		
2-1 through 2-6	Summary Charts.	2-3/2-12
4-1	63.9 hour Nominal Trajectory.	4-8
4-2	Reduction in RMS Position Estimation Error	4-44

TABLE OF CONTENTS (Continued)

Fig. No.		Page
5-1	Orbital Plane at time of Midcourse Termination	5-3
5-2	Plan View of Lunar Flight Path	5-9
5-3	Schematic of Lunar Navigation Simulation	5-25
5-4	Final Position Deviations vs. RMS Measurement Error	5-33
5-5	Final Position Uncertainties vs. RMS Measurement Error	5-34
5-6	Final Velocity Uncertainties vs. RMS Measurement Error	5-35
5-7	Total Position Uncertainty vs. Time	5-37
5-8	Total Velocity Uncertainty vs. Time	5-38
6-1	Block Diagram of Guidance System Analytical Model	6-11
6-2	Block Diagram of Guidance System Analyzed by Ames Research Laboratory	6-12
6-3	Reference Trajectory: Altitude vs. Time	6-20
6-4	Reference Trajectory: Altitude Rate vs. Time	6-21
6-5	Reference Trajectory: Velocity vs. Time	6-22
6-6	Reference Trajectory: Altitude vs. Angular Displacement from Landing Site	6-23
6-7	Landing Geometry - Illustrating Observable Quantities	6-25
6-8	Final Error Components Attributable to Range Measurement Errors	6-51
6-9	Final Error Components Attributable to Range Rate Measurement Errors	6-52
6-10	Final Error Components Attributanle to Angle Measurement Errors	6-53
6-11	Final Error Components Attributable to Angle Rate Measurement Errors	6-54
6-12	Final Error Components Attributable to Thrust Magnitude Mechanization Errors	6-55
6-13	Final Error Components Attributable to Thrust Orientation Mechanization Errors.	6-56

6-14 Auto-correlative Function of Thrust Errors 6-60

6-15 Power Spectral Density Corresponding to Triangular Auto-correlation Function 6-61

8.3-1 Types of Ascent to Rendezvous 8-5

8.4-1 Total Required Velocity Increment -- 8-17

8.4-2 System for Boost Trajectory and Sensor Error Analysis 8-21

8.4-3 Constant Thrust Optimized Lunar Boost-- 8-24

8.4-4 Nominal Boost Acceleration Profiles 8-25

8.4-5 Orientation and Axes Definition -- 8-31

8.5-1 Parking Orbit Sensitivity Coefficients 8-38

8.5-2 Effect of Initial State Errors on Final State Position Errors-. 8-42

8.5-3 Effect of Initial State Errors on Final State Velocity Errors-. 8-43

8.5-4 Total Velocity Requirements vs. Parking Altitude-- 8-44

8.5-5 Percentage of Fuel Required for Transfer vs. Parking Altitude-. 8-45

8.5-6 Percentage of Fuel Required for Transfer vs. Central Transfer Angle--- 8-46

8.5-7 Total Required Transfer Velocity Increment vs. Parking Altitude-. 8-47

8.5-8 Total Required Velocity Increment for Minimum Energy--. 8-48

9-1 Lunar Orbital Rendezvous 9-3

9-2 Rendezvous Guidance (Lunar Orbit) 9-11

9-3 Digital Smoother (Range Components) 9-19

Fig. No.		Page
9-4	Effect of Transfer Angle on Eccentricity of Cotangential Transfer Orbit (From 30 km Lunar Parking Orbit to 200 km Circular Target Orbit)	9-25
9-5	Effect of Transfer Angle on Incremental Velocities of Cotangential Transfer Orbit (From 30 km Lunar Parking Orbit to 200 km Circular Target Orbit)	9-26
9-6	Effects of Initial Conditions on Propellant Consumption (Lunar Orbit)	9-29
9-7	Vertical Phase Plane (Lunar Orbit)	9-33
9-8	Horizontal Phase Plane (Lunar Orbit)	9-34
9-9	Range Diagram (Lunar Orbit)	9-35
9-10	Effect of Rendezvous Sensor Errors on Propellant Consumption (Lunar Orbit)	9-36
9-11	Effect of Rendezvous Sensor Errors on Propellant Consumption (Lunar Orbit)	9-37
11-1	Earth Orbital Rendezvous	11-3
11-2	Rendezvous Guidance (Earth Space Station)	11-7
11-3	Digital Smoother (Range and Angle)	11-11
11-4	Range vs. Transit Time	11-15
11-5	Elevation Angle vs. Transit Time	11-16
11-6	Effects of Initial Conditions on Propellant Consumption (Earth Space Station)	11-19

Fig. No.		Page
11-7	Velocity Applications for a Nominal Trajectory (Earth Space Station)	11-20
11-8	Phase Plane of Active Rendezvous (Earth Space Station)	11-21
11-9	Variation in Elevation Angle With Range (Earth Space Station)	11-22
11-10	Effect of Rendezvous Sensor Errors on Propellant Consumption (Earth Space Station)	11-23
21-1	Velocity-Acceleration Diagram of Landing Maneuver	21-3
21-2	Vector Diagram of Landing Maneuver	21-13
22-1	Orbit Diagram (Lunar Orbit Rendezvous)	22-3
22-2	Diagram of Orbital Elements	22-13
22-3	Diagram of Eccentric Anomaly	22-15
22-4	Orbit Diagram (Earth Space Station Rendezvous)	22-21
23.1-1	Tangential Capture for Transfer between Circular Orbits	23-2
23.1-2	Total Required Velocity Increment	23-8
23.3-1	Coordinate System for Small Perturbations	23-12
23.4-1	Orientation and Axis Definition of	23-15
23.4-2	Misalignment Angles of Accelerometer Input Axes	23-17

List of Tables

Table No.		
4-1	Computer Program Inputs	4-25
4-2	Printout	4-27

Table No.		Page
4-3	Standard Input Conditions	4-30
4-4	Trial Schedules for 63.9 and 72.2-Hour Trajectories	4-32
4-5	Comparison of Results at Perilune for Different Star-Planet Angle Measurements	4-34
4-6	RMS Results at Perilune with Trial Schedules	4-35
4-7	"Optimization" of 72.2-hour Trajectory	4-39
4-8	Scheduling Runs on 63.9-hour Trajectory	4-41
4-9	Improved Schedules for Lunar Trajectories	4-42
4-10	Variation of Parameters for 72.2-hr. Trajectory (45 observations)	4-45
4-11	Variation of Parameters for 63.9-hr. Trajectory (45 observations)	4-46
4-12	Comparison of 45 and 90 Measurement Schedules	4-48
6-1	Definition of Recurrent Symbols	6-6
6-2	Digital Program Results	6-48
6-3	Results of Sample Computation	6-57
8.4-1	Optimized Boost Trajectory Parameters	8-23
8.4-2	Estimated Pre-Launch Uncertainties for the Lunar Interceptor	8-34
8.5-1	Error Coefficients, Propogation, and Evaluation at Thrust Termination	8-39
8.5-2	Velocity Errors at Thrust Cut-off	8-40
8.5-3	Position Errors at Thrust Cut-off	8-41
8.7-1	Sensor Requirements for Lunar Parking Ascent	8-55
12-1	Ground Command Midcourse Guidance	12-2
23.4-1	Inertial Measurement Error Sources	23-14
23.4-2	Miss Coefficient Integral Set for Sensor and Platform Error-Forcing Functions	23-17

This page intentionally left blank

ABSTRACT

13013

This document is the second part of a two part engineering report submitted by the Atomic, Defense and Space group of the Westinghouse Electric Corporation, under contract to NASA Headquarters (OART), for the purpose of consolidating and extending studies of detection, tracking, and navigation systems for future space missions. This Part II document determines sensor requirements for space missions as selected and defined in the Part I report.

The Part I report establishes the nature, relative importance, and growth potential of missions to be attempted in the near future, and it provides a "Problem Definition" to serve as a basis for this Part II analytical study.

In the Part II report, sensor and guidance control methods are selected; sensor measurement accuracies are specified after, and on the basis of, a study and evaluation of the resulting system performance. As a part of the analysis, control and data processing methods and mathematical techniques are considered, selected and evaluated, and digital programs employed are presented and discussed. This report provides the "Analytical Solution" or Part II for the NASA OART analytical effort.

AUTHOR

This page intentionally left blank

PROBLEM STATUS

This Analytical Solution (Part II) is a final report and completes the present contract.

A proposal to make further use of the mathematical techniques and methods and the resultant digital programming employed under this contract has been submitted to NASA Hq.

AUTHORIZATION

NASA Contract NASw 460

Westinghouse G.O. No. 51052

This page intentionally left blank

SCOPE:

In accordance with the NASw 460 contract requirements, the study and analysis, of which this report is Part II, has been organized along the guidelines furnished by MIL-D-8684A, paragraphs 3.4.3.1 and 3.4.3.2. The Problem Definition Approach, as outlined in the introduction to Part I, has allowed benefit to be gained from the vast amount of analytical work of various kinds which has been done in recent years. It is hoped that as a result of the literature survey conducted for the Part I document, the study and analysis presented in Part II will be pertinent, and applicable, and will have taken maximum advantage of similar work already done with a minimum of duplication of effort.

The Part I document consists of a general and a specific definition of the problem requirements derived from an overall examination of the problem. The Part II document consists of the analytical operation on the problem requirements of Part I to provide an analytically based survey of sensor requirements for selected space missions. Principal emphasis has been placed on the Manned Lunar Mission and on Rendezvous. In accordance with contract specification the analysis stops short of detailed hardware requirements.

This page intentionally left blank

ANALYTICAL SOLUTION

1.0 INTRODUCTION

This report examines in turn the Manned Lunar Mission, Earth Space Station Rendezvous and the Unmanned Lunar Mission. Where possible, the results are extended to Interplanetary Missions. The Manned Lunar Mission is treated by phases, the principal emphasis being placed on the Midcourse, Parking and Descent Orbit, Descent Trajectory, Lunar Ascent and Rendezvous phases. As stated in Part I, it was concluded that a detailed study of Earth Launch-To-Injection or Earth re-entry would constitute a duplication of effort. This phase is presented in summary form only.

While Space Missions in general may be divided into the classifications, Manned and Unmanned, they may equally well be grouped into the two classifications, Earth-controlled and Local-controlled. Unmanned missions tend to be Earth-controlled wherever feasible, in part because this allows a maximum of vehicle weight for experimental and measuring equipment for a minimum of control equipment. Manned missions tend to be local controlled, in part because this allows the feature of redundant earth control as a back-up system. The Unmanned Lunar Mission is treated, in this report, by phases as with the Manned Lunar Mission. Because the DSIF will logically play the principal part in Unmanned Midcourse, this phase has been treated in somewhat summary fashion, the DSIF requirements having been covered in available literature extensively and fairly completely. In addition, certain phases of the Manned Lunar Mission, such as the Descent Trajectory may equally well be considered manned or unmanned.

The major effort in this report, therefore, has been expended on the Midcourse through Ascent phases of the Manned Lunar Mission, and on Rendezvous. Each phase of each mission selected is treated in turn, in this docu-

ment, as a separate study. As stated in Part I, the separate phases are not treated as integrated phases of a coherent mission, but are treated as separate studies each assuming a nominal set of conditions (end conditions, trajectories, etc.). Because a certain amount of integration between phases, without restrictions on the separate studies, is possible, this is treated in a separate section. The control systems necessarily assumed for each phase are as general and flexible as possible, are based on present work being done, are in general a logical extension thereof, and in most cases, are different for the different phases.

The immediate results and principal objective of the Part II study are representative sensor schemes stopping short of mechanization specification for each phase, and the required sensor accuracies for each sensor scheme for each phase of each mission. Optimization is employed where possible.

Additional results which follow as a byproduct of the principal objective are also presented, such as the control schemes employed for each phase and their performance, the mathematical techniques used and their applicability, and the digital programs employed and their possible further application.

2.0 SUMMARY

The following sections comprise a phase-by-phase analytical study of the successive phases of the Manned Lunar Mission, an analysis of Lunar Rendezvous and Earth Orbiting Space Station Rendezvous, and a summary analysis of the successive phases of the Unmanned Lunar Mission. The objective in each analysis is a survey of guidance and control sensor accuracy requirements. Attitude control is not considered except in terms of directional thrust control. As stated in the Part I document, Sensor Requirements Charts are drawn up for each phase in this Part II document, and are presented in this section. However, the immediate results with regard to sensor accuracy specification of some of the studies herein presented are more general (in a useful sense) than the charts would indicate, as is shown elsewhere in this summary.

The successive sections are here summarized in order as follows.

Section 3.0 examines the earth launch to injection into lunar midcourse phase of the lunar mission, and applies to both the manned and unmanned case. The certainty of a superfluous duplication of effort resulting from a detailed analysis of this phase leads to the approach taken here, as stated in Part I. The assumptions and results of a representative study are given with the object of justifying the initial conditions assumed for midcourse. A chart of assumed sensor accuracy requirements is not shown for this phase.

Section 4.0 analyzes the Manned Lunar Midcourse Phase from immediately after earth injection into lunar trajectory to immediately prior to lunar parking orbit injection. Local navigation, computation and control are assumed. Navigation along the trajectory consists of a repeated one dimensional fix obtained by successive measurements of the angle between a known point on the earth and known stars, interspersed with measurements of the angle between the

moon and known stars, according to a prescribed schedule. Minimum time spacing between one dimensional fixes is about 20 minutes and about 45 such measurements are taken altogether over the trajectory. A possible mechanization of the scheme might be a sensor system in which earth and lunar bearings are taken with respect to a celestially fixed inertial reference. Computation consists of application of the mathematical technique of minimum variance to linearization of perturbations about a nominal trajectory. Two approximately lunar-orbital-plane trajectories are considered, a 72.2 hour and a 63.9 hour trajectory. Control consists of a total of three thrust impulses at scheduled times along the trajectory.

Results of the study are various sensor measurement and control accuracies for various assumed terminal position and velocity errors, sensitivity of measurement accuracy to assumed schedules of measurements, and a digital computer program capable of further related studies. An example of sensor requirements for a particular set of assumed condition is shown in chart from in Figure 2-1.

The general conclusions reached are that the necessary measurement accuracies for on-board midcourse navigation are extremely tight in terms of present possible mechanization; angle measurement to 10 or 20 seconds of arc to a point on earth whose position is known within 1.6 KM or to a point on the moon whose position is known within 0.8 KM. It is concluded that measurement accuracy is not particularly sensitive to the schedule of stars selected for measurement (within limits) or overly sensitive to measurement timing (provided the time is known), although some optimization can be obtained; that a reduction in required accuracy can be obtained at the expense of a considerable fuel increase; and that doubling the number of measurements will roughly reduce the required sensor accuracy by 50%. A tentative conclusion is that a two-angle measurement (two dimensional fix) would not result in significant relaxation of sensor requirements.

Phase: Manned Lunar Midcourse Guidance

Navigation and Control Error Sources

a) Measurement Uncertainty due to Instrument
b) Measurement Uncertainty due to Definition of Horizon
c) Correction Thrust Magnitude
d) Correction Thrust Pointing Error

Assumed Initial Condition Errors (rms)

a) Position:	3.6 km and 7.2 km
b) Velocity:	3.1 m/s and 6.2 m/s

Assumed Allowable Terminal Errors (rms)

a) Total Miss Distance:	25 km
b) Lunar Altitude Component of Miss Distance	5 km

Allowable Measurement Uncertainties (rms)

a) Instrument Measurement Uncertainty:	12.5 seconds arc
b) Horizon or Landmark Uncertainty:	1.6 km (earth) 0.8 km (moon)

Allowable Correction Errors

Thrust Magnitude:	0.1 m/s

Figure 2-1

Phase: Manned Lunar Parking and Descent Orbit

Navigation Sensor Measurement:

Repeated one-dimensional angular measurement - star to known point on lunar surface

Control:

a) Single thrust impulse to transfer from midcourse to parking orbit
b) Single thrust impulse to transfer from parking orbit to descent orbit

Assumed Initial Condition Deviations (per axis)

a)	Position:	4.8 km
b)	Velocity:	1.2 m/sec.

Assumed Initial Condition Uncertainties (per axis)

a)	Position:	0.8 km
b)	Velocity:	0.08 m/sec.

Assumed Allowable Terminal Position Deviations:

a)	Tangential:	5.08 km
b)	Vertical:	2.54 km

Allowable Navigation Sensor Error:

2 milli-radians

Allowable Engine Control Error (per axis)

$(1/\sqrt{3})$ (1%) of total velocity impulse

Allowable Impulse Measurement Error (per axis):

$(1/\sqrt{3})$ (0.005) meters/sec.

Figure 2-2

Section 5.0 analyzes the Manned Lunar Parking and Descent Orbits from orbit injection to the final descent trajectory phase. Local navigation, computation and control are assumed and navigation consists, again, of a repeated one dimensional fix, this time, the angle between successive known stars and successive known points on the lunar surface. A possible mechanization would be one similar to that of the preceding section. The computation scheme employed is essentially that of the preceding section and assumes nominal parking orbit and descent orbit trajectories. Trajectory correction for the measured discrepancy between the actual parking orbit and the nominal is made at transition to descent orbit. Further measured discrepancy is computed in terms of terminal conditions at the end of the descent orbit, i.e. at initiation of the landing trajectory. Control, then, consists of a thrust impulse to transfer from midcourse to parking orbit and a second thrust impulse to transfer from parking to descent orbit.

Results of the study are sensor measurement and thrust control accuracy for assumed position and velocity errors at the termination of the descent orbit, sensitivity of terminal errors to assumed conditioning of measurements, and an evaluation of the applicability of the various linearization techniques to parking orbit determination. A representative example of sensor requirement accuracies for an assumed set of conditions is shown in chart form in Figure 2-2.

In the course of this study, it was determined that the method of least squares data processing is inadequate to the problem. It was verified that the sensitivity coefficients, used in Kalman's method to weight the incoming sensor measurement data, cannot be pre-computed from the nominal trajectory in an actual on-board system, but must be re-computed from the measurements. It was also verified that the success of any feasible on-board measurement system will tend to be dependent upon taking a specified measurement in a

specified direction at a specified time.

In Section 6.0, the Manned Lunar Descent (or landing) Trajectory is analyzed. This phase begins with the perilune of the descent orbit and ends with a nominal condition of zero velocity at an altitude of 500 meters over a selected landing site.

Local navigation, computation and control are assumed. Navigation for this phase consists of an approximation to a continuous measurement of range, range rate, line-of-sight angle and line-of-sight angle rate to a fixed point on the lunar surface. Choice of observables was based on assumed mechanization such as a range measuring radar, optically aimed, or a radar set tracking a beacon, although altitude and altitude rate could equally well have been assumed in place of range and range rate.

Linearized perturbation from a nominal gravity turn trajectory is the computation scheme employed. Control consists of thrust magnitude and direction increments imposed upon what would otherwise be a constant magnitude thrust in a direction opposite to the vehicle velocity vector.

The immediate results are two sets of miss coefficients which relate individual components of terminal position and velocity error to individual sensor and initial condition errors. These are presented as Table 6-2 of Section 6.0. To present the summary of sensor requirements shown in Figure 2-3, a given distribution of sensor errors was assumed and a given set of allowable terminal errors imposed which was regarded as representative. The immediate conclusion is that sensor accuracy requirements for this phase are not excessive. General conclusions are that the modification presented in this section of the Ames trajectory analysis technique, reference 6-1, provides a flexible and useful tool for analysis of continuous thrust trajectories of the type assumed and, in addition, is susceptible to mechanization for on-board guidance. It is hypothesized

Phase: Manned Lunar Descent (Landing) Trajectory

Navigation and Control Error Sources:

a) Range Measurement
b) Range Rate Measurement
c) Angle Measurement
d) Angle Rate Measurement
e) Thrust Magnitude Mechanization
f) Thrust Orientation Mechanization

Assumed Initial Condition Errors (rms Uncertainty)

a)	Range:	0.1 percent of initial range
b)	Range Rate:	0.5 percent of initial range rate
c)	Angle:	1 milli-radian
d)	Angle Rate	1 milli-radian/second
e)	Thrust magnitude:	480 newtons, (1 percent)
f)	Thrust orientation:	35 milli-radians

Assumed Allowable Terminal Errors (rms)

a)	Velocity:	9.4 meters/second
b)	Altitude:	9.4 meters
c)	Horizontal Range:	1.4 meters

Allowable Navigation Measurement (rms Accuracy)

a)	Range Measurement:	0.1 percent
b)	Range Rate Measurement:	0.5 percent
c)	Angle Measurement:	1 milli-radian
d)	Angle Rate Measurement:	1 milli-radian/second

Allowable rms Control Error:

a)	Thrust Magnitude:	480 newtons, (1 percent)
b)	Thrust Orientation:	35 milli-radians

FIGURE 2-3

Phase: Manned Lunar Rendezvous

Navigation Sensor Measurements, Range Vector to Target:

a) Range
b) Azimuth and elevation angles relative to an inertial reference system

Assumed Initial Condition Error:

0.3 m/sec. in velocity (retrograde)
(moderate position, velocity, and phasing errors can, however be accommodated).

Assumed Allowable rms Terminal Errors:

a)	Range:	25 m
b)	Range Rate:	1 m/sec.

Assumed Allowable rms Increase in Propellant Consumption:

17%

Allowable rms (1σ) Navigation Measurement Accuracy

a)	Range:	0.06% of range or 6 m
b)	Azimuth and Elevation Angles:	1.7 mr

Allowable Control Error

a)	Attitude:	0.2 deg. (during firing) 5 deg (while tracking)
b)	Velocity:	0.5 m/sec.

FIGURE 2-4

that the results derived apply approximately to any control computation scheme resulting in a gravity turn type of trajectory and using approximately continuous measurement of observables, although this is not shown.

Because any guidance system assumed aboard the landing vehicle for the descent trajectory will be adequate for the hover-to-touchdown phase, no analysis was performed for Section 7.0. However, qualitative sensor requirements are discussed.

Section 8.0 analyzes the lunar ascent phase of the manned lunar mission. It is shown that for ascent to a parking orbit prior to rendezvous, assuming a conventional inertial reference system for boost phase, present-day capabilities are sufficient. A general discussion on ascent and orbit types of trajectory for rendezvous is also presented with regard to time and fuel required.

Section 9.0 is an analytical study of the manned lunar rendezvous phase. At initiation of this phase, the chaser and target vehicles are each assumed in approximately circular lunar parking orbits; analysis terminates at the point at which the chaser reaches a preset standoff range from the target at approximately zero relative velocity, at which point manual take-over control is assumed.

Local navigation, computation and control at the chaser vehicle are assumed except for initial target orbit information. Navigation for rendezvous consists of measurement of range and angular direction to the target vehicle. Computation is based on a range-to-go and range-rate-reduction-to-go set of equations, and control is of the on-off type assuming a sequence of variable duration rocket impulses. The method of analysis of the system was Monte Carlo. Computer runs were made for a variety of initial conditions and assumed sensor accuracies, and for both 90 and 180 degree orbit transfers.

Sensor requirements for an assumed set of conditions is shown in chart form in Figure 2-4. It is concluded that sensor requirements for the guidance scheme presented in this section are not excessive and could be met by present state-of-the-art radar without excessive fuel consumption over the theoretical minimum.

Section 10.0 summarizes the manned lunar midcourse return phase. The sensor requirements of Section 4.0 are shown to apply.

Section 11.0 examines the rendezvous of a manned spacecraft with a cooperative and manned earth space station.

As in Section 9.0, the initial conditions for this phase assume chaser vehicle and target (the earth space station) in approximately circular parking orbits, this time around earth, and Navigation and Control are of the type assumed in Section 9.0. Guidance computation is a modification of that used previously. Monte Carlo methods are used for analysis. Sensor requirements for an assumed set of conditions are shown in chart form in Figure 2-5. The modifications in guidance computation are shown to give substantial improvement over the unmodified computation scheme of Section 9.0, and, as a result, sensor requirements are not as stringent.

Section 12.0 is a study of the unmanned midcourse phase. Ground control by the DSIF ground tracking system is assumed. As stated in Part I, only a summary analysis is performed. Results are shown in chart form in Figure 2-6.

Section 13.0 and 14.0 summarize the unmanned parking and descent orbits, and the unmanned lunar descent trajectory respectively, and Section 15.0 the final landing phase.

A discussion of Integration between Phases is treated in Section 16.0. It is shown that while this report consists of independent studies of the separate phases of each mission, a certain amount of integration between phases is possible,

Phase: Rendezvous With Earth Space Station

Navigation Sensor Measurements Range Vector to Target:

a) Range
b) Azimuth and elevation angles relative to an inertial reference system

Assumed Initial Condition Error:

0.3 m/sec. in velocity (retrograde)
(moderate position, velocity, and phasing errors can, however, be accommodated).

Assumed Allowable rms Terminal Errors

a)	Range:	50 m
b)	Range Rate:	1 m/sec.

Assumed Allowable rms Increase in Propellant Consumption:

17%

Allowable rms (1σ) Navigation Measurement Accuracy

a)	Range:	0.1% of range or 10 m
b)	Azimuth and Elevation Angles:	3 mr

Allowable Control Error

a)	Attitude:	0.2 deg. (during firing) 5 deg. (while tracking)
b)	Velocity:	1 m/sec.

FIGURE 2-5

Phase: Unmanned Lunar Midcourse Guidance

Navigation and Control Error Sources

a) Errors in tracking information
b) Uncertainty in station locations, astrodynamic constants
c) Correction Thrust Magnitude
d) Correction Thrust Orientation

Assumed Initial Condition Errors

Contour guidance capabilities

Assumed Allowable Terminal Errors

Correction accuracy required to add less than 10% to miss-distance and fuel consumption caused by other uncertainties

Required Data Rate

1 pt/minute

Allowable Correction Errors (rms)

a) Thrust Magnitude: .041 m/s
b) Thrust Orientation: 1 milliradian

FIGURE 2-6

and can be done utilizing the data given in this report.

While specific conclusions and recommendations are drawn for each section of this report, general conclusions concerning the overall approach of this Part II study and its results are discussed in Section 17.0.

In accordance with the general procedure followed for the Part I and Part II documents, the subsequent document would normally be the Part III "Mechanization" report. This is treated in Section 18.0.

The appendices begin with Section 19.0 and are given consecutively for each of the various phases. Each gives a complete detailed summary of the mathematical approach for each section analyzed.

This page intentionally left blank

3.0 Earth Launch to Injection, Manned

3.1 Introduction

As indicated in the Part I document, earth launch is considered only to the extent necessary to establish feasibility for injection into the cis-lunar trajectory. The results of a representative study are given, thus avoiding repetition of error analyses of well-established guidance schemes.

Launches from the surface of the earth usually comprise several powered boosts, a free-flight coasting period, and a final boost to mid-course injection. The vehicle is guided by inertial sensors to pre-selected thrust termination points. Thus, it is relevant to provide miss distances and velocities at these points.

3.2 Approach

The following chart is a summary of earth-launch cut-off errors taken from a report concerning the guidance systems for an unmanned lunar logistics vehicle (ref. 3-1). In this report three powered boost phases were followed by a circular parking orbit defining the free-flight mode. This orbit was selected to facilitate launch every day of the month. After a dwell time equivalent to $\frac{1}{4}$ of an orbit, the vehicle was boosted from a parking velocity of 26,000 feet/sec. to a near parabolic transfer orbit of velocity 36,400 feet/sec. The miss distances and velocities attained were based on 1 σ uncertainties available in state-of-the-art inertial navigation configurations.

Earth-Launch Phase	R.M.S. Miss Value Uncertainties			
	Velocity (m/sec.)		Position (km)	
	Range	Track	Range	Track
1. Boost I ΔV = 2310 m/sec.	0.0933	0.122	0.00583	0.00610
2. Boost II ΔV = 4090 m/sec.	0.305	0.302	0.0384	0.0469
3. Boost III to Parking ΔV = 1003 m/sec.	0.305	0.303	0.0625	0.0677
4. Parking $\frac{1}{4}$ Orbit	1.63	1.63	2.12	2.12
5. Boost IV To Parab. Trans. ΔV = 3078 m/sec.	1.54	1.54	2.03	2.02

Table 3-1: Representative Earth-Launch Guidance Errors

3.3 Summary of Results

Referring to section 4.6.3, the following 1 σ r.m.s. uncertainties were assumed at the beginning of the mid-course analysis:

σ_x = 2 km. $\dot{\sigma}_x$ = 2 m/sec.

σ_y = 1 km. $\dot{\sigma}_y$ = 1.2 m/sec.

σ_z = 3 km. $\dot{\sigma}_z$ = 2 m/sec.

It was subsequently shown that for the selected mid-course scheme, these values could be doubled with no significant increase in target uncertainty prediction; a fuel penalty of no more than 20 m/sec. was required at the first correction.

Comparison of the above tables establishes feasibility. Verification of the above miss value uncertainties could be established by the methods outlined in section 8 concerning the lunar ascent.

4.0 MANNED LUNAR MIDCOURSE GUIDANCE

4.1 Introduction

The objective of the midcourse guidance study is defined as follows: to determine the sensor requirements for onboard mid-course guidance of a manned space vehicle to the moon.

It was decided to concentrate effort in this analysis on the manned lunar mission, since the orbiting space station is essentially a rendezvous problem and the unmanned lunar missions will presumably be guided from Earth during the mid-course phase.

On-board navigation was chosen for the study for several reasons:

(1) Onboard guidance is required in the vicinity of the moon or planet.

(2) Applicability to lunar and follow-on missions. Because of the range limitations on ground-tracking, an onboard guidance technique is required for missions more distant than the moon.

(3) A technique for ground-command guidance during midcourse has already been developed by JPL and extensively reported.

(4) The use of onboard guidance allows the use of DSIF as a backup.

4.2 Background and Problem Approach

In this section, the fundamental problems involved in onboard guidance of a manned vehicle on a lunar flight and the approach taken toward solving them, are considered in a semi-quantitative way, indicating some of the preliminary considerations for study and the broad system constraints. Included is a review of some of the important papers in this field.

4.2.1 Geometry and Physics of Midcourse Problem

A typical lunar trajectory is shown in Sketch I. The vehicle is

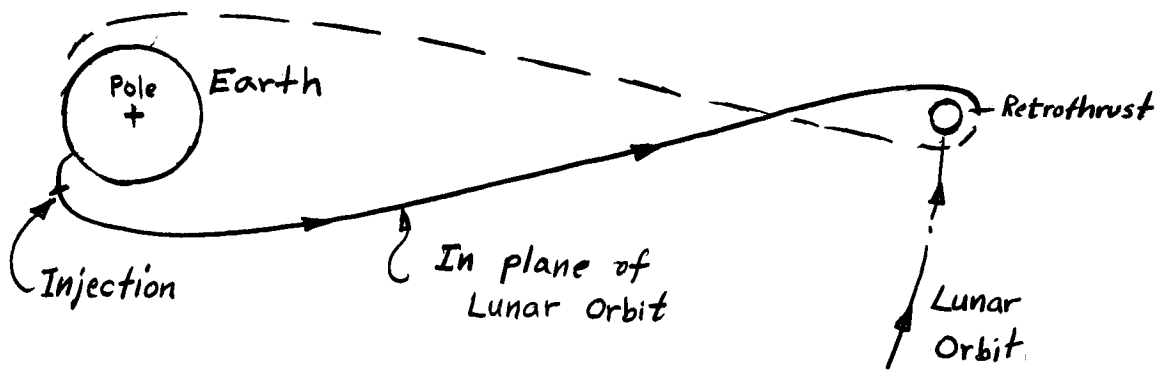

Sketch I.

fired into an elliptical trajectory at the earth having approximately .99 earth escape velocity. Near the vicinity of the moon, the lunar gravity deflects the vehicle around the moon and back toward the earth. This circumlunar trajectory can be used to obtain a lunar orbit by initaiting a large retro-thrust as the vehicle goes around the back side of the moon. In this way, an automatic return to the vicinity of the earth is obtained if it is decided not to descend to the moon.

Note that the plane of the trajectory around the earth is coincident with the plane of the moon's orbit around the earth. A trajectory of this type will result in an equatorial path around the moon, a desirable situation for rendezvous and for operations requiring mapping of the lunar surface, since the geography of the moon is best known near its equator. In order to obtain an

in-plane trajectory with a direct launch from Cape Canaveral, one must accept either a very small launch window or make an expensive velocity correction in order to re-orient the plane of the initial launch. These problems can be averted, as shown in Ref.4-6 by use of a coasting orbit. In this report, it will be assumed that a "variable launch window" coasting orbit has been used to obtain an in-plane trajectory. In order to obtain a non-equatorial orbit, the trajectory plane should be a few degrees above or below the plane of the moon's orbit.

The launch accuracy requirements for a purely ballistic flight to the moon have been developed in Ref.4-7. Since present-day inertial devices and engines cannot normally be expected to achieve injection conditions required for precise lunar trajectories, it is required that the trajectory be corrected at least once during the flight in order to reduce the miss distance and uncertainty at the moon.

The Ranger shots have employed ground tracking of radio signals from the spacecraft, and a single correction of the trajectory early in the flight to reduce the miss distance. This method is adequate for unmanned probes where the terminal accuracy requirements may not be stringent, and the practical difficulties in making velocity corrections are a limitation. However, for manned lunar orbital missions, the assignment of a small target on the moon increases the trajectory accuracy requirements and makes the use of additional corrections later in the flight mandatory.

The mission time required for the lunar flight is a function of injection velocity from the earth orbit. The minimum velocity required to reach the moon from an earth orbit of 300 km is about 10,800 m/s. However, use of this injection velocity would result in a prohibitively long flight time.

An increase in injection velocity to 11,750 m/s would result in a reasonable flight time of 3 days. The curve of flight time vs. injection velocity rises very steeply for trip times greater than 60 hours (ref.4-8).

Determination of the position and velocity of the vehicle by ground-tracking is difficult in the vicinity of the moon for two reasons: (1) no data is available when the vehicle is on the far side of the moon and (2) the angle and angle-rate measurement accuracy, being an inverse function of range is degraded at great distances from the earth. Therefore, the usefulness of on-board guidance near the vicinity of the moon is indicated.

4.2.2 System Constraints and Assumptions

A list of the preliminary system constraints assumed for this study and the effect on the analysis follows.

Vehicle

The proposed Apollo vehicle is used as a model vehicle for this study. This is done primarily to impose field-of-view limitations on sensors.

Launch and pre-injection guidance

It was assumed that launch into a coasting orbit and injection into a lunar trajectory from this orbit is used. Considerations of launch window and launch latitude were not studied in the midcourse analysis.

Launch vehicle

During the time period (1968-75) when manned lunar expeditions will be made, the primary boost vehicle in use by NASA will be the Saturn C-5, which has a planned lunar payload of about 41,000 kg (90,000 lbs.).

Criteria

The primary criteria for selction of guidance systems are (1) ability to perform desired mission, (2) reliability, (3) weight, (4) mechanizability.

4.2.3 Problem Approach

The problem of determining sensor requirements for a manned lunar mission was attached from two aspects:

(1) A review and interpretation of existing literature on the problem (Section 4.2.4 and Appendix IC, Section 19).

(2) Analysis of a specific model (Section 4.4).

This approach was chosen because of the difficulty in performing a generalized analysis for midcourse guidance of all missions, the limited time available for the study, and the broad scope of the contract. The difficulty in making a generalized analysis is caused by the dependence of sensor accuracy upon a wide variety of parameters such as target planet, mission time, available energy, observables used, number and accuracy of velocity corrections, etc.

4.2.4 Literature Search and Interpretation

In this section, the results of an evaluation of literature pertaining to midcourse guidance are presented. Although not all-inclusive, these papers develop reasonable solutions to some of the problems in midcourse guidance, especially in the areas of data processing and guidance schedules.

The problem of optimum scheduling was not specified as an output of this study. However, since it will be shown that the sensor requirements depend strongly on the number and type of observations made, some consideration of the scheduling problem must be made in order to make a sensible evaluation of sensor accuracies.

As pointed out in Appendix IC, (Section 19.0), much work has been done at Ames Research Center on the problem of optimum scheduling for various sensor configurations. The numerical results obtained are not directly

applicable to this study due to the different trajectories employed. However, wherever possible, results of the optimization work done at Ames were incorporated into development of useful schedules for this study.

A review of the general results of other analyses which formed the foundation for selection of schedules in this study is given:

(1) A reasonably optimum number of optical measurements on a lunar flight is in the range of 35-45 for measurement errors of 10 secs. of arc.

(2) For sextant-type measurements, the choice of stars has a definite effect on system performance.

(3) For sextant-type measurements, a ratio of about 5 "azimuth"-type measurements to 1 "elevation"-angle measurement is approximately correct. "Azimuth"-type angle here means measurement of the angle between a star and a planet where the star is in the trajectory plane. "Elevation" angles are measured from star and planet where the star-planet angle is in a plane perpendicular to the trajectory plane.

(4) Interchanging the order of measurements has little effect.

(5) Grouping of the observations toward the end of an interval bounded by velocity corrections is beneficial.

(6) In general, making more Earth-Star observations near the Earth and more Moon-Star observations near the moon is desired.

The papers from which these conclusions were drawn are discussed in more detail in Appendix IC, Section 19.3.

4.3 Problem Definition

In order to define the sensor requirements for a manned lunar mission,

a specific model was hypothesized for analysis. Although the sensor requirements are thus derived from a specific example, variations in the critical parameters of the model chosen will illustrate their effect on the sensors. A detailed description of the analytical model chosen and the reason for the choices follows.

4.3.1 Mission

The mission chosen for analysis is a manned lunar mission designed to achieve a low altitude lunar orbit.

4.3.2 Astronomical Model

The forces acting on the vehicle in free-flight are assumed to be the gravitational fields of spherical, homogeneous earth and moon; restricted 3-body equations are used, with the moon assumed to be rotating in a circular path about the earth at an inclination of 28° to the earth's equator. This is an approximation of the true physical situation which is considered adequate for the determination of sensor requirements, and desirable for the sake of simplifying computations.

4.3.3 Trajectory

The nominal trajectory employed is shown in Figure 4-1. This analysis is concerned with the portion of the trajectory from injection from a coasting orbit into a trans-lunar trajectory at t=0 hours, until the initiation of a retrothrust to being the vehicle into a 133-km lunar orbit at t=63.9 hours. The trajectory is approximately in the plane of the lunar orbit. Although the mission is for a lunar orbit, the trajectory would be circumlunar and return to earth if the retrothrust into lunar orbit is not made.

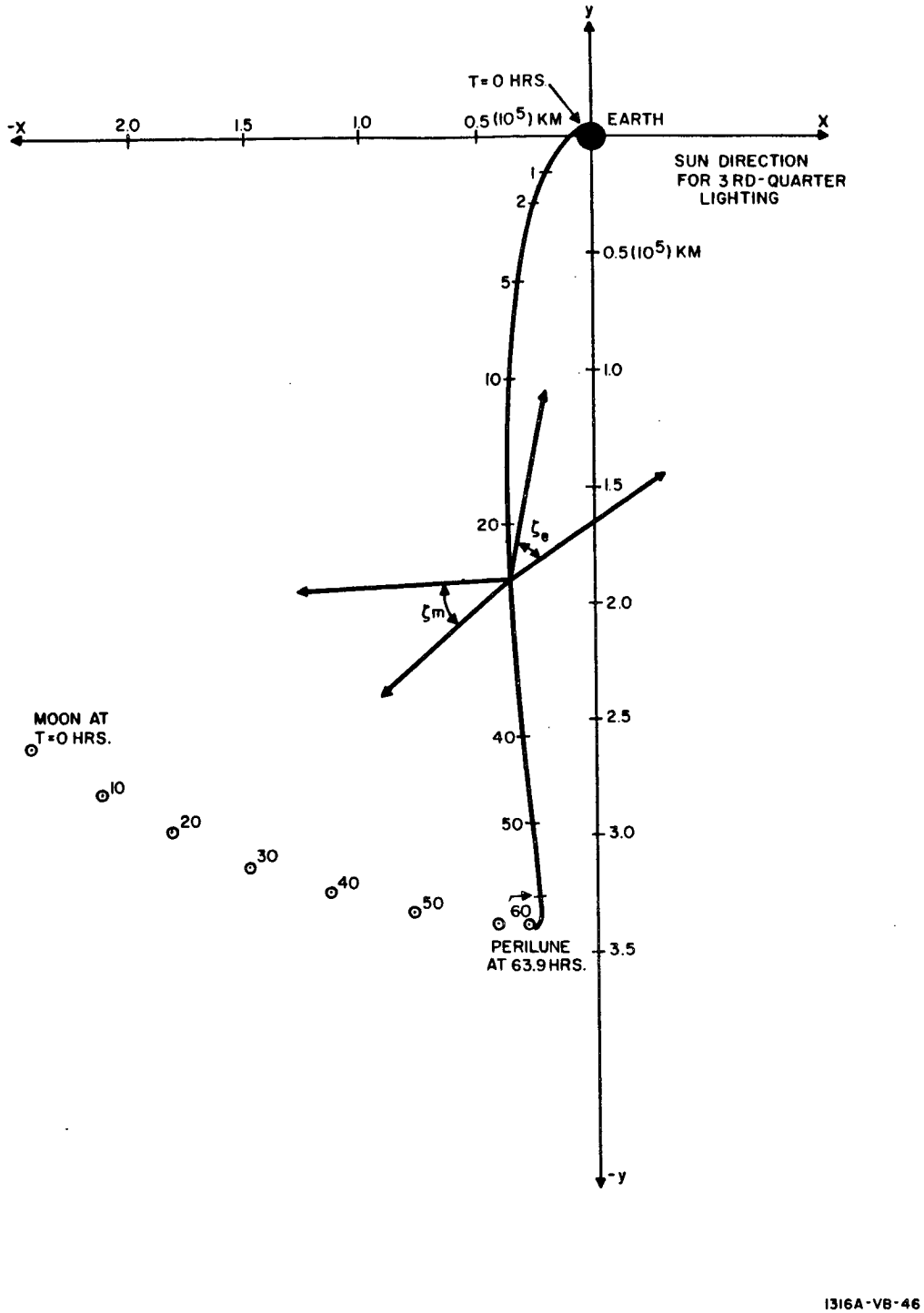

FIGURE 4-1: 63.9 Hour Nominal Trajectory

The lunar orbital altitude of 133 km is considered typical of what might be used on a mission which involves lunar rendezvous and descent to the surface.

The parameter of this trajectory which would be expected to have the greatest effect on sensor accuracy is mission time. The relatively short mission time chosen for this trajectory made the sensor requirements somewhat more severe than for the 72-hour trajectory which is presently being considered for the Apollo program. This is due to the higher velocities involved on a short mission. Because of this factor, a 72-hour trajectory was also analyzed to indicate the dependence of sensor requirements on flight time.

4.3.4 Observables

The observables chosen for estimation of position and velocity onboard the spacecraft consist of measurements of the angle between a star and a planet (earth or moon) landmark or horizon. The advantages of using optical measurements for spacecraft navigation are obvious: no power is required as would be the case in the use of some ranging device, and the system is not range-limited in its scope of applicability as would be a ground-tracking system. In addition, this type of measurement can also be employed for orbital determination around the moon. (Section 5).

Single-angle measurements are assumed here. It was shown in ref 4-4 that such measurements are nearly as effective in reducing estimation uncertainties and the stabilization requirements are expected to be simpler than would be the case for a 2-angle measurement.

4.3.5 Data-handling

The trajectory estimation scheme assumed in this analysis is essentially the same as that employed in refs 4-1 and 4-2 with modifications for the incorporation of single-angle data. This scheme, employs linear filtering theory, developed in ref 4-5 to make an optimal estimate of position and velocity based on measured deviations from the nominal trajectory. The equations of motion are linearized over short intervals, so the estimation scheme is actually "optimum" to the extent that linear relationships about the nominal trajectory are valid.

This scheme was shown to give good results for trajectory calculations in refs 4-1 and 4-2. One of the features of the scheme is the incorporation of a priori knowledge of injection accuracy and measurement accuracy to efficiently weight the data from each observation. In addition, since the scheme involves the recursive calculation of the covariance matrix of the errors in estimate, it is particularly convenient for parametric analyses such as this study. In fact, statistical data about a class of trajectories having certain things in common can be developed without resorting to Monte Carlo methods requiring many integrations of the entire trajectory.

4.3.6 Guidance Logic

A fixed-time-of-arrival guidance logic is assumed in which each midcourse correction is calculated to null out the predicted position error at t_A, the nominal time of arrival at perilune. In general, only 3 components of the vehicle's "state" (position and velocity) at perilune can be corrected by applying a single impulsive thrust and since the mission requires a large

velocity correction at perilune to achieve an orbit, and since the position at perilune is critical in determining orbital altitude, only the predicted position errors will be corrected. The fixed-time-of-arrival guidance logic was chosen for simplicity, both in the analysis and in the mechanization of an on-board system.

4.3.7 Vehicle

For purposes of using a realistic model, it was assumed that the Apollo vehicle will be used. This selection will primarily effect (1) field-of-view requirements on optical sighting and (2) stabilization and weight requirements.

4.3.8 Assumptions on Corrections and Observations

In this analysis, it will be assumed that pre-programmed observations of the angle between a star and planet are made, and that the measurement errors have gaussian statistics with zero mean and are uncorrelated from one measurement to another. This last is not unrealistic due to the time ($\frac{1}{2}$-hour minimum) between measurements. Battin (ref 4-3) has derived methods of handling time-correlated measurement error, but there is some difficulty in predicting how these correlations really occur.

4.3.9 Independence of System

It was assumed that the system was capable of independent operation without ground-tracking.

4.4 Description of Analysis

4.4.1 Introduction

Sensor requirements were developed for the model described in

Section 4.3 by determining the observation and correction accuracy required to achieve desired end conditions at the moon. This was done by setting up a digital computer program (Section 4.5) to statistically analyze the effects of various system parameters on:

1) The rms miss distance at the moon.
2) The rms error in estimation of the miss distance.
3) The cost of midcourse maneuvers in fuel.
4) The total number of corrections and observations.

The system parameters of most interest in this study were:

1) Number and accuracy of observations.
2) Number and accuracy of corrections.
3) Injection accuracy required.
4) Mission time.
5) Scheduling of operations.
6) Selection of "optimum" star-planet combinations for measurement.

4.4.2 Onboard System Model

The operation of a data-processing scheme for estimation of position and velocity from noisy optical measurements is described in Appendix IA, Section 19.

Estimates of the position and velocity deviations from the reference trajectory are developed by updating the previous estimates with each new measurement. The incorporation of new data into the estimate each time a measurement is made can best be shown by a discussion of equations A-20, 21, 22 which are written here for convenience.

After $[\hat{x}]$ and P are updated, the estimation process (Equations (A-20), (A-21) and) (A-22) goes on as before.

For the purpose of analysis, pre-set observation and correction schedules were assumed. Though this may not necessarily be the case in an onboard system, it has been shown (Ref.4-4) that the results in either case will not be widely divergent.

4.4.3 Development of Statistical Information For Parametric Analysis

The estimation and correction process described in the previous section and Appendix IA is one which may be used for the guidance of a space vehicle employing optical measurements. In fact, with some modifications the same process might be employed to accept other sensor information such as radar or radio signals to a ground tracking station.

In order to make some statistical analyses on the performance of such a system and the attendant requirements on sensors one might run a Monte Carlo analysis of many trajectories, with randomly varying correction, injection and observation errors. The trouble with such an approach is that it would consume huge amounts of computer time, primarily due to the many parameters of interest in this study and the necessity of integrating the equations of motion on each run, a lengthy process even on the IBM 7094.

In order to avoid Monte Carlo analysis, statistical information about a class of flights having certain parameters in common may be developed. These parameters are $P(t_o)$, the injection accuracy, Q, the instrument variance, C, the correction accuracy, the nominal trajectory and the observation and correction schedules.

The quantities of interest for a parametric study are P, the

covariance matrix of estimation errors, R, the covariance matrix of deviations from the nominal trajectory and u, the rms value of velocity corrections. The development of these matrices at various times of interest is shown in Appendix IB. In addition, the rms deviations from the nominal trajectory in position and velocity are given by:

$$\text{(B-2)} \qquad r = \sqrt{Tr\,(R_1)}$$

$$v = \sqrt{Tr\,(R_4)}$$

The rms errors in estimation of position and velocity are given by:

$$\text{(B-2)} \qquad \tilde{r} = \sqrt{Tr\,(P_1)}$$

$$\tilde{v} = \sqrt{Tr\,(P_4)}$$

(In the above equations, Tr indicates the trace of a matrix and R_1, R_4, P_1 and P_4 are 3 x 3 submatrices of R and P).

$$\text{(B-10)} \qquad u = \sqrt{Tr\,(G'(R-P)G')}$$

where G' is the guidance matrix which relates deviations from the reference trajectory to the commanded Δv.

The quantities r, v, $\tilde{r}$, $\tilde{v}$ and u will be used as indicators of system performance, in addition to r_H, the component of position deviation in the radial direction at the moon.

The errors in making the corrections were described by the 3 x 3 C matrix, and the injection uncertainties by the 6 x 6 matrix, P (t_o). In

$$\text{(A-20)} \quad [\hat{x}] = \Phi[\hat{x}]_{k-1} + K\left[y - H\Phi[\hat{x}]_{k-1}\right]$$

$$\text{(A-21)} \quad K = \begin{bmatrix} P_1 \\ P_2 \end{bmatrix} H_1^T \left[H_1 P_1 H_1^T + Q\right]^{-1}$$

$$\text{(A-22)} \quad P_{k+1} = \Phi_{k+1}\left[P - KHP\right]\Phi_{k+1}^T$$

In the matrix equation (A-20), $[\hat{x}]$ is a 6-vector whose components are the estimate of deviations from the reference trajectory in position and velocity ($\hat{\delta x}$, $\hat{\delta y}$, $\hat{\delta z}$, $\hat{\delta \dot{x}}$, $\hat{\delta \dot{y}}$, $\hat{\delta \dot{z}}$). Φ is a 6 x 6 linear matrix derived from the reference trajectory that relates deviations from the reference trajectory at some time t_{k-1} to deviations at t_k. K is a weighting vector, y is the deviation of the measured angle from its reference value, and H is a row matrix which converts the position deviations from the reference to an angle deviation.

The estimation process works as follows: At each observation time, t_k, there is an estimate of the deviations $\Phi[\hat{x}]_{k-1}$, based on the estimate at t_{k-1} and the transition matrix Φ. There is also an estimate of the angle deviation, $H\Phi[\hat{x}]_{k-1}$, which will be measured at t_k. When the measurement is made, this predicted angle deviation is subtracted from the measured deviation angle, y. The difference is then weighted by K and the result is added to the estimate $\Phi[\hat{x}]_{k-1}$ to obtain $[\hat{x}]$, the estimate based on k observations.

In equation (A-21), it may be seen that the weighting vector K is a function of P, which is uncertainty in the estimate before the measurement is made and H, which is a geometric measure of the efficiency of the chosen star-planet combination (P_1, P_2 and H_1 are submatrices of P and H). K is also an inverse function of Q, the measurement error. In other words, the higher is the ratio of initial uncertainties to the assumed measurement errors, the more heavily will a measurement be weighted, for a given star-planet combination.

Equation (A-22) is the recursion relationship for the development of the matrix P which is a measure of the uncertainty in the estimation. The quantity in the brackets $\left[P - KHP\right]$ is the decrease in P obtained by each measurement. The operation $\Phi(\quad)\Phi^T$ shows the change in P over an interval when no observation is made.

The estimation system, then, is a recursive operation in which $[\hat{x}]$, the estimated position and velocity deviations and P, the uncertainty in the estimate are developed throughout the trajectory. Note that this process includes the effects of Q, the assumed instrument variance, P_o, the injection errors and H, the measurement geometry.

As was stated in Section 4.3.6, a fixed time-of-arrival guidance logic was assumed for the computation of midcourse corrective thrusts. This thrust was assumed to be impulsive and applied in such a manner as to null out the predicted position error at t_A, time of perilune. The reasons for this choice are given in 4.3.6.

In Appendix IA, the computation of the thrust command as a function of the estimated position and velocity deviation is given by the matrix equation:

$$\text{(A-31)} \qquad [\Delta v] = G_k' [\hat{x}] \ (t_k)$$

After a velocity correction is made, the velocity components of the estimate are updated and the uncertainty matrix, P, is incremented:

$$\text{(A-31)} \qquad P_c = \begin{bmatrix} P_1 & P_2 \\ P_3 & (P_4 + C) \end{bmatrix}$$

The P matrix is thus changed by C, the matrix of assumed errors in making the correction.

each case, a diagonal matrix was assumed.

The statistical evaluation of trajectories used in this study ignores three pertinent error sources: nonlinearity errors, bias errors and uncertainty in the knowledge of astrodynamic constants, especially in μ_m, the lunar gravitational constant. Nonlinearity errors are caused by the use of linearized prediction matrices in the estimation and guidance scheme and may cause appreciable errors in the vicinity of the moon. This trouble may be alleviated by the use of second partial derivatives in computing the prediction matrices or recomputation of prediction matrices during the flight at some expense to the computer. Since this will require a greater computer capability, but not necessarily make sensor requirements more stringent, this problem was not considered in detail in this study. Uncertainty in the knowledge of astrodynamic constants also falls outside the range of sensor problems, and these uncertainties will have been reduced somewhat by data analysis of unmanned lunar flights. Bias errors are certainly in the realm of sensor requirements, but an analysis of these errors was not made in the study, since bias errors will not cause uncertainties as large as the uncertainties due to random errors of the magnitude considered in this study. (Reference 4-2).

4.4.4 Geometric Considerations

It was previously stated that the observables selected for this analysis consisted of angle measurements from a star to some planet landmark or horizon. If the horizon is being measured, the geometric situation is illustrated in Sketch III.

Sketch III.

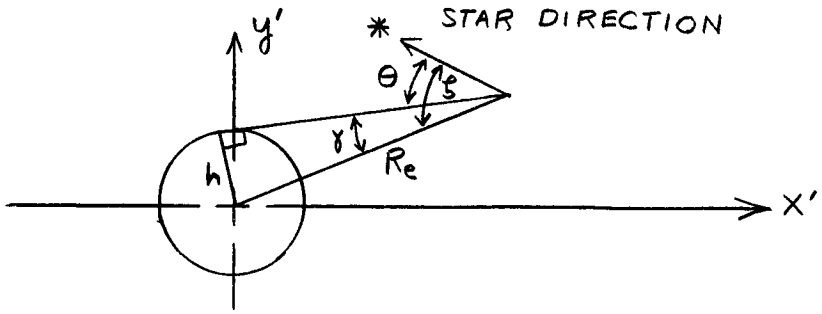

The sketch is planar, with x'y' defining the plane of the measurement angle. θ is the angle from the horizon to the star direction and h is the assumed planet radius at the horizon where the measurement is taken.

$$\frac{\partial\theta}{\partial h} = -\frac{\partial\gamma}{\partial h} = \frac{-1}{R_e\sqrt{1-(h/R_e)^2}} \cong \frac{-1}{R_e}$$

$$\Delta\theta = \left(\frac{\partial\theta}{\partial h}\right)\Delta h \cong -\frac{h}{R_e}$$

In this study, it was assumed that the rms uncertainty in defining the planet horizon was some constant k_1 for the Earth and k_2 for the Moon where k_1 and k_2 are in km. Then the variance of the uncertainty in each measurement is given by:

$$Q = \sigma^2 + (k_i/R_i)^2$$

where σ^2 is the variance of the errors in making the measurements and the subscript i refers to the particular planet being observed. In the numerical re-results, k_1 was assigned values of 3.2 km and 1.6 km, while k_2 had values of 1.6 km and 0.8 km.

If a landmark is being observed, then the uncertainties will not be as large. Timing of the measurements may then be a problem, though, due to the rotation of the planet, expecially in the case of the Earth. Although this again is essentially a computer problem, it may be shown that for the worst

possible geometric configuration, a timing error of 22 seconds would be required to cause an error of 1.6 km. Therefore, in this study, it was assumed that the angles were being measured with respect to the planet horizon, since the errors will have a small effect in either case.

In Ref. 4-3, a mathematical determination of the optimum plane in which to make a measurement has been given. Since the results depend on a step-by-step optimization procedure which is not necessarily useful, a simpler method has been used for this study. Since the uncertainties in the nominal trajectory plane are much larger than the uncertainties out of the trajectory plane, most of the measurements should be made in the trajectory plane. In Ref. 4-4, it was stated that optimum system performance resulted from taking a ratio of about 5 "azimuth" measurements to 1 "elevation" measurement where "azimuth" is the measurement of a star-planet angle in the trajectory plane and "elevation" is the measurement of an angle perpendicular to the trajectory plane. Taking azimuth measurements in this manner, it is clear that the direction of the sightline to the star being measured is irrelevant so long as the star is in the trajectory plane. This is illustrated in Sketch IV.

Sketch IV

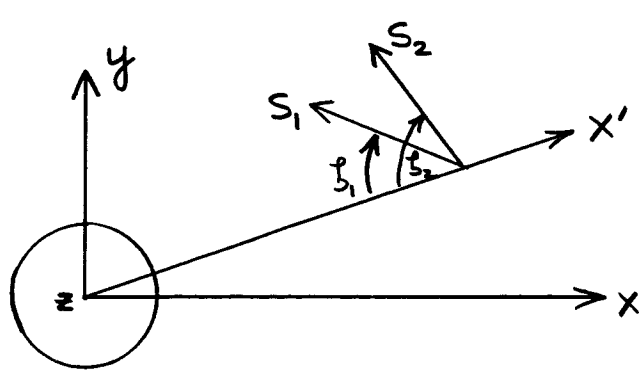

In the planar sketch, xy defines the trajectory plane and S_1 and S_2 are star directions in the trajectory plane. Then obviously:

$$\frac{\partial b_1}{\partial x} = \frac{\partial b_2}{\partial x}$$

$$\frac{\partial b_1}{\partial y} = \frac{\partial b_2}{\partial y}$$

$$\frac{\partial b_1}{\partial z} = \frac{\partial b_2}{\partial z} = 0$$

Since the partials are identical for either S_1 or S_2, then measurement to either star would be equally effective in reducing in-plane uncertainties. This and the result that relatively few out-of-plane measurements are required was verified in the computer runs (Section 4.6.1).

The point of all this as it affects optical angle-measuring systems is that stars in precise "optimum" directions are not required so long as there are some stars available in the trajectory plane which are practical to use from the standpoint of brightness, recognizability, field-of-view required and sun direction. For the 2 nominal trajectories considered in this study, the trajectory plane makes an angle of about 4.5° with the ecliptic.

Sketch IV also shows that the partial derivative $\partial b_1/\partial x'$ is zero along the line of sight to the planet being observed. Thus, no information about the uncertainties along the sightline to the planet is obtained, regardless of the star being used. For lunar flights, this fact limits the usefulness of an optical angle-measuring system during long periods of time since

it may be seen on Fig. 4-1 that the sightlines to the Earth and Moon rotate very little during midflight. The sudden improvement in the efficiency of angle measurements as the vehicle nears the Moon and the sightline to that planet begins rotating rapidly is shown in Fig. 4-2, Section 4.6.2. This also indicates that the type of measurement system assumed would be more effective on a slower trajectory, due to the greater curvature.

4.5 Digital Program

4.5.1 General Description of Inputs, Outputs

A digital computer program for the IBM 7094 has been written to perform the computations shown in Section 4.4.3 and appendix IB for various lunar trajectories. As shown in Section 4.4.3, the output quantities of interest for a parametric analysis are as follows:

- P Covariance Matrix of Estimation Errors
- R Covariance Matrix of Deviations from the nominal trajectory.
- u rms value of Δv applied at each correction time.
- r rms value of position deviations from the nominal trajectory.
- v rms value of velocity deviations from the nominal trajectory.
- $\tilde{r}$ rms value of errors in position estimate.
- $\tilde{v}$ rms value of errors in velocity estimate.

In each computer run, statistical estimates of the above quantities are printed out at all time-points of interest (observation and correction times and perilune) for the ensemble of trajectories having the following things in common:

Nominal trajectory

Observation schedule

Correction schedule

Observation Accuracy

Correction Accuracy

Injection Accuracy

All of the above quantities except the "nominal trajectory" are program inputs for a particular run. Generation of a new nominal trajectory requires a little more work, but a separate program using trial and error and linear - interpolation methods was written to generate new nominal trajectories quickly.

4.5.2 Development of Computer Program

Integration of the equations of motion, (A-1) Section 19, for a particular nominal trajectory was carried out by using a fourth-order Runge-Kutta numerical integration routine. This routine, written in double-precision, selects the size of the integration step automatically to reduce the truncation error to less than some required amount. If the step size is made too small, round-off error can become a problem, but successive runs of the same trajectory employing different values of truncation error criteria resulted in nearly identical numerical results, indicating that round-off error problems had been eliminated by use of a double precision routine.

Two nominal trajectories were used in the analysis, one having a flight time of 63.9 hours (to perilune), the second having a 72.2-hour flight time. Initial conditions for the first trajectory were generated using 2-body equations and trial and error integrations of the equations of motion. Since this was a time-consuming process, a program was written for the IBM 7094 to

perform these trial and error computations automatically until a trajectory was obtained which met the desired end conditions. This process consisted of setting the initial position and velocity of the vehicle at some values according to the type of trajectory desired, and varying the initial position of the moon by linear interpolation. The Φ matrices described in Appendix IA, Section 19 could also have been used, but the above approach was quicker and simpler.

In addition to the program inputs listed in Section 4.5.1, the transition matrices $\Phi(t_k, t_{k-1})$, which are 6 x 6 matrices relating deviations at some time t_{k-1} to deviations at t_k were developed. These Φ matrices were generated as shown in Appendix IA, equations A-1 through A-6, by simultaneously solving linearized perturbation equations and the equations of motion for a particular nominal trajectory. The Φ matrices were computed, at 6 minute intervals ($t_k = t_{k-1} + 6$) then stored on magnetic tape and used for every run involving this particular nominal trajectory.

Since the Φ matrices are linear approximations to a non-linear process, a comparison was made of a trajectory computed by use of these matrices and the actual integration of equations of motion, in order to test the validity of the Φ matrices. The use of prediction matrices were accurate to within .05% in predicting deviations from nominal until near the vicinity of the moon. The indication is that, while these prediction matrices are adequate for parametric analyses, an actual flight would require recomputation of these matrices later in the flight.

4.5.3 Operation of the Computer Program

A sample of the program for a given nominal trajectory is given in Table 4-1 for a particular run. As previously stated, it was assumed that the variance of the errors in angle measurement could be represented by

$$Q = \sigma^2 + (K_i/R_i)^2$$

This page intentionally left blank

TABLE 4-1 COMPUTER PROGRAM INPUTS

```
PHI  =  27.5500          PSI = -129.5300          TE=  3834.00
SIG2 = 0.23503999E-08    K1     1.6000            K2=   0.8000

CORRECTION SCHEDULE
 11.0000 35.0000 55.0000

OBSERVATION SCHEDULE
  2.0000  2.5000  3.0000 - - - - - - - - - - - - - - - - - - - - - - - - - - - - - - - - - - - - - 63.5000

STAR SCHEDULE
 1 1 1 2 4 4 4 - - - - - - - - - - - - - - - - - - - - - - - - - - - - - - - - - - - - - - - - - - - - 8

PLANET SCHEDULE-EARTH=0-MOON=1
 0 0 0 1 1 1 0 0 0 1 - - - - - - - - - - - - - - - - - - - - - - - - - - - - - - - - - - - - - - - - 1

STAR     DIRECTION COSINES
  1        0.92512000E 00  0.33671000E-00   0.17564999E-00
  2        - - - - - - -   - - - - - - - -   - - - - - - -
  -        - - - - - - -   - - - - - - - -   - - - - - - -
  -        - - - - - - -   - - - - - - - -   - - - - - - -
  -        - - - - - - -   - - - - - - - -   - - - - - - -
  8        - - - - - - -   - - - - - - - -   - - - - - - ---

P    0.4  (01)     0.          0.          0.          0.          0.
P    0.          0.1  (01)    0.          0.          0.          0.
P    0.          0.          0.9  (01)    0.          0.          0.
P    0.          0.          0.          0.4  -(05)   0.          0.
P    0.          0.          0.          0.          0.15  -(05)  0.
P    0.          0.          0.          0.          0.          0.4  -(05)

C       0.25 -(08)    0.          0.
C       0.            0. -(08)    0.
C       0.            0.          0.25 -(08)
```


Westinghouse

where σ^2 is the variance in radians^2 of the measurement uncertainty and the term (k_i/R_i) is a range-dependent quantity which reflects the rms uncertainty in defining a landmark or the horizon on the planet from which the star angle is being measured. Thus, the input quantities k_1 (earth) and k_2 (moon) may be varied.

The correction and observation schedules are simply lists of the times at which these operations are to be performed.

The star schedule is a list of the stars to which the angles are measured at the observation times. The direction cosines of each of the stars (1, 2 - -n) are precomputed and stored in the program. The planet schedule simply shows whether the earth (0) or moon (1) is being measured to.

The matrix $P(t_o)$ statistically describes the assumed injection accuracy. The terms in the major diagonal are the variances of the deviations in 6 components of position and velocity at $t = 0$. The matrix C is the covariance matrix of errors in making velocity corrections. Constant values were used for the accuracy, and no attempt was made to separate errors in applying this Δv from errors in measuring the Δv. Although this is an oversimplification, it was shown that the accuracy requirements on making the corrections are not severe and that system performance is not greatly affected by Δv errors on the order of .1 m/s, which is within state-of-the-art capabilities.

Printouts were made at every observation and correction time and at t_A (nominal time of perilune). These printouts are shown in Table 4-2.

The matrices P* and P are the covariance matrices of the errors in estimate before and after the observation was made. By comparing these matrices and the corresponding quantities $\tilde{r}$, $\tilde{v}$, $\tilde{r}^*$ and $\tilde{v}^*$, an assessment could be

TABLE 4-2 PRINTOUT

TIME = 120.0000

K	0.58	-0.46	-0.26	0.96	0.20	0.14

RRMS= 0.47 VRMS= 0.81 SRRMS= 0.19 SVRMS= 0.35

P*	0.16	0.93	0.51	0.33	0.19	0.88
P*	0.93	0.77	0.85	0.19	0.13	0.34
P*	0.51	0.85	0.12	0.11	0.23	0.17
P*	0.33	0.19	0.11	0.68	0.40	0.18
P*	0.19	0.13	0.23	0.40	0.27	0.49
P*	0.88	0.34	0.17	0.18	0.49	0.27
R	0.20	-0.51	0.43	0.33	0.84	0.53
R	-0.51	0.88	-0.78	-0.44	0.88	-0.38
R	0.43	-0.78	0.12	0.97	0.20	0.17
R	0.33	-0.44	0.97	0.57	0.14	0.92
R	0.84	0.88	0.20	0.14	0.50	0.20
R	0.53	-0.38	0.17	0.92	0.20	0.38

PRMS= 0.47 PVRMS= 0.81

P	0.20	-0.51	0.42	0.33	0.84	0.53
P	-0.51	0.88	-0.78	-0.44	0.88	-0.38
P	0.43	-0.78	0.12	0.97	0.20	0.17
P	0.33	-0.44	0.97	0.57	0.14	0.92
P	0.84	0.88	0.20	0.14	0.50	0.20
P	0.53	-0.38	0.17	0.92	0.20	0.38

made of the value of each measurement in reducing the estimation uncertainties.

In addition to the quantities shown in Table 4-2, the rms value of the velocity correction was printed out at times when corrections were made.

4.6 Program Results

Computer runs were made, using the digital program described in Section 4.5 to determine the effects of varying the system parameters of interest on the overall performance of the onboard guidance system. Since the runs were made on a cut-and-try basis, the results are presented chronologically as they were actually obtained and the reasons for each new "cut" are given. In section 4.7, the results of the computer program are summarized and interpreted.

4.6.1 Preliminary Runs

In order to develop some familiarity with the problem of scheduling observations and corrections, and to get a rough idea of the numerical results to be expected, some preliminary runs were made.

Two nominal trajectories were employed, the 63.9-hour flight described in Section 4.3 illustrated in Figure 4-1, Section 4.3.3 and a 72.2 hour trajectory. The geometry of the 72.2 hr. trajectory is similar to the faster flight except that it has greater curvature near the planets, and has a 210-km perilune rather than 133 km.

Certain preliminary ground-rules were assumed, with regard to the scheduling of observations and corrections. These ground rules are as follows:

1. The observations and corrections are at least 1/2-hour apart, except for the final sequence of moon observation which are 18 minutes apart. This would allow sufficient time to sight on the desired star and planet or to stabilize the vehicle for the application of a corrective thrust.

2. The observations are grouped such that there is a minimum of switching from one star-planet combination to another. For instance, if in one group of observations, the earth and moon are each to be measured to 6 times, first all 6 earth measurements are made, then 6 moon measurements. In addition, observations of a particular star are grouped together.
3. The total Δv requirements for midcourse corrections must be less than 20 m/s. This is about .5% of the payload at injection from parking orbit, assuming a specific impulse of 424 seconds.
4. Angles must be measured to the lighted portion of the planet involved.

It is recognized that any of the above assumptions may lower the guidance system capabilities, but it was felt that some such assumptions must be made in order that the resulting sensor requirements would not be based on schedules which would unduly penalize or complicate the rest of the system.

For preliminary runs, a "standard" set of input conditions were used. These are listed in Table 4-3. These conditions were assumed initially for comparison of results with similar work (Ref. 4-3). For the preliminary runs, the trial schedules listed in Table 4-4 for each trajectory were used. These schedules were later revised (Section 4.6.2) to

TABLE 4-3

Standard Input Conditions

Measurement Variance Q $\qquad Q = \sigma^2 + (k_i/R_i)^2 \text{ radians}^2$

where $\sigma = 10$ secs. of arc

k_1 (earth) = 1.6 km

k_2 (moon) = 0.8 km

and R_i is the range to the planet being measured

Injection errors: $r_o = 3.6$ km

$v_o = 3.1$ m/s

Correction Errors = .1 m/s

Total number of observations: 45

Total number of corrections: 3

obtain better overall performance. The number of measurements (45) and the number of corrections (3) were kept fixed in the preliminary runs to assess the effect of different observation and correction schedules on system performance.

As was pointed out in Section 4.4.4, the in-plane components of the position and velocity uncertainties will be considerably greater than the uncertainties perpendicular to the trajectory plane. For this reason, many more measurements must be made of in-plane angles than out-of-plane. The results of several preliminary runs indicated that for a 45-observation schedule, 6 observations of angles perpendicular to the trajectory were sufficient to reduce the out-of-plane uncertainties to a level considerably below that of the in-plane uncertainties.

In section 4.4.4, it was stated that the direction of the star-sightline from which the angle was measured made no difference, so long as the sightline was in the trajectory plane. This was verified numerically by comparison of 3 runs.

These runs, made with the 63.9-hour trajectory, each had 45 observations, 39 "azimuth" and 6 "elevation", where azimuth measurements mean measurements of an angle in the trajectory plane, and elevation measurements perpendicular to the trajectory plane. For the azimuth measurements, on one run it was assumed that the Moon-Star angle was measured from the line of intersection of the trajectory plane and the yz-axis and the Earth angle measured from the x-axis, on another run both planet angles were measured from the same sightline lying in the trajectory plane, and on the

TABLE 4-4

Trial Schedules for 63.9 and 72.2-Hour Trajectories

2.5 - 10.0 hrs. ½ hr. spacing	a a a a a a a a d | a a a a a a a a d 9E | 8M	Δv at 11 hours
22 - 32 hours 1-hour spacing	a a a a a d | a a a a a d 6E | 6M	Δv at 33 hours
60 - 65 hours ½ hr. spacing	a a a | a a d 3E | 3M	Δv at 66 hours
67 - 71.8 hours ½ hr. spacing	a a a a a d a a a a 10 M	Perilune at 72.2 hours
1.5 - 9.5 hours ½ hr. spacing	a a a a a a a a d | a a a a a a a a 9E | 8M	Δv at 10 hours
23 - 34 hours 1 hour spacing	a a a a a d | a a a a a d 6E | 6M	Δv at 35 hours
53 - 59 hours 1 hour spacing	a a a a | a a d 4E | 3M	Δv at 59.5 hours
60 - 63.9 hours .3 hour spacing	a a a a d a a a a 9M	Perilune at 63.9

M = Moon Δv = correction a = azimuth measurement
E = Earth d = elevation measurement

third, a mixture of various sightlines in the trajectory plane was used. The results of these three runs were almost identical numerically.

The main conclusions from the above are that:

(1) Since there is no particular "optimum" direction for the star sightline, as long as it is in the trajectory plane, then field-of-view requirements are affected only by the availability of a noneclipsed, recognizable star of sufficient magnitude in the trajectory plane.

(2) For the purposes of analysis, one may assume that all azimuth measurements are made with reference to a single star direction. In this analysis, since the x-axis lies in the trajectory plane, it was assumed that all azimuth measurements were made with reference to this axis.

For elevation measurements, comparison was made between runs taking these 6 measurements with reference to a polar star (z-axis) and a sightline perpendicular to the trajectory plane. Since there was a negligible difference in the results, it was assumed that elevation measurements are taken with reference to a polar star, since the field-of-view requirements for this are only 65°, while the other case would require 90°.

In order to investigate the effect of the azimuth angle being measured to a star somewhat out of the trajectory plane, a run was made in which this star-sightline was 15° above the trajectory plane. In addition, a run was made in which all 45 measurements were made to this sightline. The results are listed in Table 4-5.

TABLE 4-5

Comparison of Results at Perilune For Different Star-Planet Angle Measurements (72.2-hour Nominal Trajectory)

	r, km	v, m/s	$\tilde{r}$, m/s	$\tilde{v}$, km	$\Sigma\Delta v$, m/s
In-Plane Azimuth Measurements	24.8	13.4	2.52	1.55	19.11
Out-of-Plane (by 15°) Azimuth Measurements	25.6	13.6	3.42	2.06	19.46
All Measurements to same Star	51.3	38.2	3.49	2.11	23.52

The quantities presented for comparison in the table are r and v, the deviations from the nominal trajectory, in position and velocity at time of reference perilune (t_A), $\tilde{r}$ and $\tilde{v}$, the errors in estimate of position and velocity at t_A, and $\Sigma\Delta v$, the total correction velocity applied during the flight.

Although the figures shown in Table 4-5 are not particularly good, a comparison of the 3 cases shows that there is little decrease in miss distance (r), due to the azimuth measurements being made 15° out of the trajectory plane. Measurements to a single star, however, gave much worse results.

In conclusion, the results of the preliminary runs show that location of stars in some "desirable" pattern is not of critical importance in the overall performance of the guidance system being studied.

4.6.2 Improvement of Schedules

The perilune results obtained by using the trial schedules in Table 4-4 and standard input conditions (Table 4-3) are shown in Table 4-6 for each trajectory:

Table 4-6. RMS Results at Perilune with Trial Schedules

	r, km	v, m/s	$\tilde{r}$, km	$\tilde{v}$, m/s	$\Sigma\Delta v$, m/s
63.9 hour trajectory	21.7	12.1	2.96	1.81	20.0
72.2 hour trajectory	24.8	13.4	2.52	1.55	19.11

It is to be emphasized here that these results are not intended to show that a smaller rms miss distance (21.7 km to 24.8 km) is obtained by using the faster trajectory. This lower miss-distance was the result of making

the last velocity correction 2 hours closer to perilune on the 63.9 hour trajectory than on the 72.2 hour trajectory. As the result, the rms propellant cost for midcourse corrections was increased.

Also note that r is the rms position deviation from the nominal trajectory at time of reference perilune, not the geometric miss distance. In fact, the radial (altitude) component of miss distance is about one fifth of r. This point is discussed further in Section 4.7.2.

In ref.4-3(see Appendix IC), a decision logic was employed for optimizing the schedule of operations on a circumlunar mission. It was claimed in ref.4-4,however, that by deciding which was the "best" operation to make at any time on a step-by-step basis would not yield an optimum schedule, since then the operation would be based only on what had occurred previously, and might preclude doing the operation (observation or correction) at some later, more favorable time.

Actually, the choice depends on the criterion employed for optimization. If one were strictly interested in reducing target errors, then a step-by-step decision process would not be optimum. However, if one were interested in reducing the position and velocity estimation errors as quickly as possible (in case an abort is required), then the approach used in ref.4-3 would be desirable. In this study, schedules were revised to reduce errors at perilune.

As was shown in Section 4.6.1, the selection of star directions is not critical. Therefore, for a given number of observations and corrections, the scheduling parameters which may be varied to improve system performance are:

1) the timing of the observations and corrections and,

2) the ratio of earth measurements to moon measurements.

Concerning the timing of observations and corrections, it is clear that by making corrections later in the trajectory one reduces the miss distance at the target at the cost of making a larger correction. As for the timing of observations, in general it is best to make many measurements while on the curved portion of the trajectory (near the planets). The reasons are, as pointed out in Section 4.4.4 that more information about the trajectory is obtained when the sightline to the planet is rotating rapidly and the distance to the planet is small. (This last criterion is somewhat degraded by the larger range-dependent errors at small distances from the planet). The ratio of earth-to-moon measurements is dependent upon the same factors that influence timing of the measurements.

With the above considerations in mind, additional computer runs were made, employing different observation and correction schedules to improve upon the results obtained with the trial schedules, shown in Table 4-6. Since the rms miss distances shown in that table were large, the criterion used for schedule "optimization" was reduction in r.

Four computer runs were made to improve upon the 72.2 hour trajectory. Since the sightline to the moon was relatively constant over the second and third "legs" of the flight (22-32 hours and 60-65 hours), the trial schedule was amended in Run A7 to make 9 earth observations and 3 moon observations instead of 6 of each in the second leg. In Run A8, the timing of the third correction was changed from 66 hours to 68 hours. In Run A9, both the changes described above were made. The rms perilune results of

these three runs, together with Run A1, the trial schedule and Run A10, the improved schedule decided upon are shown in Table 4-7.

Although no striking improvements in system performance have been produced as a result of schedule changes, several points are noteworthy. Replacement of moon measurements by earth measurements in the second and third legs reduced the rms miss distance from 24.8 km to 21.7 km. Making the third correction two hours later also reduced the miss distance, but not as sharply, and also caused the rms correction velocity total to increase. Therefore, it was decided to add still another earth measurement (in place of a moon measurement) to the second leg. No further attempts at optimizing the schedule for this trajectory were made, in this sensor study. The resulting schedule A10, was used for system parameter variations (Section 4.6.3).

It can be seen that for all five runs, the estimation errors at perilune are nearly equal. This is because these errors are primarily dependent upon the last series of observations after the third correction.

The increase in correction velocity required when more earth measurements are made seems paradoxical at first. The reason is as follows: the optimization criterion used here, e.g., reduction of r at perilune requires that the uncertainties $\tilde{r}$ and $\tilde{v}$ be made smaller at the time of the third correction. It turns out that by taking more earth measurements in the second leg, $\tilde{r}$ and $\tilde{v}$ at the time of the second correction are larger, but the effectiveness of the measurements in the third leg has been enhanced by previously taking more earth measurements, so that $\tilde{r}$ and $\tilde{v}$ at the time of the third correction have been reduced. Thus r at perilune is reduced, but since the correction essentially makes up for errors made in applying the second correction, it is larger than the third

TABLE 4-7

"Optimization" of 72.2 hr.
Trajectory

Run	Description	r, km	v, m/s	$\tilde{r}$, km	$\tilde{v}$, m/s	$\Sigma\Delta v$, m/s
A-1	Trial Schedule	24.8	13.4	2.52	1.55	19.11
A-7	More E Measurements	21.7	11.9	2.52	1.55	19.16
A-8	3d Δv Later	23.4	13.0	2.53	1.56	19.96
A-9	Both A7 and A8	21.0	11.9	2.54	1.57	20.00
A-10	Improved Schedule	21.4	11.8	2.53	1.55	19.45

r = rms position deviation at t_A, nominal time of perilune

v = rms velocity deviation at t_A

$\tilde{r}$ = rms position estimation error at t_A

$\tilde{v}$ = rms velocity estimation error at t_A

$\Sigma\Delta v$ = rms correction velocity required

Westinghouse

correction on the trial schedule, and the total corrective velocity required is increased. Again, this is a result of the fact previously stated, that in order to optimize performance for some quantity at perilune, one must consider the entire sequence of observations and corrections.

Some computer runs were made using the 63.9 hour nominal trajectory. Run B-1 was the trial schedule. In Runs B-2, and B-3, the first group of 17 measurements was changed from 9 earth, 8 moon to 12 earth, 5 moon. In Run B-2, the second group of 12 measurements was changed from 6 earth, 6 moon to 4 earth, 8 moon, while Run B-3, had 8 earth and 4 moon measurements on the second leg. In Run B-4, the final velocity correction was changed from 59.5 hours to 62 hours and the observations of the moon after 60 hours were re-timed. The results of these runs are presented in Table 4-8.

Runs B-2 and B-3 resulted in a larger miss distance, although both required less $\Sigma \Delta v$. Run B-4 resulted in a significantly lower miss distance (17.5 km), than the trial schedule. In addition, the estimation errors at perilune were reduced by re-timing of the final group of moon observations.

It was not the intent of this section to determine optimum schedules for the trajectories used, since the criteria for optimization are, in general, not well-defined. The purpose of making the runs shown was to arrive at some reasonable operational schedules for further analysis, and to show how various aspects of system performance (miss distance, estimation errors, fuel costs) vary according to the schedule used.

The schedules used for Runs A-10 and B-4 were used in Section 4.6.3 for variation of system parameters for the 72.2-hour and 63.9-hour trajectories, respectively. Table 4-9 shows both schedules and the results at each Δv and perilune.

TABLE 4-8

Scheduling Runs on 63.9 Hour Trajectory

Nr.	Description	r, km	v, m/s	$\tilde{r}$, km	$\tilde{v}$, m/s	$\Sigma\Delta v$, m/s
B-1	Trial Schedule	21.7	12.1	2.96	1.81	20.0
B-2	More E Measurements	22.5	12.4	2.97	1.81	18.8
B-3	Moon Measurements Later	24.6	13.6	2.96	1.81	19.3
B-4	Last Δv at 62 hours	17.5	11.5	2.64	1.60	23.5

TABLE 4-9

Improved Schedules for Lunar Trajectories

2.5 - 10.5 hrs. 1/2 hr. spacing	a a a a a a a a d | a a a a a a a a d 9E 8M Δv at 11	$\tilde{r}$ = 26.3 km $\tilde{v}$ = .992 m/s	Δv = 14.93 m/s
22 - 33 hrs. 1 hr. spacing	a a a a a d a a a a | a d 10E 2M Δv at 34 hrs.	$\tilde{r}$ = 15.6 km $\tilde{v}$ = .178 m/s	Δv = 2.52 m/s
60-65 hrs. 1 hr. spacing	a a a a | a d 4E 2M Δv at 66 hrs.	$\tilde{r}$ = 9.41 km $\tilde{v}$ = .096 m/s	Δv = 2.00 m/s ΣΔv = 19.45 m/s
67-72.2 hrs. 1/2 hr. spacing	a a a a a d a a a a 10M Perilune at 72.2 hrs	$\tilde{r}$ = 2.53 km $\tilde{v}$ = 1.55 m/s	r = 21.4 km v = 11.8 m/s
1.5 - 9.5 hrs. 1/2 hr. spacing	a a a a a a a a d | a a a a a a a a 9E 8M Δv at 10 hrs.	$\tilde{r}$ = 31.0 km $\tilde{v}$ = 1.20 m/s	Δv = 14.10 m/s
23 - 34 hrs. 1 hr. spacing	a a a a a d | a a a a a d 6E 6M Δv at 35 hrs.	$\tilde{r}$ = 14.3 km $\tilde{v}$ = .180 m/s	Δv = 3.80 m/s
53 - 61.5 hrs. 1/2 & 1 hr. spacing	a a a a | a a d a a a a d 4E 8M Δv at 62 hrs.	$\tilde{r}$ = 9.23 km $\tilde{v}$ = .261 m/s	Δv = 5.56 m/s ΣΔv = 23.46 m/s
62.6 - 63.5 hrs. .3 hr. spacing	a a a a 4M Perilune at 63.9 hours	$\tilde{r}$ = 2.64 km $\tilde{v}$ = 1.60 m/s	r = 17.5 km v = 11.5 m/s

A-10

B-4

E = Earth a = azimuth measurement
M = Moon d = elevation measurement

In Figure 4-2, the reduction in rms position estimation error at each measurement and correction is shown for the 72.2-hour trajectory. Although reduction in rms position uncertainty is not necessarily a criterion for scheduling, the graph illustrates several interesting points. Note that when a particular star-planet combination has not been measured for some time, there is a sharp drop in the uncertainty due to measuring this combination. For instance, the first measurement and the first elevation measurement produce sharp reductions in the uncertainty. Two of the measurements (10.5 hours and 70.9 hours) were relatively useless and could have been dropped or replaced.

Note that the position estimation error propagates rapidly early in the flight and also near the vicinity of the moon. Near the moon, however, the effectiveness of the measurements are enhanced by the rapid change of direction of the sightline to the moon. This point was discussed in Section 4.4.4. This is one reason why delaying the last correction until near the vicinity of the moon will sharply reduce the miss distance, since the estimation errors can be reduced drastically in this region.

Velocity estimation errors propagate much less rapidly (due to the gradual decrease in velocity) except in the vicinity of the moon.

4.6.3 Variation of Parameters

Computer runs were made using schedules A-10 and B-4 described in the previous section, in which system parameters were varied to indicate their importance in determining the guidance system performance. The rms results at perilune for these runs are listed in Tables 4-10 and 4-11 for the two trajectories. The standard parameters referred to are listed in Table 4-3.

For these runs, the target criterion assumed was that the rms miss distance at perilune, r, was not to exceed 25 km.

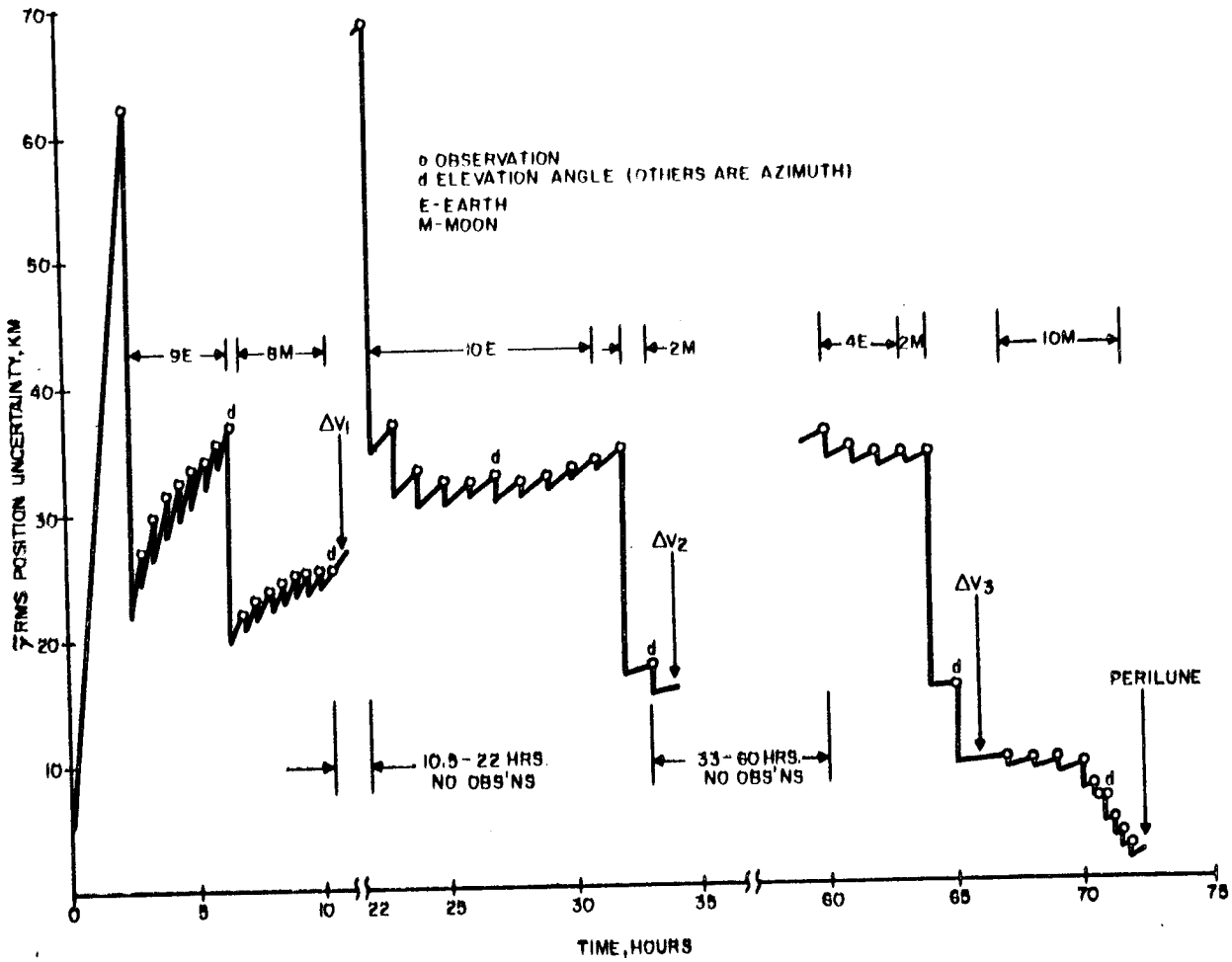

FIGURE 4-2: Reduction in RMS Position Estimation Error Due to Observations

TABLE 4-10

Variation of Parameters for 72.2-Hour Trajectory (45 Observations)

Inputs	r, km	v, m/s	$\tilde{r}$, km	$\tilde{v}$, m/s	$\Sigma\Delta v$, m/s
Standard Case	21.4	11.8	2.53	1.55	19.5
σ = 5 secs. arc	13.0	7.29	2.40	1.47	17.6
σ = 20 secs. arc	35.4	19.5	2.84	1.76	23.1
σ = 40 secs. arc	49.6	27.4	3.32	2.07	26.8
k_1 = 3.2 km, k_2 = 1.6 km	21.8	12.1	4.05	2.43	19.7
Zero Correction Errors	16.9	9.42	1.93	1.14	19.4
1.5 x Standard Correction Errors	23.5	13.0	2.75	1.71	19.5
2 x Standard Injection Errors	21.5	12.2	2.53	1.56	34.6

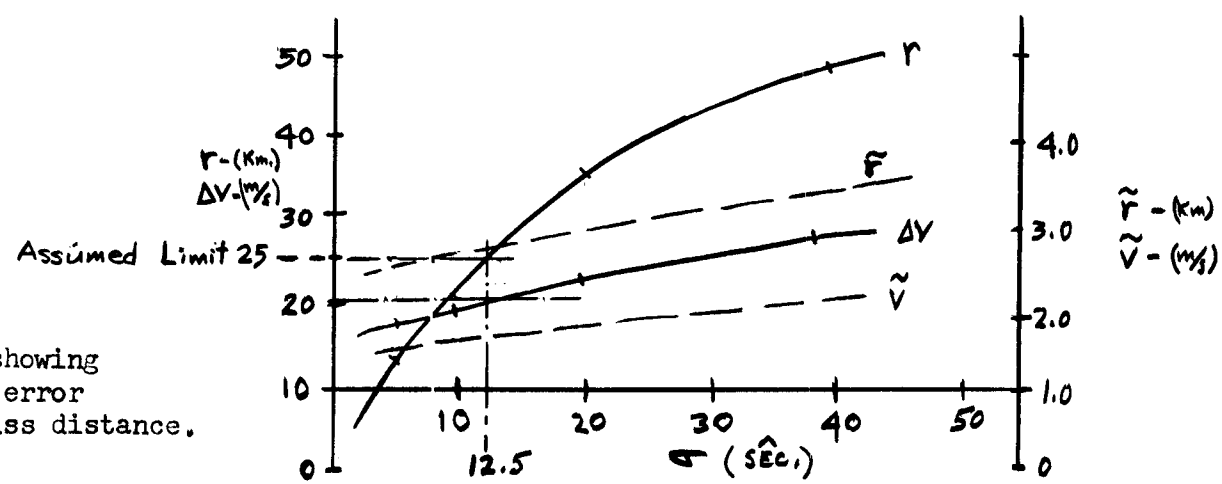

Sketch of data showing limit of sensor error for a limited miss distance.

TABLE 4-11

Variation of Parameters for 63.9-In. Trajectory (45 Observations)

Inputs	r, km	v, m/s	$\tilde{r}$, km	$\tilde{v}$, m/s	$\Sigma\Delta v$, m/s
Standard Case	17.5	11.5	2.64	1.60	23.5
σ = 5 secs. of arc	11.0	7.16	2.35	1.42	19.8
σ = 20 secs. of arc	28.7	19.5	3.22	1.97	30.4
σ = 40 secs. of arc	40.9	28.6	3.96	2.44	37.8
k_1 = 3.2 km, k_2 = 1.6 km	19.2	12.4	4.11	2.42	24.3
Zero Correction Errors	14.2	9.86	2.18	1.27	23.2
1.5 x Correction Errors	18.9	12.3	2.91	1.79	23.7
2 x Injection Errors	17.6	11.8	2.65	1.61	38.2

The results in Table 4-10 show that for the assumed 45 measurement schedule, the most important system parameter is, as expected, σ, the rms measurement error. The position deviation, r, at t_A is greater than the 25 km desired for the σ = 20 seconds and σ = 40 seconds cases. In addition, there is a weight penalty incurred by the increased Δv required when the instrument errors are this large. It is interesting to note, however, that the estimation errors ($\tilde{r}$ and $\tilde{v}$) are not too bad for σ = 20 seconds. This suggests that the use of a less accurate instrument would be feasible if the increased cost and complications of making the third velocity correction nearer the moon were acceptable.

Doubling the range-dependent errors (k_1, and k_2) has little effect on the miss distance, but does cause a significant increase in $\tilde{r}$ and $\tilde{v}$ due to the degrading effect of these errors on the last group of measurements near the moon.

The assumption of zero correction error reduced the miss distance from 21.4 km to 16.9 km and significantly decreased the estimation errors. This shows that the primary factor in determining the miss distance is the uncertainty in estimate at the time of the last correction, rather than the error in making the correction itself. In fact, the correction error assumed in this program was rather crude and the importance of the correction accuracy is even less than these results show.

Doubling the injection errors causes negligible change in the accuracy at perilune, but does incur a significant fuel penalty due to the larger first correction required.

The results in Table 4-11, for the 63.9 hour trajectory are similar to those of Table 4-10.

4.6.4 Increased Number of Measurements

All of the previous runs used a 45-measurement schedule. In order to determine the effect of taking more measurements, a computer run using the 72.2 hour nominal trajectory, was made in which a 90 observation schedule and standard conditions were used. Although no attempt was made at "optimizing" this schedule, a comparison with the 45 measurement schedule is made in Table 4-12.

Table 4-12

Comparison of 45 and 90 Measurement Schedules

	r, km	v, m/s	$\tilde{r}$, km	$\tilde{v}$, m/s	$\Sigma\Delta v$, m/s
45 Measurements	21.4	11.8	2.53	1.55	19.5
90 Measurements	16.6	9.22	1.68	1.06	18.2

This comparison shows a significant decrease in miss distance, $\Sigma\Delta v$ and estimation errors, when more measurements are made.

4.6.5 Comparison with 2 Angle Measuring Device

In all of the previous computer runs, it was assumed that each observation consisted of the measurement of the angle between some point on a planet and a star direction. A theodolite is a device which is stabilized to an inertial reference coordinate system (2 stars) and measures the elevation and azimuth angle of a planet in this reference system. In order to compare the results obtained by measuring a single angle at a time with a 2-angle measuring device a computer run was made with the 72.2 hour trajectory in which both azimuth and elevation angles were measured. The results obtained with the 2-angle device were only slightly better than those obtained by measuring a single angle. This may have been due to an inefficient schedule or the fact that the 2-angle device was assumed stabilized in the trajectory plane and the additional elevation measurements were practically worthless. The problem of determining a better orientation or schedule for the 2-angle device was not investigated.

4.7 Summary of Computer Results and Discussion

4.7.1 Summary of Computer Results

A summary of the results of the computer program, as they relate to sensor requirements, is given.

1. A sufficient set of guidance parameters for the 72.2 hour nominal trajectory, employing a single-angle measuring device for measuring angles from a point on the earth or moon to a star is obtained from interpolating the data in Table 4-10 as follows:

RMS Measurement Accuracy,	$\leq$ 12.5 secs. arc
Horizon or Landmark Uncertainties	$\leq$ 1.6 km (earth)
	$\leq$ 0.8 km (moon)
Field-of-view required	$\geq$ 65°
Correction Accuracy	$\leq$ .1 m/s
Number of Measurements required	$\geq$ 45
Number of Corrections required	3
$\Sigma\Delta V$ Correction required, rms	20.4 m/s

These parameters, coupled with rms injection errors of 3.6 km in range and 3.1 m/s in velocity give results at perilune as follows:

RMS Position Estimation Error ($\tilde{r}$)	2.61 km
RMS Velocity Estimation Error ($\tilde{v}$)	1.60 m/s
RMS Position Deviation from Nominal (r)	24.9 km
RMS Altitude Component of r	5 km
RMS Velocity Deviation from Nominal (v)	13.73 m/s

2. The most significant parameters in the assumed guidance system, as they affect sensor requirements are:

1) measurement accuracy

2) total number of observations

3) weight allowance for making corrections, and the minimum time allowed between operations (especially near perilune).

3. Correction errors on the order of .1 m/s do not greatly degrade guidance system performance. Large injection errors cause an increase in the required correction fuel, but have little effect on perilune accuracy.

4. The use of a faster trajectory makes more stringent the guidance system requirements. Equivalent results for a faster trajectory may be obtained by taking more measurements, or more accurate measurements, or by allowing more fuel for corrections.

5. Selection of stars for the guidance system is not critical as long as some stars are available which are approximately in the trajectory plane.

4.7.2 Discussion of Results

The computer runs discussed previously have shown the importance of the number and accuracy of measurements and the Δv budget for midcourse corrections. The results show that there is a tradeoff between these three parameters, and that a change in one will have a direct effect on requirements for the other two. These trade-off studies were not conducted since detailed analysis of such factors as the "cost" of making measurements were considered beyond the scope of the present study.

The geometry of lunar trajectories of 72 hours or less is such that over a great deal of the flight (about 8-20 hours before perilune) little useful information can be gained by taking optical angle measurements. As a result, improvement in the estimation errors before the third velocity correction requires a large number of observations early in the flight or the

postponement of the third velocity correction until very late in the trajectory, when the propellant cost of this correction is large. Studies conducted at Ames Research Center (Ref. 4-2), assuming a theodolite device and a 79-hour flight to perilune came up with better numerical results than those shown here, for similar conditions. The reason is that the slower trajectory has a greater curvature and the value of a given number of measurements is thereby increased, as was shown in Section 4.4.4.

Throughout Section 4.6, the rms position deviation from nominal at t_A, nominal time of perilune, is referred to as the "miss distance". This is not exactly true in a geometric sense. Since most of the error is in the down-range direction, a better measurement of miss distance might be the geometric miss distance and some timing error in arrival. However, the matrix rotation necessary to convert r in xyz coordinates into a "down-range, cross-range, altitude" coordinate system was not included in the computer program. A few hand calculations indicated that the altitude component of r was about .2 r. The cross range errors were even smaller.

The significance of down-range deviations from nominal depends upon the requirements for the lunar orbit to be achieved. If it is required to achieve a precise lunar orbit at a precise time, then the entire miss distance must be considered in determining midcourse guidance requirements, and the resulting sensor requirements would be rather severe. A more reasonable approach is to consider a variable time of injection into lunar orbit so that only the down-range and cross-range components of miss distance and the velocity deviations need be considered in determining midcourse requirements.

4.7.3 Determination of Sensor Requirements

Sections 4.6, 4.7.1 and 4.7.2 describe the work that has been done to evaluate the effect of varying system parameters of an onboard guidance system, and to identify the parameters which most strongly affect sensor requirements. The results show that one cannot define sensor requirements except in terms of an assumed trajectory and operational schedule. The method employed in this study has seen to assume an operational procedure, then determine the sensor requirements necessary to achieve the desired end conditions. Thus, the sensor recommendations given below were based on the assumption of 64-73 hour flights having the following operational constraints:

1) 45 observations
2) 3 corrections
3) 1/2 hour minimum preparation for corrections
4) 18 minute minimum time between observations
5) 25 m/s maximum $\Sigma\Delta v$ allowance.

A relaxation of these constraints will result in a corresponding relaxation of sensor requirements as was indicated by the comparison of 90-measurement and 45-measurement schedules in Section 4.6.4. Finally, the sensor requirements for flight times greater than 73 hours will be less stringent than for those listed here, and flight times of less than 64 hours will require more $\Sigma\Delta V$, but not necessarily better sensors.

4.8 Sensor Requirements

On the basis of the analytical work done in this study, the following sensor specifications are recommended for onboard guidance of manned lunar missions:

Type - Optical device for measuring the angle between a star and a planet landmark or horizon.

Accuracy - 12.5 seconds of arc, rms.

Range of Operation - 5° to 65°.

Magnification - undetermined.

4.9 Recommendations

Since the sensor requirements stated in the previous section apply to a particular set of observables and operational procedures, it is recommended that further study be made in the following areas:

1) Further analysis of the trade-offs between the number of measurements required, the measurement accuracy and the requirements for corrections, with consideration of the cost of making measurements.
2) Comparison of optical angle measurements with other sensor observables such as range, range rate, etc.
3) Analysis of the effects of bias errors, non-linearities and uncertainties in the knowledge of astrodynamic constants. Analysis of these errors has been done at Ames Research Center, but results have not yet been published.
4) Determination of the "cost" of making measurements (in fuel, operator requirements, stability requirements, etc.)
5) More precise target definition.

The computer program used in this study would be an effective tool for performing analyses in Topic 1) system tradeoffs and Topic 2) comparison with other sensor methods. In addition, the computer program could be modified to perform the analyses indicated under Topic 3).

This page intentionally left blank

5.0 LUNAR PARKING AND DESCENT ORBITS, MANNED

The study of these phases of the lunar mission included an analysis which is considerably more sophisticated than originally envisioned. The computer program used for this analysis consumes the entire core space of the IBM 7094; it represents a parallel effort for navigation system evaluation, consisting of:

(1) A completely linearized analysis of trajectory errors, from parking orbit initiation to termination of the descent orbit, referred to the terminal state vector as computed by a linearized on-board guidance and navigation system. These errors include the effects of sensor inaccuracies.

(2) A Monte Carlo simulation of the same system with the same input errors, but including nonlinearities, which is used to provide an indication of the effects of inherent dynamic nonlinearities on the accuracy of the proposed on-board navigation system.

The guidance and navigation system is characterized by Kalman's (ref. 5-1) recursive minimum variance processing of optimally selected on-board space angle measurements, and fixed time-of-arrival, end point guidance.

Although the prescribed on-board system computes a new estimate of its trajectory after each measurement, the fundamentally important decision remains whether or not to compute new sensitivity coefficients from each new estimate. Such an on-board data processor would be quite complex; for this study it was decided to determine whether a set of recursion formula matrices which are computed from the nominal orbit would suffice. Unfortunately,

it was determined that they do not suffice over the time arcs considered here; this soon became evident from the Monte Carlo simulation.

By reason of the above discussion, it is expected that the on-board computer actually required for lunar navigation will employ the nonlinear equations of motion, and will recompute all sensitivity coefficients from each new estimate. As a result of this study, it is recommended that the present analysis be modified accordingly, and that a performance evaluation be made, without invoking the usual assumptions regarding linearization. The use of additional observables (e.g., beacons, altitudes) is also advocated, as explained in the latter part of this section.

5.1 Introduction

As stated in the Part I document, the nominal lunar orbit and descent trajectory were chosen on the basis of the following considerations:

a. The midcourse trajectory, from which the vehicle is launched into lunar orbit, is the familiar "figure-eight" circumlunar path. This condition provides a nominal figure for velocity prior to injection.

   The choice of this initial condition is consistent with commonly accepted mission plans; trajectories with this energy level provide an automatic return to earth if no departure is made from the midcourse phase.

b. The desired landing site will presumably be located on the lighted side of the moon (due to temperature considerations), with the lunar phase as shown in the top view of figure 5-1.

c. A significantly large velocity impulse will be required to inject the vehicle out of the midcourse phase prior to landing.

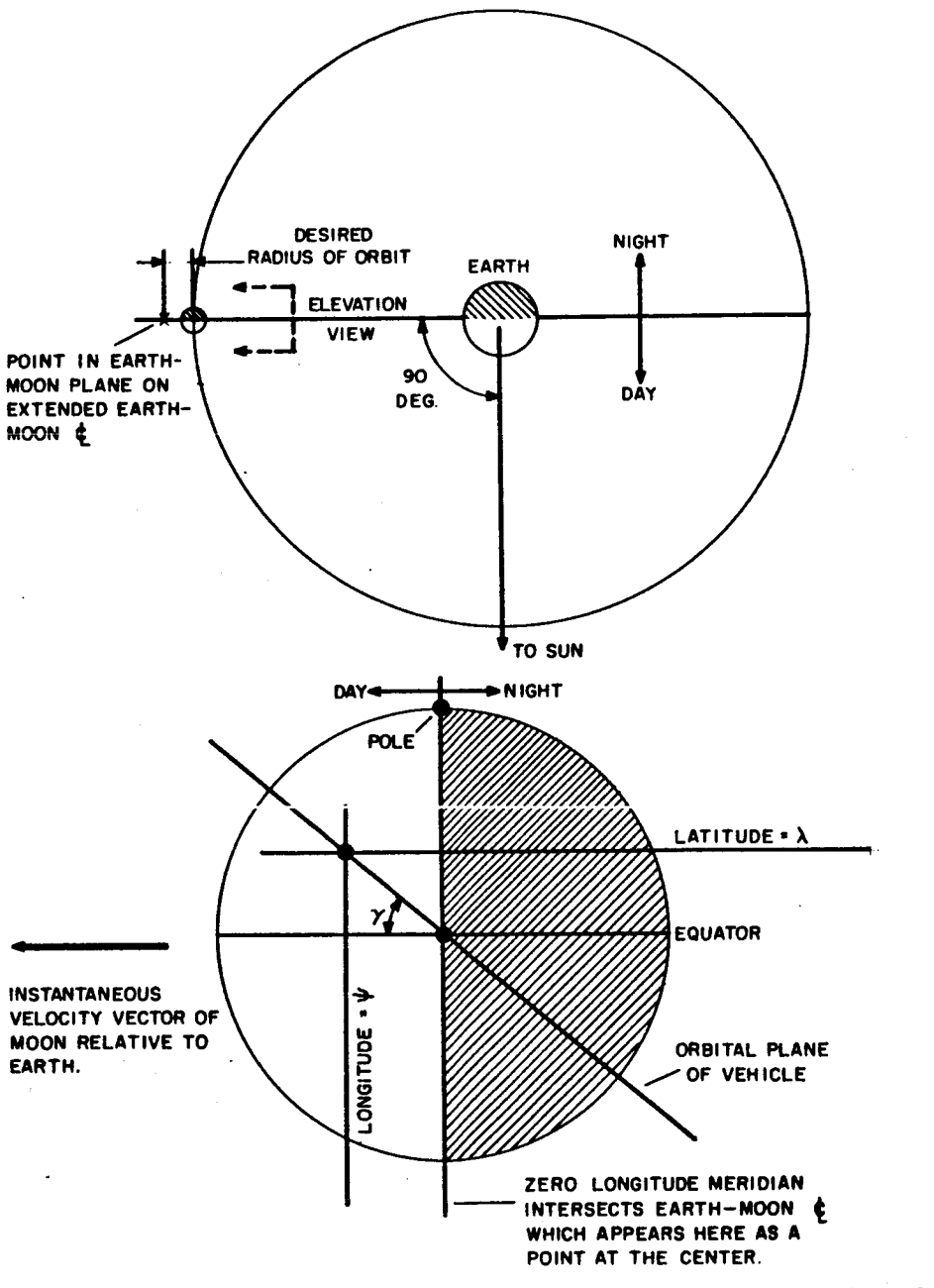

Figure 5-1. Orbital Plane at Time of Midcourse Termination

This page intentionally left blank.

c. (Cont'd)

The trajectory obtained immediately after midcourse is therefore subject to deviations from the nominal, due to injection errors. A lunar parking orbit is therefore prescribed, whereby on-board navigation will provide a corrected estimate of the true course. A nominal circular orbit of 200 kilometers is assumed; this is a typical figure in current mission analyses.

d. The midcourse trajectory is assumed to be designed such that perilune, (point X in the top view of figure 5-1) is located directly above a point on the lunar equator, on the extended earth-moon centerline at the time of arrival. In addition, the midcourse velocity vector at perilune is assumed to be inclined with respect to the lunar equator, at an angle equal to (γ) in the elevation view of figure 5-1. It is noted that (γ) is the inclination required for an orbit to pass over the point shown (latitude = λ ; longitude = ψ) when the longitude of the ascending node (Ω) of the orbit is zero. It will therefore be possible to inject tangentially at perilune (at 180 degrees longitude and zero latitude) into a circular orbit which passes over the desired point. It follows from the preceding discussion that the earth-moon plane is considered synonymous with the lunar equator. This is consistent with the practice of ignoring second-order effects (e.g., tilting of the lunar polar axis) in the sensor requirements analysis.

e. The circular orbit will be followed by a descent orbit which is nominally an elliptical arc, passing over the desired point

e. (Continued)

(λ, Ψ in figure 5-1) with a perilune altitude of twenty kilometers. These conditions, plus the angles (γ) and (Ω = 0) previously determined, constitute only a partial definition of descent trajectory geometry. It is also necessary to specify the central angle of the elliptical arc. A reasonable choice can be made from a knowledge of the basic approach to guidance, described in the item which follows.

f. Although deviations are expected from the nominal parking orbit due to injection errors, no attempt will be made to correct this error. Instead, the on-board navigation system will be used to compute adjustments to the nominal thrust vector to be applied for descent injection. This is basically a fuel economy measure. It can be shown that the desired velocity impulse vector for orbital transfer at any time is uniquely determined by the initial state at that time and the desired position vector (latitude, longitude, and altitude) at the time of reference perilune. This is the computation which will be carried out by the on-board system. With this navigation scheme, a small plane change may be called for at descent initiation, to offset parking orbit deviations. There is no immediate objection to this since, with no plane correction at descent, additional translation would be required in landing.

It would be desirable to prescribe a central angle for the elliptical descent arc which would lead to a minimum fuel transfer. With no plane change, the optimum arc would be 180 degrees,

f) Continued

corresponding to a Hohman transfer. However, to obtain the greatest translation on the surface due to a plane correction, made at the start of the descent, a 90 degree arc would be required to minimize the fuel expenditure. The optimum arc for the complete maneuver depends upon the rms plane change called for at descent initiation. This is, of course, unknown at present; it is part of the analytical solution. A nominal value of 90 degrees has been chosen for this study, with the understanding that the scheme could be improved in the future. About one hundred feet per second of velocity increment could possibly be saved by optimization. This optimization, however, is outside the scope of the sensor requirements analysis.

g. Precision guidance computations will not be carried out during descent; parking orbit navigation is expected to be sufficiently accurate to allow landing at the desired site. Initiation of the landing phase will occur nominally at perilune of the descent ellipse. The desired landing site will therefore lie a short distance beyond descent perilune.

A summary of the flight path sequence is indicated in Figure 5-2. The tangential injection from midcourse begins at point (A) and ends at point (O).* The vehicle enters a circular orbit, from which measurements are made for the purpose of trajectory determination. At least one full revolution is set aside for measurements; consequently the descent initiation takes place

* In this analysis, the injection is assumed to be impulsive; points (A) and (O) are coincident. The same is true of points (E) and (F).

This page intentionally left blank.

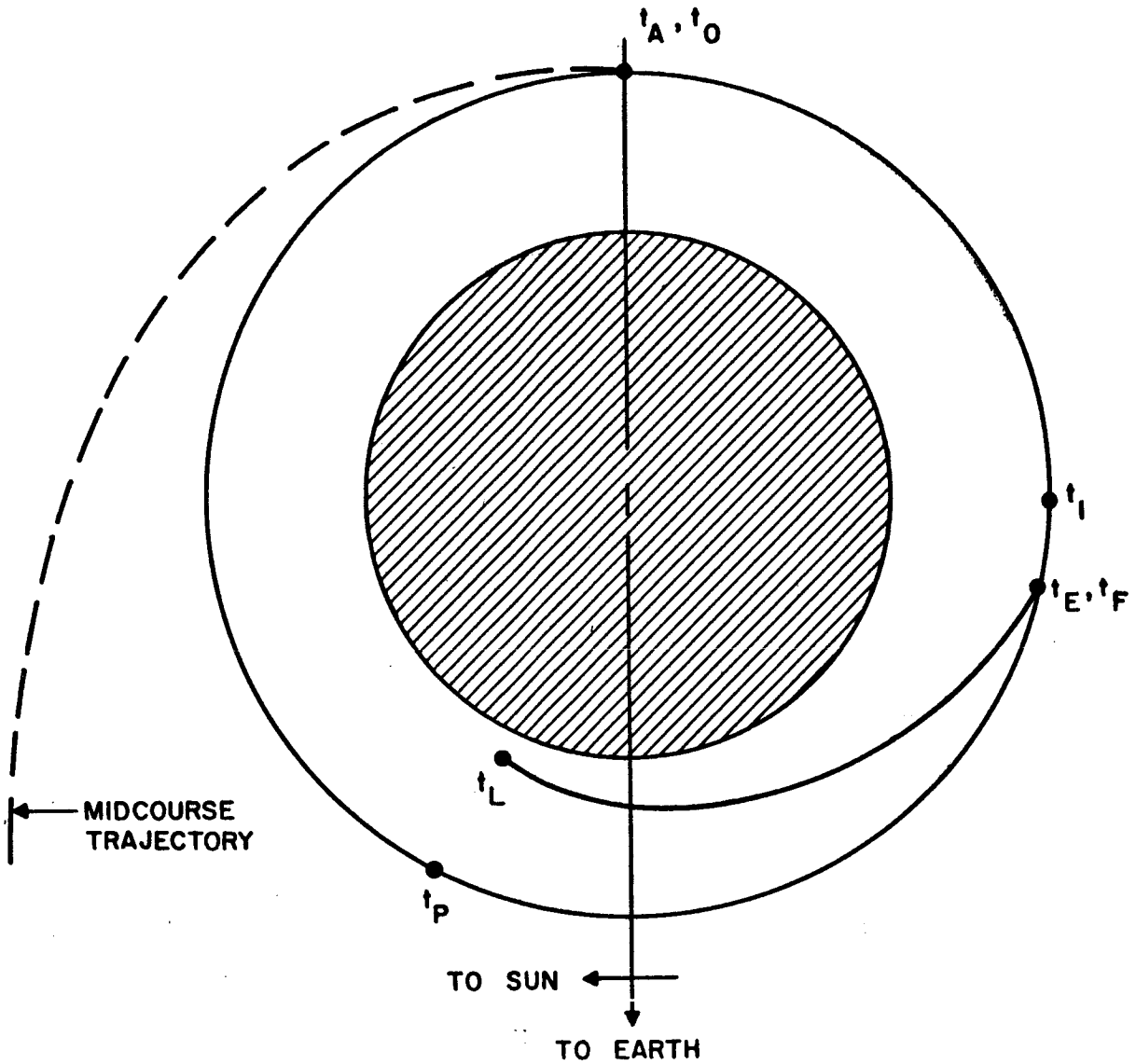

IDENTIFICATION OF EVENTS

t_A — TIME OF MIDCOURSE PHASE TERMINATION

t_O — TIME AT BEGINNING OF PARKING ORBIT

t_I — TIME OF FIRST OBSERVATION ON FIRST REVOLUTION

t_P — TIME AT FIRST PASS OVER PERILUNE

t_E — TIME AT END OF PARKING ORBIT (ON SECOND REVOLUTION)

t_F — TIME AT INITIATION OF DESCENT ORBIT

t_L — TIME AT END OF DESCENT ORBIT

1316A—VB—54

Figure 5-2. Plan View of Lunar Flight Path

on the second passage through point E. The arc $(\widehat{EL})$ is a segment of an ellipse, with perilune at point (L).

It is seen that the true anomaly ($\angle$ ECL = $\angle$ FCL) is greater than ninety degrees. The term "ninety degree descent" refers to the eccentric anomaly of the elliptical segment. When this is ninety degrees, the periods of the ellipse and the circular orbit are equal, providing an "automatic rendezvous" feature in the event that a decision is made not to initiate a landing.

In the Part I document, the nominal parking orbit and descent trajectory were expressed in terms of the ellipse parameters (semi-major axis, eccentricity, inclination, etc.). The computer program has since been designed to accept the following inputs:

Latitude of injection point (λ_o)

Longitude of injection point (ψ_o)

Latitude of perilune (λ_p)

Longitude of perilune (ψ_p)

Circular orbit radius (r_o)

Perilune radial distance (p)

Descent angle (eccentric anomaly) (E_F)

These familiar quantities are sufficient to define the parking and descent orbit geometries completely.

5.2 Background and Approach

In anticipation of the thrust errors previously described, an on-board navigation scheme has been prescribed for this phase of the mission. For the sake of on-board computer simplicity, it is desirable to prescribe a linearized system, if this will provide adequate performance. Kalman's formulation (Ref. 5-1) of the recursive optimum linear estimator appears especially attractive for this purpose.

The application of Kalman's theory to space navigation was pioneered by Dr. Stanley F. Schmidt and his associates (Refs. 5-2 and 5-3), and also by Dr. R. H. Battin (Ref. 5-4). In this latter reference, a method was included whereby the measurement to be taken at each observation time could be optimized. This data conditioning procedure was found to be indispensable for the navigation system described herein.

The above studies were applied to the midcourse phase of a lunar mission. The use of Kalman's theory in a two-body trajectory has been proposed by Pines (Ref. 5-5) and an investigation of minimum variance earth navigation has already been published by Levine (Ref. 5-6).

All of the documents referenced above have been used extensively in the formulation of this study. In fact, all of the equations involving the optimum linear estimator, and the effect of time translation, celestial measurements, and velocity changes upon trajectory deviations and uncertainties, were taken directly from refs. 5-2 and 5-3. The vector formulation of two-body motion developed in ref. 5-5 is quoted here without further proof; this was in a form convenient for determination of the state transition matrix. As mentioned earlier, every measurement was optimized by the minimum error criteria described in ref. 5-4.

In view of all this apparent duplication, the question might be raised whether the analysis described herein was necessary. It is clear, however, that no quantitative results for a lunar parking orbit can be extracted from studies of midcourse trajectories or earth parking orbits (which are the subjects of the above mentioned references). Of equal significance is the difference between the purposes of the studies. In the determination of sensor requirements, there are certain considerations which would not apply

to a trajectory analysis, or to a study performed to illustrate feasibility of a particular navigation scheme. One such consideration, which was not definitely established previously, is the question of whether the sensitivity coefficients could be precomputed from the nominal orbit and prestored in the on-board computer. The Monte Carlo simulation of the actual nonlinear dynamics, described herein, removed all doubt; the precomputation of coefficients is not sufficiently accurate for navigating in a lunar orbit with the proposed measurements.

5.3 Problem Description

The study described in this section is an error analysis of an on-board guidance and navigation system, in the lunar flight paths of Figure 5-2. The on-board systems in brief, is characterized by angle measurements between known stars and lunar landmarks, Kalman's minimum variance data processing, and fixed time-of-arrival end point guidance.

5.3.1 Ground Rules and Assumptions

The details of the analysis were governed largely by the emphasis placed upon sensor requirements throughout this study. For instance, one way of asking what the required accuracies are for this phase of a mission, is to pose this question: How large can the initial trajectory deviations, uncertainties, thrust errors, and measurement errors be, before the system fails to perform adequately? At the upper limit of these errors, it seems possible that nonlinear effects could introduce significant discrepancies into the navigation system. Therefore, although the minimum variance estimator is optimum for truly linear systems, it is not necessarily adequate for navigation around a circular path. It was decided at the outset of this study to include a Monte Carlo simulation in the circular orbit analysis. This provided an indication of the errors introduced by nonlinearities by comparison of the simulation results

with ensemble data from the usual linearized covariance matrix analysis.

While the foregoing discussion indicates a degree of complexity added to the analysis, there are also some simplifications allowed by the sensor requirements stipulation. Since it is the required sensor performance, and not the precise trajectories themselves which must be determined, orbital perturbations due to multibody effects and lunar oblateness can be ignored. The geometry is idealized, then, to a Keplerian form, and the moon is assumed stationary.

Because of time limitations placed upon this study, the following assumptions were also adopted:

a) Uncertainties in physical constants were ignored. (a study of these uncertainties, already conducted for the midcourse phase, is described in ref. 5-7).

b) All velocity changes were assumed impulsive,

c) The time at which a measurement is taken, or thrust is applied, is known exactly,

d) All random errors are pairwise independent and normally distributed with zero mean. The effects of bias errors, therefore, have not been taken into account,

e) Existence of a known visible star and landmark is assumed, in the directions determined by the optimum measurement criteria (Ref. 5-4), at each measurement time,

f) The possibility of instrument failure or gross measurement errors is not considered.

5.3.2 Quantitative Inputs to Analysis

For ease in interpretation, an effort was made to express all parameters in terms of quantities which are most familiar, and which can be varied most conveniently when necessary.

5.3.2.1 Nominal Trajectory Geometry

The flight paths shown in Figure 5-2 are defined by the latitude (λ_0), longitude (ψ_0) and radial distance (r_0) of the injection point, the latitude (λ_p), longitude (ψ_p), and radial distance (p) of descent perilune, and the descent angle (E_F) defined in Section 5.1. The direction (posigrade or retrograde) is expressed in terms of the algebraic sign of the initial true anomaly $\{ sgn(\theta_0) \}$.

In accordance with the considerations expressed in the Part I (Problem Definition) study, the following geometric parameters have been chosen for the nominal orbit:

a) (λ_0) is zero degrees,

b) (ψ_0) is 180 degrees (the sightline to the earth marks the zero longitude reference),

c) (r_0) is the mean lunar radius plus 200 kilometers,

d) (λ_p) is thirty degrees positive,

e) (ψ_p) is twenty degrees negative (twenty degrees off the terminator on the lighted side of the moon).

f) (p) is the mean lunar radius plus twenty kilometers,

g) (E_F) is ninety degrees negative, as previously explained,

h) A retrograde orbit was chosen.

5.3.2.2 Navigation Parameters

Measurement geometry is defined by the following inputs:

a) The time delay (t_{d1}) between injection and the first measurement,

b) Time interval (τ_1) between measurements on the first pass, or revolution,

c) The fraction (f_1) of a period for which measurements can be taken on the first revolution,

d) The time delay (t_{d2}) between the last measurement on the first revolution, and the first measurement on the second revolution. (This is necessitated by the absence of any light during part of the orbit, and/or the fact that part of the lunar surface is unknown. A discussion follows shortly),

e) Time interval (τ_2) between measurements on the second revolution,

f) The fraction (f_2) of a period for which measurements can be taken on the second revolution, before descent,

g) The angle (α_L) at the moon center, between a radial line to the mth landmark and the radius vector to the nominal vehicle position, at the time of the mth measurement. (For this analysis, a constant value was chosen. This is discussed in Section 20.3.3).

It can be seen from Figure 5-2 that no visual observations can be made during the first quarter of the parking orbit. At the lunar phase shown, there is no light during this period.* For the next two quadrants of the parking orbit, earth shine and sun, respectively, will illuminate the known side of the lunar surface. The vehicle will then pass over the unknown side of the moon* for a half revolution, during which time no measurements have been prescribed. At one full period after t_1, measurements can be re-initiated for a short time prior to descent.

In accordance with the above discussion, the following logic applies to the selection of the measurement scheduling parameters:

a) (t_{d1}) is one-fourth of the orbital period,

b) (τ_1) can be between five and ten minutes,

c) (f_1) is one-half period,

d) (t_{d2}) is essentially one-half period,

e) (τ_2) can be set at five minutes,

f) (f_2) is limited to only (0.04) for a perilune longitude of minus twenty degrees. This value, and the interval (τ_2), will allow two measurements to be made on the second revolution prior to descent.

5.3.2.3 Astronomical Constants

The lunar gravitational constant (μ) and the mean lunar radius (q) were taken from ref. 5-3 and the Part I document, respectively:

$$\mu = 4.8982 \times 10^{12} \text{ meters}^3/\text{sec}^2$$

$$q = 1.73807 \times 10^6 \text{ meters}$$

* This suggests the desirability of additional observables for this phase of the mission. See Section 5.9, Recommendations.

5.3.2.4 Input Error Statistics

The following random errors were taken into account:

a) Position deviations at time of injection (Γ_1),

b) Velocity deviations at time of injection (Γ_2),

c) Position uncertainties at time of injection (Γ_3),

d) Velocity uncertainties at time of injection (Γ_4),

e) Error in application of injection velocity increment (Γ_5),

f) Error in measurement of injection velocity increment (Γ_6),

g) Errors in navigation measurements (including landmark position uncertainty)(Γ),

h) Errors in application of descent velocity increment (Γ_7),

i) Errors in measurement of descent velocity increment (Γ_8).

Aside from the navigation measurement errors, each of the above errors consists of three mutually orthogonal components. The values of error considered are discussed in Section 20.5.

5.3.3 Quantitative Outputs of Analysis

The outputs of the simulation are simply the statistics of:

a) The final miss vector,

b) The final dynamic uncertainty (both position and velocity),

c) The total excess (above nominal) velocity impulse used in injection and descent.

The coordinate system used for the final deviations and uncertainties is the Cartesian set with vectors in the directions of:

a) The nominal descent perilune velocity vector,

b) The nominal descent perilune radius vector,

c) The nominal transverse perilune vector.

5.4 Summary of Analytical Techniques

5.4.1 Acquisition of Results

The analysis of this phase consists of two parallel but separate determinations of navigation system performance. In order to include non-linear effects, a deterministic analysis was performed by the Monte Carlo technique whereby random numbers* were selected for each input error, and squared errors at the output were accumulated from one hundred repeated trials. The positive and negative final errors were also accumulated, and a student's t-test (ref. 5-9) was applied to test the hypothesis that the mean value of each error component is small.

As a logical extension of the Monte Carlo simulation, the linearized covariance matrices of the deviations and uncertainties in state at the last measurement were linearly transformed into final deviations and uncertainties at descent perilune. A comparison of the two methods provided an indication of the error in an on-board trajectory computation due to the proposed linearization.

5.4.2 Summary of Notation

The nomenclature used in subsequent discussion and in the corresponding Appendix (Section 20) is defined below.

ENGLISH ALPHABET

B	Product of H and corresponding transition matrix
E	Eccentric anomaly beyond perilune
F	Velocity increment vector
G	Guidance law matrix

*Random numbers were generated by the power residue method described in Ref. 5-8.

H	Row vector of partial derivatives of observables
I	Identity matrix
K	Six-dimensional weighting factor
L	Selenocentric landmark vector
M	Total number of observations
N	Covariance matrix of deviations from nominal state
P	Covariance matrix of errors in estimated state
Q	Selenocentric star sightline vector of magnitude q
R	Selenocentric instantaneous vehicle position vector
T	Period of parking orbit
U	Unit eigenvector corresponding to maximum position uncertainty
V	Selenocentric instantaneous vehicle velocity vector
X	Six-dimensional state vector
a	Parking orbit radius
a_d	Descent orbit semimajor axis
d	Dot product of R and V
e_d	Descent orbit eccentricity
f	Deviation from nominal velocity increment vector
f_1	Fraction of a period for which measurements can be taken on first parking orbit revolution
f_2	Fraction of a period for which measurements can be taken on second parking orbit revolution
l	Magnitude of L

q	Mean lunar radius
r	Magnitude of R
t	Time
t_{d1}	Time delay between injection and first observation
t_{d2}	Time delay between last observation on first parking orbit revolution and first observation on second revolution
v	Magnitude of V
x	Deviation from nominal state vector

GREEK ALPHABET

α_L	Angle subtended at moon center between L and local vertical
Γ_n	Covariance matrix of input errors*
θ	True anomaly
λ	Selenocentric latitude
μ	Lunar gravitational constant
ν	Incremental eccentric anomaly
$\varkappa$	Angle between Q and sightline from vehicle to landmark
ξ	Deviation from reference value of $\varkappa$
ρ	Unit vector in the direction of R
σ	Standard deviation (general)
τ_1	Time interval between observations on first parking orbit revolution
τ_2	Time interval between observations on second parking orbit revolution
Φ	State transition matrix
ψ	Selenocentric longitude

*See Section 5.3.2.4

SUPERSCRIPTS

$[\ ]^T$	Matrix transpose
$[\ ]^{-1}$	Matrix inverse

SUBSCRIPTS

A	Pertaining to termination of midcourse
E	Pertaining to termination of parking orbit
F	Pertaining to beginning of descent orbit
i,j	Vector or matrix components *
L	Pertaining to termination of descent orbit
m	Pertaining to the mth observation
M	Pertaining to the last observation
O	Pertaining to the beginning of parking orbit
P	Pertaining to the first pass over desired perilune

SYMBOLS ABOVE LETTERS

$(\ )'$	Actual value
$(\tilde{\ })$	Uncertainty; error in estimated value
$(\hat{\ })$	Indicated or observed value

5.4.3 Determination of Nominal Orbits

The first step in the computation is to determine, from the parameters in Section 5.3.2.1, all of the following quantities:

a) All parking and descent orbit parameters (e.g. period, semimajor axis, etc.)

b) The time, true anomaly, and eccentric anomaly at all key points of Figure 5-2 and at all measurement times,

* For time-varying vectors and matrices, the first subscript denotes the time.

c) Vehicle position and velocity vectors at all key points on the orbits,

d) Nominal velocity impulse vectors for injection into parking orbit and descent initiation.

This computation is described fully in Section 20.1 of Appendix II.

5.4.4 On-Board Navigation Technique

The various quantities associated with the observations are computed in the following order:

a) From the parameters in Section 5.3.2.2, the time of each observation is determined,

b) The nominal vehicle state is computed at each observation time,

c) From the vehicle state, and the star and landmark vectors associated with each measurement, the nominal space angle is determined,

d) All partial derivatives of space angles follow readily.

A complete set of equations appears in Section 20.2 of Appendix II.

5.4.5 On-Board Linear Prediction

Section 20.3 of Appendix II describes:

a) Computation of the state transition matrix,

b) The recursion relations used for linear prediction, and the literature from which they are taken,

c) A method of data conditioning based upon the eigenvectors of the position uncertainty covariance matrix (ref.4).

5.4.6 Linearized Dynamic Equations

Ref. 3 provides the basis for computation of:

a) A linearized guidance command, based on the definition of an orbital arc from two position vectors and a fixed time interval,

b) Transformation of error covariance matrices with velocity impulses.

The corresponding equations appear in Section 20.4 of Appendix II. Also included in that section is a transformation of final errors into tangential, vertical, and transverse coordinates.

5.4.7 Typical Input Errors

Section 20.5 of Appendix II contains a discussion of:

a) Thrust measurement errors, based on typical accelerometer inaccuracy and the estimated thrust pulse width,

b) Thrust application error, from estimated engine control accuracy,

c) Effect of landmark uncertainties on angular measurements at 200 KM altitude,

d) Initial condition errors, from final errors of midcourse phase.

5.5 Digital Program

The major inputs and outputs of the program, the equations used for the solution, and even the order of computation for the linearized analysis are described in Section 20. Concurrent with that computation, a Monte Carlo simulation was performed as a check on linearization errors. A block diagram of the deterministic solution for each repeated trial is shown in Figure 5-3. All random errors, of course, are multidimensional, and all components were generated independently.

This page intentionally left blank.

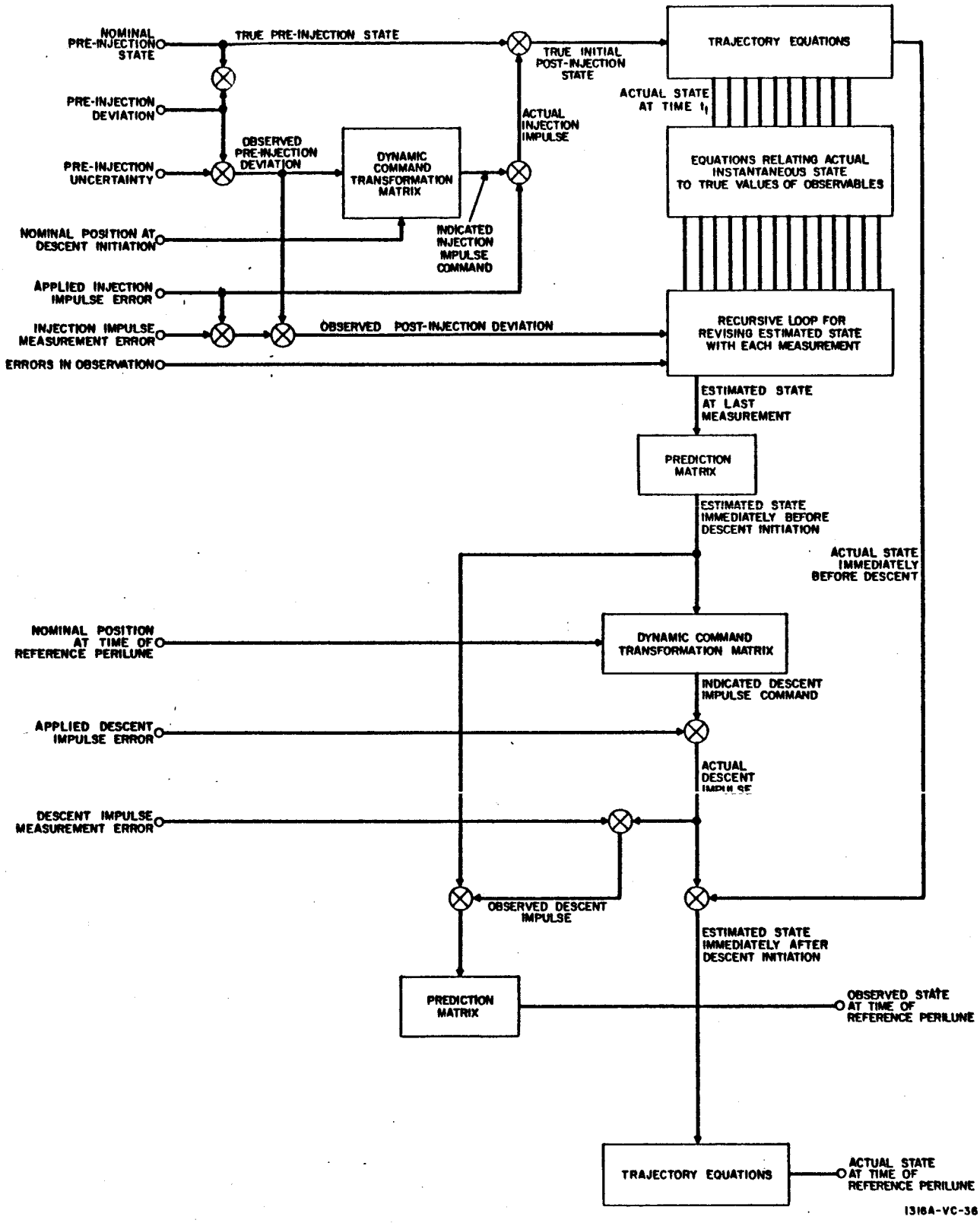

Figure 5-3. Schematic of Lunar Navigation Simulation

As a check on the validity of the various steps in the computation, several additional features were added to the program. For instance, a very extensive set of data was printed out, including:

a) All nominal and actual orbit elements,

b) Nominal state vector components, true anomaly, eccentric anomaly, time, etc., at all key points in the orbits and at all measurement times,

c) True and observed values of measurements, state, etc., at all measurement times,

d) Measurement derivative row vectors (H), state transition matrices (Φ), their product (B), weighting vector (K), and uncertainty covariance matrix (P) at all measurement times.

A considerable amount of hand computation was carried out with the above figures, to establish confidence in the program. In addition, a number of tests were added to the program which, if not passed, would stop the program immediately. These include:

a) Comparison of quantities computed twice, by independent methods,

b) Coplanarity test (by the scalar triple product) for vectors in the same orbit. This test was made for every vector computed in both the nominal and the actual orbits;

c) Vanishing dot product for vectors known to be orthogonal,

d) Convergence of quantities computed by transcendental equations (e.g., the incremental eccentric anomaly),

e) Verification of defining equations for the chosen landmark vector.

The computation was performed in double precision on the IBM 7094.

5.6 Summary of Digital Computation

From this program a number of results were obtained which are more appropriately described as qualitative, rather than numerical. In early computer runs, for example, it was quickly learned that certain practices regarding selection of observables, data processing, etc., were grossly inadequate for orbital navigation. In these instances, improvements were quickly sought and adopted; little effort was made to collect large amounts of data on a prescribed system which is known to be inferior. The qualitative results to be discussed here are theoretically acceptable and no large amount of data is required to verify them. In chronological order, the conclusions reached were:

a) There is an inherent ambiguity in the measurement of the deviation from a 180 degree angle. The sightlines from the vehicle to the landmark and to the star should not be nearly collinear;

b) A double precision program is necessary to insure accuracy of the computation;

c) The fixed time of arrival end point guidance law is effective, even over a time arc exceeding one period. With a 5 KM initial radial deviation at (t_A) and no other errors in the system, the total position deviation at (t_E) for an equatorial orbit was about 60 meters. Nonlinearities were, of course, the sole cause of this error;

d) The use of simple least squares data processing with these angle measurements is inadequate. As stated in Ref. 5-5, data should not be fitted over a long time arc. Initially, the unweighted least squares estimate was used in this program. This was soon discarded in favor of the minimum variance technique;

e) For these single angle measurements, a data conditioning procedure is essential, even when the input errors and the time between measurements are relatively small;

f) With properly conditioned data and no measurement error, the P matrix elements experience a rather sharp drop in the vicinity of the sixth and seventh measurement. This is reasonable, since there are six unknowns;

g) Results of the Student's t-test indicate, as expected, that the mean value of each error is appreciably less than its standard deviation;

h) The most important qualitative result was the conclusion that a linearized on-board data processing system with precomputed sensitivity coefficients does not represent the inherent dynamic nonlinearities with a sufficient degree of accuracy to provide adequate computation of a lunar trajectory.

As an illustrative example of the nonlinearity present, the estimation errors were read out for a typical member of an ensemble with rms initial uncertainties of 1 KM and 1 meter per second in position and velocity, respectively, and all other input errors set at zero.* The delay time (t_{dl}) and the interval between measurements (τ_l) were both set at five minutes for this (purely academic) trial.

After the eighth observation in this orbit the total rms position uncertainty was only 57 meters, but the uncertainty increased steadily after this reading until after the thirty-fifth observation, an error of 28.5 kilometers was reached. At the same time, the covariance matrix of estimation errors indicated an rms uncertainty well below one meter. The initial reaction

*(Γ) of equation 20-51 was set at 10^{-12} radians squared to prevent possible singularity.

to this result was skepticism in regard to the validity of such a large discrepancy.

The above computation prompted further test runs (e.g., accumulation of squared errors from 100 repeated trials, re-runs with different inputs, etc.) which consistently led to the conclusion that this method of data processing is inadequate for the navigation problem considered. The space angle derivatives (elements of the H-vector), simply are not linear over a long time arc. It is insufficient to recalculate a new estimated state after each observation without also calculating a complete new set of matrices.

To prescribe an on-board system which recomputes new sensitivity coefficients after each measurement did not seem logical at the outset of this analysis, since its complexity made it appear somewhat unattractive. Furthermore, a recent (January 1963) paper indicated that the linearized navigation technique is suitable, provided that the deviation from a reference state remain small (Ref. 5-6). However, even for reasonably small initial errors, such as those reported in the NASA midcourse study (Ref. 5-3), performance of the prescribed system is unacceptable in a trajectory with long time arcs. Consequently, no further Monte Carlo simulation results were made after the inadequacy of the linearized system was revealed.

It must be emphasized that inadequacy of the particular system originally prescribed does not preclude the possibility of approximating the performance of a truly optimum system by linearized techniques.* The lack of agreement between the linearized analysis and the Monte Carlo simulation stems, of course, from one underlying assumption. In the matrix error analysis, using Kalman's method, the weighting vector (K) is assumed to be truly optimum, and

* In fact, all of the NASA and MIT studies referenced here utilize linearization throughout the analysis.

the state transition matrix is assumed to represent the actual physical law to which the motion conforms. In each Monte Carlo trial, actual vehicle state and true measurement values are computed deterministically without using linear approximations. Operating on actual observations, obtained in this way, and in an actual orbit, the weighting vector computed from linearized physical laws is not really optimum. Over a long time arc, in fact, the practice of using this non-optimum weighting vector results in gross errors. By using the Monte Carlo analysis in this study, the terminal state errors due to linearization were determined.

An on-board system is now hypothesized in which the sensitivity coefficients used to weight each observation are recalculated after each observation. The analytical simplification commonly adopted for performance evaluations, even in the most advanced recent studies (refs. 5-2 through 5-7), can be re-stated as follows: a true optimum data processor operating in the presence of the nonlinearities, is able to provide the same performance as a linearized data processor would provide if there were no nonlinearities present. Future verification of this assumption is discussed in Section 5.9, "Recommendations".

5.7 Numerical Results

On the basis of the foregoing discussion, the linearized matrix computation used in this study was carried out for the following values of RMS input errors to determine the effects of the sensor errors in the final state vector accuracy.

Initial State Deviations:	4.8 KM & 1.2 m/sec.
Initial State Uncertainties:	0.8 Km & 0.08 m/sec.
Applied Impulse Error:	1% of total velocity increment
Impulse Measurement Error:	0.005 m/sec.
Landmark Uncertainty:	1 KM

The above error values are discussed in Section 20.5. The RMS instrument error was varied from zero to three milliradians.

In view of the 3-sigma pre-landing miss distance tolerance expressed in Section 6.3.1, the allowable final RMS deviations for this computation were set at:

a) 5.08 kilometers tangential error

b) 2.54 kilometers vertical error

for descent trajectory perilune. Sensor requirements for this phase were determined exclusively from these figures; excess fuel consumption was dropped from consideration.

It is seen from figure 5-4 that from the standpoint of allowable vertical error, an RMS instrument error of two milliradians forms the borderline case. Much of the final position deviation is obviously caused by the error (1 meter/sec.) in the applied descent impulse, approximately one half hour ahead of descent perilune.

Because the trajectory which follows this descent orbit is self-correcting (Section 6), the final uncertainty requirements are not stringent; it is merely necessary that the vehicle be observed within its required miss distance tolerances. This condition is met with the aforementioned borderline case of Figures 5-4 to 5-6.

This page intentionally left blank.

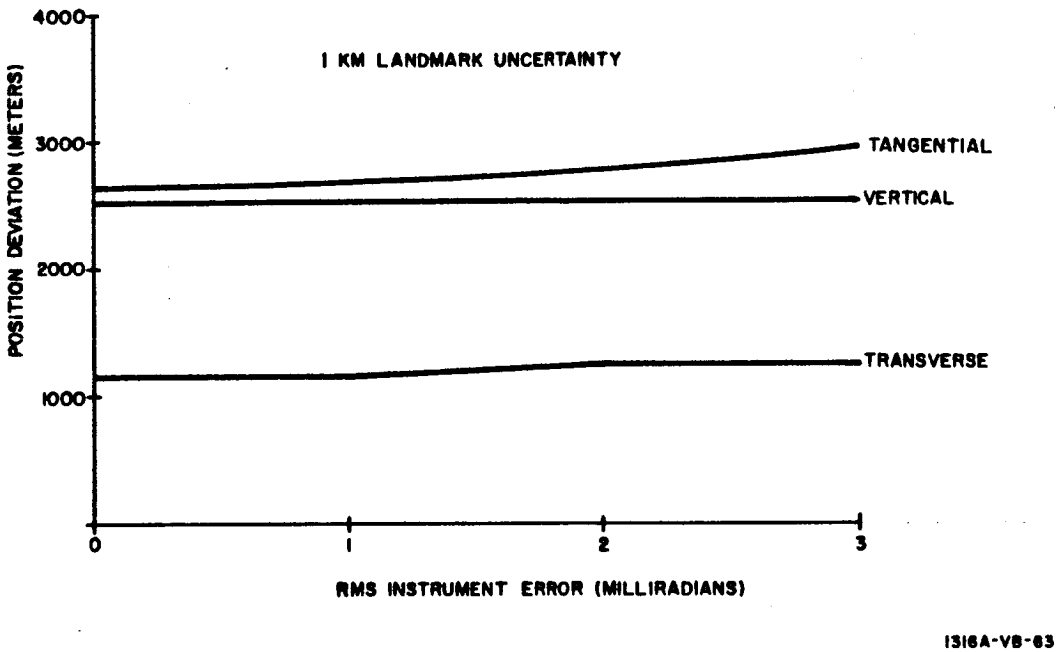

Figure 5-4. Final Position Deviations vs. RMS Measurement Error

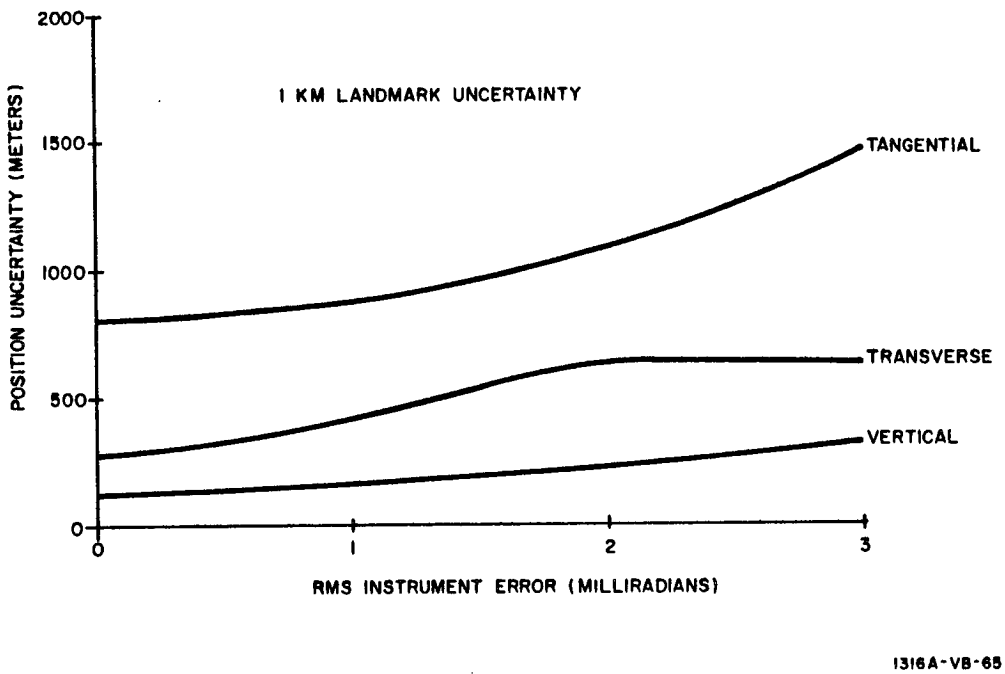

Figure 5-5. Final Position Uncertainties vs. RMS Measurement Error

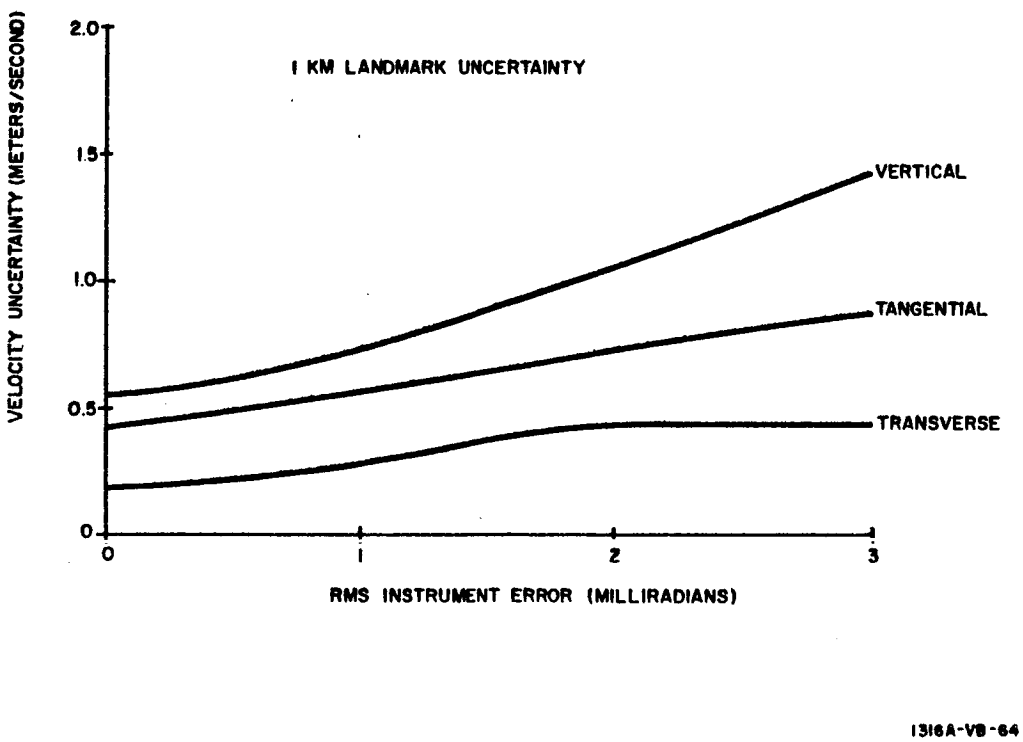

Figure 5-6. Final Velocity Uncertainties vs. RMS Measurement Error

Three further behavior characteristics deserve mention at this point:

1. The transverse error seems to have reached a saturation level. Clearly, there must be such a level since, with excessive instrument error, navigation measurements would be unable to reduce estimation errors below the extrapolated initial uncertainties. The optimum linear weighting factor takes this into account, by diminishing the influence of navigation measurements with large inaccuracies (Equation 20-51).

2. Figures 5-7 and 5-8 illustrate the total rms uncertainties* after each measurement. The abcissa is broken before the first and fourteenth observations, to indicate the associated time delays (Section 5.3.2.2). The points cannot be connected by a smooth curve, because the uncertainty is always increasing between measurements.

   As expected, the uncertainty grows considerably during the excursion over the dark portion of the moon. The possibility of obtaining other measurements (e.g., altitudes, beacons) during these intervals is discussed in Section 5.9.

3. The borderline case was recomputed with applied thrust errors reduced to four-tenths of their original value. Final miss distance components were roughly halved, and uncertainties remained unchanged. The fact that the applied impulse errors consume most of the allowable final error is also mentioned in Section 5.9.

* As explained in Ref. 5-3, these are computed as the square roots of the traces of the partitioned covariance matrix of estimation error.

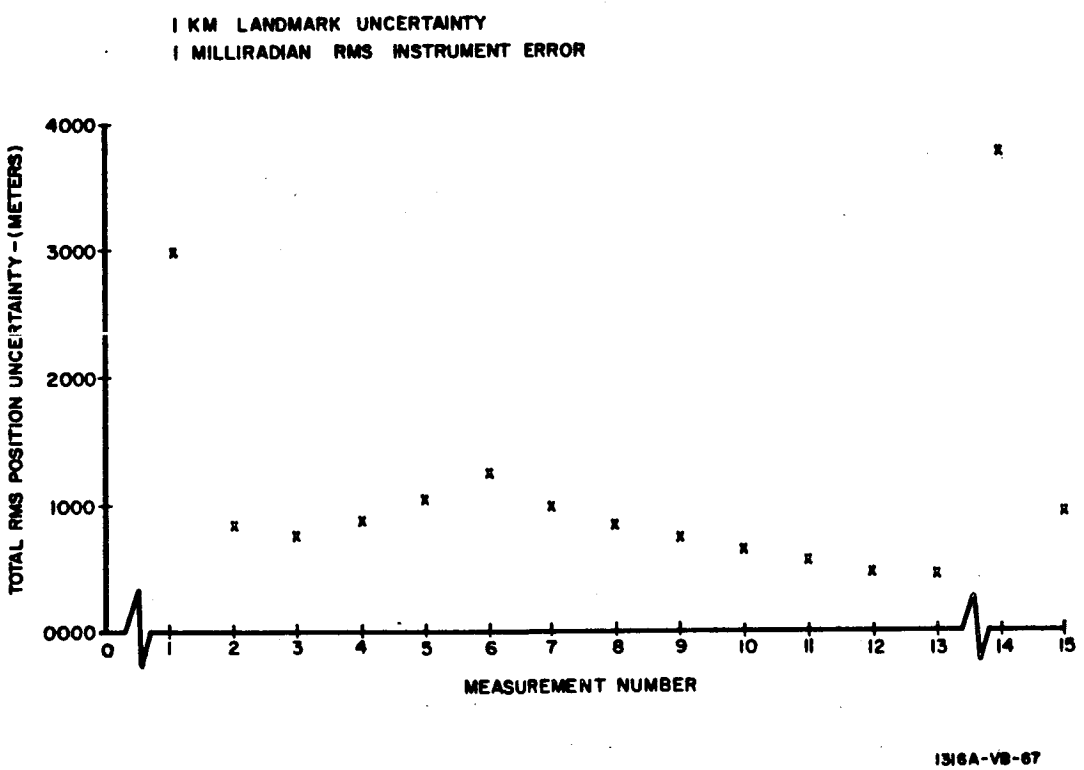

Figure 5-7. Total Position Uncertainty vs. Time

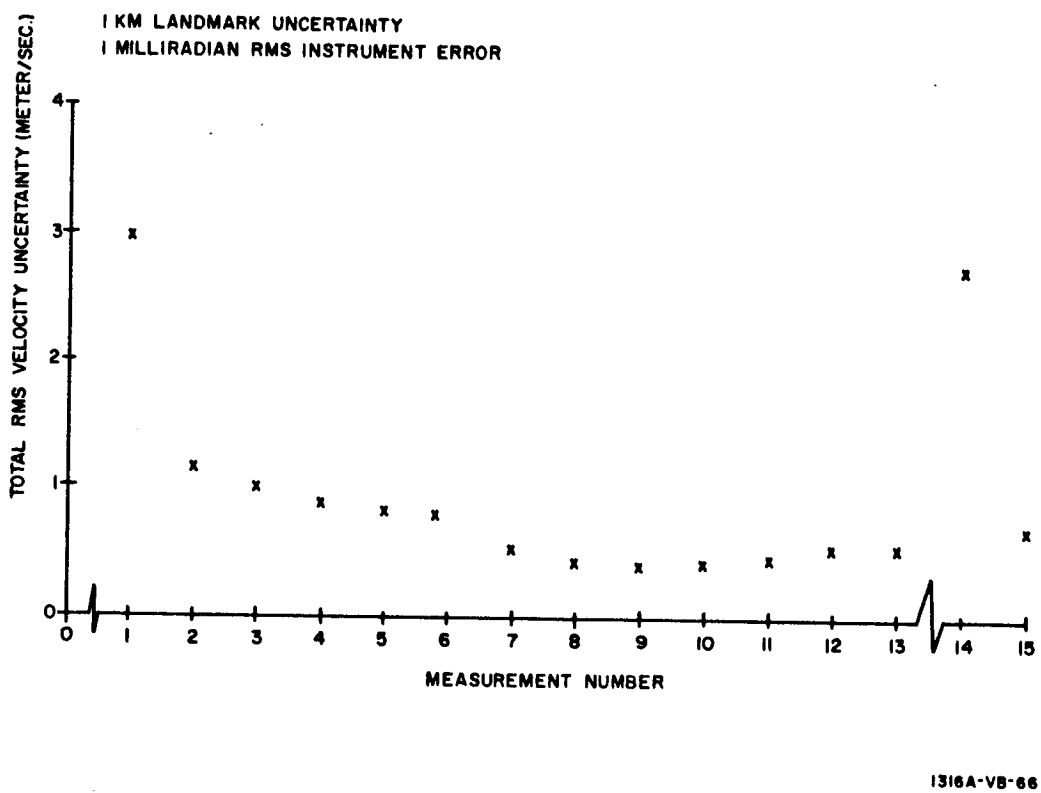

Figure 5-8. Total Velocity Uncertainty vs. Time

5.8 Sensor Requirements

With the initial condition errors given in Section 20.5 and a landmark uncertainty of one kilometer, the following combination of RMS control and sensor errors results in a maximum allowable final miss distance:

Applied Thrust Error:	1% of Total Impulse
Incremental Velocity Measurement Error:	0.005 meters per second
Angular Measurement Error:	2 milliradians

5.9 Recommendations

The lunar orbit navigation problem requires further study in the following areas:

a) A more complete specification is needed for the on-board data processor;

b) It must be verified that the above system is sufficiently accurate to hold the final errors to an acceptable level. Verification should not be subject to the linearization assumption discussed in Section 5.6;

c) The utilization of more observables should be considered;

d) A different set of orbit parameters should be considered;

e) Errors in applying velocity increments should be reduced;

f) After the above items have been sufficiently treated, the assumptions adopted for this analysis (Section 5.3.1) should be examined more critically.

In regard to the first item, the data processor needed for orbital navigation will most likely be nonlinear* and will probably recompute all sensitivity coefficients after each observation.

A system of the type described above must have some limiting combination of input errors, beyond which convergence to the actual trajectory is either impossible or too slow for some finite observation rate. An analysis based on the linearity approximation would be invalid at this point. Fortunately, however, since the performance analysis is conducted on the basis of two-body dynamics, it would be possible to obtain adequate statistical data by Monte Carlo methods, without consuming excessive IBM machine time. In view of the extent of nonlinearity found in this study, and because a Monte Carlo simulation would be quite straightforward for a two body navigation problem, it certainly appears advisable to analyze the dynamical situation in its true form. To the best of this writer's knowledge, this has not yet been done.**

In regard to the third item, there are (aside from the possibility of a failure) four reasons why the addition of more observables (e.g. beacons, instantaneous altitude) is advocated:

a) With landmarks as the only near observable, it will be necessary to obtain, prior to the manned mission, detailed lunar terrain maps. These would have to include the unknown side of the moon;

*In the on-board system described in Refs. 5-2 and 5-3, the estimated trajectory is used directly in the equations of motion.

** Nonlinearity in the state transition matrix was investigated in Ref. 5-3 (the third item of Section 5.6 conforms to the results of that investigation). No study was made, however, of nonlinearity in the measurement sensitivity coefficients.

b) Lack of sunlight or earth shine during part of the orbit will interrupt the desired continuous accumulation of landmark data;

c) Actual landmark uncertainties may prove excessive;

d) Availability of sufficient landmarks (or beacons) for consistently well conditioned measurements appears difficult to achieve.

The use of various nonsingular orbital parameter sets (Refs. 5-10 and 5-5) is also worthy of further investigation. As explained in this latter reference, partial derivatives are more stable when only one parameter depends upon the energy.

Reduction of applied velocity impulse tolerances can be achieved by improving the present state of the art in engine control and/or by lengthening the thrust pulse width. A reduction would be desirable, since the impulse errors assumed typical for this study seem to be borderline values, even with no appreciable instrument error.

This page intentionally left blank

6.0 Lunar Descent (Landing) Trajectory, Manned

6.1 Introduction

As was indicated in Part I of this report, landings which include atmospheric entry are not considered to be within the scope of this study. This restriction limits the problem to the consideration of such targets as natural planetary satellites and the planet Mercury. Within the era being considered, only the moon of Mars and the Earth's moon would appear to be feasible mission targets. As a further limitation, the Part I document indicated that the Earth's moon would be used in any analysis of non-atmospheric landing operations.

The landing phase can be the terminal portion of a manned or an unmanned lunar mission. As indicated in Part I, the landing operation is to be initiated at perilune of an elliptical lunar orbit, and the nominal initial conditions for the landing phase are: altitude, 20,000 meters, horizontal velocity, approximately 1750 meters per second (5750 feet per second); vertical velocity, zero; and distance from landing site, approximately 300 kilometers. During the first sub-phase of the landing operation, thrust is applied to reduce vehicle velocity and altitude to zero and roughly 500 meters respectively at a point directly over the landing site. The second sub-phase starts at the zero velocity, or hover condition and continues until actual vehicle touchdown on the surface.

6.2 Background and Approach

The aim of the analysis performed in connection with lunar landing is to obtain estimates of sensor accuracy requirements for manned and unmanned lunar landings. Information forthcoming from this initial study will indicate areas in which further analytical and/or developmental effort needs to be expended. This study is not engaged in such activities as trajectory, guidance

law, control system, or mission optimization. Therefore, in these areas, particular techniques have been selected from those available.

To arrive at intelligent selections in the above areas, the techniques under consideration should be examined in the light of certain other considerations based on study goals and limitations. The following group of statements indicate some factors which may be helpful in reaching conclusions concerning which system should be analyzed, and what analytical techniques should be employed.

1) Since the study objective is to determine the effects of sensor errors, the appropriate error sources should be separated if possible (both from each other, and from other error sources). This approach would allow final error to be divided properly among the error sources.

2) The guidance law selected should be applicable in as many different situations as possible. It would be excellent, for example, if the same guidance law, or very similar guidance laws could be used for both manned and unmanned landings, and for landings with and without surface navigation aids (beacons).

3) It is felt that extreme analytical accuracy is not essential to the successful completion of this effort. Rather the intent is to obtain reasonable estimates which will indicate areas in which sensor requirements exceed, or approximate existing sensor capabilities. These areas would then be selected for detailed study to determine associated sensor requirements more exactly.

4) The guidance technique selected should be able to make up as large an initial deviation from nominal conditions as possible. This is not meant to imply that guidance law optimization will be required for this study. It simply means that the capability of guidance laws considered to reduce initial errors will be an important factor in guidance law selection; by making the zone of acceptable landing initiation parameters as large as possible, accuracy requirements on earlier mission phases are relaxed.

With these considerations in mind, it is possible to proceed to a broad description of the system to be analyzed, and the analytical approach that will be taken.

The first decision reached was in regard to the use of a reference trajectory. The system to be analyzed will be based on linearization about a nominal reference trajectory. The primary factors governing this decision are the complexity of computer equipment on the landing vehicle, and the advantages associated with the guidance law selected. The guidance law which will be discussed shortly, requires knowledge of a reference trajectory. The reference trajectory which has been used, a constant thrust gravity turn, is a reasonably good trajectory from a fuel standpoint and also has many characteristics desirable in a landing trajectory. For example, the landing vehicle is automatically rotated to the proper hover and landing attitude during the first sub-phase of landing so that no separate attention need be given to this problem. More will be said concerning the reference trajectory in a succeeding section.

The guidance law that seemed most advantageous in light of the considerations outlined above is one that Ames Research Center has been investigating which computes corrections to be applied to the nominal thrust vector

based on known deviations from the nominal trajectory. The corrections are computed from linearized equations valid in a small region close to the nominal path. This guidance law was chosen for several reasons.

1) It is general in that it may be adapted to both manned and unmanned spacecraft. It will also function with or without surface navigation aids, and with or without direct observation of the state variables.

2) The guidance law possesses the capability of reducing relatively large known initial errors (deviations from the nominal initial conditions) to a comparatively small final error. In fact, it is possible to reduce the ideal value of final error to zero by addition of an "over-control" multiplier which will be described later.

3) The nature of the guidance technique allows for an analysis that will permit easy identification of the final error component produced by each error source.

Details of the selected guidance technique will be discussed in a later section of this report.

In keeping with the broad study concepts presented previously, it was decided to pursue a linearized analysis. Although there is a loss of accuracy by not simulating inherent nonlinearities, it is more than offset by the decrease in complexity, the relative ease of data processing, and the generality allowed by the linearization approach. Concerning this latter quality, the linearization approach allows one to analyze different sensor combinations without repeating the entire analysis. Thus, one technique for providing input information to the guidance system can be compared to another with relative ease.

Further, it is felt that comparisons of this nature do not suffer particularly from the loss of absolute accuracy associated with the linearization process.

6.3 Preliminary Analysis

Before proceeding to the actual error analysis of the lunar landing, there is some preliminary work which must be done in certain areas. Unfortunately, it does not seem possible to study the landing phase sensor requirements without giving some definition to the guidance technique. This is true because errors caused by sensor inaccuracies will propagate through the guidance system to the thrust control system. Therefore, thrust command errors will be affected by the nature of the guidance technique under consideration.

In view of this restriction, it is necessary to select a guidance law from among those that have been proposed, to observe the effect of data processing. After consideration of a number of guidance laws, one that is currently under study by Ames Research Center was selected for this analysis. This guidance technique, its capabilities, and modifications introduced during this study will be discussed in Section 6.3.1.

The guidance law selected requires knowledge of a reference trajectory. The trajectory selected, the constant thrust, gravity turn type used by Ames is described more fully in Section 6.3.2.

The last item of preliminary analysis is the selection of a group of observables to be analyzed. An observable is a quantity that may be observed by sensors on board the landing vehicle. The thrust command errors are dependent upon the particular observables selected as data inputs to the guidance system. Therefore, before the analysis can proceed, a specific set of observables must be selected and the relationships between observed quantities and guidance quantities need to be established as described in Section 6.3.3.

TABLE 6-1

Definition of Recurrent Symbols

A. Quantities

1. e : an error. When used with a subscript, it indicates an error in the subscript quantity; i.e., e_v is an error in velocity.

2. h : vehicle altitude above a reference sphere

3. I_{SP} : fuel specific impulse

4. K_{ij} : error transformation coefficient (constant rms error source)

5. K'_{ij} : error transformation coefficient (constant rms percent error source)

6. m : vehicle mass

7. R : line-of-sight range from vehicle to landing site.

8. r_o : radius of moon at landing site

9. $S_1, S_2, \ldots, S_8$: guidance terms stored in the guidance computer

10. T : vehicle thrust magnitude

11. t : time

12. Δt_i : the ith small increment of time along the trajectory

$$\sum_{i=0}^{i=N} (\Delta t_i) = \text{total time of flight}$$

13. V : vehicle velocity (magnitude)

14. α : angle between vehicle velocity vector and thrust axis

15. γ : angle between local horizontal and the velocity vector (in the plane of motion).

16. θ : angular displacement of vehicle from landing site in moon centered coordinates. (Measured in the plane of motion).

17. μ : lunar gravitational constant

18. σ : rms value of an error distribution. Subscripts are used to denote which error distribution, i.e., σ_V is the rms error in velocity.

19. σ_{ij} : the final rms value of the ith state variable error caused by the jth error source

20. σ_j : the effective rms error of the jth error source

21. ϕ : angle between local vertical and the line-of-sight from vehicle to landing site.

B. Standard Subscripts

1. a : actual value
2. f : final value
3. o : initial value
4. r : reference value

C. Operators

1. δ : indicates a small deviation from nominal value
2. ∂ : indicates partial derivative
3. dot over quantity: indicates time differentiation.

Table 6-1 defines symbols which are repeated throughout this analysis.

6.3.1 Guidance Law

The guidance law selected for analysis is patterned after one which was first encountered at the Ames Research Center during a visit to this center. A working paper describing the technique was obtained from Ames and used as a basis for the guidance technique finally settled upon. Before discussing the differences between the Ames approach and the model to be analyzed here, it would be best to explain why this particular system was chosen, and also how it functions.

The guidance capabilities of the selected system are such that it comes closest to fulfilling the criteria suggested for guidance law selection in Section 6.2. It is a guidance technique with a broad range of application; and it is capable of correcting large, known deviations from the nominal trajectory.

In regard to the generality of the guidance technique, it can be used in conjunction with both manned and unmanned landing vehicles, it will function using input data from inertial sensors such as accelerometers, or environmental sensors, e.g. radar that observe position and velocity relative to the vehicle surroundings. Ames found that the guidance technique as they were studying it was capable of placing the landing vehicle within a final position box whose demensions were ±152 meters (500 ft.) in altitude and ±304 meters (1000 ft.) in range if the initial deviations from the nominal were within ±7.6 KM (25,000 ft.) in altitude and ±15.2 KM (50,000 ft.) in range. The maximum increase in fuel consumption for this capability was found to be around 10 percent. For more information concerning the performance capabilities of this system, see reference 6-1.

In essence, the guidance law may be described as follows. (See Figure 6-1 for block diagram). The position and velocity of the vehicle are observed at a certain time. During the descent to hover phase of the landing operation, time is referenced to the time of thrust initiation which is allowed to be zero. The vehicle state variables computed from the observed data are compared with the state variables which would exist at the same time if the vehicle were on the nominal trajectory. The results of these comparisons are observed deviations from the nominal case. On the basis of observed deviations the guidance system computes corrections to the nominal thrust magnitude and direction values. Ideally, the new thrust parameters are just sufficient to reduce final position deviations to zero if no other corrections are made throughout the landing maneuver. Practically this is not strictly true because the corrections are based on equations linearized around the nominal trajectory and the presence of linearization errors will mean that the computed corrections are not quite correct. For large initial deviations from the nominal, linearization errors may become appreciable. Nevertheless, the thrust corrections are in the proper direction. The vehicle is therefore forced to move closer to the nominal trajectory, and as a consequence the linearization errors are continually reduced.

Through analog simulation, Ames has found that positive initial deviations from the nominal result in positive final deviations. This implies that the actual trajectories flown by this guidance law never cross the nominal trajectory.

In fact, a trajectory not subjected to the effects of random observation and thrust errors will still exhibit small deviations from the nominal at the final time. Thus, for any arbitrary trajectory with initial deviations from the nominal trajectory, the mean values of final error distributions are

not zero. Rather, they are equal to the final deviations which would exist if no random errors were present. Only the ensemble mean values, over all possible trajectories, are zero. There is at least one way to avoid the above condition. That is to add some "over control" to the guidance system. The computed thrust commands are multiplied by a constant, K_c, which is greater than one. The intent is to compensate for the fact that the corrections computed from the linearized technique of the guidance system are too small. The effect is to drive the actual trajectory back to the reference trajectory before the nominal end conditions are reached. The magnitude of K_c could be determined from a simulation analysis such as performed by Ames. K_c must be large enough to insure that the actual trajectory will intersect the nominal; and small enough so that control oscillations about the nominal trajectory are damped out quickly.

Guidance terms relating observed deviations from the nominal and time to thrust deviations are stored in the guidance computer, and used to compute thrust correction commands. These guidance terms are determined through the use of equations adjoint to the dynamic perturbation equations as explained in Appendix III-A.

The nominal values of state variables describing landing vehicle position and velocity vs. time along the reference trajectory are also stored in the guidance computer. The following state variables are used throughout this analysis.

1) h = The altitude above a reference sphere with radius equal to lunar radius at the landing site,

2) θ = The angular displacement of the vehicle from the landing site measured in the plane of motion with the origin of the angle at the moon's center,

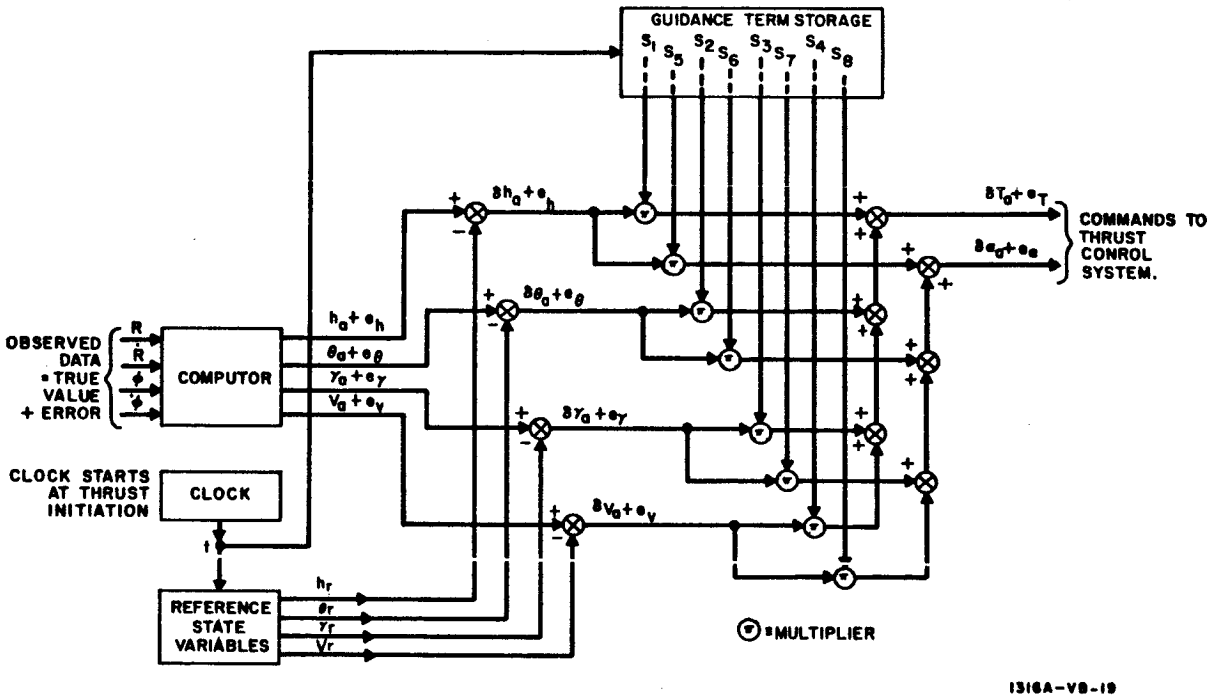

FIGURE 6-1: Block Diagram of Guidance System Analytical Model

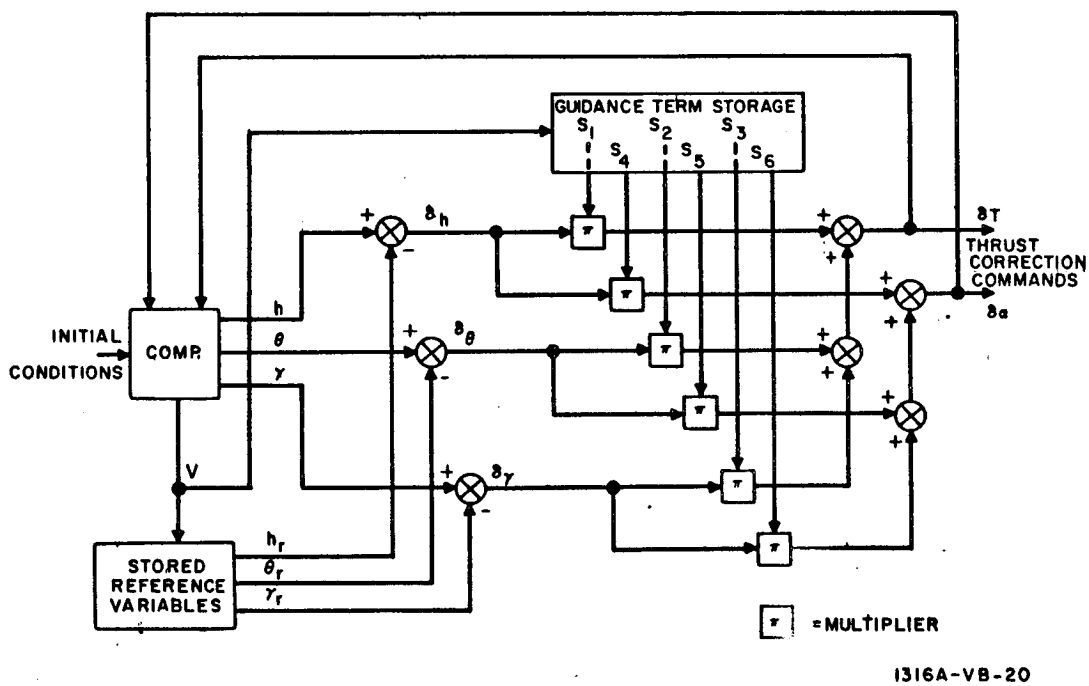

FIGURE 6-2: Block Diagram of Guidance System Analyzed By Ames Research Laboratory

3) γ = The angle between local horizontal and the vehicle's velocity vector measured in the plane of motion

4) V = The magnitude of the velocity vector

For a mathematical description of the guidance system, see Appendix III-A.

There are two points of difference between the system described by a working paper obtained from Ames and the system as it was analyzed during this study. (See Figure 6.2 for a block diagram of the Ames' system.) The Ames approach allowed velocity to be the independent variable and stored the reference variables h_r, θ_r, and γ_r and the guidance terms S_1 through S_6 as functions of velocity. The advantage of the Ames approach is that it reduces storage requirements in the guidance computer. The disadvantage is that it allows the reference quantities h_r, θ_r, and γ_r; and also the guidance terms to become random variables because they are determined as functions of the random variable V. It was decided, therefore, to use time as the independent variable, and to assume that the reference clock introduces no error. This prevents the stored quantities from taking on any random properties. There is implied in this change of independent variable a subtle change in the nature of the guidance law. The Ames approach produced what might be referred to as a fixed velocity at arrival system. That is, the thrust corrections are computed such that the position and velocity deviations from nominal will be reduced to zero when the vehicle velocity is zero. Time is not constrained to be the same as nominal flight time at this point. The changeover to time as the independent variable produces a fixed time of arrival guidance law in which commands are computed on the basis of reducing position errors to zero for time equal to the nominal final time with no explicit constraint on final velocity.

The second alteration to the system being studied by Ames involves the method of determining the values of the state variables. Ames computes the initial command on the basis of the best available estimate of initial conditions. Thereafter the thrust deviation commands are fed back into a computer containing the equations of motion where updated values of h, θ, γ, and V are computed based on the estimated initial conditions and commanded thrust levels. This model is adequate for demonstration of the guidance technique where perfect knowledge of initial conditions and perfect thrust control can be assumed. However, for error analysis where initial uncertainties and thrust control mechanization are important sources of error this approach did not appear to be the most appropriate model. The model analyzed here makes use of sensed data from which the state variables can be computed.

Through the use of observed data rather than values of state variables which are based on the integration of initial condition estimates, a possible source of large final position uncertainties is eliminated. Essentially, the guidance technique that will be analyzed treats each set of simultaneous observations as a new set of initial conditions and computes a set of thrust corrections based on the latest information. Thus, the initial state uncertainties do not remain as constant bias errors over the entire landing trajectory, but rather are only the random errors on the first set of observations. Each set of observations will include a different and independent set of random errors. Therefore, a source of constant error over the flight has been eliminated and replaced by a source of random error. Over the ensemble of all possible flights the mean squared value of the final errors will be much smaller for the case of continuous observation if the initial state variable uncertainties are considered to be approximately the same for each technique.

6.3.2 Reference Trajectory

It was pointed out in Section 6.3.1 that the guidance law selected requires the determination of a nominal trajectory. The values of h, θ, γ, V, and the eight guidance terms stored in the guidance computer are calculated beforehand, based on the nominal path. It was decided to use the same class of trajectory selected by Ames, namely a constant thrust, gravity turn from periselene of a descent orbit to a hovering state a small distance above the lunar surface. There are several reasons for selecting this type of trajectory. These include:

1) Continuous thrust is selected over impulsive thrust because the use of a two or three impulse landing scheme would imply high acceleration levels and large engines. The use of large engines would incur a weight penalty over the smaller engines required for a continuous thrust trajectory. Furthermore, continuous thrust does not demand the shutdown and re-start capabilities of a multiple impulse landing trajectory,
2) A constant or approximately constant thrust level provides the minimum engine size, and minimizes throttling during the descent trajectory,
3) A gravity turn trajectory is near optimum from the standpoint of fuel consumption because the thrust is always in the direction to reduce the velocity most effectively,
4) The gravity turn trajectory automatically rotates the vehicle to the proper hovering attitude during the descent so that no last second, high rate rotations are required.

Since knowledge of nominal trajectory parameters is required for the error analysis, a computer program was developed to provide the necessary

information. Given initial values of vehicle velocity (V_o), attitude (γ_o), and altitude (h_o), this program computes the initial value of angular displacement from the landing site (θ_o) and the thrust level (T_o) required to produce a hover state directly over the nominal landing site at an altitude of 500 meters.

The method of this program is to assume a complete set of initial conditions, integrate the equations forward in time until $V = 0$, and compare the computed values of h_f and γ_f corresponding to $V = 0$ with the desired nominal values of h_f and γ_f which are 500 meters and -90° respectively. This computed deviation from nominal hover conditions provides information helpful in determining changes to be made in the assumed initial conditions before making the next run through the trajectory.

The general equations of motion used for the nominal trajectory determination program are:

$$\text{(a)} \quad \dot{h} = V \sin \gamma$$

$$\text{(b)} \quad \dot{\theta} = -\frac{V}{r_o + h} \cos \gamma$$

$$\text{(c)} \quad \dot{V} = -\frac{T \cos \alpha}{\left(m_o - \int_{t_o}^{t} kT \, dt\right)} - \frac{\mu}{(r_o + h)^2} \sin \gamma$$

$$\text{(d)} \quad \dot{\gamma} = \frac{V \cos \gamma}{(r_o + h)} - \frac{T \sin \alpha}{V\left(m_o - \int_{t_o}^{t} kT \, dt\right)} - \frac{\mu \cos \gamma}{V(r_o + h)^2}$$

where h, θ, V, and γ have been defined previously, and:

$r_o \equiv$ radius of reference lunar sphere.

$T \equiv$ thrust vector magnitude

$\alpha \equiv$ angle between vehicle velocity vector and thrust vector

$m_o \equiv$ vehicle mass at time of landing trajectory initiation

$k \equiv$ constant of proportionality, relating instantaneous thrust vector magnitude to instantaneous mass rate of flow.

$\mu \equiv$ gravitational constant of the moon.

For the ideal, nominal constant thrust, gravity turn trajectory,

$$T = T_o = \text{a constant}$$

and,

$$\alpha = 0$$

along the nominal path. Substituting these values into the equations of motion produces the following set of expressions:

(a) $\dot{h} = V \sin \gamma$

(b) $\dot{\theta} = \dfrac{-V}{(r_o + h)} \cos \gamma$

(c) $\dot{V} = -\dfrac{T_o}{m_o - kT_o t} - \dfrac{\mu \sin \gamma}{(r_o + h)^2}$

(d) $\dot{\gamma} = \dfrac{V \cos \gamma}{r_o + h} - \dfrac{\mu \cos \gamma}{V(r_o + h)^2}$

These are the equations mechanized in the trajectory determination program.

There are three classes of outputs directly available from the program. First are the nominal initial values of T_o and θ required to produce the desired hover condition from the given initial values of h, γ, and V. Secondly, values of the state variables h, θ, γ, and V can be printed out at any desired time intervals along the flight path. Finally, two matrices of partial derivatives, relating deviations in state variable derivatives to deviations in the state variables, and to deviations in the thrust control quantities; may be printed out at specified time intervals along the trajectory.

If the operator δ is used to represent a deviation in the value of the parameter on which it operates, the matrices of partial derivatives mentioned above are contained in the following matrix equation;

$$\begin{bmatrix} \delta\dot{h} \\ \delta\dot{\theta} \\ \delta\dot{\gamma} \\ \delta\dot{V} \end{bmatrix} = \begin{bmatrix} \frac{\partial\dot{h}}{\partial h} & \frac{\partial\dot{h}}{\partial\theta} & \frac{\partial\dot{h}}{\partial\gamma} & \frac{\partial\dot{h}}{\partial V} \\ \frac{\partial\dot{\theta}}{\partial h} & \frac{\partial\dot{\theta}}{\partial\theta} & \frac{\partial\dot{\theta}}{\partial\gamma} & \frac{\partial\dot{\theta}}{\partial V} \\ \frac{\partial\dot{\gamma}}{\partial h} & \frac{\partial\dot{\gamma}}{\partial\theta} & \frac{\partial\dot{\gamma}}{\partial\gamma} & \frac{\partial\dot{\gamma}}{\partial V} \\ \frac{\partial\dot{V}}{\partial h} & \frac{\partial\dot{V}}{\partial\theta} & \frac{\partial\dot{V}}{\partial\gamma} & \frac{\partial\dot{V}}{\partial V} \end{bmatrix} \begin{bmatrix} \delta h \\ \delta\theta \\ \delta\gamma \\ \delta V \end{bmatrix} + \begin{bmatrix} \frac{\partial\dot{h}}{\partial T} & \frac{\partial\dot{h}}{\partial\alpha} \\ \frac{\partial\dot{\theta}}{\partial T} & \frac{\partial\dot{\theta}}{\partial\alpha} \\ \frac{\partial\dot{\gamma}}{\partial T} & \frac{\partial\dot{\gamma}}{\partial\alpha} \\ \frac{\partial\dot{V}}{\partial T} & \frac{\partial\dot{V}}{\partial\alpha} \end{bmatrix} \begin{bmatrix} \delta T \\ \delta\alpha \end{bmatrix}$$

If the deviations δh, $\delta\theta$, $\delta\gamma$, and δV are allowed to equal $\delta\xi_1$, $\delta\xi_2$, $\delta\xi_3$, and $\delta\xi_4$ respectively, the matrix expression can be written more compactly as

$$\left[\delta\dot{\xi}_i\right] = \left[A_{ij}\right]\left[\delta\xi_j\right] + \left[B_{ij}\right]\begin{bmatrix} \delta T \\ \delta\alpha \end{bmatrix}$$

where

$$A_{ij} \equiv \frac{\partial\dot{\xi}_i}{\partial\xi_j}$$

and

$$B_{ij} \equiv \left.\frac{\partial\dot{\xi}_i}{\partial T}\right|_{j=1} ; \quad \left.\frac{\partial\dot{\xi}_i}{\partial\alpha}\right|_{j=2}$$

This is a linearized relationship which is valid only in a small region near the trajectory on which the partial derivatives are computed.

To determine the nominal trajectory that was used during the remainder of this study the following fixed initial and final conditions were set into the computer program.

h_o = 20.0 Km

γ_o = 0.0 rad.

V_o = 1752 m/sec.

t_o = 0.0 sec.

h_f = 500 m

V_f = 0.0 m/sec.

γ_f = $-\pi/2$ rad.

θ_f = 0.0 rad.

The following values were used for the various constants required by the program.

m = 11,340 kg

μ = $0.489820 \times 10^{13} \frac{m^3}{sec^2}$

r_o = 1739 Km (mean lunar radius)

$k = 2.54929 \times 10^{-4}$ sec/m

(based on I_{sp} of 400 sec.)

The remaining initial and final values of the state variables as determined by the computer are:

T_o = 48,061 Newtons

θ_o = 0.18028 rad.

t_f = 346.52 sec.

Some of the pertinent characteristics of the reference trajectory are plotted in figures 6-3 through 6-6.

6.3.3 Observables

It was mentioned in Section 6.3.1 that one of the differences between the Ames guidance technique and the one under investigation here pertains to the method of updating state variable information. Ames uses initial conditions, computed thrust commands, and integration to compute state variables during the landing trajectory. The modified system being analyzed in this report uses direct measurement of environmental observables as a source of

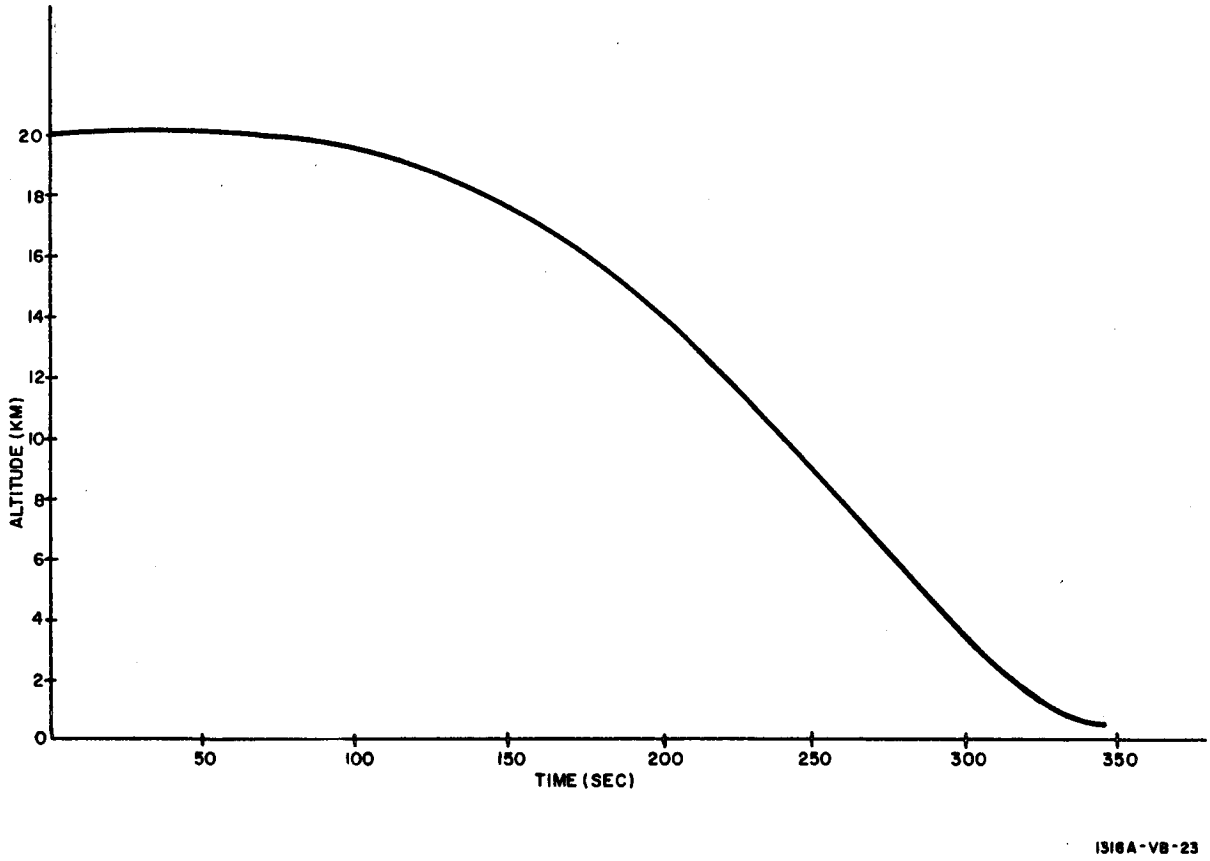

FIGURE 6-3: Reference Trajectory: Altitude vs. Time

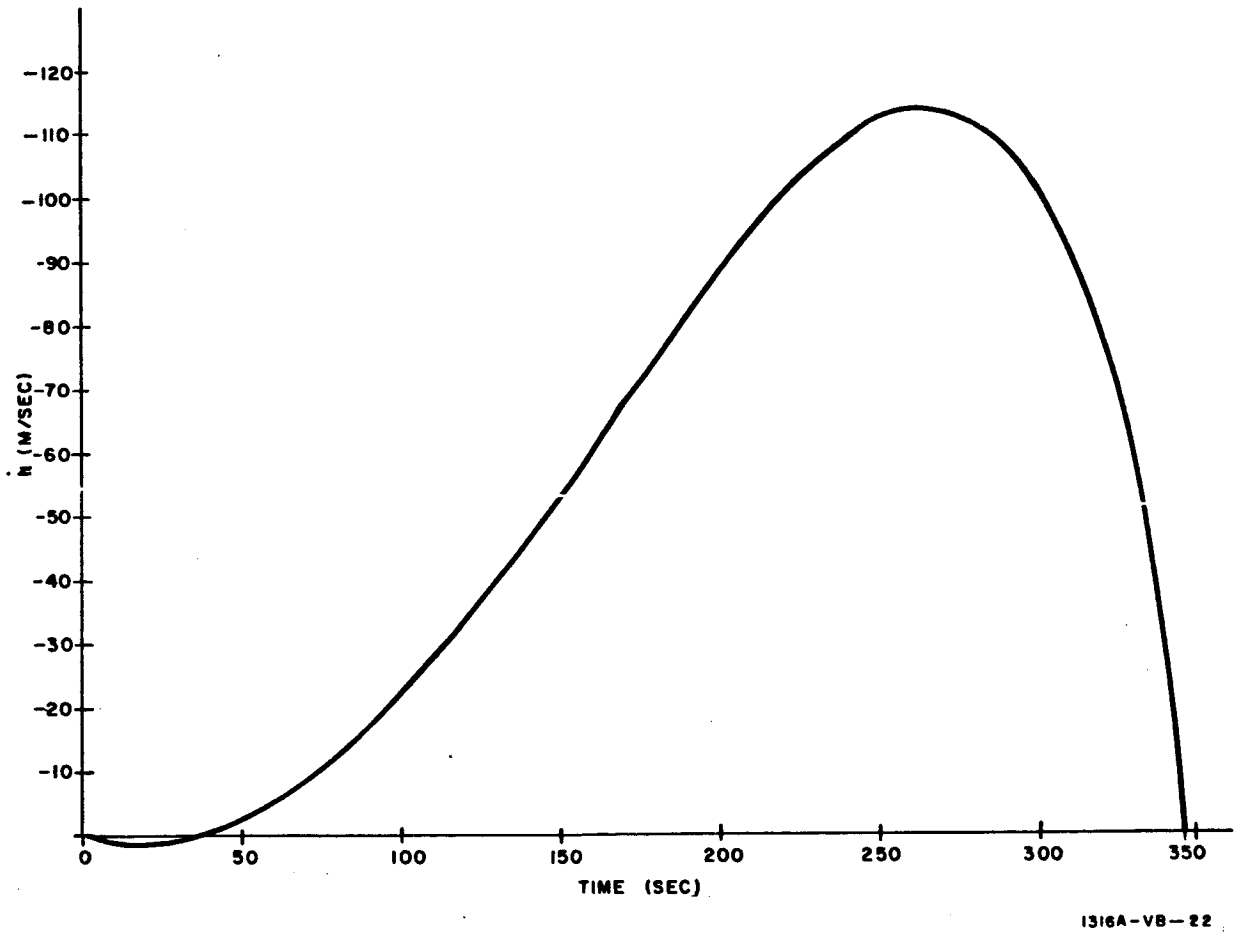

FIGURE 6-4: Reference Trajectory: Altitude Rate vs. Time

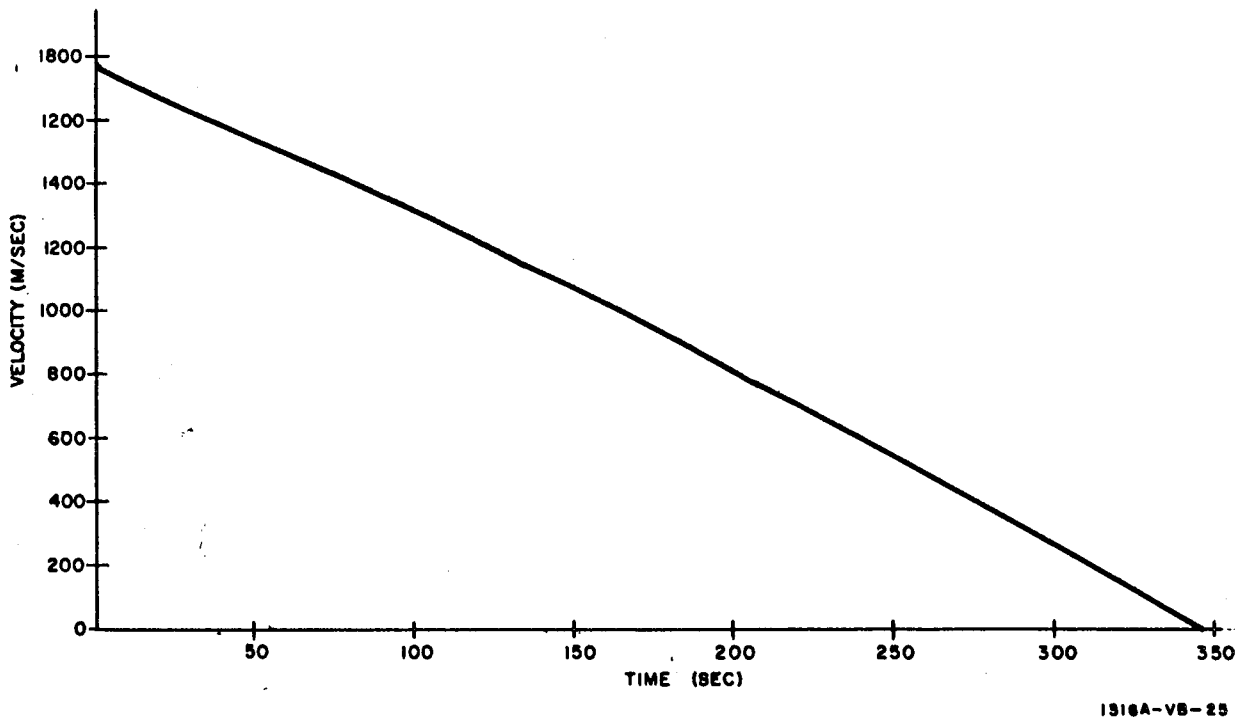

FIGURE 6-5: Reference Trajectory: Velocity vs. Time

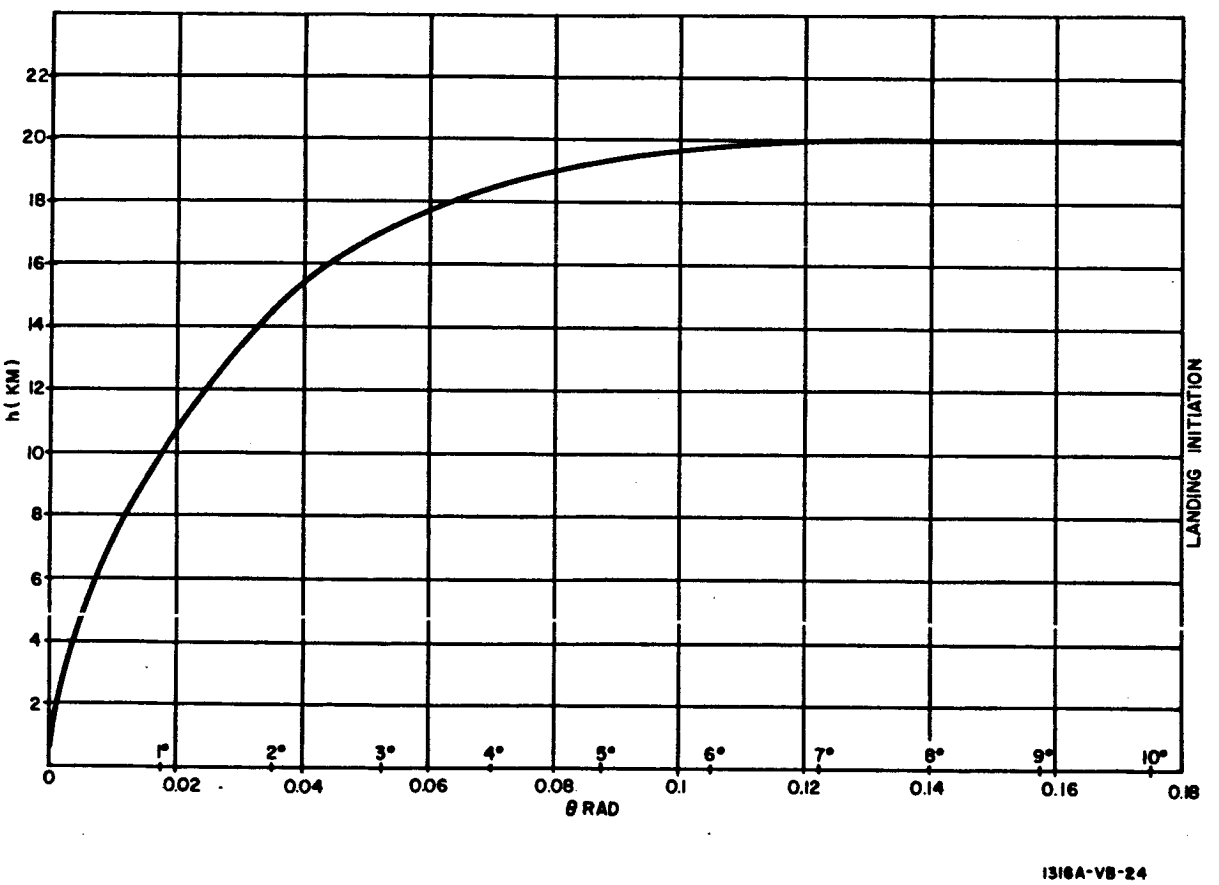

FIGURE 6-6: Reference Trajectory: Altitude vs Angular Displacement from Landing Site

state variable information. The advantage of this modification has been discussed previously.

To function, this approach requires the selection of a set of observables from which the state variables can be computed. A list of the possible observables includes:

(a) altitude = h

(b) Altitude rate = $\dot{h}$

(c) Range to a surface beacon or landmark = R

(d) Range rate to a surface beacon or landmark = $\dot{R}$

(e) Angle between local vertical and the line-of-sight to a surface landmark or beacon = ϕ

(f) Angular rate of line-of-sight to a surface landmark or beacon = $\dot{\phi}$

(g) Acceleration in three mutually perpendicular axes

(h) Vehicle velocity relative to the lunar surface (three mutually perpendicular components).

The angular observables imply that the direction of local vertical is available. In practice, local vertical is an observed quantity which is therefore subject to observational error. However, in this analysis, local vertical will be treated as a known quantity and any measurement errors associated with the determination of local vertical will be lumped with measurement errors associated with the observable angle (ϕ).

The combination of observables that seem particularly desirable for advanced missions includes range, range rate, line-of-sight angle, and angular rate to a point on the surface. (See Figure 6-7 for geometrical relationships). Range to a single point of the surface of the moon seems preferable to an altitude measurement, because it requires less apriori knowledge of surface selenography. By using line-of-sight range, instantaneous altitude can be referenced

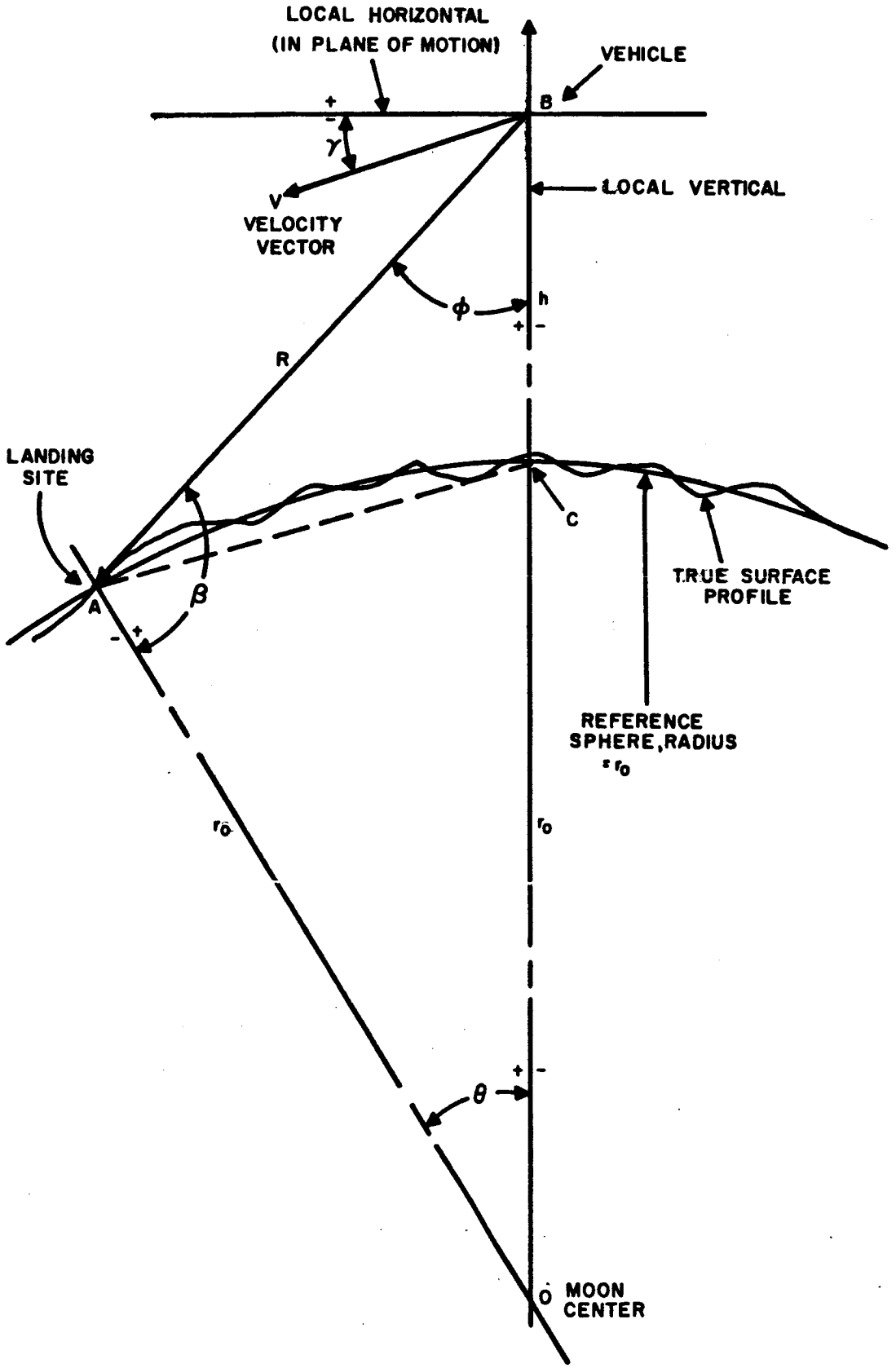

FIGURE 6-7: Landing Geometry - Illustrating Observable Quantities

This page intentionally left blank

to the lunar radius at the landing site, whereas, direct altitude measurements would require topographical knowledge over a large region surrounding the landing site to prevent the injection of additional uncertainty errors which may exhibit a high degree of correlation.

It is shown in Appendix III-A that the observables R, $\dot{R}$, ϕ and $\dot{\phi}$ provide sufficient information to calculate the state variables h, θ, γ, and V for the case of a beacon or landmark at the chosen landing site.* With this restriction, the equations relating the state variables to the observables are:

$$\text{(a)} \quad h = R \cos \phi - r_o + (r_o^2 - R^2 \sin^2 \phi)^{\frac{1}{2}}$$

$$\text{(b)} \quad \theta = \sin^{-1} \left(\frac{R}{r_o} \sin \phi\right)$$

$$\text{(c)} \quad \gamma = \phi - \frac{\pi}{2} + \tan^{-1} \frac{R(\dot{\phi} + \dot{\theta})}{\dot{R}}$$

$$\text{(d)} \quad V = \left[\dot{R}^2 + R^2 (\dot{\phi} + \dot{\theta})^2\right]^{\frac{1}{2}}$$

where:

$$\dot{\theta} = \frac{R \dot{\phi} \cos \phi + \dot{R} \sin \phi}{(r_o^2 - R^2 \sin^2 \phi)^{\frac{1}{2}}}$$

These expressions will be used throughout the remainder of this report, and represent the computed values of the state variables.

---

* If the angle ϕ is split into azimuth and elevation components, enough information is available for generalized placement of the surface feature.

6.4 Analytical Techniques Description or Analytical Plan

With the preliminary analysis of section 6.3 completed, it is possible to proceed to the actual error analysis which is the principal product of this effort. Section 6.4.1 presents a description of the analytical approach and the techniques that have been used to determine the effects of sensor errors. Following that, section 6.4.2 covers the application of the analytical techniques to the guidance system selected for study. Derivations have been restricted to the several appendices, with only procedures and resulting equations appearing in the text.

6.4.1 Discussion of Available Analytical Technique

The guide lines used to determine the analytical approach were described in section 6.2. The most accurate analysis would be a simulation of the guidance and control system. A multitude of simulated landings together with Monte Carlo statistical methods would be necessary to produce statistical estimates of sensor requirements. To set up a simulation, two preliminary computer programs are required--one to determine nominal trajectory, and initial state conditions, and a second to compute the eight guidance terms (S_1, S_2,... S_8) as time functions along the nominal flight path. Simulation of the landing phase would be considerably more complicated than the simulation of the orbital phase that has been developed (section 5). The principal complication is introduced by the continuous thrust condition which makes it impossible to determine end point errors as functions of initial errors alone. It is also not possible to continually improve estimates of end conditions through data processing of redundant measurements as is done in the midcourse and orbital mission phases, because the vehicle no longer remains in a single orbit.

As an alternative to a simulation analysis, linearization techniques are available. These are based on an assumption pertaining to the evaluation of partial derivatives in the neighborhood of a known point.

Let,

$$y = f(x_1, x_2, x_3, \ldots, x_n) = f(x_i) \qquad (6.4.1)$$

where the x_i variables are implicit functions of time. If the nominal value of y at some particular instant is y_o and the nominal value of x_i is denoted by x_{io}, then

$$y_o = f(x_{io}) \qquad (6.4.2)$$

A linearized analysis is based on the assumption small deviation of the x_i variables away from the nominal values will cause a small deviation in y that may be approximated by the expression:

$$\delta y \equiv y - y_o \doteq \sum_{i=1}^{n} \left(\frac{\partial y}{\partial x_i} \bigg|_{x_{io}} \right) \left(\delta x_i \right) \qquad (6.4.3)$$

$$\delta x_i \equiv x_i - x_{io}$$

Notice that the indicated partial derivatives are evaluated with the x_i variables taking on their nominal values.

It was determined that an error analysis using linearization techniques would be much faster than a simulation approach; also it is extremely flexible, allowing changes to be made in sensor capabilities, trajectory characteristics and observables with only minor alterations of the computer programs involved. The computer programs required are essentially the same two required as preliminary steps in a simulation analysis. Furthermore, the simpler and faster linearized analysis is a logical and valuable step in the

development of an efficient simulation program.

In the light of the preceding statements, a linearized approach seemed most in line with the considerations of section 6.2, and it was decided to pursue a linearized analysis.

6.4.2 Analysis

The analysis divides conveniently into two parts. The first is concerned with the propagation of observation errors through the guidance system to the thrust correction commands. The second part of the analysis relates to the effect of thrust command errors and thrust mechanization errors on final values of position and velocity.

6.4.2.1 Propagation of Observation Errors Through Guidance System

The first step in the linearized analysis is to develop relationships between the instantaneous thrust command errors, and the observation errors which cause them. The thrust correction commands are calculated from the computed state variables, the stored state variables, and the stored guidance terms S_1 through S_8. The correction commands are computed from the following equations:

$$\delta\Gamma = S_1\,\delta h + S_2\,\delta\theta + S_3\,\delta\gamma + S_4\,\delta V \qquad (6.4\text{-}4a)$$

$$\delta\alpha = S_5\,\delta h + S_6\,\delta\theta + S_7\,\delta\gamma + S_8\,\delta V \qquad (6.4\text{-}4b)$$

where:

$$\delta h = h - h_r \qquad (6.4\text{-}5a)$$

$$\delta\theta = \theta - \theta_r \qquad (6.4\text{-}5b)$$

$$\delta\gamma = \gamma - \gamma_r \qquad (6.4\text{-}5c)$$

$$\delta V = V - V_r \qquad (6.4\text{-}5d)$$

The subscript r denotes reference values which are stored in the guidance computer as functions of time. All of the state variables are implicit functions of time. The computed value of a state variable is made up of two components: the actual value, denoted by the subscript "a" and an error term denoted by e_h, e_θ, e_γ, and e_V for the respective variables. Then:

$$h = h_a + e_h \tag{6.4-6a}$$

$$\theta = \theta_a + e_\theta \tag{6.4-6b}$$

$$\gamma = \gamma_a + e_\gamma \tag{6.4-6c}$$

$$V = V_a + e_V \tag{6.4-6d}$$

It follows that:

$$\delta h = \delta h_a + e_h = h_a - h_r + e_h \tag{6.4-7a}$$

$$\delta\theta = \delta\theta_a + e_\theta \tag{6.4-7b}$$

$$\delta\gamma = \delta\gamma_a + e_\gamma \tag{6.4-7c}$$

$$\delta V = \delta V_a + e_V \tag{6.4-7d}$$

The computed thrust deviation commands can be written as:

$$\delta T = \delta T_a + e_{Tc} = S_1 \left[\delta h_a + e_h\right] + S_2 \left[\delta\theta_a + e_\theta\right] + S_3 \left[\delta\gamma_a + e_\gamma\right] + S_4 \left[\delta V_a + e_V\right] \tag{6.4-8a}$$

$$\delta\alpha = S\alpha_a + e_{\alpha c} = S_5 \left[\delta h_a + e_h\right] + S_6 \left[\delta\theta_a + e_\theta\right] + S_7 \left[\delta\gamma_a + e_\gamma\right] + S_8 \left[\delta V_a + e_V\right] \tag{6.4-8b}$$

where:

e_{Tc} = computed error in the thrust magnitude command

$e_{\alpha c}$ = computed error in the thrust orientation command

$$e_{Tc} = S_1 e_h + S_2 e_\Theta + S_3 e_\gamma + S_4 e_V \qquad (6.4\text{-}9a)$$

$$e_{\alpha c} = S_5 e_h + S_6 e_\Theta + S_7 e_\gamma + S_8 e_V \qquad (6.4\text{-}9b)$$

If h, Θ, γ, and V were measured directly, the expressions for e_{Tc} and $e_{\alpha c}$ would complete the first part of the analysis. In general, however, these quantities cannot be observed directly, but rather must be computed from other observed variables. For this analysis it is assumed that the variables R, $\dot{R}$, ϕ and $\dot{\phi}$ as defined in section 6.3.3 are the observable quantities. Before determining expressions for e_h, e_Θ, e_γ, and e_V it is first necessary to relate the state variables to the observables.

$$h = f_1 (R, \dot{R}, \phi, \dot{\phi}) \qquad (6.4\text{-}10a)$$

$$\Theta = f_2 (R, \dot{R}, \phi, \dot{\phi}) \qquad (6.4\text{-}10b)$$

$$\gamma = f_3 (R, \dot{R}, \phi, \dot{\phi}) \qquad (6.4\text{-}10c)$$

$$V = f_4 (R, \dot{R}, \phi, \dot{\phi}) \qquad (6.4\text{-}10d)$$

The functions F_1, F_2, F_3, and F_4 derived in Appendix III-B are presented in Section 6.3.3. They are restated below for convenience.

$$h = R \cos \phi - r_o + \left(r_o^2 - R^2 \sin^2 \phi\right)^{\frac{1}{2}} \qquad (6.4\text{-}11a)$$

$$\Theta = \sin^{-1} \left(\frac{R \sin \phi}{r_o} \right) \qquad (6.4\text{-}11b)$$

$$\gamma = \phi - \frac{\pi}{2} + \tan^{-1}\left[\frac{R(\dot{\phi} + \dot{\theta})}{\dot{R}}\right] \tag{6.4-11c}$$

$$V = \left[\dot{R}^2 + R^2 \ (\dot{\phi} + \dot{\theta})^2\right]^{\frac{1}{2}} \tag{6.4-11d}$$

where

$$\dot{\theta} = \frac{R\dot{\phi}\cos\phi + \dot{R}\sin\phi}{\left[r_o^{\ 2} - R^2 \sin^2\phi\right]^{\frac{1}{2}}} \tag{6.4-11e}$$

With these expressions available, it is possible to proceed to the next step which is the linearization process. It is desired to develop expressions relating errors in the computed values of the state variables to the observation errors which caused them. The application of linearization techniques yields these relationships in a small region near the nominal trajectory.

$$\begin{bmatrix} e_h \\ e_\theta \\ e_\gamma \\ e_V \end{bmatrix} \doteq \begin{bmatrix} \frac{\partial F_1}{\partial R} & \frac{\partial F_1}{\partial \dot{R}} & \frac{\partial F_1}{\partial \phi} & \frac{\partial F_1}{\partial \dot{\phi}} \\ \frac{\partial F_2}{\partial R} & \frac{\partial F_2}{\partial \dot{R}} & \frac{\partial F_2}{\partial \phi} & \frac{\partial F_2}{\partial \dot{\phi}} \\ \frac{\partial F_3}{\partial R} & \frac{\partial F_3}{\partial \dot{R}} & \frac{\partial F_3}{\partial \phi} & \frac{\partial F_3}{\partial \dot{\phi}} \\ \frac{\partial F_4}{\partial R} & \frac{\partial F_4}{\partial \dot{R}} & \frac{\partial F_4}{\partial \phi} & \frac{\partial F_4}{\partial \dot{\phi}} \end{bmatrix} \begin{bmatrix} e_R \\ e_{\dot{R}} \\ e_\phi \\ e_{\dot{\phi}} \end{bmatrix} \tag{6.4-12}$$

All the partial derivatives are evaluated on the nominal trajectory. The equations for the 16 partial derivatives are given in Appendix III-B.

The thrust correction command errors can then be approximated by the matrix equations:

$$\begin{bmatrix} e_{Tc} \\ e_{\alpha c} \end{bmatrix} \doteq \begin{bmatrix} S_1 & S_2 & S_3 & S_4 \\ S_5 & S_6 & S_7 & S_8 \end{bmatrix} \begin{bmatrix} e_h \\ e_\theta \\ e_\gamma \\ e_V \end{bmatrix} \tag{6.4-13}$$

The S terms are defined in Appendix III-A. Substituting equation 6.4-12 into 6.4-13 and performing the indicated matrix multiplication yields a matrix expression of the following form.

$$\begin{bmatrix} e_{Tc} \\ e_{\alpha c} \end{bmatrix} \doteq \begin{bmatrix} K_1 & K_2 & K_3 & K_4 \\ K_5 & K_6 & K_7 & K_8 \end{bmatrix} \begin{bmatrix} e_R \\ e_{\dot{R}} \\ e_\phi \\ e_{\dot{\phi}} \end{bmatrix} \qquad (6.4\text{-}14)$$

The observation errors are assumed to be from independent populations displaying gaussian statistics. The mean value of e_R, $e_{\dot{R}}$, e_ϕ, and $e_{\dot{\phi}}$ are all assumed to be zero; and the mean squared values are σ_R^2, $\sigma_{\dot{R}}^2$, σ_ϕ^2, and $\sigma_{\dot{\phi}}^2$ respectively. Multiplication of a gaussian distributed random variable by a constant results in a second gaussian distributed random variable. The mean and mean squared values of the new distribution are related to those of the old distribution by the constant multiplier and its square respectively. Let e_1, be a gaussian random variable with mean value μ_1 and mean squared value σ_1. If

$$e_2 = Ke_1$$

then

$$\mu_2 = K\mu_1$$

and

$$\sigma_2^2 = K^2 \sigma_1^2$$

From equation (6.4-14)

$$e_{Tc} \doteq K_1 e_R + K_2 e_{\dot{R}} + K_3 e_\phi + K_4 e_{\dot{\phi}} \qquad (6.4\text{-}15a)$$

$$e_{\alpha c} \doteq K_5 e_R + K_6 e_{\dot{R}} + K_7 e_\phi + K_8 e_{\dot{\phi}} \qquad (6.4\text{-}15b)$$

Since the observation errors are assumed to be independent random variables with zero mean values, the mean values of e_{Tc} and $e_{\alpha c}$ are also zero and the mean squared values, σ^2_{Tc} and $\sigma^2_{\alpha c}$ respectively can be approximated by:

$$\sigma^2_{Tc} \doteq K_1^2 \sigma_R^2 + K_2^2 \sigma_{\dot{R}}^2 + K_3^2 \sigma_\phi^2 + K_4^2 \sigma_{\dot{\phi}}^2 \qquad (6.4\text{-}16a)$$

$$\sigma^2_{\alpha c} \doteq K_5^2 \sigma_R^2 + K_6^2 \sigma_{\dot{R}}^2 + K_7^2 \sigma_\phi^2 + K_8^2 \sigma_{\dot{\phi}}^2 \qquad (6.4\text{-}16b)$$

The thrust error statistical parameters σ^2_{Tc} and $\sigma^2_{\alpha c}$ will vary in magnitude during the landing maneuver, because the eight multiplying factors K_1 through K_8 and the statistical quantities describing the observation error distributions are functions that vary during the landing. The method of dealing with these time varying error distributions will be discussed in the next section.

6.4.2.2 <u>Propagation of Thrust Errors Along the Landing Trajectory</u>

The expressions generated in the last section by no means complete the error analysis. Determining the relationships between errors in the computed thrust commands and the observation errors is a necessary step toward the desired end point, but does not contribute much in itself. The desired end point, is a linearized expression relating the mean squared values of the position and velocity errors at the end of the landing trajectory to the mean squared values of the observation error distributions and the mean squared values of thrust errors introduced by the control system itself. These latter errors will be referred to as thrust mechanization errors, and denoted by:

e_{Tm} = Thrust magnitude mechanization error

$e_{\alpha m}$ = Thrust orientation mechanization error

The observation errors manifest themselves as thrust command errors at the output of the guidance system. There are then two sources of thrusting errors, one related to sensors, and one related to control system mechanization. The

total thrust error is equal to the sum of these two components.

$$e_T = e_{Tc} + e_{Tm} \tag{6.4-17a}$$

$$e_\alpha = e_{\alpha c} + e_{\alpha m} \tag{6.4-17b}$$

Rewriting the expressions for e_{Tc} and $e_{\alpha c}$ (egs. 6.4-15), including the time arguments which now become important yields;

$$e_{Tc}(t) \doteq K_1(t)\, e_R(t) + K_2(t)\, e_{\dot{R}}(t) + K_3(t)\, e_\phi(t) + K_4(t)\, e_{\dot{\phi}}(t) \tag{6.4-18a}$$

$$e_{\alpha c}(t) \doteq K_5(t)\, e_R(t) + K_6(t)\, e_{\dot{R}}(t) + K_7(t)\, e_\phi(t) + K_8(t)\, e_{\dot{\phi}}(t) \tag{6.4-18b}$$

Then the total thrust error expressions can be written as:

$$e_T(t) \doteq K_1(t)\, e_R(t) + K_2(t)\, e_{\dot{R}}(t) + K_3(t)\, e_\phi(t) + K_4(t)\, e_{\dot{\phi}}(t) + e_{Tm}(t) \tag{6.4-19a}$$

$$e_\alpha(t) \doteq K_5(t)\, e_R(t) + K_6(t)\, e_{\dot{R}}(t) + K_7(t)\, e_\phi(t) + K_8(t)\, e_{\dot{\phi}}(t) + e_{\alpha m}(t) \tag{6.4-19b}$$

The time variability of coefficients K_1 through K_8 and the observation error statistics cause the thrust error distribution to exhibit time varying statistics. Recalling that all the random error inputs are assumed to be independent and gaussian with zero mean values, the mean squared values of the thrust error distributions may be expressed as functions of time.

$$\sigma_T^2(t) \doteq K_1^2(t)\, \sigma_R^2(t) + K_2^2(t)\, \sigma_{\dot{R}}^2(t) + K_3^2(t)\, \sigma_\phi^2(t) + K_4^2(t)\, \sigma_{\dot{\phi}}^2(t) + \sigma_{Tm}^2(t) \tag{6.4-20a}$$

$$\sigma_\alpha^2(t) \doteq K_5^2(t)\, \sigma_R^2(t) + K_6^2(t)\, \sigma_{\dot{R}}^2(t) + K_7^2(t)\, \sigma_\phi^2(t) + K_8^2(t)\, \sigma_{\dot{\phi}}^2(t) + \sigma_{\alpha m}^2(t) \tag{6.4-20b}$$

These equations determine the instantaneous statistics of the thrust errors.

The procedure used to determine the final state error statistics can be described as follows. First, the landing trajectory is divided into small time segments which are numbered sequentially from zero to N. The ith segment is Δt_i seconds long, and the sum of all the small time segments is equal to the total time required by the nominal landing maneuver. It is assumed that the thrust error components and their statistics are constant over each Δt_i time segment, but independent of the errors existing in any other time segment, Δt_j.

Next, linearized expressions relating the constant thrust errors within a Δt_i time interval to the state variable errors resulting at the end of the interval are derived. The partial derivatives associated with the linearization process are evaluated on the nominal trajectory.

Finally, assuming that the thrust errors in each small time interval are statistically independent of the errors in each other interval implies that the final state variable errors which are the sum of all the small errors occurring in each time interval will have mean squared values which can be expressed as the sum of the mean squared errors of each interval.

The first step then is to determine the position and velocity errors in a small time interval that are caused by thrust errors. Thrust errors manifest themselves directly as acceleration errors. Therefore, thrust errors e_T and e_α can be related directly to errors in $\dot{V}$, $\ddot{h}$, and $\ddot{\theta}$ which are denoted $e_{\dot{V}}$, $e_{\ddot{h}}$, and $e_{\ddot{\theta}}$ respectively. The relationships are obtained by linearization about the nominal trajectory and may be expressed as:

$$e_{\dot{V}}(t) \doteq \frac{\partial \dot{V}}{\partial T}(t)\, e_T(t) + \frac{\partial \dot{V}}{\partial \alpha}(t)\, e_\alpha(t) \qquad (6.4\text{-}21a)$$

$$e_{\ddot{h}}(t) \doteq \frac{\partial \ddot{h}}{\partial T}(t)\, e_T(t) + \frac{\partial \ddot{h}}{\partial \alpha}(t)\, e_\alpha(t) \qquad (6.4\text{-}21b)$$

$$e_{\ddot{\theta}}(t) \doteq \frac{\partial \ddot{\theta}}{\partial T}(t)\, e_T(t) + \frac{\partial \ddot{\theta}}{\partial \alpha}(t)\, e_\alpha(t) \qquad (6.4\text{-}21c)$$

The partial derivatives are evaluated on the nominal trajectory. (Expressions for these partials are given in Appendix III-C). These acceleration errors are essentially constant over the small intervals of time Δt_i so that the position and velocity errors in the ith interval are:

$$e_{V_i} \doteq \left[\frac{\partial \dot{V}}{\partial T} e_T + \frac{\partial \dot{V}}{\partial \alpha} e_\alpha\right]_{t=t_i} \Delta t_i \qquad (6.4\text{-}22a)$$

$$e_{h_i} \doteq \left[\frac{\partial \ddot{h}}{\partial T} e_T + \frac{\partial \ddot{h}}{\partial \alpha} e_\alpha\right]_{t=t_i} \frac{(\Delta t_i)^2}{2} \qquad (6.4\text{-}22b)$$

$$e_{\theta_i} \doteq \left[\frac{\partial \ddot{\theta}}{\partial T} e_T + \frac{\partial \ddot{\theta}}{\partial \alpha} e_\alpha\right]_{t=t_i} \frac{(\Delta t_i)^2}{2} \qquad (6.4\text{-}22c)$$

where:

$$t_i \equiv \sum_{i=0}^{i=i} \Delta t_i$$

The final position and velocity errors are obtained by summing the errors in each interval:

$$e_{Vf} = \sum_{i=0}^{i=N} e_{V_i} \doteq \sum_{i=0}^{i=N} \Delta t_i \left[\frac{\partial \dot{V}}{\partial T} e_T + \frac{\partial \dot{V}}{\partial \alpha} e_\alpha\right]_{t=t_i} \qquad (6.4\text{-}23a)$$

$$e_{hf} = \sum_{i=0}^{i=N} e_{h_i} \doteq \sum_{i=0}^{i=N} \frac{(\Delta t_i)^2}{2} \left[\frac{\partial \ddot{h}}{\partial T} e_T + \frac{\partial \ddot{h}}{\partial \alpha} e_\alpha\right]_{t=t_i} \qquad (6.4\text{-}23b)$$

$$e_{\theta f} = \sum_{i=0}^{i=N} e_{\theta_i} \doteq \sum_{i=0}^{i=N} \frac{(\Delta t_i)^2}{2} \left[\frac{\partial \ddot{\theta}}{\partial T} e_T + \frac{\partial \ddot{\theta}}{\partial \alpha} e_\alpha\right]_{t=t_i} \qquad (6.4\text{-}23c)$$

The functions, $e_T(t)$ and $e_\alpha(t)$ can be expanded as per equations (6.4-19) to give functions relating final state errors to observation and thrust mechanization errors.

$$e_{Vf} \doteq \sum_{i=0}^{i=N} \Delta t_i \Big\{ \Big[\frac{\partial \dot{V}}{\partial T} K_1 + \frac{\partial \dot{V}}{\partial \alpha} K_5 \Big]_{t=t_i} e_R(t_i)$$
$$+ \Big[\frac{\partial \dot{V}}{\partial T} K_2 + \frac{\partial \dot{V}}{\partial \alpha} K_6 \Big]_{t=t_i} e_{\dot{R}}(t_i)$$
$$+ \Big[\frac{\partial \dot{V}}{\partial T} K_3 + \frac{\partial \dot{V}}{\partial \alpha} K_7 \Big]_{t=t_i} e_{\phi}(t_i)$$
$$+ \Big[\frac{\partial \dot{V}}{\partial T} K_4 + \frac{\partial \dot{V}}{\partial \alpha} K_8 \Big]_{t=t_i} \sigma_{\dot{\phi}}(t_i)$$
$$+ \Big[\frac{\partial \dot{V}}{\partial T} e_{Tm} + \frac{\partial \dot{V}}{\partial \alpha} e_{\alpha m} \Big]_{t=t_i} \Big\} \qquad (6.4\text{-}24a)$$

$$e_{hf} \doteq \sum_{i=0}^{i=N} \frac{(\Delta t_i)^2}{2} \Big\{ \Big[\frac{\partial \ddot{h}}{\partial T} K_1 + \frac{\partial \ddot{h}}{\partial \alpha} K_5 \Big]_{t=t_i} e_R(t_i)$$
$$+ \Big[\frac{\partial \ddot{h}}{\partial T} K_2 + \frac{\partial \ddot{h}}{\partial \alpha} K_6 \Big]_{t=t_i} e_{\dot{R}}(t_i)$$
$$+ \Big[\frac{\partial \ddot{h}}{\partial T} K_3 + \frac{\partial \ddot{h}}{\partial \alpha} K_7 \Big]_{t=t_i} e_{\phi}(t_i)$$
$$+ \Big[\frac{\partial \ddot{h}}{\partial T} K_4 + \frac{\partial \ddot{h}}{\partial \alpha} K_8 \Big]_{t=t_i} e_{\dot{\phi}}(t_i)$$
$$+ \Big[\frac{\partial \ddot{h}}{\partial T} e_{Tm} + \frac{\partial \ddot{h}}{\partial \alpha} e_{\alpha m} \Big]_{t=t_i} \Big\} \qquad (6.4\text{-}24b)$$

$$e_{\theta f} \doteq \sum_{i=0}^{i=N} \frac{(\Delta t_i)^2}{2} \Big\{ \Big[\frac{\partial \ddot{\theta}}{\partial T} K_1 + \frac{\partial \ddot{\theta}}{\partial \alpha} K_5 \Big]_{t=t_i} e_R(t_i)$$
$$+ \Big[\frac{\partial \ddot{\theta}}{\partial T} K_2 + \frac{\partial \ddot{\theta}}{\partial \alpha} K_6 \Big]_{t=t_i} e_{\dot{R}}(t_i)$$
$$+ \Big[\frac{\partial \ddot{\theta}}{\partial T} K_3 + \frac{\partial \ddot{\theta}}{\partial \alpha} K_7 \Big]_{t=t_i} e_{\phi}(t_i)$$
$$+ \Big[\frac{\partial \ddot{\theta}}{\partial T} K_4 + \frac{\partial \ddot{\theta}}{\partial \alpha} K_8 \Big]_{t=t_i} e_{\dot{\phi}}(t_i)$$
$$+ \Big[\frac{\partial \ddot{\theta}}{\partial T} e_{Tm} + \frac{\partial \ddot{\theta}}{\partial \alpha} e_{\alpha m} \Big]_{t=t_i} \Big\} \qquad (6.4\text{-}24c)$$

It is true that the mean squared value of a sum of independent variables is the sum of the mean squared values of the individual random variables. In general, this may be expressed as follows:

$$\sigma_y^2 = \overline{\Big[\sum_{i=0}^{i=N} k_i x_i \Big]^2} = \sum_{i=0}^{i=N} k_i^2 \sigma_{x_i}^2 \qquad (6.4\text{-}25)$$

The bar denotes mean value.

Applying equation 6.4-25 to the set of equations, 6.4-24, the following expressions emerge for the mean squared values of final position and velocity error distributions.

$$\sigma_{\dot{v}f}^2 \doteq \sum_{i=0}^{i=N} (\Delta t_i)^2 \Bigg\{ \left[\frac{\partial \dot{v}}{\partial T} K_1 + \frac{\partial \dot{v}}{\partial \alpha} K_5\right]^2_{t=t_i} \sigma_R^2(t_i) + \left[\frac{\partial \dot{v}}{\partial T} K_2 + \frac{\partial \dot{v}}{\partial \alpha} K_6\right]^2_{t=t_i} \sigma_{\dot{R}}^2(t_i) + \left[\frac{\partial \dot{v}}{\partial T} K_3 + \frac{\partial \dot{v}}{\partial \alpha} K_7\right]^2_{t=t_i} \sigma_{\phi}^2(t_i) + \left[\frac{\partial \dot{v}}{\partial T} K_4 + \frac{\partial \dot{v}}{\partial \alpha} K_8\right]^2_{t=t_i} \sigma_{\dot{\phi}}^2(t_i) + \left[\frac{\partial \dot{v}}{\partial T} \sigma_{Tm}\right]^2_{t=t_i} + \left[\frac{\partial \dot{v}}{\partial \alpha} \sigma_{\alpha m}\right]^2_{t=t_i} \Bigg\} \tag{6.4-26a}$$

$$\sigma_{hf}^2 \doteq \sum_{i=0}^{i=N} \frac{(\Delta t_i)^4}{4} \Bigg\{ \left[\frac{\partial \ddot{h}}{\partial T} K_1 + \frac{\partial \ddot{h}}{\partial \alpha} K_5\right]^2_{t=t_i} \sigma_R^2(t_i) + \left[\frac{\partial \ddot{h}}{\partial T} K_2 + \frac{\partial \ddot{h}}{\partial \alpha} K_6\right]^2_{t=t_i} \sigma_{\dot{R}}^2(t_i) + \left[\frac{\partial \ddot{h}}{\partial T} K_3 + \frac{\partial \ddot{h}}{\partial \alpha} K_7\right]^2_{t=t_i} \sigma_{\phi}^2(t_i) + \left[\frac{\partial \ddot{h}}{\partial T} K_4 + \frac{\partial \ddot{h}}{\partial \alpha} K_8\right]^2_{t=t_i} \sigma_{\dot{\phi}}^2(t_i) + \left[\frac{\partial \ddot{h}}{\partial T} \sigma_{Tm}\right]^2_{t=t_i} + \left[\frac{\partial \ddot{h}}{\partial \alpha} \sigma_{\alpha m}\right]^2_{t=t_i} \Bigg\} \tag{6.4-26b}$$

$$\sigma_{\theta f}^2 \doteq \sum_{i=0}^{i=N} \frac{(\Delta t_i)^4}{4} \Bigg\{ \left[\frac{\partial \ddot{\theta}}{\partial T} K_1 + \frac{\partial \ddot{\theta}}{\partial \alpha} K_5\right]^2_{t=t_i} \sigma_R^2(t_i) + \left[\frac{\partial \ddot{\theta}}{\partial T} K_2 + \frac{\partial \ddot{\theta}}{\partial \alpha} K_6\right]^2_{t=t_i} \sigma_{\dot{R}}^2(t_i) + \left[\frac{\partial \ddot{\theta}}{\partial T} K_3 + \frac{\partial \ddot{\theta}}{\partial \alpha} K_7\right]^2_{t=t_i} \sigma_{\phi}^2(t_i) + \left[\frac{\partial \ddot{\theta}}{\partial T} K_4 + \frac{\partial \ddot{\theta}}{\partial \alpha} K_8\right]^2_{t=t_i} \sigma_{\dot{\phi}}^2(t_i) + \left[\frac{\partial \ddot{\theta}}{\partial T} \sigma_{Tm}\right]^2_{t=t_i} + \left[\frac{\partial \ddot{\theta}}{\partial \alpha} \sigma_{\alpha m}\right]^2_{t=t_i} \Bigg\} \tag{6.4-26c}$$

If the mean squared values of the observation and mechanization errors are constant, so that these quantities can be removed from the summations, the following expressions result.

$$\sigma_{Vf}^2 \doteq \sigma_R^2 \sum_{i=0}^{N} (VP)_{1i} + \sigma_{\dot{R}}^2 \sum_{i=0}^{N} (VP)_{2i} + \sigma_{\phi}^2 \sum_{i=0}^{N} (VP)_{3i} + \sigma_{\dot{\phi}}^2 \sum_{i=1}^{N} (VP)_{4i} + \sigma_{Tm}^2 \sum_{i=0}^{N} (VP)_{5i} + \sigma_{\alpha m}^2 \sum_{i=0}^{N} (VP)_{6i} \qquad (6.4\text{-}27a)$$

$$\sigma_{hf}^2 \doteq \sigma_R^2 \sum_{i=0}^{N} (HP)_{1i} + \sigma_{\dot{R}}^2 \sum_{i=0}^{N} (HP)_{2i} + \sigma_{\phi}^2 \sum_{i=0}^{N} (HP)_{3i} + \sigma_{\dot{\phi}}^2 \sum_{i=0}^{N} (HP)_{4i} + \sigma_{Tm}^2 \sum_{i=0}^{N} (HP)_{5i} + \sigma_{\alpha m}^2 \sum_{i=0}^{N} (HP)_{6i} \qquad (6.4\text{-}27b)$$

$$\sigma_{\theta f}^2 \doteq \sigma_R^2 \sum_{i=0}^{N} (TP)_{1i} + \sigma_{\dot{R}}^2 \sum_{i=0}^{N} (TP)_{2i} + \sigma_{\phi}^2 \sum_{i=0}^{N} (TP)_{3i} + \sigma_{\dot{\phi}}^2 \sum_{i=0}^{N} (TP)_{4i} + \sigma_{Tm}^2 \sum_{i=0}^{N} (TP)_{5i} + \sigma_{\alpha m}^2 \sum_{i=0}^{N} (TP)_{6i} \qquad (6.4\text{-}27c)$$

Another common way of expressing observation error statistics is in terms of a percent of the quantity being observed. That is,

$$\sigma_x = \eta_x x \qquad \text{where } (\eta_x)(100) = \text{percent}$$

Then

$$\sigma_x^2 = \eta_x^2 x^2$$

Equations expressing final error mean square values would then be written as,

$$\sigma_{Vf}^2 \doteq \eta_R^2 \sum_{i=0}^{N} (VP)_{1i} R^2(t_i) + \eta_{\dot{R}}^2 \sum_{i=0}^{N} (VP)_{2i} \dot{R}^2(t_i) + \eta_{\phi}^2 \sum_{i=0}^{N} (VP)_{3i} \phi^2(t_i) + \eta_{\dot{\phi}}^2 \sum_{i=0}^{N} (VP)_{4i} \dot{\phi}^2(t_i) + \eta_{Tm}^2 \sum_{i=0}^{N} (VP)_{5i} T^2(t_i) + \eta_{\alpha m}^2 \sum_{i=0}^{N} (VP)_{6i} \alpha^2(t_i) \qquad (6.4\text{-}28a)$$

$$\sigma_{hf}^2 \doteq n_R^2 \sum_{i=0}^{N} (HP)_{1i} R^2(t_i) + n_{\dot{R}}^2 \sum_{i=0}^{N} (HP)_{2i} \dot{R}^2(t_i) + n_\phi^2 \sum_{i=0}^{N} (HP)_{3i} \phi^2(t_i)$$

$$+ n_{\dot{\phi}}^2 \sum_{i=0}^{N} (HP)_{4i} \dot{\phi}^2(t_i) + n_{Tm}^2 \sum_{i=0}^{N} (HP)_{5i} T^2(t_i) + n_{\alpha m}^2 \sum_{i=0}^{N} (HP)_{6i} \alpha^2(t_i) \qquad (6.4\text{-}28b)$$

$$\sigma_{\theta f}^2 \doteq n_R^2 \sum_{i=0}^{N} (TP)_{1i} R^2(t_i) + n_{\dot{R}}^2 \sum_{i=0}^{N} (TP)_{2i} \dot{R}^2(t_i) + n_\phi^2 \sum_{i=0}^{N} (TP)_{3i} \phi^2(t_i) \qquad (6.4\text{-}28c)$$

$$+ n_{\dot{\phi}}^2 \sum_{i=0}^{N} (TP)_{4i} \dot{\phi}^2(t_i) + n_{Tm}^2 \sum_{i=0}^{N} (TP)_{5i} T^2(t_i) + n_{\alpha m}^2 \sum_{i=0}^{N} (TP)_{6i} \alpha^2(t_i)$$

Combinations of equations 6.4-27 and 6.4-28 are also possible when certain of the error sources display constant statistical parameters and others show rms errors which are a percentage of the observable.

The values of $(VP)_{ji}$, $(HP)_{ji}$, and $(TP)_{ji}$ can be inferred by comparison with equations (6.4-26). For example:

$$(VP)_{ji}\Big|_{j=1} = \left\{ (\Delta t_i) \left[\frac{\partial \dot{V}}{\partial T} K_1 + \frac{\partial \dot{V}}{\partial \alpha} K_5 \right]_{t=t_i} \right\}^2 \qquad (6.4\text{-}29)$$

For the given guidance law, nominal trajectory and observables, the summations of equations 6.4-27 and 6.4-28, once computed, represent the linearized transformations between the input errors (caused by imperfect observation or mechanization) and the resulting position and velocity uncertainties at the end of the landing trajectory. The principal digital computer program developed for the landing analysis determines the values of these summations. This program and its capabilities are discussed in Section 6.5 and Appendix III-C.

6.5 Digital Program

This section presents a qualitative discussion of the digital computer program developed for the IBM 7094 in conjunction with the analysis discussed in Section 6.4. Items discussed include program inputs and available outputs, variations, and programming difficulties that were encountered. More technical aspects of the program are treated in Appendix III-C.

6.5.1 Qualitative Program Description

The only inputs required by the program are the final conditions of the nominal trajectory as determined from the preliminary trajectory program mentioned in Section 6.3. These values, along with pertinent astronomical constants are the only numbers which must be entered into the computer. By application of the equations of motion, equations adjoint to the equations of motion (see Appendix III-C), and the transformation equations outlined in Section 6.4, it is possible to compute the constants relating final state position and velocity error distributions to the observation and mechanization error statistics existing along the trajectory. The reason for using final trajectory values as inputs to the error analysis program is that backward integration along the nominal trajectory is required to compute the adjoint variables which in turn are required to determine the guidance terms S_1 through S_8 as defined in equations 21-17. Since the other integrals involved (see appendix III-A) and the summations specified in Section 6.4.2.2 can be calculated using either forward or backward steps of time, it was decided to compute everything by stepping back from the nominal final time of the landing trajectory. This approach offers considerably reduced storage requirements compared to a program which would compute and store the guidance terms

(S_1 to S_8) over the entire nominal trajectory and then compute the summation terms by stepping forward in time for landing trajectory initiation.

The principal outputs of this program, are the summations indicated in section 6.4.2.2. These are the quantities relating final errors to input error sources computed from a linearized analysis. It is also possible to find the contribution of any particular segment, or group of segments, to the overall summations. The ability to evaluate sums over portions of the trajectory makes it possible to observe the effect of changing sensor error statistics during the landing maneuver. This type of sensor accuracy alteration might be introduced by a scale change, for example.

Other quantities that are available from the program include the guidance terms, all the partial derivatives required for the linearized equations, the nominal values of state variables, and the adjoint variables at small intervals of time along the trajectory.

6.5.2 Program Flexibility

The summations representing the primary printout of the computer program used in this study, relate the statistical quantities describing final state errors to observation and mechanization errors. They are valid for only one combination of nominal trajectory, observables, and guidance law. The limitation to one combination is not inherent in either the analytical approach, or in the computer program. It could be modified to include additional combinations. Different constant thrust gravity turn reference trajectories can be handled with no modification to the existing program. Changing the nature of the reference trajectory would require some minor modifications. To change the set of observables used new functions relating

the new group of observables to the state variables and a new matrix of partial derivatives for the linearized error transfer expressions would have to be derived. These new transformation equations would replace the old ones in the program.

A change in guidance law would require extensive program modification. However, for many other guidance laws, the modification would be of simplifying nature. The guidance technique employing guidance terms computed with the aid of equations adjoint to the dynamic perturbation equations is one of the most complicated guidance laws to deal with analytically.

6.5.3 Program Mechanization Difficulties

There were no particular difficulties during the mechanization of this program.

6.6 Program Results

The primary results obtained from the computer program are the values of the error transformation summations derived in Section 6.4. These summations relate the mean squared values of the observation and mechanization errors to the mean squared errors in final position and velocity.

If σ_{ij}^2 denotes the mean squared error in the final value of the ith state variable, attributable to the jth error source; where i = 1, 2, 3 corresponds to final velocity, altitude and horizontal range errors respectively, and j = 1, 2, 3, 4, 5, 6 corresponds to (1) range observation, (2) range rate observation, (3) angle measurement (ϕ), (4) angle rate observation ($\dot{\phi}$), (5) thrust magnitude errors caused by mechanization, and (6) thrust orientation errors caused by mechanization imperfections. For example, σ_{24}^2 is the mean squared value of final altitude errors caused by errors in observing $\dot{\phi}$. Since all the error sources are assumed independent, the total final mean squared errors are:

$$\sigma_i^2 = \sum_{j=1}^{j=6} \sigma_{ij}^2$$

If the statistics of each error source are constant, $\sigma_{ij}^2 = K_{ij}^2 \sigma_j^2$ where σ_j^2 is the effective mean squared error of the jth error source and K_{ij}^2 is the appropriate error transformation summation determined from the computer program.* If the r.m.s. error in the jth error source is allowed to be a constant percentage of the observed or controlled quantity, a different set of equations result:

$$\sigma_{ij}^2 = (K'_{ij})^2 n_j^2$$

Where $(K'_{ij})^2$ is a modified error transformation coefficient and n_j^2 is the constant error percentage (expressed as a fraction of unity) squared. There are two options to the computer program — one computes the coefficients K_{ij}^2 and the second is a composite program which computes $(K'_{i1})^2$, $(K'_{i2})^2$, $(K_{i3})^2$, $(K'_{i4})^2$, $(K_{i5})^2$ and $(K_{i6})^2$. That is, r.m.s. errors in range, range rate, and angle rate measurements are taken to be a constant percent of the measured quantities; while errors in angle measurement and thrust mechanization are allowed to have constant statistics.

For the group of observables selected for analysis it was felt that range and range rate measurement errors would be best treated as having a constant percent of error, while the remaining error sources would exhibit error distributions with nearly constant statistical parameters over the landing trajectory. Therefore, values of the error transformation coefficients $(K_{i1})^2$ $(K_{i2})^2$ $(K_{i3})^2$ $(K_{i4})^2$ $(K_{i5})^2$ $(K_{i6})^2$ $(K'_{i1})^2$ $(K'_{i2})^2$ and $(K'_{i4})^2$ have been computed and appear in Table 6-2. The

---

* See Section 6.7.2.2 for a discussion of σ_j^2

square root of each coefficient is also presented. This quantity relates the r.m.s. value of any particular final error component to the r.m.s. error, or percent error, of the appropriate error source.

For the computer program, all of the small time intervals (Δt_i) were allowed to have equal length. The program was run with Δt_i equal to one second, two seconds, and three seconds. The meaning of this time interval, and the effects of variations in its length will be discussed in Section 6.7.

6.7 Discussion and Interpretation of Results

6.7.1 Presentation of Results and Example

To examine sensor and mechanization effects on the final values of the state variables, the error transformation coefficients were used to generate the curves shown in figures 6-8 through 6-13. These figures show the final position and velocity errors (rms) plotted against the rms observation and mechanization errors. As mentioned above, a composite of K_{ij} and K'_{ij} coefficients best represents the lunar landing situation. Figure 6-8 shows the r.m.s. values of final position and velocity errors resulting from range observation errors along the trajectory. The r.m.s. value of the range observation errors is equal to $\eta_1 \times 100$ percent of the range measurement at any point in the trajectory. As a typical example, if η_1 equals 0.01, (1%), the resulting position and velocity error components are:

Velocity error (rms) = 18.5 meters/sec.

Altitude error (rms) = 6.2 meters

Horizontal range error (rms) = 1.44 meters

TABLE 6-2 DIGITAL PROGRAM RESULTS

STATE VARIABLE AFFECTED	ERROR SOURCE	Δt_i = 1 sec.		Δt_i = 2 sec.		Δt_i = 3 sec.	
		K^2_{ij}	K_{ij}	K^2_{ij}	K_{ij}	K^2_{ij}	K_{ij}
FINAL VELOCITY	R OBSERVATION	1.38×10^{1}	3.72×10^{0}	1.35×10^{1}	3.68×10^{0}	1.46×10^{0}	1.21×10^{0}
	$\dot{R}$ OBSERVATION	6.31×10^{0}	2.52×10^{0}	7.02×10^{0}	2.63×10^{0}	5.93×10^{0}	2.44×10^{0}
	ϕ OBSERVATION	4.56×10^{5}	6.76×10^{2}	4.40×10^{5}	6.64×10^{2}	1.03×10^{5}	3.21×10^{2}
	$\dot{\phi}$ OBSERVATION	1.88×10^{6}	1.37×10^{3}	3.59×10^{6}	1.87×10^{3}	5.29×10^{6}	2.30×10^{3}
	T MECHANIZATION	4.30×10^{-6}	2.08×10^{-3}	8.58×10^{-6}	2.93×10^{-3}	1.28×10^{-5}	3.58×10^{-3}
	α MECHANIZATION	0.0	0.0	0.0	0.0	0.0	0.0
FINAL ALTITUDE	R OBSERVATION	1.49×10^{0}	1.22×10^{0}	1.88×10^{0}	1.37×10^{0}	1.80×10^{0}	1.34×10^{0}
	$\dot{R}$ OBSERVATION	5.01×10^{-1}	7.09×10^{-1}	1.67×10^{0}	1.29×10^{0}	3.09×10^{0}	1.76×10^{0}
	ϕ OBSERVATION	3.54×10^{4}	1.88×10^{2}	5.52×10^{4}	2.36×10^{2}	7.41×10^{4}	2.73×10^{2}
	$\dot{\phi}$ OBSERVATION	8.34×10^{7}	9.14×10^{3}	6.70×10^{8}	2.59×10^{4}	2.27×10^{9}	4.77×10^{4}
	T MECHANIZATION	9.59×10^{-8}	3.10×10^{-4}	7.49×10^{-7}	8.65×10^{-4}	2.40×10^{-6}	1.55×10^{-3}
	α MECHANIZATION	2.26×10^{3}	4.76×10^{1}	1.81×10^{4}	1.35×10^{2}	6.10×10^{4}	2.48×10^{2}
FINAL HORIZONTAL RANGE	R OBSERVATION	7.40×10^{-2}	2.72×10^{-1}	1.15×10^{-1}	3.40×10^{-1}	1.49×10^{-1}	3.86×10^{-1}
	$\dot{R}$ OBSERVATION	5.30×10^{-1}	7.28×10^{-1}	2.31×10^{0}	1.52×10^{0}	5.35×10^{0}	2.31×10^{0}
	ϕ OBSERVATION	5.33×10^{3}	7.30×10^{1}	1.01×10^{4}	1.00×10^{2}	1.62×10^{4}	1.28×10^{2}
	$\dot{\phi}$ OBSERVATION	1.34×10^{6}	1.16×10^{3}	9.53×10^{6}	3.09×10^{3}	3.06×10^{7}	5.54×10^{3}
	T MECHANIZATION	9.64×10^{-7}	9.82×10^{-4}	7.71×10^{-6}	2.78×10^{-3}	2.60×10^{-5}	5.10×10^{-3}
	α MECHANIZATION	2.21×10^{2}	1.49×10^{1}	1.73×10^{3}	4.16×10^{1}	5.52×10^{3}	7.44×10^{1}

$(K_{ij})^2$ relates final errors to error sources with constant statistical parameters.

$(K'_{ij})^2$ relates final errors to error sources with rms error expressed as a percentage of the observable.

TABLE 6-2: DIGITAL PROGRAM RESULTS (continued)

STATE VARIABLE AFFECTED	ERROR SOURCE	$\Delta t_i = 1$ sec.		$\Delta t_i = 2$ sec.		$\Delta t_i = 3$ sec.	
		$(K'_{ij})^2$	K'_{ij}	$(K'_{ij})^2$	K'_{ij}	$(K'_{ij})^2$	K'_{ij}
FINAL VELOCITY	R OBSERVATION	3.49×10^6	1.87×10^3	3.40×10^6	1.84×10^3	4.05×10^5	6.36×10^2
	$\dot{R}$ OBSERVATION	3.41×10^4	1.85×10^2	6.82×10^4	2.61×10^2	1.05×10^5	3.20×10^2
	ϕ OBSERVATION	-	-	-	-	-	-
	$\dot{\phi}$ OBSERVATION	1.30×10^2	1.14×10^1	2.56×10^2	1.60×10^1	3.68×10^2	1.92×10^1
	T MECHANIZATION	-	-	-	-	-	-
	α MECHANIZATION	-	-	-	-	-	-
FINAL ALTITUDE	R OBSERVATION	3.80×10^5	6.16×10^2	5.07×10^5	7.12×10^2	5.52×10^5	7.43×10^2
	$\dot{R}$ OBSERVATION	4.74×10^2	2.18×10^1	3.74×10^3	6.11×10^2	1.23×10^4	1.11×10^2
	ϕ OBSERVATION	-	-	-	-	-	-
	$\dot{\phi}$ OBSERVATION	1.22×10^2	1.10×10^1	9.77×10^2	3.12×10^1	3.30×10^3	5.74×10^1
	T MECHANIZATION	-	-	-	-	-	-
	α MECHANIZATION	-	-	-	-	-	-
FINAL HORIZONTAL RANGE	R OBSERVATION	2.06×10^4	1.44×10^2	4.51×10^4	2.12×10^2	9.04×10^4	3.05×10^2
	$\dot{R}$ OBSERVATION	8.55×10^3	9.24×10^1	6.84×10^4	2.62×10^2	2.31×10^5	4.81×10^2
	ϕ OBSERVATION	-	-	-	-	-	-
	$\dot{\phi}$ OBSERVATION	1.62×10^2	1.28×10^1	1.28×10^3	3.57×10^1	4.05×10^3	6.36×10^1
	T MECHANIZATION	-	-	-	-	-	-
	α MECHANIZATION	-	-	-	-	-	-

STATE VARIABLE NOTATION

$i = 1$: FINAL VELOCITY ERROR COMPONENT
$i = 2$: FINAL ALTITUDE ERROR COMPONENT
$i = 3$: FINAL HORIZONTAL RANGE ERROR COMPONENT

ERROR SOURCE NOTATION

$j = 1$: RANGE OBSERVATION
$j = 2$: RANGE RATE OBSERVATION
$j = 3$: ANGLE OBSERVATION
$j = 4$: ANGLE RATE OBSERVATION
$j = 5$: THRUST MAGNITUDE MECHANIZATION
$j = 6$: THRUST ORIENTATION MECHANIZATION

Similarly, through application of curves 6-9 to 6-13 the final error components produced by the other five error sources can be estimated. Of the remaining five sources only one, the range rate observation has statistical parameters that vary along the trajectory. The range rates that will occur generally fall well within the dynamic range of range rate detectors. The observation accuracy is then limited by non-linearities which produce a constant per cent type of error. The angular rate observation errors are allowed to be from a time invariant population because the angular rates encountered during the trajectory are near the lower end of the dynamic range of angle rate measuring techniques. Thrust magnitude errors can be expressed either in terms of percent error or in the units of thrust since the thrust level is essentially constant throughout the maneuver. Angle measurement errors are hardly ever expressed in terms of percent of the angle measured, so that it was not deemed necessary to consider this representation for angular error sources.

If numbers which are considered to be typical of the extrapolated state of the art are used as sensor capabilities, and some mechanization errors are assumed, it is possible to generate estimates of final position and velocity rms errors. Let the error sources have the following rms values.

a) Range observation: 0.1% of range

b) Range rate observation: 0.5% of range rate

c) Angle observations: 1 milli-radian

d) Angle rate observation: 1 milli-rad/sec.

e) Thrust magnitude: 1 percent = 480 Newtons

f) Thrust orientation: 35 milli-radians

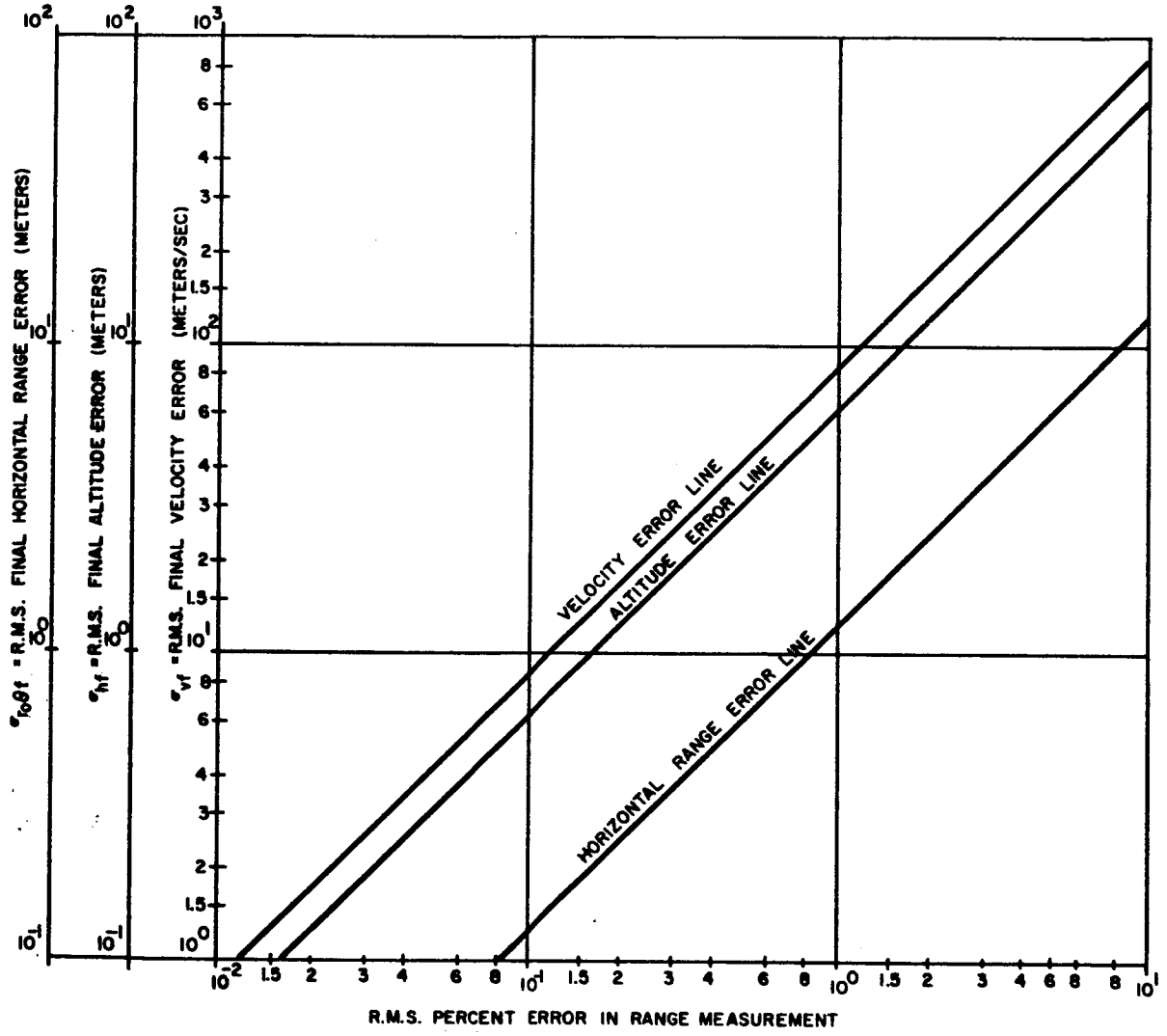

FIGURE 6-8: Final Error Components Attributable to Range Measurement Errors

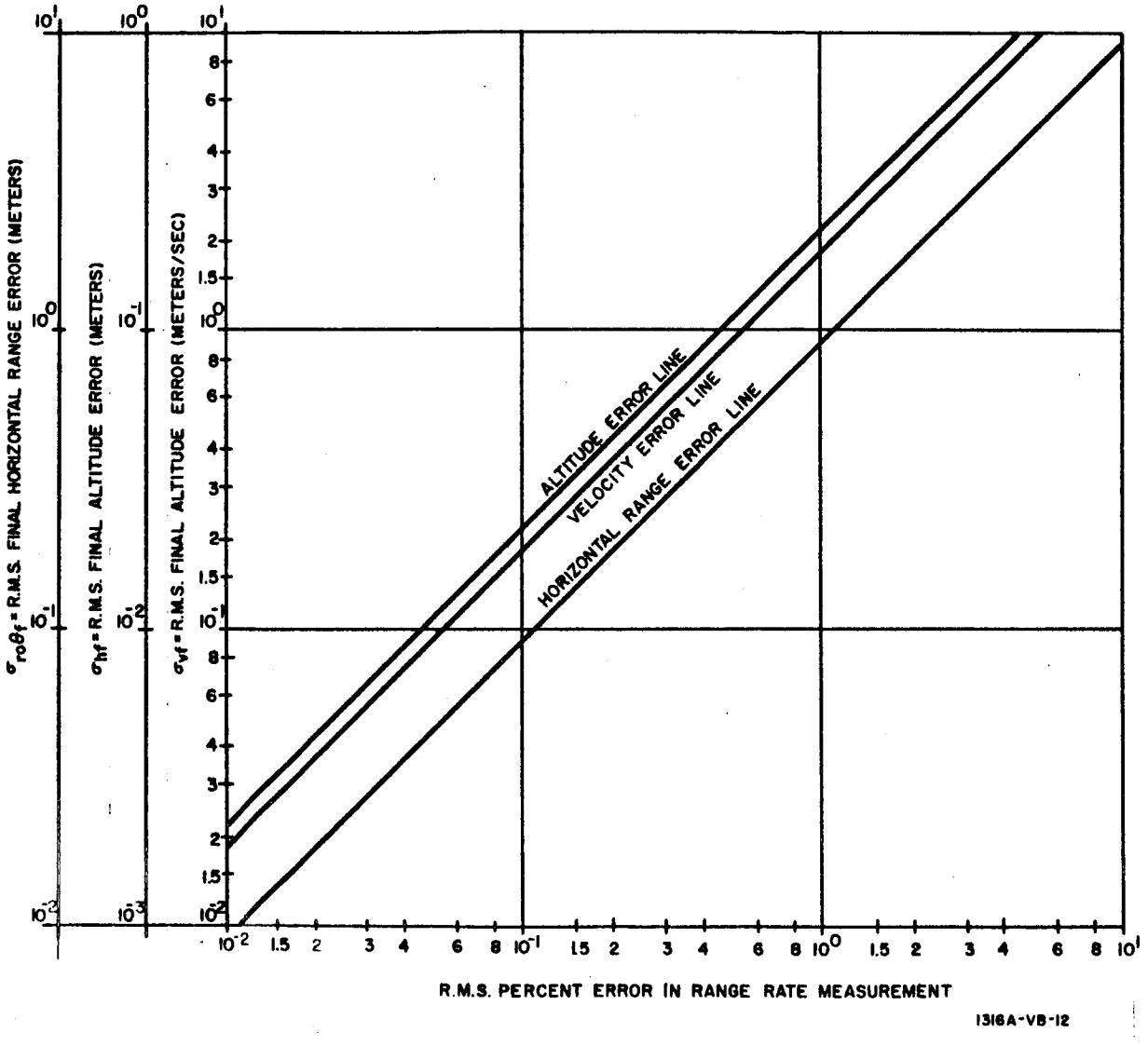

FIGURE 6-9: Final Error Components Attributable to Range Rate Measurement Errors

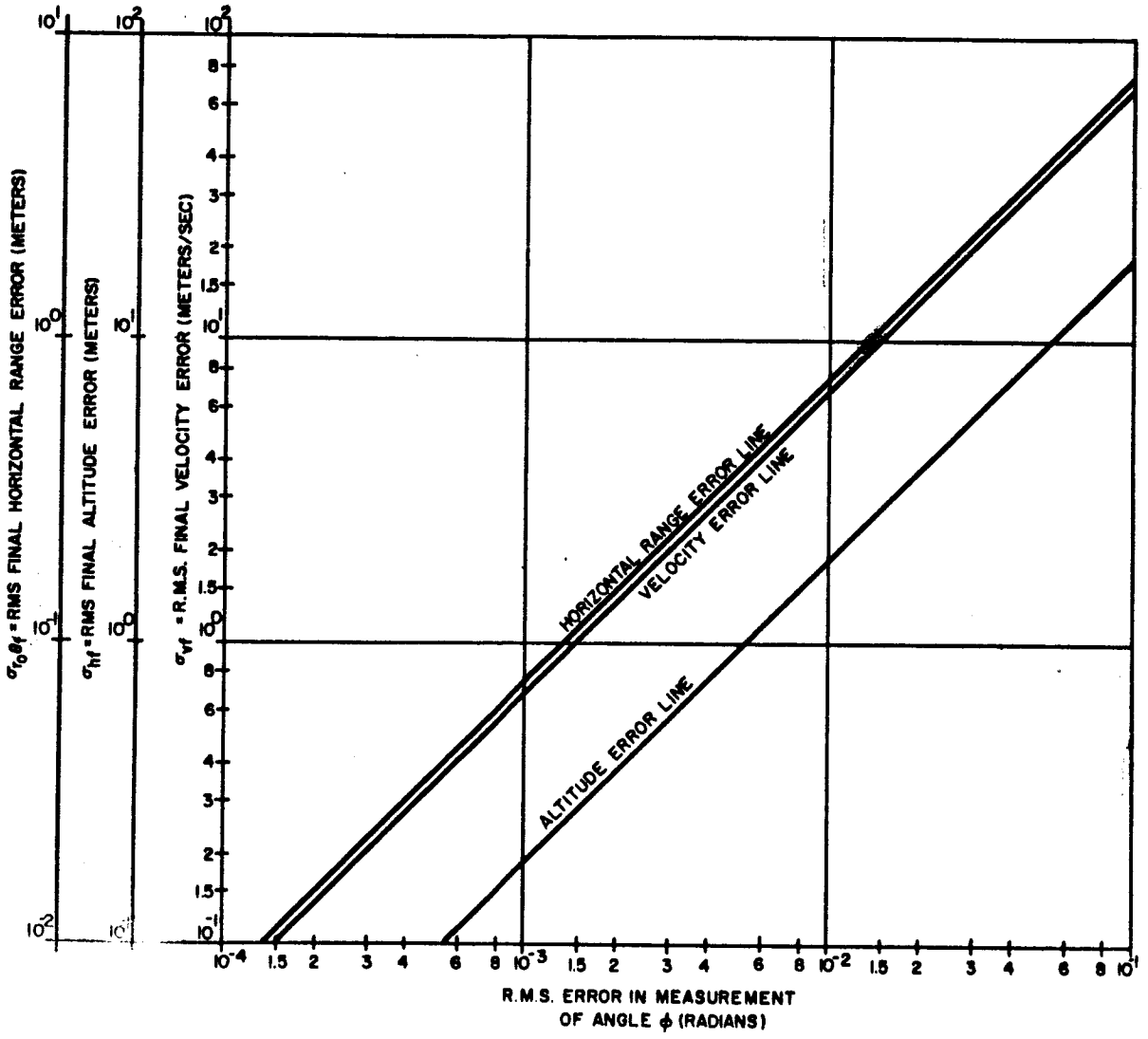

FIGURE 6-10: Final Error Components Attributable to Angle Measurement Errors

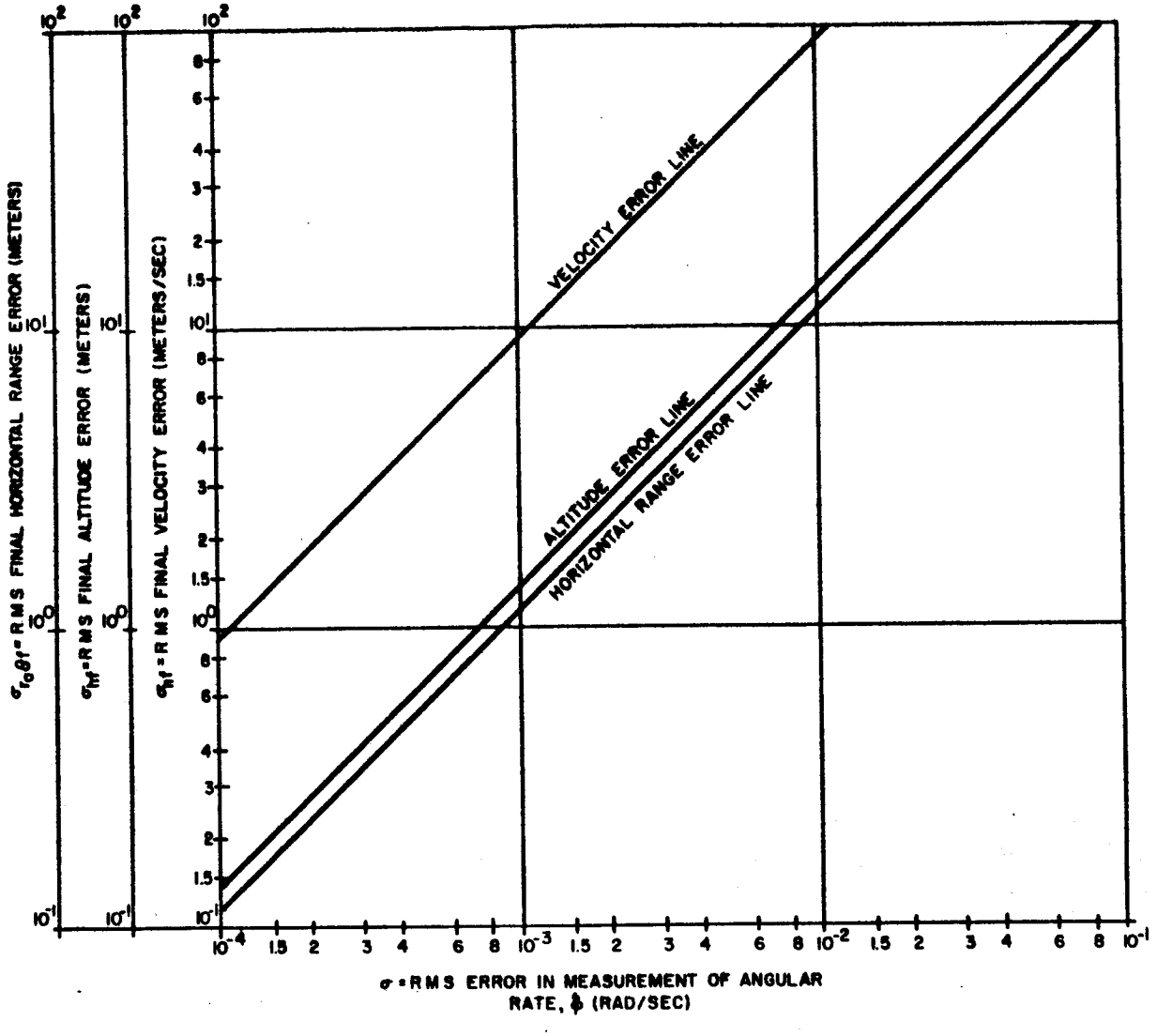

FIGURE 6-11: Final Error Components Attributable to Angle Rate Measurement Errors

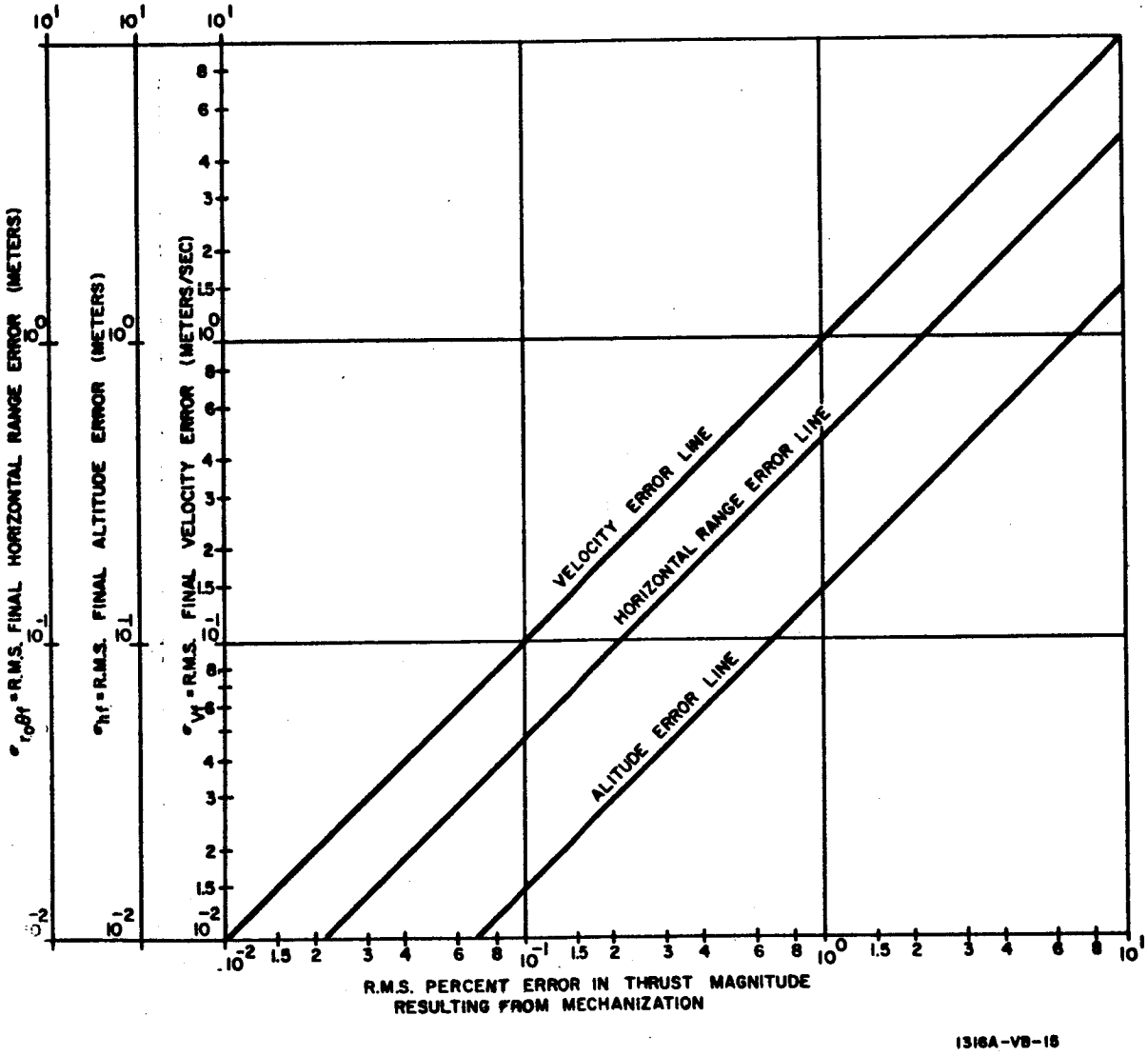

FIGURE 6-12: Final Error Components Attributable to Thrust Magnitude Mechanization Errors

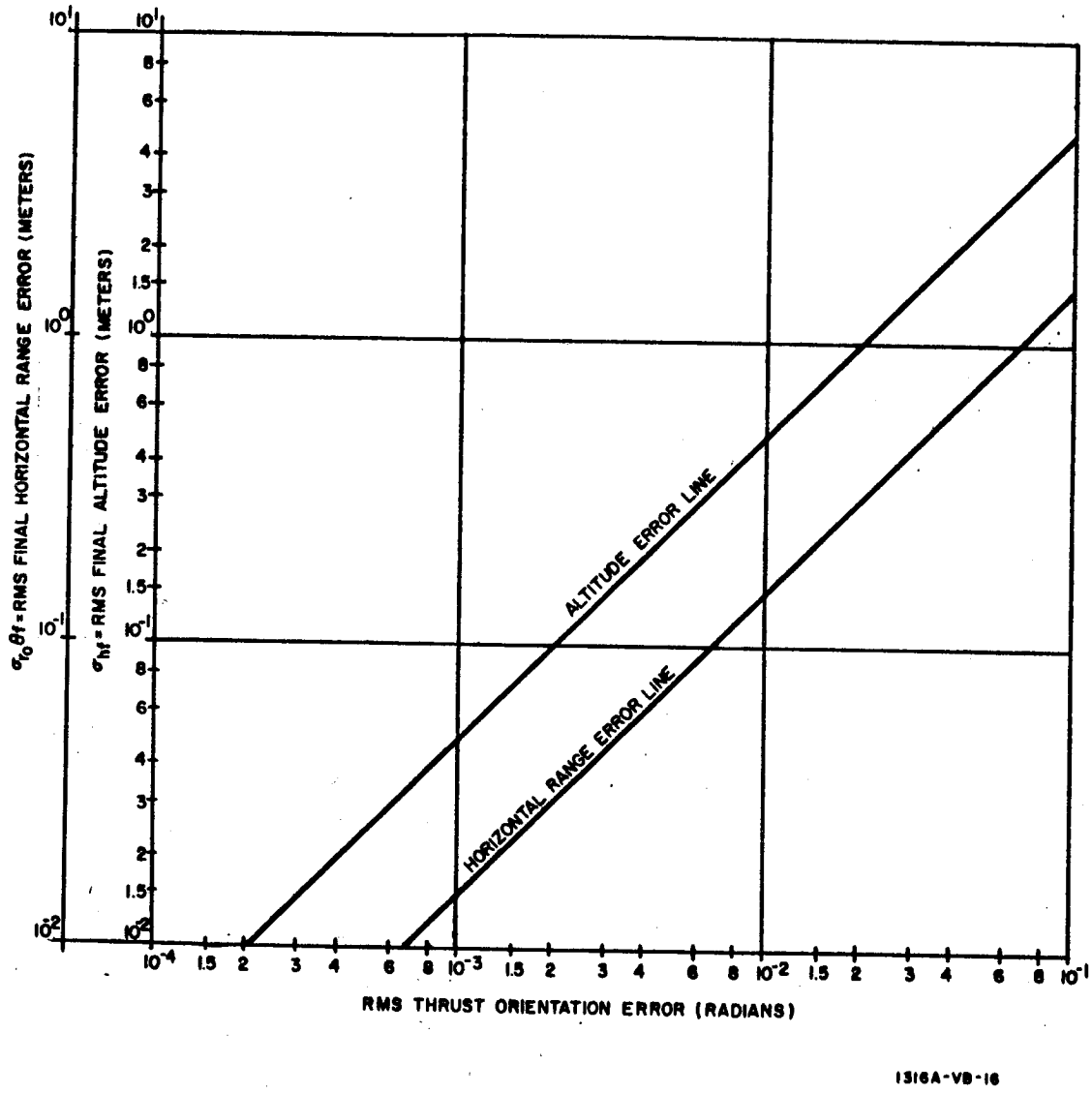

FIGURE 6-13: Final Error Components Attributable to Thrust Orientation Mechanization Errors

For these numbers, which represent but small advances over present radar capabilities if the radar is used in conjunction with a beacon on the surface, the rms values of the final position and velocity error components have been computed and appear as Table 6-3. (Table 6-3 is compiled for $\Delta t_i = 1$ sec.)

Table 6-3

a) RMS Velocity Errors (meters/sec.)

1)	caused by range observation errors	1.87
2)	caused by range rate observation errors	0.93
3)	caused by angle observation errors	0.68
4)	caused by angle rate observation errors	9.1
5)	caused by thrust magnitude errors	1.00
6)	caused by thrust orientation errors*	0.0
	TOTAL RMS VELOCITY ERROR	9.41 m/sec.

b) RMS Altitude Errors (meters)

1)	caused by range observation error	0.617
2)	caused by range rate observation errors	0.109
3)	caused by angle observation errors	0.188
4)	caused by angle rate observation errors	9.14
5)	caused by thrust magnitude errors	0.15
6)	caused by thrust orientation errors	1.67
	TOTAL RMS ALTITUDE ERROR	9.40 meters

* Linearization about the nominal trajectory results in $K_{16} = 0$.

c) RMS Horizontal Range Errors (meters)

1)	caused by range observation errors	0.144
2)	caused by range rate observation errors	0.462
3)	caused by angle observation errors	0.073
4)	caused by angle rate observation errors	1.16
5)	caused by thrust magnitude errors	0.475
6)	caused by thrust orientation errors	0.52
	TOTAL RMS HORIZONTAL RANGE ERROR	1.44 meters

It is obvious from examination of the table that the largest single contribution to the final position and velocity errors comes from the measurement of angle rate. The position errors caused are not dangerous, but the r.m.s. velocity error of better than 9 meters per second is a fairly large item. The landing vehicle will have an upward acceleration of approximately one earth g, or 9.8 meters/sec.^{2} at the end of the nominal trajectory. If the velocity error were in the downward direction, this thrust level would have to be maintained for an extra second or a maximum of three extra seconds (3 sigma velocity error = 3 x 9.4 meters/sec.). This extra firing time would use an amount of fuel equal to a maximum of $\frac{\Delta t_{max}}{t_f} \times 100 = 3/346 \times 100 = 1\%$ extra fuel. This extra fuel required for the descent to hover portion of the landing operational is partially, if not entirely made up during the hover-to-touch-down maneuver because the vehicle is hovering at a lower altitude during the extra time required to reduce the velocity to zero, the vehicle cannot travel downward more than 14.1 meters (3σ). This might be regarded as an additional component of altitude error. However, the altitude error, even with this additional component, is only 10.5 meters(rms) and 31.5 meters(3σ). These

values do not represent dangerous excursions from the nominal end altitude of 500 meters.

The errors that are described are deviations from the end conditions which would result in the absence of any control and sensor uncertainties. They do not necessarily represent deviations from the nominal end point. The reason is that in the absence of any over-control, initial deviations from the nominal are never quite completely compensated for, even if there are no sources of random error present. For each initial point away from nominal initial point, there is a specific final position in the neighborhood of the nominal final position. The errors computed during this study represent displacements from this pseudo-nominal end point which are caused by random observation errors and mechanization errors which exist during the flight. (see Reference 6-1 for information concerning the distribution of these pseudo-nominal end points).

6.7.2 Discussion

In this section several brief discussions appear that relate to the interpretation and use of the analytical results.

6.7.2.1 Effects of Over-Control

To implement over-control, the thrust control commands are multiplied by a constant whose value is greater than unity (see Section 6.3.1). This will also multiply the thrust command errors by the same constant. If the over-control multiplier is K_c then, in Table 6-2, the error transformation coefficients $(K_{ij})^2$ and $(K'_{ij})^2$ for $j = 1, 2, 3$, and 4 are multiplied by K_c^2. The thrust mechanization errors $(K_{ij})^2$ and $(K'_{ij})^2$ for

j = 5 and 6 are not affected by the addition of over-control.

None of the data presented in Table 6-2 and 6-3 include the effects of over-control.

6.7.2.2 Effect of Changing Time Interval

It has been assumed in the analysis that the error in thrust (caused by both observation and mechanization) is constant over one of the small time segments Δt_i seconds long. Also, the errors in one time segment are independent of the errors in all other segments. In the computer program, all time segments were of equal duration. This assumption is equivalent to specifying an auto-correlation function, $\Psi(\tau)$, for the thrust error function. The form of the auto-correlation function specified is shown in figure 6-14.

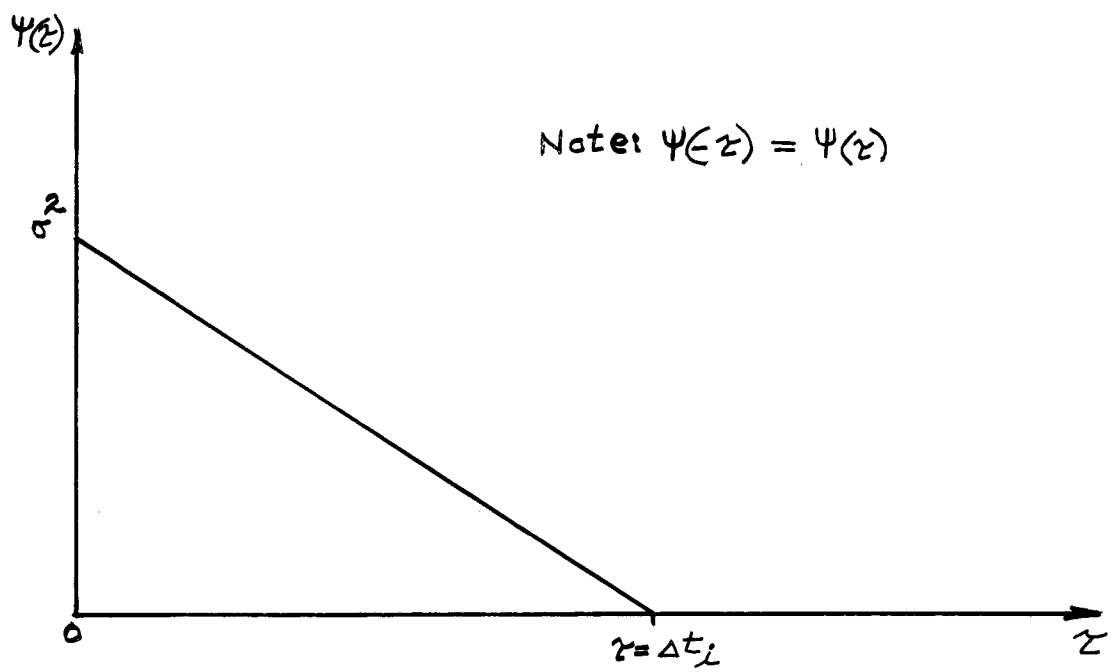

Figure 6-14 Auto correlation Function of Thrust Errors

The frequency response (power spectrum) that is associated with this type of autocorrelation function is of the form $\frac{\sin^2 x}{x^2}$ illustrated in figure 6-15. The response associated with a triangular autocorrelation function is

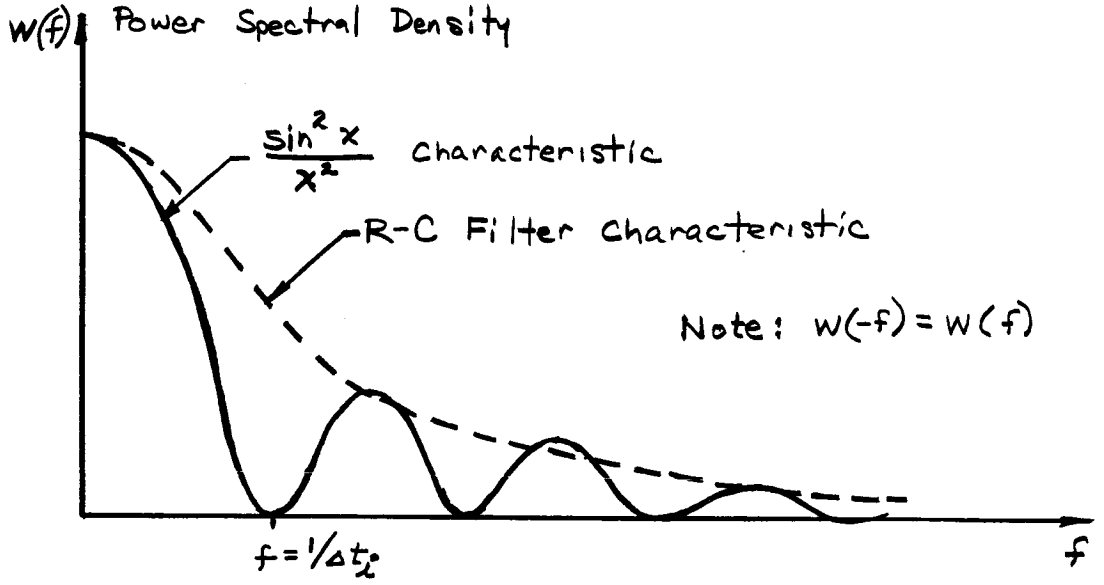

Fig. 6-15 Power Spectral Density Corresponding to Triangular Autocorrelation Function

essentially being used to approximate the frequency response of the entire guidance and control system. The assumed time segment lengths, 1, 2, and 3 seconds correspond to systems of three different bandwidths with longer time intervals implying more sluggish systems. It is this change in the frequency response that causes the error transformation coefficients to change when the length of Δt_i is altered.

It is assumed that sensor noise bandwidths are greater than the control system bandwidth. With this condition, σ_j^2, the effective mean square sensor error of the jth error source, is defined;

$$\sigma_j^2 = \frac{\text{Average Sensor Noise Power}}{\text{Sensor Noise Bandwidth}} \times \text{control system bandwidth}$$

In this definition, the control system bandwidth, B, is approximately equal to $1/\Delta t_i$ where Δt_i is the correlation interval. It is important to recall this definition when determining the effect of control system bandwidth variation on system performance. If a value for σ_j^2 is assumed for some particular value of Δt_i, then the sensor noise power spectral density $W_s(f)$ can be determined*.

$$W_s(f) = \frac{\text{Average Sensor Noise Power}}{\text{Sensor noise bandwidth}} = \frac{\sigma_j^2}{B} = (\sigma_j^2)(\Delta t_i)$$

For some other control system bandwidth, $B' = 1/(\Delta t_i)'$ the effective mean square sensor error is $(\sigma_j')^2$: $(\sigma_j')^2 = W_s(f)B' = \sigma_j^2 \frac{B'}{B} = \sigma_j^2 \frac{(\Delta t_i)}{(\Delta t_i)'}$

6.7.2.3 Validity

It must be remembered, when using the results of this analysis, that the techniques used are only approximations to reality. For this reason, the resulting numbers are only estimates of the errors that will exist. The linearized expressions are not necessarily good approximations at the initiation of the landing maneuver because of the large initial deviations from nominal that are allowed. However, as the flight progresses and the landing vehicle is corrected toward the nominal trajectory, the linearized equations become more accurate. Adding an over-control multiplier to the control system will cause the actual trajectory to converge on the nominal trajectory more rapidly which implies that the numerical results of this study become more accurate for an over-controlled system. To determine the errors caused by observation uncertainties more accurately, a deterministic simulation using Monte Carlo

* The quantity $W_s(f)$ is often used as an indication of sensor quality.

techniques is required.

The program used to compute the results has been checked against the equations of Section 6.4 and Appendix III-C and a sufficient number of results have been verified by hand computation to allow a high degree of confidence in the performance of the computer program.

6.7.2.4 Bias Error Effects

The effects of sensor and control mechanization bias errors on system performance are not determined by the analysis described previously. Bias errors in the control system will tend to produce bias errors in the thrust quantities that are constant over the landing maneuver. Thrust errors caused by sensor biases will vary in magnitude over the flight because of the time variation of the guidance terms stored in the guidance system.

Although analysis has not been performed to determine the effects of bias errors, there is one comment which is applicable. Bias errors are a much less important problem in the type of guidance system analyzed in this report than in one which does not derive information from sensors along the flight path. An example of the latter guidance scheme would be an inertial system which starts with initial conditions and computes position and velocity at any later time by measureing acceleration and integrating the equations of motion. By using sensed information to determine position and velocity, the guidance system is able to correct for deviations caused by bias errors which have occurred earlier in the flight. In fact, this type of system can correct for nearly all of the bias error effects which occur preceding an interval of time at the end of the trajectory equal in length to a correlation interval of the thrust control system. The control system performance is too sluggish to correct for errors existing during the final correlation

interval of the trajectory. Furthermore, it will be desirable to reduce sensor bias errors below the level of rms errors since this will result in final error components that can be attributed to bias errors which will be negligible compared to the errors caused by rms measurement and control uncertainties.

6.7.2.5 Remarks Concerning Generalization of the Analysis

There does not seem to be any factor limiting this control system to two dimensional landing trajectory. Furthermore, the error components perpendicular to the plane of motion are generally the smallest in magnitude, so that generalization to three dimensions is not expected to place increased demands on sensor accuracy. The additional dimension will require that the angle and angle rate measurements be resolved into azimuth and elevation components to provide sufficient guidance information.

The analytical results are valid for any vehicle displaying the same thrust to mass ratio as that used to determine the reference trajectory. The reference trajectory upon which the linearized analysis is based is determined using an initial thrust to mass ratio of 4.23 Newtons/Kg. This is an initial acceleration of 0.432 Earth g. Since thrust is constant, fuel is used at a constant, rate and the final acceleration can be determined for the specified initial conditions, the final acceleration is 0.521 Earth g. These values of acceleration depend only on the thrust to mass ratio. Any vehicle with the same initial thrust to mass ratio will follow the same reference trajectory, and undergo the same acceleration levels, regardless of the actual size of the vehicle.

6.7.2.6 Sensor Mechanization

The rms sensor errors which were assumed in the sample computation of Section 6.7.1 can be realized with little and in some cases no advance in present state-of-the-art capabilities of airborne radar systems. Specifications that have been generated for rendezvous radar systems are in general, more stringent than the values used in the sample. Thus, mechanization of the sensor scheme analyzed would not appear to be difficult.

6.7.2.7 The Role of the Pilot

Man has not been included in the discussion prior to this point because the aim was to perform an analysis which would be applicable to both manned and unmanned landing vehicles. That a system of the type discussed is capable of operating without man in the loop has been adequately demonstrated by the automatic guidance and control modes of modes of modern airborne manned and unmanned interceptors. If it is desired to include man in the guidance and control system, there are tasks he is capable of performing. These tasks are similar in nature to those he can perform during rendezvous. These include, monitoring of system performance, interpreting displayed information and executing the thrust commands, and perhaps, most important, acting as a terminal controller in guiding from hover to touch-down.

6.8 Sensor Requirement

Sensor requirements per se cannot be specified until limits are placed on the allowable final r.m.s. position and velocity errors. It has been shown in Section 6.7 that the extrapolated state-of-the-art sensor

capabilities appear to be sufficient for the landing maneuver. This does not necessarily mean that the sensor accuracies specified for the example are required. It can be seen in the example, that specifications for range measurement, range rate measurement, angle measurement, and the two thrust mechanization errors yield final error components considerably smaller than those stemming from angular rate measurements. One possible conclusion is that these five error sources have been over-specified and that less accurate sensors can be used without impairing performance. There is little to be gained by reducing the magnitude of any of the six error components, comprising each of the 3 final state variable errors, very much below the level of the error produced by the most highly developed sensor. In the case of the extrapolated state-of-the-art discussed earlier, the limiting sensor is obviously that which determines angular rate ϕ.

The primary output of this study are the trade-off curves relating sensor and mechanization errors to final state errors. When more information is available concerning the characteristics of landing vehicles, and the magnitudes of final errors that can be tolerated, these trade-off curves, or others like them that are easily generated from the data presented (curves for other values of Δt_i for example), can be used to determine appropriate sensor and mechanization accuracy requirements.

6.9 Recommendations

6.9.1 Extended Use of Linearized Analysis

The analysis performed indicates that the guidance system studied is capable of excellent performance in connection with lunar landing

maneuvers. The term guidance system is here construed to include the sensors which have been studied. However, no specific attempt was made during this study to determine the optimum landing trajectory, or the optimum combination of observables for lunar landing. It is recommended that other combinations of sensors be studied, particularly, a set that includes both inertial sensors and observations to the surface. This type of sensor grouping may be required to counter visibility constraints imposed by lunar surface curvature which limit the distance from which surface landmarks or beacons can be observed. The effect of changing the nominal trajectory or changing the guidance law have not been determined by the analysis contained in this report, and should be investigated.

The additional studies recommended above represent further steps toward mechanization that can be accomplished through the use of techniques and programs which have been developed with minor supplemental computer programming.

6.9.2 Simulation

In view of the system performance capability indicated by linearized analysis, the guidance law and sensor combination that has been analyzed seems to warrant further study more closely concerned with the problems of mechanization. For this purpose, dynamic simulation of the landing vehicle and its guidance and control system would be required. Monte Carlo statistical methods applied to the simulation model will yield more accurate data concerning the effects of observation and mechanization errors than has been

obtained by linearized analysis. Simulation is the final step before mechanization. It is required to confirm the results of linearized analyses and for final parameter optimization. However, the complexity of an accurate simulation requires that an efficient simulation program be based on the results of objective studies of the type performed here.

7.0 LUNAR LANDING, HOVER-TO-TOUCHDOWN, MANNED

7.1 Introduction

The emphasis, for this phase, tends to fall almost entirely upon the requirements for the particular mission envisioned, and the importance of a given sensor and control scheme for a given mission takes precedence over sensor accuracy requirements, which are not stringent. The hover phase is necessarily of short duration due to fuel limitations, and the inertial system possessed by the landing vehicle is more than sufficient for this phase. This phase, then, is not to be covered except to summarize several qualitative sensor requirements which are generally applicable, as follows.

7.2 Summary

Lunar terrain, as seen from any distance, however short, can be expected to appear quite unfamiliar with regard to sizes and shapes and, in addition, will be illuminated in a totally unfamiliar manner. Any visual judgement of distance or altitude, then, is very difficult so that an altimeter, which, in combination with the inertial system possessed by the landing vehicle, is accurate to within a range of 3 meters of the surface is a necessity, for the landing phase.

Because the hover phase is necessarily of minimum duration to conserve fuel, sensing equipment is required to determine a lunar surface condition suitable for landing from an altitude of at least 500 meters. Such a device would be a surface roughness sensor capable of distinguishing surface protruberances 1 meter or higher from the average surface level and capable of indicating slopes of 20 degrees or greater. Illumination conditions, particularly near the terminator region would dictate a radar or other active illumination type of device.

The high variability of surface temperature with location due to lack of atmosphere would indicate the need for a sensor to measure surface temperature at a distance of 500 meters or more.

The surface roughness sensor requirement would appear to indicate an area where a research program is needed to create the basic operating principles of a sensor device to determine unknown landing surface conditions with the degree of accuracy indicated.

8.0 LUNAR ASCENT TRAJECTORY, MANNED

8.1 Introduction

This section describes the method of specifying sensors required for the boost phase of a lunar ascent to an orbit from which a rendezvous with another orbiting vehicle can be made. Only conventional navigation schemes are considered, and evaluated only to the extent necessary to establish sensor requirements.

Although optimizing techniques are used wherever possible, absolute optimization is characterized as second order effects insofar as sensor requirements are concerned. Providing that the system has the capability of compensating for lesser effects, the method of specification and hence, the results, are valid.

To insure integration of this section with the following section concerning terminal rendezvous, an extensive discussion of the entire initial-to-terminal maneuvers is presented as part of this section. Over-all fuel and flight-time trade-offs are considered as an important aspect of this section, regardless of their effect on boost sensor requirements. Therefore, much of the presentation is an objective study of those methods required to insure an efficient over-all ascent.

The class of trajectories is characterized by near minimal fuel requirements. Results are given in terms of the total theoretical velocity increment required for the entire ascent and rendezvous. Thus, fuel, boost cut-off altitude, transfer angles, flight-time, etc., are the dependent parameters of this study.

Although the accuracy required of the boost sensors is shown to be well within the capabilities of state-of-the-art mechanization, areas requiring additional investigation have been indicated. These areas are characterized by mission constraints which may impose requirements on the selected boost and

rendezvous system more severe than expected. Such areas necessarily include abort and emergency situations.

8.2 Background and Approach

An inertial reference system has been selected to provide position and velocity information during boost. The nature of the boost phase practically implies such a choice, i.e., the trajectory is characterized by continuous power, short duration, short distances and angular displacements, high thrust acceleration, and reasonable knowledge of the launch site and target kinematics. The advantage of this choice is that such a system offers a guidance technique capable of furnishing all of the elements required for guidance in a self-contained unit, relying only upon the relationship between acceleration, angular measurements, and time. It is further assumed that the inertial system does not contain an external monitoring source. The purpose of this assumption is to provide conservative results as well as include missions in which external monitoring imposes difficult or excessive mechanization.

Generally speaking, the accuracy of a long-range ballistic missile or satellite launch guidance scheme is primarily limited by the source generating position and velocity information. With this type of relatively short powered trajectory, incorrect information from the inertial navigator contributes the major portion of system inaccuracy. It is not necessary for the purposes of this study to presume a control technique. Thus, sensor requirements are simply determined by the errors associated with position and velocity prediction.

Although a wide class of trajectories are analyzed to obtain fuel trade-offs, only two trajectories are used to determine boost sensor requirements. Both ascent trajectories are consistent with the minimum fuel constraint, but differ primarily by flight time and altitude of the thrust termination point. One trajectory terminates in an orbit at a low altitude selected by terrain

avoidance considerations whereas the other terminates at an altitude very close to that of the target vehicle in a higher orbit. Thus, these two trajectories are, in a sense, upper and lower bounds of the class of trajectories considered. If sensor requirements are established for the most stringent of these cases, then these requirements are necessarily adequate for attaining any intermediate thrust termination point.

Considering the previous objectives, the following approach has been established:

- General discussion and selection of type of ascent
- Selection of boost sensor and associated system
- Analytical trajectory and sub-phase definition
- Boost error specification, i.e., the nature and propagation of errors caused by both the sensor-system scheme and the inputs to the sensors
- Error summation and trajectory trade-off results

Once the preceding information is available an evaluation of the results is performed. A criteria for evaluation is established in view of the obvious trade-offs involving fuel, time, and sensor requirements.

8.3 Preliminary Analysis and Problem Definition

8.3.1 Trajectory Determination

8.3.1.1 Introductory Discussion

Problem definition consists of defining, analyzing, and selecting that type of ascent which is best suited to a manned lunar rendezvous. The following discussion is presented as background material for the construction of an optimized ascent trajectory.

Ultimately, any rendezvous involving a target and an interceptor terminates when the kinematic states of both vehicles are identical in space, time, and velocity. Since the end-points may be undefined, trajectory

This page intentionallyleft blank

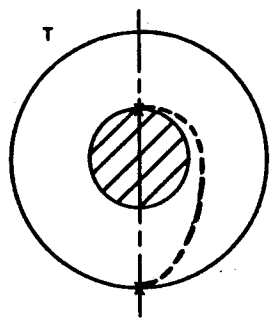

FIG. 8.3-1-A: TWO-IMPULSE MINIMUM ENERGY ASCENT

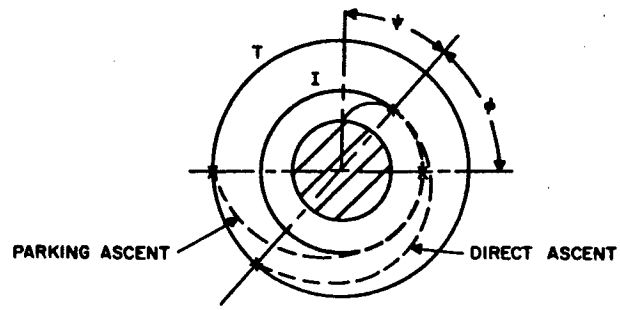

FIG. 8.3-1-B: MINIMUM FUEL ASCENT (HOHMANN TRANSFER)

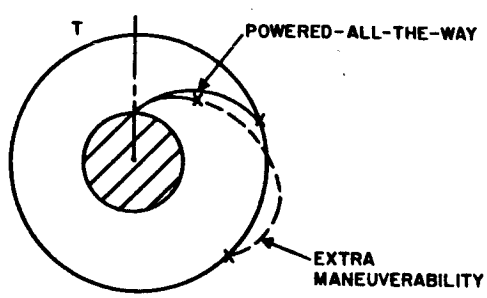

FIG. 8.3-1-C: DIRECT ASCENT

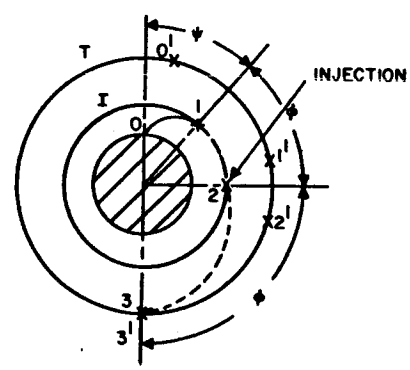

FIG. 8.3-1-D: RELATIVE POSITIONS IN PARKING ASCENT

SUB-PHASES:

0-1 = BOOST (ψ)
1-2 = PARKING (φ)
2-3 = TRANSFER (θ)

T = TARGET ORBIT
I = INTERMEDIATE ORBIT

FIG. 8.3-1: TYPES OF ASCENTS TO RENDEVOUS

1316A-VB-34

solution in its general form is indeterminate, and solvable only when suitable constraints are imposed. Typical examples of these constraints are: minimum energy, bounded energy, minimum time, or transfer in a specified time interval. Since the minimum energy constraint has been selected, the problem can be further narrowed by considering only those minimum energy trajectories which terminate with target velocity at arbitrary points on the target trajectory. Theoretically, the entire maneuver may be accomplished without geometrical or kinematic limitations on the end-points with two impulses, see Fig. 8.3-1-A and Ref. 8-1.

Consistent with a minimum fuel constraint are two methods of ascent, differing only by a delay in time as illustrated in Fig. 8.3-1-B. In the first method the boost cut-off velocity yields a Hohmann transfer if the target orbit is circular. In the second method the cut-off velocity yields an intermediate or "parking" orbit. This orbit may be selected concentric with the outer orbit so that the subsequent transfer orbit is identical to the above Hohmann transfer. Both methods require the same minimum fuel, i.e., the former is simply a bounding trajectory of the latter.

8.3.1.2 Definition and Comparison of Parking and Direct Ascents

Based on the above considerations, the following definitions have been adopted:

1. Direct: Powered boost directly yielding a transfer orbit which nominally terminates in target acquisition. Powered-all-the-way ascents could fall into this class, but are not considered in this study since the fuel penalty is generally too severe (see ref. 8-3 and Fig. 8.3-1-C).
2. Parking: Powered boost yielding an intermediate orbit followed by injection into a transfer orbit which terminates in target acquisition (see Fig. 8.3-1-D).

The boost phase of the direct ascent requires minimal timing errors prior to launch and during the burning period. Any timing deviations at the cut-off point must be made up by fuel expenditure some time during the transfer orbit. For a typical lunar rendezvous with a low altitude target orbit, orbital velocity is approximately 1 mi/sec.(1.6 km/sec). Hence, a count-down delay of a few tens of seconds results in a miss distance of a few tens of miles if uncorrected. Should there be insufficient fuel to compensate for this delay, the only choice with a passive target is to allow the target to complete another orbit and repeat the operation. However, the angular velocity of the launch site is in general not perpendicular to the target plane and an out-of-plane launch and hence, additional fuel is required. Although an in-plane launch is virtually impossible, plane changes should be held to a minimum.

For the parking orbit ascent, the powered boost yields an intermediate lower altitude orbit. This orbit, having an angular rate greater than that of the target orbit, permits the interceptor to advance upon the target prior to injection into the transfer ellipse. Thus, an unfavorable in-plane angular position at launch and known launch-boost time delays can be made up by remaining in the parking orbit for a greater or lesser time. The parking orbit therefore functions as a synchronizing phase for the target and interceptor trajectories. If additional scientific data or check-outs are desired, the parking orbit offers extra time between boost and transfer. However, there are three main disadvantages for the parking orbit ascent (ref. 8-4):

1. Boost cut-off errors are a function of the parking dwell time. These errors have both secular and periodic propagation characteristics.
2. A long period of ascent and rendezvous may require excessive

life-support equipment. Also, errors in target ephemeris prediction increase with time and thus updated target information may be necessary prior to transfer injection.

3. After the coast period, the engines must be ignited once additionally to initiate transfer.

Comparison of both ascents shows that the total allowable flight time and launch delays are primary factors in selecting the nominal trajectory. By maintaining very small launch delays, both ascents require nearly the same fuel if the rotational effect of the launch site is negligible.

Regardless of the method selected many techniques and equations are common to both, especially when a near minimum fuel trajectory is employed. However, if a large fuel penalty is relatively unimportant and a very quick ascent is required, i.e., one in which the total flight time is a small fraction of the orbital half-period, a direct ascent is far more efficient. On the other hand, the parking orbit facilitates launch at all times during the exploration period. Operationally, this is a distinct advantage especially if abort or emergency situations arise. It should be noted that the parking dwell time can be selected as long or short as desired, depending on the period of the target orbit and the relative positions of the two vehicles at launch.

It is not to be assumed that the sensor requirements for a direct ascent are less stringent than the parking ascent simply because the flight time for the direct ascent may be shorter. It is difficult to recommend either method on the basis of sensor requirements alone unless several other constraints are well-defined. Clearly, this objective study attempts to minimize the number of these constraints and thus has the advantage of offering methods for sensor specification applicable to many situations.

8.3.1.3 Ascent Trajectory Selection and Division into Sub-Phases

Since this section is concerned with general surface-to-orbit rendezvous, the parking ascent has been selected because of its inherent flexibility. It must be emphasized that while a direct ascent for a lunar rendezvous is entirely feasible, such a choice imposes limitations on the mission which may or may not be relevant.

The trajectory is conveniently divided into five sub-phases with the analytical description of each proceeding in reverse order: target definition, orbital transfer, parking, boost, and pre-launch. The errors associated with each phase will, in the end, be expressed as normalized miss distances and velocities at the point where orbital transfer is initiated. This point represents an interface between section 8 and section 9.

8.3.2 Selection of Boost Sensors and Observables

As indicated previously, the choice of inertial sensors was dictated primarily by the salient features of the boost trajectory and degree of certainty with which the initial and final kinematic end states are known. Functionally, a set of gyros, accelerometers and integrators, a gravity computer, a clock, and a navigation computer comprise the system. The gyros supply inertial angular measurements; accelerometers and integrators supply inertial acceleration, velocity, and position; the gravity computer supplies gravitational acceleration which must be distinguished from vehicle accelerations; the clock supplies time for the computation of central body rotation; and the computer provides the measurements in a useable reference frame.

The only observables during flight are inertial acceleration and angular displacement, and time. Pre-launch determination of initial and target kinematics are not included as part of this study although uncertainties in these end points are error sources and will be discussed in section 8.4.3.4

In the absence of other constraints, determination of the following parameters is sufficient:

A. Prior to lift-off:

1. Vector position and velocity of the launch site in space.
2. Vector position and velocity of the target in the region of target acquisition.
3. Total flight time and fuel requirements for the interceptor.

B. After lift-off:

1. Vector position and velocity of the interceptor trajectory.
2. Stored or possibly updated target information.
3. Flight time elapsed, or time to go.

The type of inertial system selected is usually dictated by the nature of the trajectory, i.e., the acceleration level and flight time. Once the nominal trajectory is established the choice is narrowed into one of the following system categories: vertical-seeking, space-stabilized, base-point, or gimballess. Extensive discussions of each of these systems may be found in the literature (refs. 8-5, 8-6, and 8-7).

Generally speaking, if the thrust period is normally within a limit of 10 to 20 minutes, space-stabilized systems are attractive. The usual applications of such systems are in ballistic missiles, satellite launchings, or launches for outer space probes. Since the lunar take-off falls into this boost category, this system has been selected. The next step involves the determination of analytical error models of each error producing source within the system.

Three error analysis procedures are discussed in detail in section 8.4.3.3. In general, all three require the use of a computer program since the propagation of errors depends on trajectory "coefficients". However,

simplifying assumptions may be used to obtain linearization and thus, analytical solution. It will be shown that the use of a digital program is warranted only when fine-grain analysis, system optimization, or the inclusion of a wide class of trajectories is necessary.

This page intentionally left blank

8.4 Analytical Description

8.4.1 Restrictions:

Prior to trajectory definition, the following restrictions are imposed:

1. The attracting body and orbiting vehicle are assumed to be constant point-masses in an idealized two-body system. The interceptor is analyzed on the same basis during parking and transfer.
2. All trajectories are two-dimensional. Error sensitivity to the non-coplanar situation is treated independently.
3. Velocity increments necessary to effect the various transfers are treated as impulses. It is assumed that finite thrusting time has a negligible effect on propellant consumption (ref. 8-8). Although finite thrusting does yield different conics at different thrust levels, the effect on boost sensor specification should also be negligible.
4. Transfers requiring more than two impulses are not considered.
5. The trajectory is characterized by near minimal velocity requirements. This is consistent with the second restriction concerning coplanar trajectories. However, fast transfer and high altitude boosts will also be considered.
6. All acceleration levels must not exceed boundaries imposed by physiological (ref. 8-9) and structural constraints.

7. The target is assumed completely passive with one exception, vehicle-to-vehicle tracking and/or communication is available to determine when and where to launch. Although more accurate information about target ephemeris prediction may be available during boost and subsequent parking and transfer, the boost sensors will be specified in the absence of up-dated information. Note that one of the reasons for selecting the parking ascent was the possibility of obtaining more accurate measurements of range and range rate prior to transfer.

All sub-phases are subject to the above restrictions, when relevant.

8.4.2 Analytical Trajectory Description

8.4.2.1 Target Definition

Operationally, the most appropriate distance of the target from the planet under consideration would depend on the mission. One application, determining the true shape of the Moon, requires very close proximity. On the other hand detailed surface observations from a satellite may require higher orbital altitudes. Since a near minimal fuel constraint was imposed on the ascent vehicle, a low altitude near-circular target orbit has been selected. Obviously, near-circular parameterization reduces fuel, time, and sensor requirements for the interceptor while predisposing severe requirements on the mid-course trajectory. Based on the previous mid-course analysis, this choice is well-justified. For interplanetary probes involving surface-to-orbit rendezvous, further analysis is required to validate this decision.

The selection of a near-circular (low eccentricity) orbit as a constraint implies the use of a circular orbit as a functional target, i.e., fuel, time, and sensor requirements imposed on the nominal ascent trajectory are assumed to be the same in both cases. The circular orbit enables analytical simplification while imposing only second order effects on the primary requirements. Again, as long as the system has correction capability, these effects are unimportant for sensor specification.

It now follows that only two parameters are necessary to define the two-dimensional target trajectory, e.g., the gravitational constant μ, and circular radius, r. Since the former is fixed, the problem is reduced to altitude selection, which in turn, is determined by the mid-course transfer and capture maneuver. A representative altitude of 200 km. above the lunar surface has been chosen to maintain consistency with Section 9.

8.4.2.2 Orbital Transfer Trajectory

In transferring between two coaxial orbits, co-tangential transfers are often thought to be the most efficient under all circumstances. Several authors have shown that using fewer than three impulses, the minimum energy transfer for non-interesting orbits is the Hohmann transfer connecting the higher altitude apogee to the perigee of the inner orbit (ref 8-2). In the cases where the terminals are arbitrary, and faster transfers may be required at a fuel penalty, the corresponding transfer path which requires minimum energy is not initially tangent to the inner orbit. However, the minimum energy transfer ellipse to a circular target orbit from an inner ellipse requires tangential target contact (Reference 8-10).

This page intentionally left blank

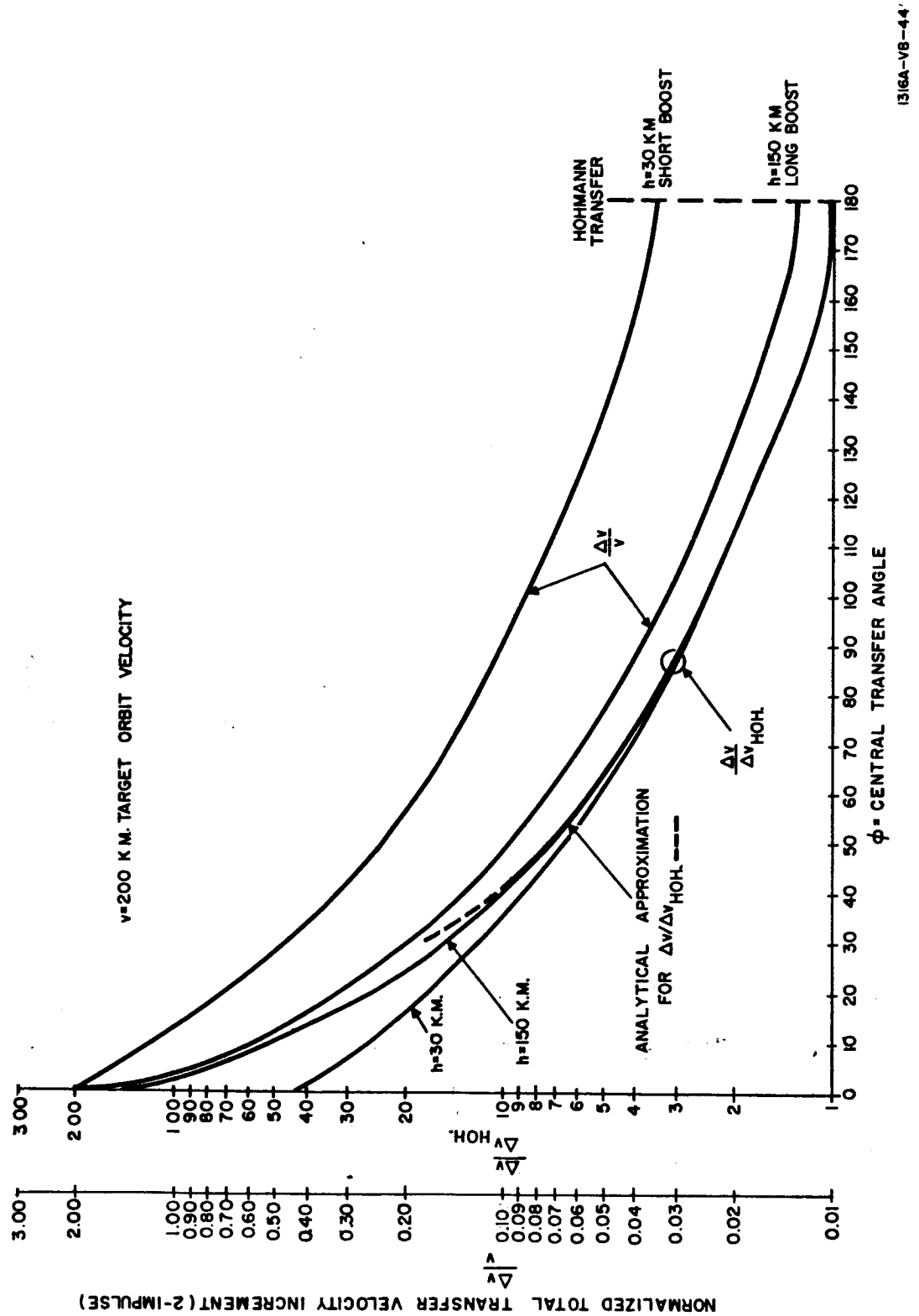

FIGURE 8.4-1: Total Required Velocity Increment for Minimum Energy Circle-to-Circle Transfer

To allow for faster flight times and possible error reduction the trajectory has been defined as a minimum energy transfer between arbitrary terminals located on two circular coplanar orbits, the parking and target orbits. Therefore, tangential target contact is required. The derivation of the total required velocity increment as a function of the radii ratio (parking and target) and central transfer angle is given in Appendix 23.1. Note that the Hohmann transfer is simply the bounding trajectory.

In addition to the exact solution of these trajectories, an approximate solution is given for obtaining quick and accurate estimates for cases where the radii ratio is near unity and the central transfer angle is above 40°. For transfers below 40°, severe fuel requirements are imposed on the interceptor for circle-to-circle transfer.

Although the analysis is restricted to transfers between two circular orbits, differences in the total velocity increment resulting from the two orbits not being exactly circular will produce only second order effects. There are no restrictions on the transfer ellipse other than intersection with the parking orbit and apogee at the target. Hence, transfers from 0° to 180° or eccentricities from unity to that corresponding to the Hohmann transfer are allowed.

Since the period of Hohmann transfers is very nearly equal to the period of the target or parking orbit if the radii ratio is close to unity, the maximum transfer time for a lunar rendezvous is roughly one hour. Referring to Fig. 8.4-1, for a 90° transfer, the transfer time is

roughly halved at a fuel penalty of only three times that required for the Hohmann transfer. It is obvious that for very small transfer angles the fuel penalty is significant, i.e., a direct ascent is much more economical. Therefore, an ascent in which the flight time is restricted to a very small fraction of the half period of the target orbit suggests that the boost phase should yield the transfer ellipse directly. Thus, fuel is not wasted in obtaining injection velocity.

8.4.2.3 Parking Orbit Trajectory

As indicated previously the boost phase requires cut-off at the lowest feasible altitude. Since the parking dwell time may be considerable, it is preferable to choose a near-circular orbit. This choice is dictated by minimal over-all fuel requirements and terrain avoidance during parking. Again, a circular orbit is used for analytical simplification as a functional trajectory.

For a lunar ascent the best estimates of cut-off altitudes lie between ten and fifty km. Two representative altitudes of 30.5 and 152.4 km have been selected, dictated by reasons given in the following section concerning the boost trajectory. The over-all fuel requirements for both orbital transfer and boost as a function of parking orbit altitude are provided in Fig. 8.5-4.

8.4.2.4 Boost Trajectory

To obtain optimized boost trajectories for an ascent from any planet, it is necessary to program on a computer the non-linear differential equations of motion. Approximate analysis indicates that a thrust schedule which demands linear-tangent attitude control maximizes the mass in orbit,

This page intentionally left blank

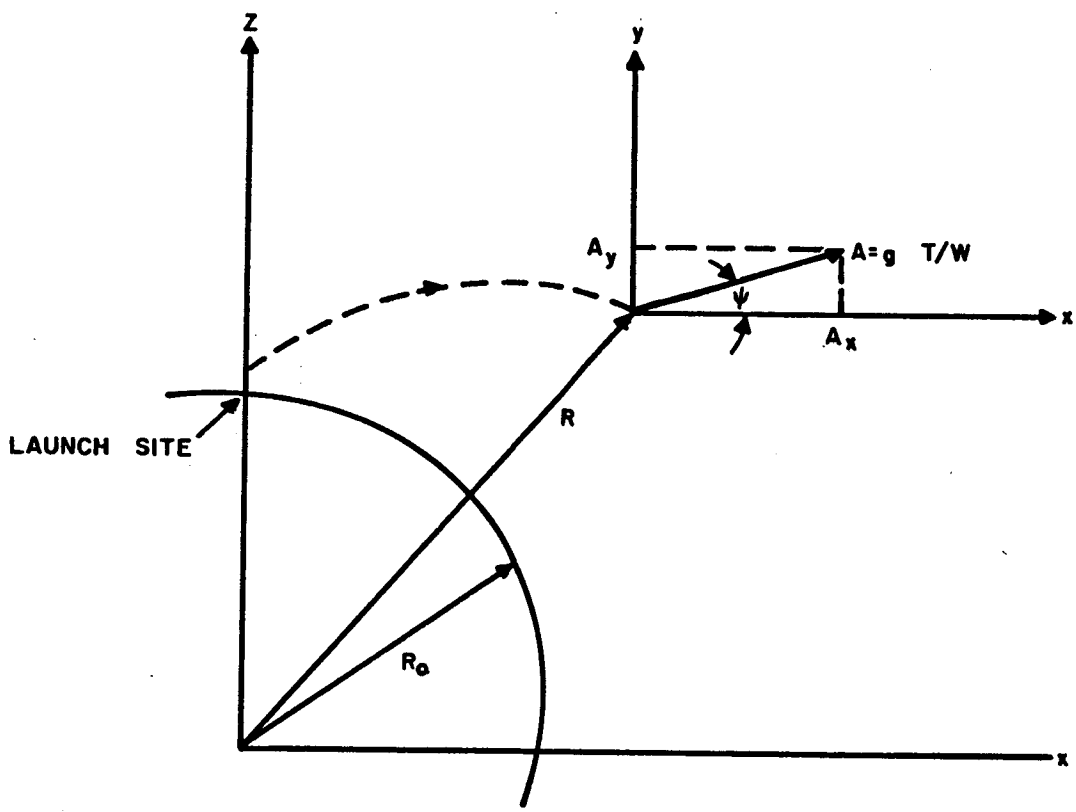

1316A-VB-29

FIGURE 8.4-2: Moon Centered, Non-Rotating Coordinate System for Boost Trajectory and Sensor Error Analysis

or, maximizes horizontal velocity for a specified altitude (ref. 8-3 and 8-11). Theoretically, this schedule should always be used, but for atmospheric ascent in which large angles of attack are structurally undesirable, near-zero lift is preferable. Therefore, for a lunar take-off, the linear-tangent schedule is especially attractive.

Neglecting drag, the equations of motion of a two-dimensional boost trajectory are,

$$\ddot{x} + \frac{\mu}{R^3} x = A_x = g_c \frac{T}{W} \cos \psi$$

$$\ddot{z} + \frac{\mu}{R^3} z = A_z = g_c \frac{T}{W} \sin \psi$$

with the linear-tangent relation defined as,

$$\tan \psi = a - bt$$

Fig. 8.4-2 illustrates the coordinate system selected.

Assuming R = constant, constant thrust T, constant mass flow rate reduction, and a small angle assumption,

$$\sin \omega t \cong \omega t, \qquad \cos \omega t \cong 1$$

where,

$$\omega = \sqrt{\frac{\mu}{R_0^3}} = 0.0548\ ^\circ/\text{sec. for a lunar boost}$$

Mackay (ref. 8-12) has obtained a closed form analytical solution for final position and velocity. Note that $\omega t = 16.5°$ for a 300 sec. lunar boost.

Using these equations with a calculus of variations program performed on an IBM 704, Burley and Weber (ref. 8-13) obtained optimized lunar boost trajectories for continuous and discontinuous application of thrust. For reasons of reliability, system and analysis simplicity, only the results of continuous thrust will be used. The effect of optimum T/W and characteristic velocity vs. altitude are given in Fig. 8.4-3.

TABLE 8.4-1: OPTIMIZED BOOST TRAJECTORY PARAMETERS

		Short Boost	Long Boost
1.	Cut-off Altitude	30.5 km	152.4 km
	Cut-off Radius	R_o+30.5 = 1768 km	R_o+152.4 = 1886 km
2.	Cut-off Velocity	1.665 km/sec.	1.613 km/sec.
	Characteristic Velocity Increment	1.88 km/sec.	2.35 km/sec.
3.	Initial T/W_o moon	3	2
4.	Total Flight Time	255 sec.	462 sec.
	*Initial Vertical Flight	30 sec.	42 sec.
5.	Central Angle Traversed,	6.10°	8.62°
6.	$\psi = \tan^{-1} a$	30.46°	70.16°
7.	I_{sp}	300 sec.	300 sec.
8.	b	3.50×10^{-3} sec.$^{-1}$	8.76×10^{-3} sec.$^{-1}$

* The first $1\frac{1}{2}$ km. was vertical flight; the assumption was mainly for computational convenience, but insures terrain avoidance at low altitudes, Ref. 8-13.

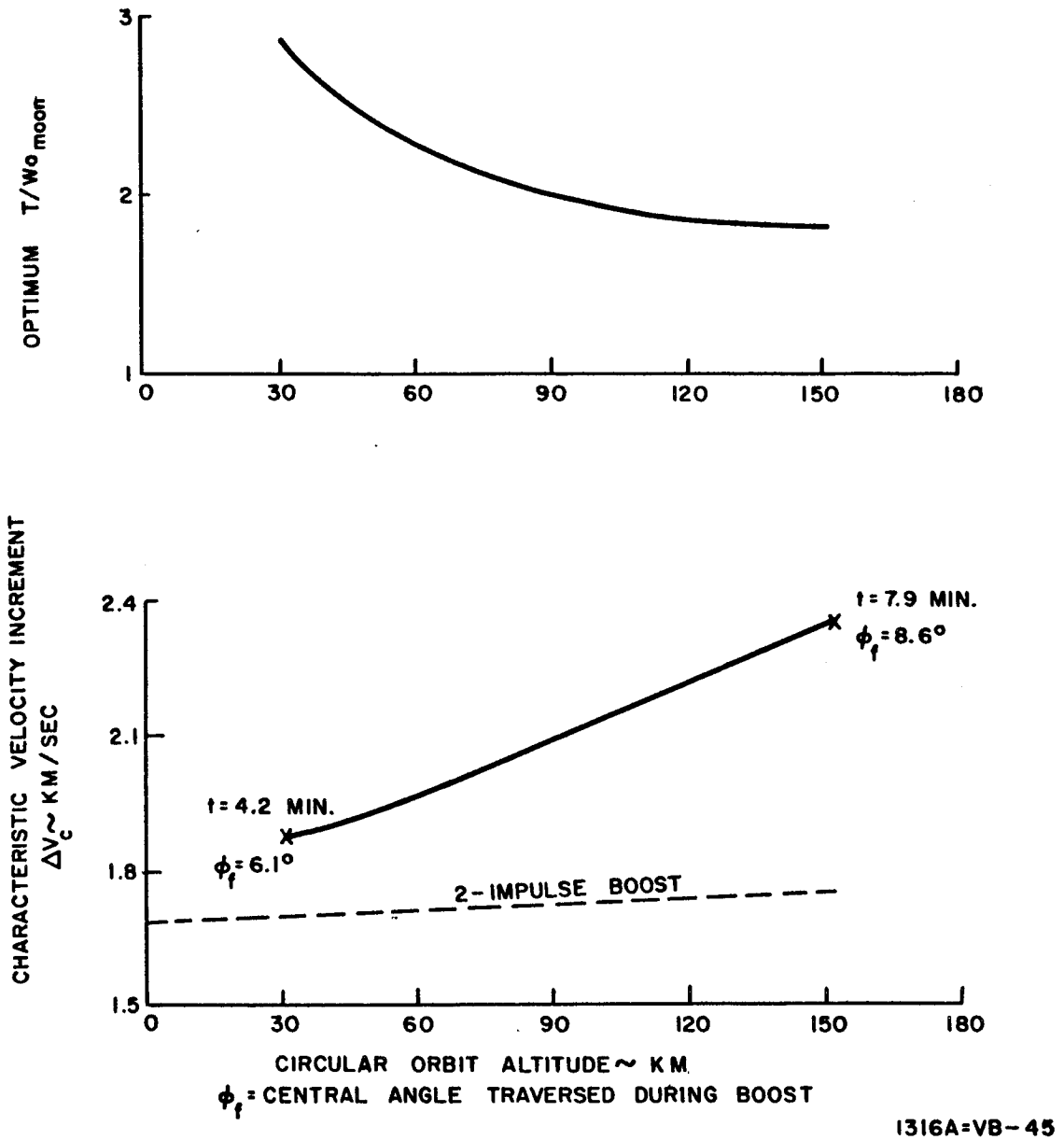

FIGURE 8.4-3: Constant Thrust Optimized Lunar Boost

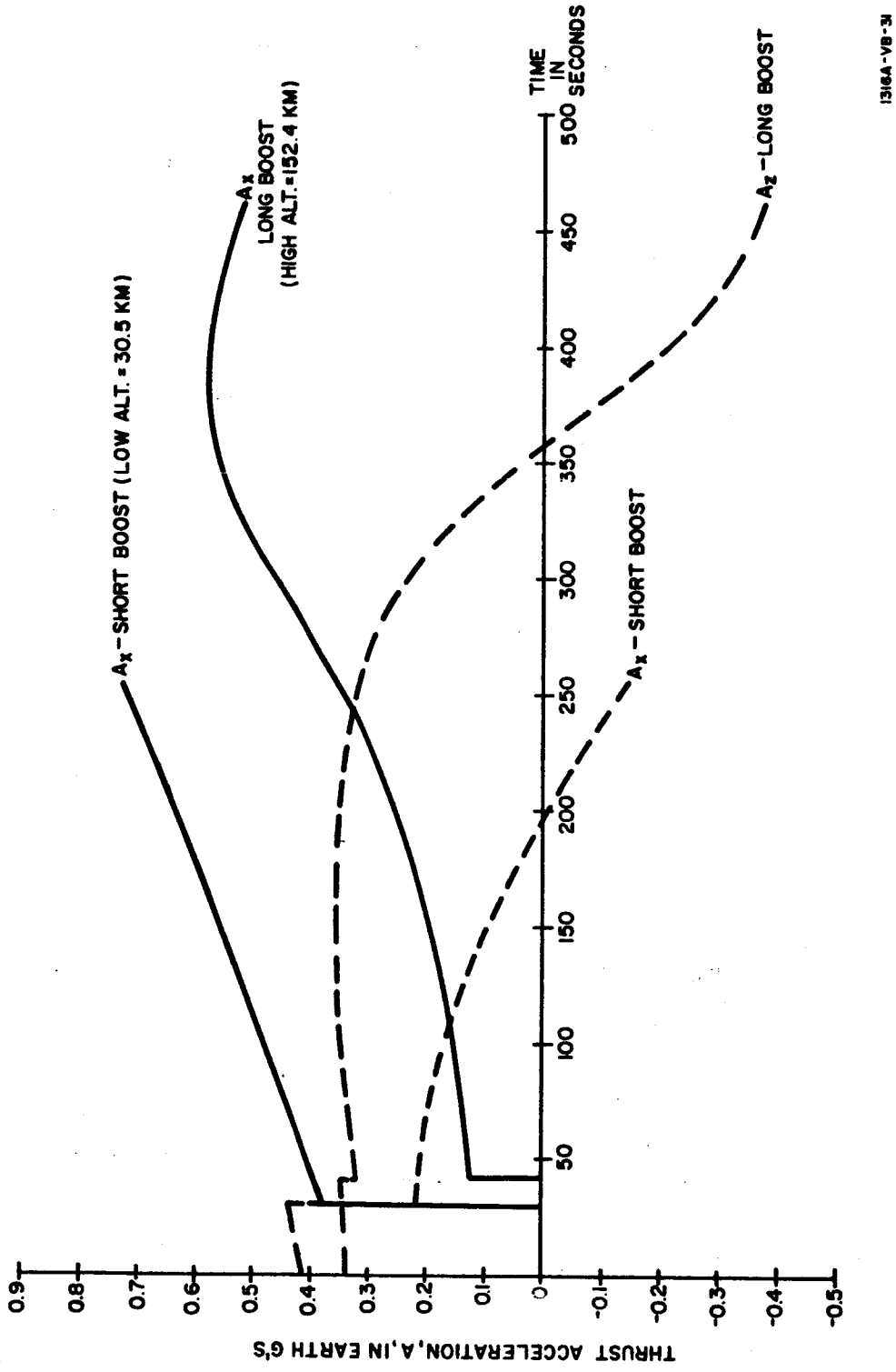

FIGURE 8.4-4: Nominal Boost Acceleration Profiles

Two of these optimized boost trajectories are considered in detail: a relatively short low-altitude boost, and a relatively long high-altitude boost. Trajectory data appearing in Table 8.4-1 has been obtained from the authors and used to plot the thrust components A_x and A_z vs. time, see Fig. 8.4-4 and Appendix 23.2. The jump in the acceleration profile results from assuming instantaneous application of the optimized attitude program after a short period of vertical flight.

The literature survey also revealed trajectory work for a lunar boost done by Burns and Singleton (ref. 8-14). The study is quite comprehensive and is not restricted to two-dimensional trajectories.

8.4.2.5 Launch-Site Definition

The nominal launch site like the target orbit is preselected from an operational view-point. For analytical simplification, the nominal boost trajectory has been two-dimensionalized. Thus, the launch site is constrained to lie in the target plane. Consideration of launch delays and out-of-plane ascents was provided in the Part I document. The following discussion summarizes the major results.

The landing site generally passes through the target plane twice during the planetary period of rotation. However, a co-planar launch is possible only if the target vehicle is at the preferred point in orbit, i.e., if the target is at the opposite side of the planet when the launch site passes through the target plane, lift-off must be delayed. In the general case, therefore, a launch plane change is required.

It was further indicated that for small planetary rotation ωt, the approximate required plane change ϕ is,

$$\phi = \omega t \sin \delta \cos \psi_0$$

where,

δ = inclination of the orbital plane with respect to the equator

ψ_0 = angle between the initial launch site position vector and the intersection of the target and equatorial planes

ω = planetary angular velocity

t = time interval between actual launch and theoretical in-plane launch.

For small plane changes the required velocity increment is approximately

$$\Delta v = v\phi = \omega t v \sin \delta \cos \psi_0$$

where v is approximately circular velocity at boost cut-off.

To obtain range requirements for sensors having input axes perpendicular to the nominal trajectory plane, consider a 6° plane change. The required Δv is then 10% v. Since the latter represents a large fuel expenditure, displacement and velocity perpendicular to the plane must be small compared to values attained within the plane. Therefore, range requirements are not critical.

However, the sensors will be specified symmetrically. The range and accuracy limitations will be dictated by the most stringent requirements on any one of the three axes. This method insures mechanization and control which may require the same minimal error characteristics on all three axes.

8.4.3 Error Analysis

8.4.3.1 Introductory Discussion

It is possible to separate error sources in the following manner:

1. Intentional analytical simplification of the actual equations of motion.
2. Intentional analytical simplification of the equations solved by the guidance system.
3. Imperfect operation of the sensors and data processing.
4. Errors in initial conditions (kinematic uncertainties of both the launch site and target) used to program the guidance system.

For the purposes of this study it is possible to work with only the last two error sources. When mechanizing the guidance scheme, it is essential to obtain error estimates from all four sources.

8.4.3.2 Parking Orbit Error Sensitivity

Problem definition consists of determining the dynamic variations at any point in a near-circular orbit as a function of miss distances and velocities at boost cut-off. Fortunately, the literature survey revealed much work in this area (refs. 8-4, 8-15, and 8-16).

For first order variations, the error coefficients are usually expressed as functions of time or one of the parametric anomalies with the choice dictated by the purpose of the analysis. In this study the true anomaly ϕ has been selected. No effort has been made to determine ϕ, i.e., the parking dwell time. The choice is of an operational nature depending primarily on the probability of launch delays and the location of the landing site relative to both the target and polar axis.

Generally speaking, the linearized analysis consists of separating

the problem into in-plane errors and errors normal to the nominal trajectory plane. The state vectors are normalized; thus the error coefficients in the transformation matrix expose the relationships between initial and final state variables. The analysis is presented in Appendix 23.3 with graphical results in section 8.5.

The results may also be used for the subsequent rendezvous phase when the transfer trajectory is near-circular. In the case of the lunar rendezvous, a very quick approximation is available for the propagation of injection errors for transfers between 75° and the Hohmann transfer.

8.4.3.3 Boost Error Analysis

The analytical formulation of the boost error analysis is given in Appendices 23.4 and 23.5. The analysis is conveniently divided into two steps: selection of system-component error models; propagation of errors as miss distances and velocities at boost cut-off. The following discussion summarizes the approach and provides the motivation for the selected method.

In an inertial system the characteristic defect is an incorrect velocity profile caused by imperfect and misaligned accelerometers. In turn, there are several error sources which affect both the profile and misalignment. The most significant sources are listed as follows:

Component	Error Source
1. Accelerometers	Input axis bias and scale factors Cross-axis sensitivity bias and scale factors
2. Gyros	Fixed drift, mass unbalance, anisoelasticity
3. Platform	Factory and launch site misalignment, and servo bias

The analytical models of each component given in the appendix indicates the mechanism by which each error source propagates its respective

This page intentionally left blank

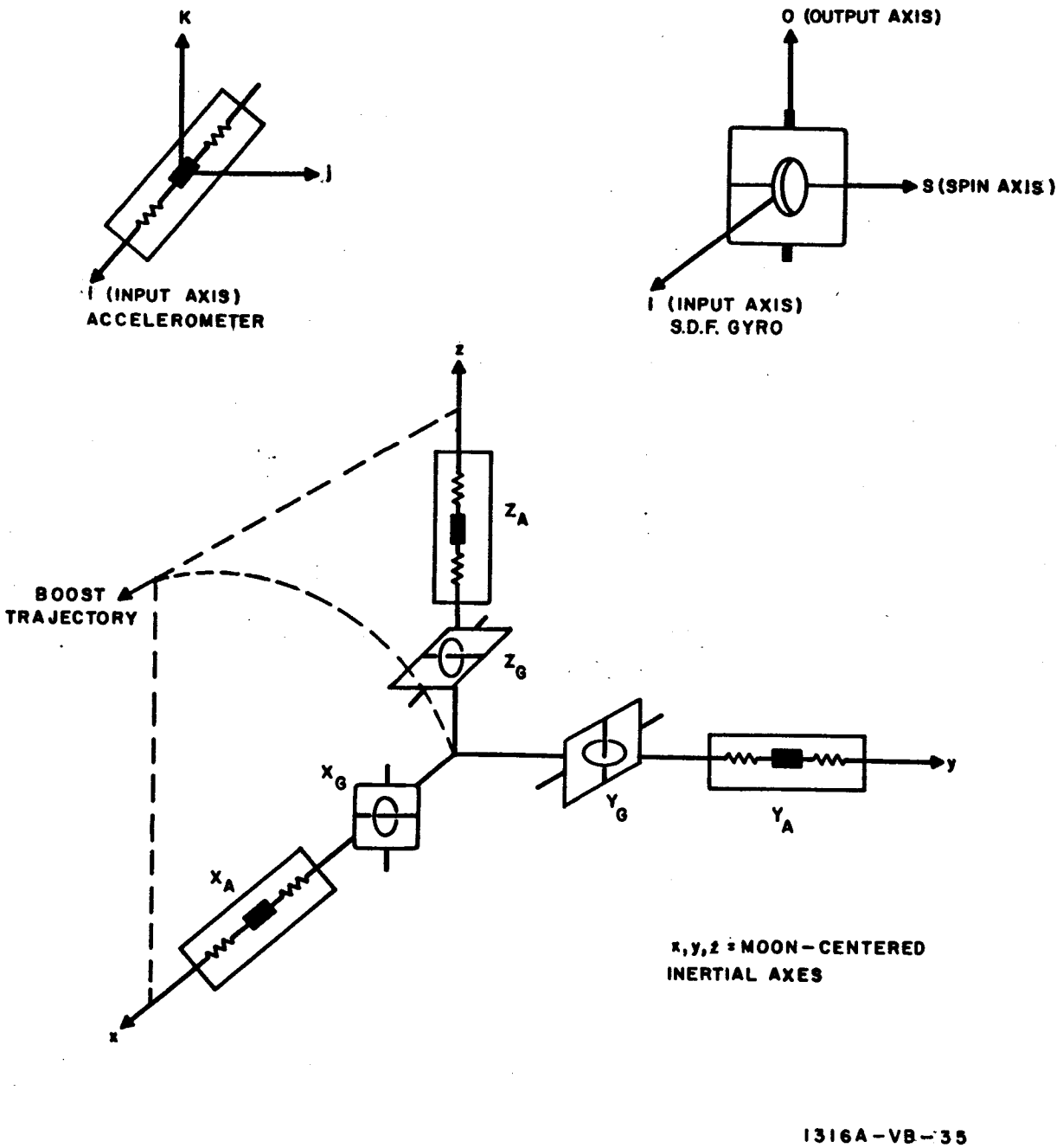

FIGURE 8.4-5: Orientation and Axes Definition of Inertial Sensors and Space-Stabilized Platform

errors. Thus, sensor orientations which reduce the over-all system inaccuracies may be selected. The orientation of gyros and accelerometers shown in Fig. 8.4-5 has been chosen on this basis. The nominal acceleration perpendicular to the trajectory plane is zero. Therefore, errors propagating as a function of this acceleration will be eliminated.

The second step involving the propagation of errors through the system requires a solution to three sets of differential error equations, each having forcing functions with trajectory dependent "coefficients". In only very specialized cases, where the trajectory parameters are extremely simple analytical functions, is it possible to avoid one of several non-analytical techniques.

For example, in a cruise mission error analysis where constant velocity and constant altitude flight characterizes the major portion of the powered trajectory, the trajectory coefficients are often approximated by step inputs. The resulting errors are then found to be simple functions of time.

If the trajectory is not simplified, three procedures are available (ref. 8-6):

1. Evaluation of a set of integrals which characterize the trajectory-dependent "coefficients" of the error forcing functions.
2. Utilization of a computer program which solves the generalized position and velocity differential error equations for all three axes.
3. Flight simulation program.

Considering the above methods in reverse order, the flight simulation program is most useful for evaluation of the entire guidance and control system. This method requires a complex computer program which is unnecessary for determining sensor requirements.

The second procedure can be utilized to obtain results for a wide

range and magnitude of error sources. In addition to optimizing the effects of error sources, it is possible to obtain the best initial orientation of the sensors. However, to make the program worthwhile results should be obtained for a wide range of nominal trajectories. In turn, variation in the selection of trajectory coefficients should be dictated by an additional computer program which optimizes the trajectory, such as the method discussed in section 8.4.2.4.

The first procedure of evaluating a set of trajectory integrals which characterize the coefficients of the error forcing functions can be accomplished several ways: digital computer computation, analytical hand integration, graphical integration, or combinations of graphical and hand integration in which polynominals are used to approximate the integrands. For a few nominal trajectories, this method is extremely useful and yields quick results.

Since the determination of many optimized trajectories is beyond the scope of this study, the method of graphical integration described in the last paragraph is the one by which sensor requirements are determined. The two boosts previously described should suffice inasmuch as they represent optimized trajectories which require both short and long flight durations. Methods involved in setting up a computer program for the second procedure are outlined in Appendix 23.5. In addition, a sample computation for non-atmospheric vertical flight is presented.

8.4.3.4 Pre-Launch Uncertainties

The uncertainty levels at launch for any rendezvous depend on the method used to determine position and velocity of the launch site. Extra-terrestrial methods may be classified as follows:

1. Earth-tracking
2. Independent surface navigation

3. Subtracting the relative motion of the target and launch site from the motion of the target.

The first method may be used to much advantage for a lunar mission especially as a back-up procedure. However, it will not be considered in this study to retain on-board independence.

Surface navigation techniques usually fall into the following categories: inertial, celestial, observations on ambient fields, and mapping (obtained prior to earth lift-off). A detailed discussion of each and hybrid techniques is beyond the scope of this study.

In the third method, relative motion between the two vehicles may be obtained by tracking equipment located in either vehicle. Since the target vehicle is usually able to determine its orbit very accurately after several revolutions, the accuracy of this method is essentially limited by the tracking equipment.

Since this study concerns itself with post-initial Apollo missions, the uncertainty levels in position and velocity of the launch site will be selected on the basis of previous probes having established better estimates in the critical areas. Evidently this is an area requiring additional investigation.

Referring to Table 8.4.2, a representative error of 100 meters in the launch site radius is chosen. The present estimates of probable error in

Position Errors	Uncompensated 1 σ Estimate
1. z-axis	Δz_0 = 100 m.
2. x-axis	$\Delta x_0/R_0$ = 30 sec. of arc
3. y-axis	$\Delta y_0/R_0$ = 30 sec. of arc

Velocity Errors - Negligible

Misalignment	Uncompensated 1 σ Estimate
1. z-axis	$\phi_z(0)$ = 30 sec. of arc.
2. x-axis	$\phi_x(0)$ = 30 sec. of arc.
3. y-axis	$\phi_y(0)$ = 30 sec. of arc.

Table 8.4-2: Estimated Pre-Launch Uncertainties for the Lunar Interceptor (external to system)

the lunar datum is of the order of 1000 meters. However, if the orbiting vehicle is capable of extreme accuracy in the measurement of orbital parameters, state-of-the-art configurations for range measurements provide much better radius determination. As an example, for a 200 km. target orbit and a 1 σ range uncertainty of 0.05%, the error in predicting the altitude of the launch site is 100 meters.

With methods such as stellar-inertial position on the earth may be established within a few thousand feet. Particular care in compensating gravitational anomalies and refinement of the optics can reduce the error to a few hundred feet. The former magnitude is equivalent to approximately 1/4 min. of arc. It is not unreasonable to estimate 30 secs. of error with similar procedures used on the lunar surface. This angle is equivalent to lateral surface uncertainty of 261 meters.

Planets whose angular velocity is extremely small yield negligible initial velocity errors. The only possible significant source is the tangential component. The accuracy of this component obviously depends on prediction of radius, latitude, and central body rotation. For a lunar equatorial landing site, the velocity is a maximum equal to approximately 4.63 m./sec. The error in its prediction can certainly be limited to 0.1% or 0.00463 m/sec. Referring to Appendix 23.5, for short burning periods the effect on thrust

cut-off position increases linearly with time; a 500 sec. boost then yields a position error of no more than 2.3 meters. Initial velocity errors and their effect on position have therefore been neglected.

The only remaining error source is initial misalignment of accelerometers. If the actual shape of the central body is best approximated by a sphere, then misalignment is defined relative to true vertical. Therefore, total misalignment is usually caused by:

1. Accelerometer-platform misalignment within the system
2. Ambient fields
3. Oblateness of the central body

The propagation of each error is the same and is given in Appendix 23.4 under platform misalignment.

The magnitude of the first error source is of course estimated by the manufacturer. Unfortunately, a brief literature survey did not reveal any estimates of the last two sources for a lunar rendezvous. There is much conjecture concerning the true shape of the moon, i.e., triaxial ellipsoid, equatorial bulges which may or may not exist, etc. The lunar anomaly has been selected on the basis of the following known earth anomalies.

Geodetic measurements of the earth's surface indicate variations due to density and form in the earth's crust from 5 to as high as 50 seconds of arc, depending on locality and terrain. At the better equipped launch sites, this error is generally held below 6 seconds. Perhaps, more significant errors on the lunar surface are those caused by the effects of local ore deposits on magnetic-sensitive leveling techniques. In this study component errors of 30 seconds on each axis have been selected. Again, further study is required in this area for all planetary rendezvous involving inertial sensors for boost.

8.5 Results

Since the boost cut-off errors are given in moon-centered inertial axes, a transformation through the central angle traversed during boost is required to obtain the errors in the coordinate system used for the parking orbit error analysis. Referring to Fig. 8.5-1 the transformation is

$$\begin{bmatrix} \Delta s_o \\ \Delta y_o \\ \Delta r_o \end{bmatrix} = \begin{bmatrix} \cos \phi_f & 0 & -\sin \phi_f \\ 0 & 1 & 0 \\ \sin \phi_f & 0 & \cos \phi_f \end{bmatrix} \begin{bmatrix} \Delta x \\ \Delta y \\ \Delta z \end{bmatrix}$$

The central angle ϕ_f traversed during both boost trajectories is less than 10°. Small angle assumptions then yield,

Error Axis	Position	Velocity
1. Radial	$\Delta r_o = \Delta z + \phi_f \Delta X$	$\Delta V_{r_o} = \Delta V_z + \phi_f \Delta V_x$
2. Track	$\Delta s_o = \Delta x - \phi_f \Delta Z$	$\Delta V_{r_o} = \Delta V_x - \phi_f \Delta V_z$
3. Cross-track	$\Delta y_o = \Delta y$	$\Delta V_{N_o} = \Delta V_y$

Table 8.5-1 provides a break-down for system-sensor and initial condition error propagation. Tables 8.5-2 and 8.5-3 provide total position and velocity errors at the initiation of parking in parking orbit coordinates. Figures 8.5-2 and 8.5-3 provide graphical illustrations of thrust cut-off errors during parking in accordance with the transformation matrix given in Figure 8.5-1.

Total and percentage values of fuel requirements for boost and orbital transfer are provided in Figure 8.5-4 through Fig. 8.5-8. These values are plotted as functions of parking altitude and central transfer angle.

The detailed discussion and interpretation of results is given in the following section.

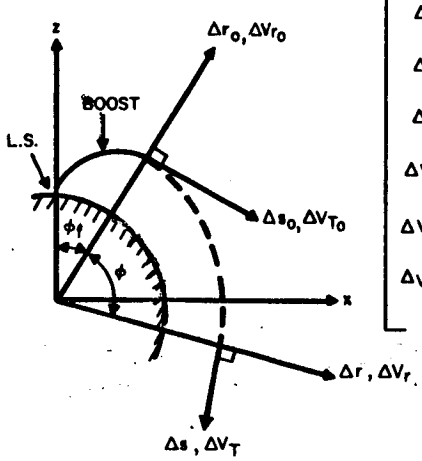

$$
\begin{bmatrix} \Delta r/r \\ \Delta s/r \\ \Delta y/r \\ \Delta V_r/V \\ \Delta V_T/V \\ \Delta V_N/V \end{bmatrix}
=
\begin{bmatrix}
2-\cos\phi & 0 & 0 & \sin\phi & 2(1-\cos\phi) & 0 \\
2\sin\phi-3\phi & 1 & 0 & -2(1-\cos\phi) & -3(\phi-4\sin\phi) & 0 \\
0 & 0 & \cos\phi & 0 & 0 & \sin\phi \\
\sin\phi & 0 & 0 & \cos\phi & 2\sin\phi & 0 \\
2\cos\phi-3 & 0 & 0 & -2\sin\phi & -3+4\cos\phi & 0 \\
0 & 0 & -\sin\phi & 0 & 0 & \cos\phi
\end{bmatrix}
\begin{bmatrix} \Delta r_o/r \\ \Delta s_o/r \\ \Delta y_o/r \\ \Delta V_{r_o}/V \\ \Delta V_{T_o}/V \\ \Delta V_{N_o}/V \end{bmatrix}
$$

1316A-VB-53

FIGURE 8.5-1: Parking Orbit Sensitivity Coefficients

SENSOR & PLATFORM ERROR COEFFICIENTS					*MISS VELOCITY COEFFICIENTS			*MISS DISTANCE COEFFICIENTS			SHORT BOOST VEL. ERROR ~ M./SEC.			LONG BOOST VEL. ERRORS ~ M./SEC			SHORT BOOST POSIT. ERRORS ~ M.			LONG BOOST POSIT. ERRORS ~ M.		
COMPONENT ERROR SOURCE	ERROR INPUT AXIS	SYMBOL	ERROR SYMBOL	UNCOMPENSATED 1 σ VALUE	ΔVx COEFF.	ΔVy COEFF.	ΔVz COEFF.	Δx COEFF.	Δy COEFF.	Δz COEFF.	ΔVx	ΔVy	ΔVz	ΔVx	ΔVy	ΔVz	Δx	Δy	Δz	Δx	Δy	Δz
ACCELER.:																						
1. BIAS	i	X_A	a_{ox}	2×10^{-5}g	t			$\frac{1}{2}t^2$			.0500			.0907			6.380			20.93		
	i	Y_A	a_{oy}	2×10^{-5}g		t			$\frac{1}{2}t^2$			.0500			.0907			6.380			20.93	
	i	Z_A	a_{oz}	2×10^{-5}g			t			$\frac{1}{2}t^2$			.0500			.0907			6.380			20.93
2. SCALE FACTOR	i	X_A	a_{1x}	2×10^{-5}g/g	I_1			$1I_1$			.0243			.0300			2.456			4.62		
	i	Y_A	a_{1y}	2×10^{-5}g/g																		
	i	Z_A	a_{1z}	2×10^{-5}g/g			I_3			$3I_3$			.0076			.0121			.862			5.21
3. CROSS-AXIS BIAS SENSIT.	j	X_A	a_{2x}	1×10^{-5}g/CROSS g																		
	j	Y_A	a_{2y}	1×10^{-5}g/CROSS g		I_3			$3I_3$			.0038			.0061			.432			2.61	
	j	Z_A	a_{2z}	1×10^{-5}g/CROSS g			I_1			$1I_1$			.0122			.0150			1.228			2.31
4. CROSS-AXIS SCALE FACTOR	j	X_A	a_{3x}	1×10^{-5}g/g/CROSS g																		
	j	Y_A	a_{3y}	1×10^{-5}g/g/CROSS g																		
	j	Z_A	a_{3z}	1×10^{-5}g/g/CROSS g			I_{11}			$11I_{11}$			.0024			.0003			.196			.46
5. CROSS-AXIS BIAS SENSIT.	k	Y_A	a_{4x}	1×10^{-5}g/CROSS g	I_3			$3I_3$			.0038			.0061			.432			2.61		
	k	Y_A	a_{4y}	1×10^{-5}g/CROSS g		I_1			$1I_1$			.0122			.0150			1.228			2.31	
	k	Z_A	a_{4z}	1×10^{-5}g/CROSS g																		
6. CROSS-AXIS SCALE FACTOR	k	X_A	a_{5x}	1×10^{-5}g/g/CROSS g	I_{11}			$11I_{11}$			.0024			.0003					.196			.46
	k	Y_A	a_{5y}	1×10^{-5}g/g/CROSS g																		
	k	Z_A	a_{5z}	1×10^{-5}g/g/CROSS g																		
GYROS:																						
1. AVG. DRIFT	i	X_G	b_{0x}	.02°/HR. = 10^{-7}RAD/SEC.		I_6			$6I_6$			.0024			.0021			.343			3.21	
	i	Y_G	b_{0y}	.02°/HR. = 10^{-7}RAD/SEC.	$-I_6$		I_4	$-6I_6$		$4I_4$	-.0024		.0215	-.0021		.0462	-.343		1.393	-3.21		5.33
	i	Z_G	b_{0z}	.02°/HR. = 10^{-7}RAD/SEC.		$-I_4$			$-4I_4$			-.0215			-.0462			-1.393			-5.33	
2. g - SENSIT. DRIFT	s	X_G	b^s_{1x}	.02°/HR./g = 10^{-7}RAD./g-SEC.		I_7			$7I_7$			.0027			-.0016			.347			.35	
	s	Y_G	b^s_{1y}	.02°/HR./g = 10^{-7}RAD./g-SEC.																		
(MASS UNBAL.)	s	Z_G	b^s_{1z}	.02°/HR./g = 10^{-7}RAD./g-SEC.		$-I_8$			$-8I_8$			-.0040			-.0193			-.331			-1.45	
3. g-SENSIT. DRIFT	i	X_G	b^i_{2x}	.02°/HR./g = 10^{-7}RAD./g-SEC.																		
	i	Y_G	b^i_{2y}	.02°/HR./g = 10^{-7}RAD./g-SEC.	I_9		I_8	$9I_9$		$8I_8$	.0126		.0040	.0447		.0193	.840		.331	.94		1.45
(MASS UNBAL.)	i	Z_G	b^i_{2z}	.02°/HR./g = 10^{-7}RAD./g-SEC.																		
4. ANISO-ELASTICITY	i	X_G	b_{3x}	.02°/HA./g^2 = 10^{-7}RAD./g^2-SEC.																		
	i	Y_G	b_{3y}	.02°/HA./g^2 = 10^{-7}RAD./g^2-SEC.																		
	i	Z_G	b_{3z}	.02°/HA./g^2 = 10^{-7}RAD./g^2-SEC.																		
PLATFORM:																						
1. INITIAL MISALIGNMENT (FACTORY)	k	X_P	$\phi_{xy}(0)$	10 SEC. OF ARC. = 5×10^{-5} RAD.																		
	j	X_P	$\phi_{xz}(0)$	10 SEC. OF ARC. = 5×10^{-5} RAD.	$-I_3$			$-3I_3$			-.0189			-.0304			-6.140			-13.03		
	k	Y_P	$\phi_{yx}(0)$	10 SEC. OF ARC. = 5×10^{-5} RAD.		$-I_1$			$-1I_1$			-.0609			-.0748			-2.155			-11.53	
	i	Y_P	$\phi_{yz}(0)$	10 SEC. OF ARC. = 5×10^{-5} RAD.		I_3			$3I_3$			.0189			.0304			6.140			13.03	
	i	Z_P	$\phi_{zx}(0)$	10 SEC. OF ARC. = 5×10^{-5} RAD.			I_1			$1I_1$			.0609			.0748			2.155			11.53
	j	Z_P	$\phi_{zy}(0)$	10 SEC. OF ARC. = 5×10^{-5} RAD.																		
2. SERVO BIAS	k	X_S	ϵ_x	10 SEC. OF ARC. = 5×10^{-5} RAD.		$-I_1$			$-1I_1$			-.0609			-.0748			-2.155			-11.53	
	k	Y_S	ϵ_y	10 SEC. OF ARC. = 5×10^{-5} RAD.		I_3			$3I_3$			.0189			.0304			6.140			13.03	
	k	Z_S	ϵ_z	10 SEC. OF ARC. = 5×10^{-5} RAD.	$-I_3$		I_1	$-3I_3$		$1I_1$	-.0189		.0609	-.0304		.0748	-6.140		2.155	13.03		11.53
								R.M.S. SUM			0.064	0.111	0.105	0.117	0.160	0.145	7.70	13.45	11.19	29.14	33.79	28.63
INITIAL CONDITION PROPOGATION																						
1. POSITION	x	-	$\Delta x_o/R_o$	30 SEC. OF ARC. = 15×10^{-5} RAD.				1									261			261		
	y	-	$\Delta y_o/R_o$	30 SEC. OF ARC. = 15×10^{-5} RAD.					1									261			261	
	z	-	Δz_o	100 m.						1									100			100
2. MISALIGNMENT	x	-	$\phi_x(0)$	30 SEC. OF ARC. = 15×10^{-5} RAD.		I_3			$3I_3$			.0567			.0912			18.42			39.09	
	y	-	$\phi_y(0)$	30 SEC. OF ARC. = 15×10^{-5} RAD	$-I_3$		I_1	$-3I_3$		$1I_1$	-.0567		.1827	-.0912		.2244	-18.42		6.47	-39.09		34.59
	z	-	$\phi_z(0)$	30 SEC. OF ARC. = 15×10^{-5} RAD		$-I_1$			$-1I_1$			-.1827			-.2244			-6.47			-34.59	
3. VELOCITY	-	-		NEGLIGIBLE																		
R.M.S. SUM (INITIAL MISALIGNMENT ONLY)											0.057	0.192	0.183	0.091	0.242	0.224	18.42	19.58	6.47	39.1	52.3	34.6

*REFER TO TABLE 23.4-2 FOR MISS COEFFICIENT INTEGRALS

TABLE 8.5-1: ERROR COEFFICIENTS, PROPAGATION, AND EVALUATION AT THRUST TERMINATION

This page intentionally left blank.

TABLE 8.5-2

Velocity Errors at Thrust Cut-Off

ERROR SOURCE	RADIAL Value m/sec ΔV_{r_o}	RADIAL Normalized x 10^{-6} $\Delta V_{r_o/V}$	TRACK Value m/sec ΔV_{T_o}	TRACK Normalized x 10^{-6} $\Delta V_{T_o/V}$	CROSS-TRACK Value m/sec ΔV_{N_o}	CROSS-TRACK Normalized x 10^{-6} $\Delta V_{N_o/V}$
System-Sensor	0.122	73	0.053	32	0.111	67
*L.S. Init.Pos.	0	0	0	0	0	0
L.S. Misalign.	0.189	115	0.038	23	0.192	115
L.S. Init.Vel.	Negligible		Negligible		Negligible	
SHORT BOOST						
System-Sensor	0.163	101	0.095	59	0.163	101
L.S. Init.Pos.	0	0	0	0	0	0
L.S. Misalign.	0.238	147	0.057	35	0.242	150
L.S. Init.Vel.	Negligible		Negligible		Negligible	
R.M.S. Sum	0.288	179	0.111	69	0.292	181

* Launch Site (L.S.)

TABLE 8.5-3

Position Errors at Thrust Cut-off

ERROR SOURCE	RADIAL Value Δr_o meters	RADIAL Normalized $\Delta r_o/r$ x 10^{-6}	RADIAL Normalized $\Delta r_o/h_T$ * %	TRACK Value Δs_o meters	TRACK Normalized $\Delta s_o/r$ x 10^{-6}	TRACK Normalized $\Delta s_o/r$ sec.of arc	CROSS-TRACK Value Δy_o meters	CROSS-TRACK Normalized $\Delta y_o/r$ x 10^{-6}	CROSS-TRACK Normalized $\Delta y_o/r$ sec. of arc
System-Sensor	12.01	6.79	0.006	6.51	3.68	0.74	13.45	7.62	1.52
** L.S. Init.Pos.	128	72.4	0.064	250	141.4	28.3	261	147.7	29.5
L.S. Misalign.	8.43	4.77	0.004	17.3	10.03	2.01	19.58	11.06	2.21
L.S. Init.Vel.	negligible			negligible			negligible		

SHORT BOOST

* Normalized with respect to 200 km. target altitude

** Launch Site (L.S.)

LONG BOOST

System-Sensor	33.0	17.0	0.017	33.4	17.7	3.54	38.8	17.9	3.58
L.S. Init.Pos.	139	73.6	0.070	246	130.1	26.0	261	138.0	27.6
L.S. Misalign.	40.5	21.5	0.020	33.9	17.9	3.59	52.3	27.7	5.54
L.S. Init. Vel.	negligible			negligible			negligible		

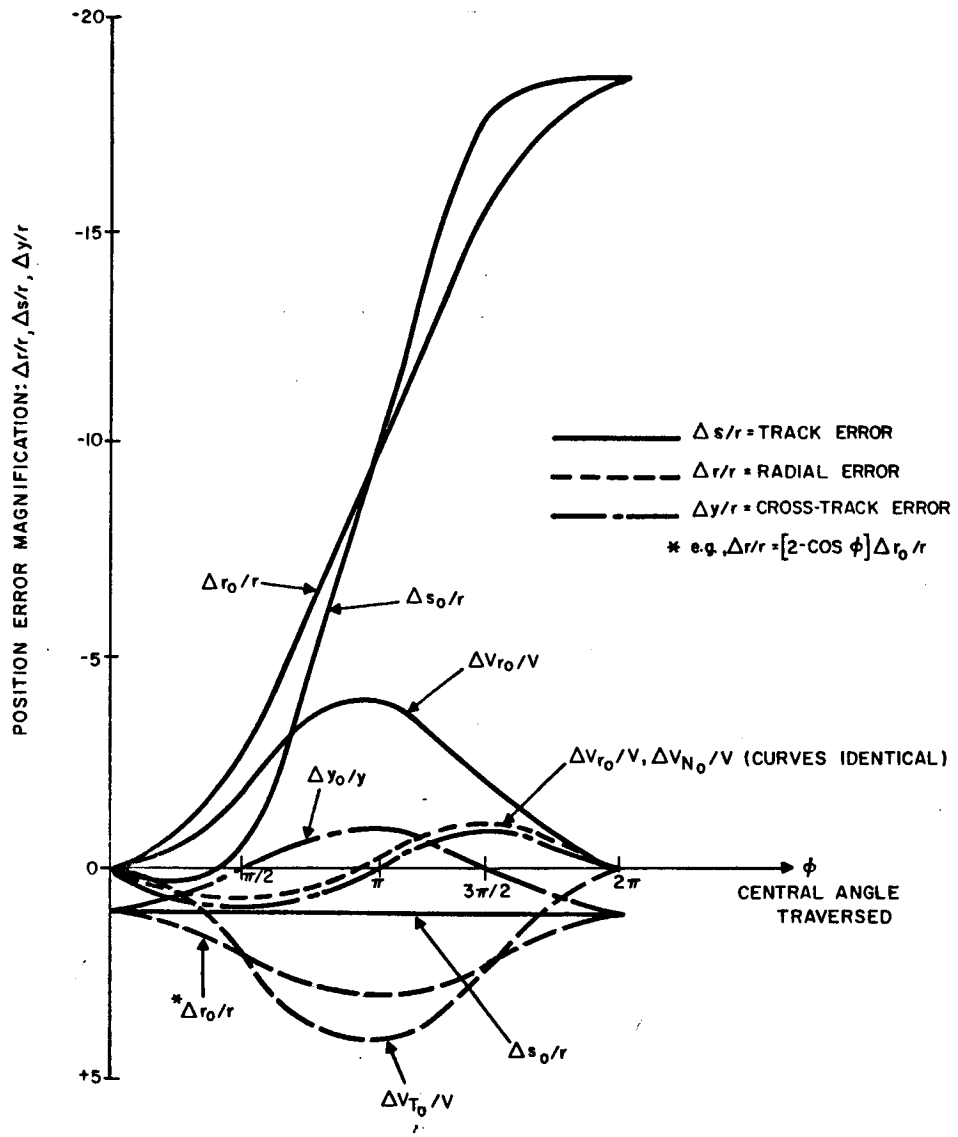

1316A-VB-38

FIGURE 8.5-2: Effect of Initial State Errors on Final State Position Errors for Near Circular Orbits

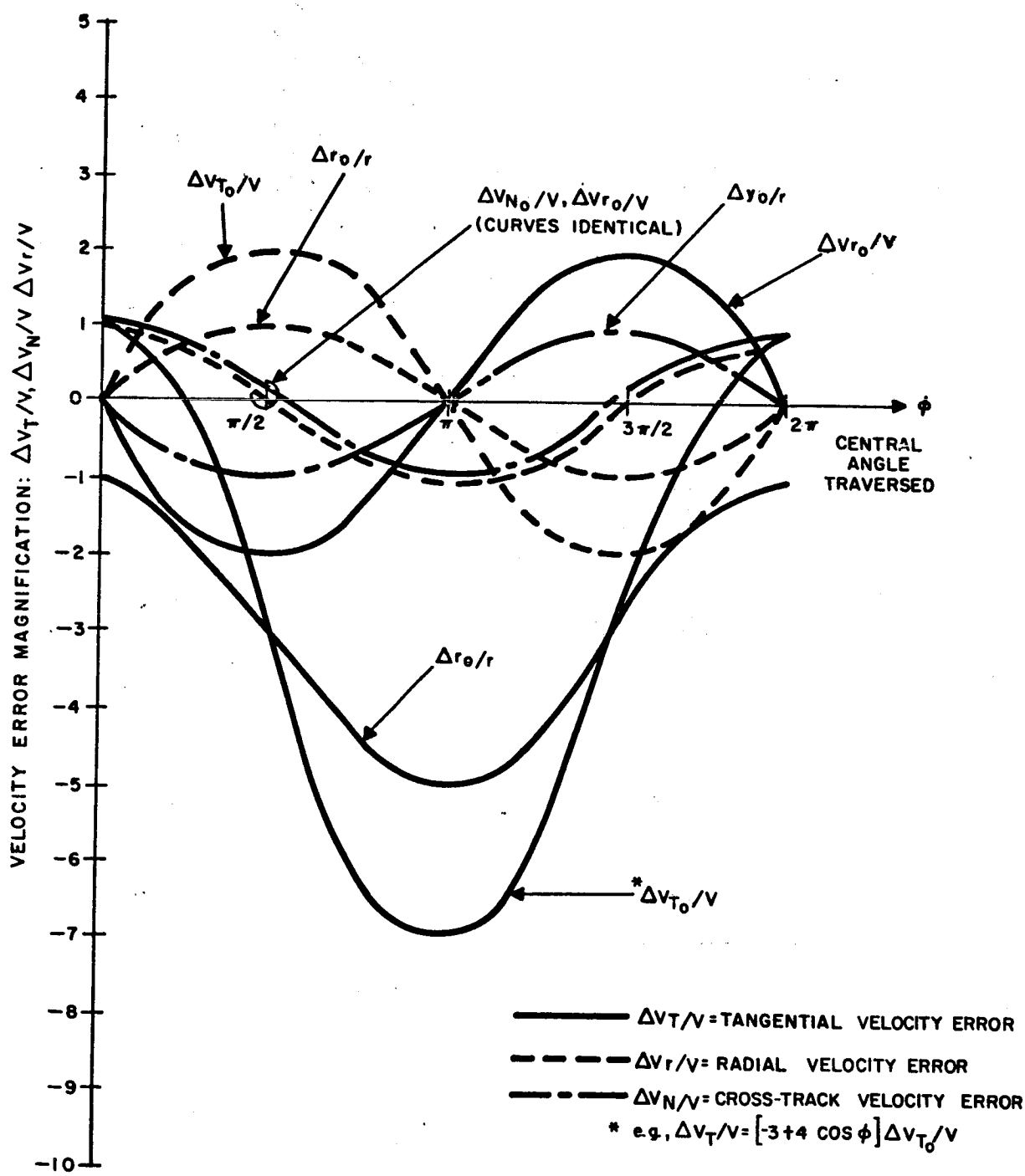

FIGURE 8.5-3: Effect of Initial State Errors on Final State Velocity Errors for Near-Circular Orbits

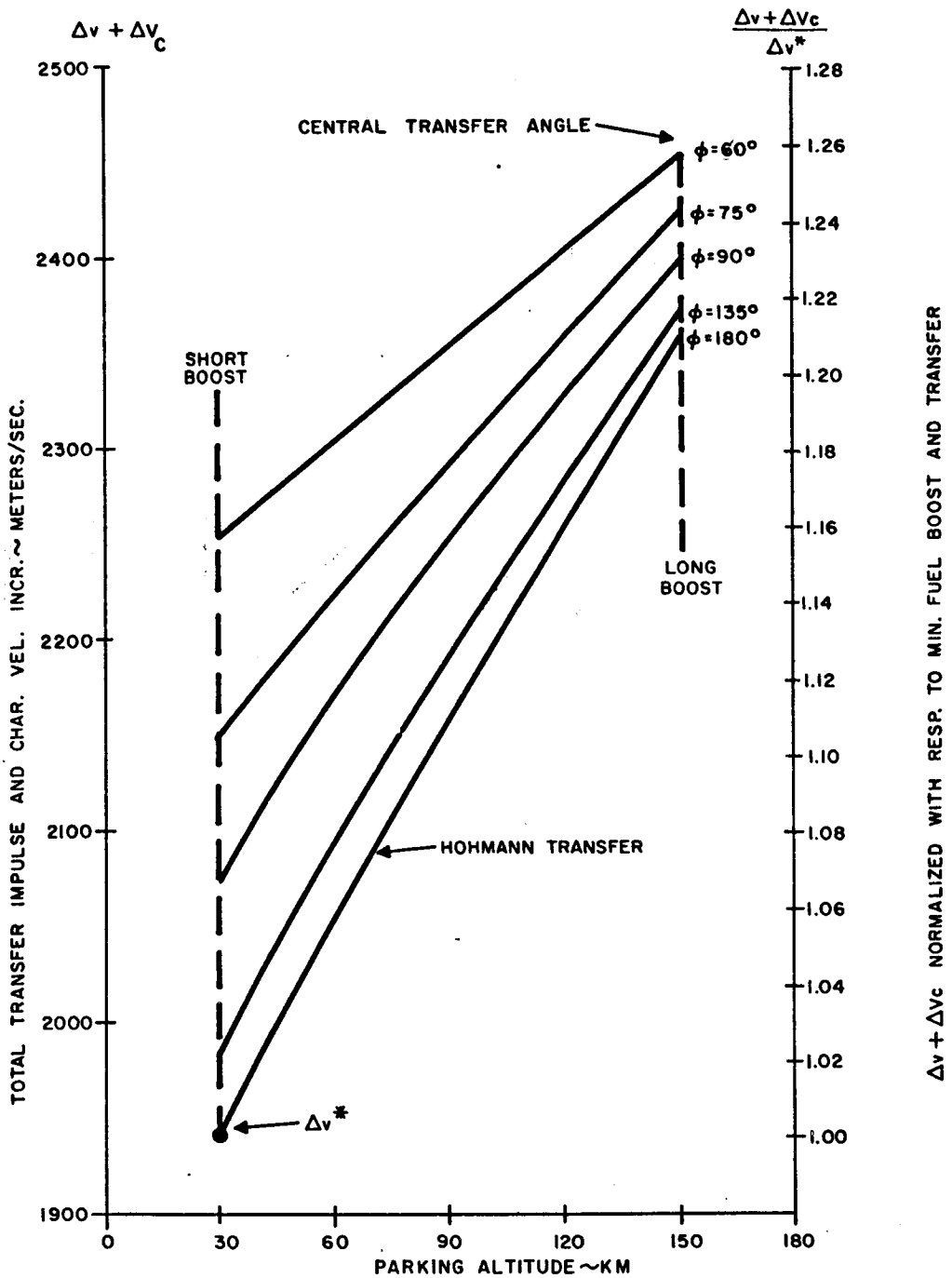

FIGURE 8.5-4: Total Velocity Requirements vs. Parking Altitude for Various Central Transfer Angles (200 km Target Orbit)

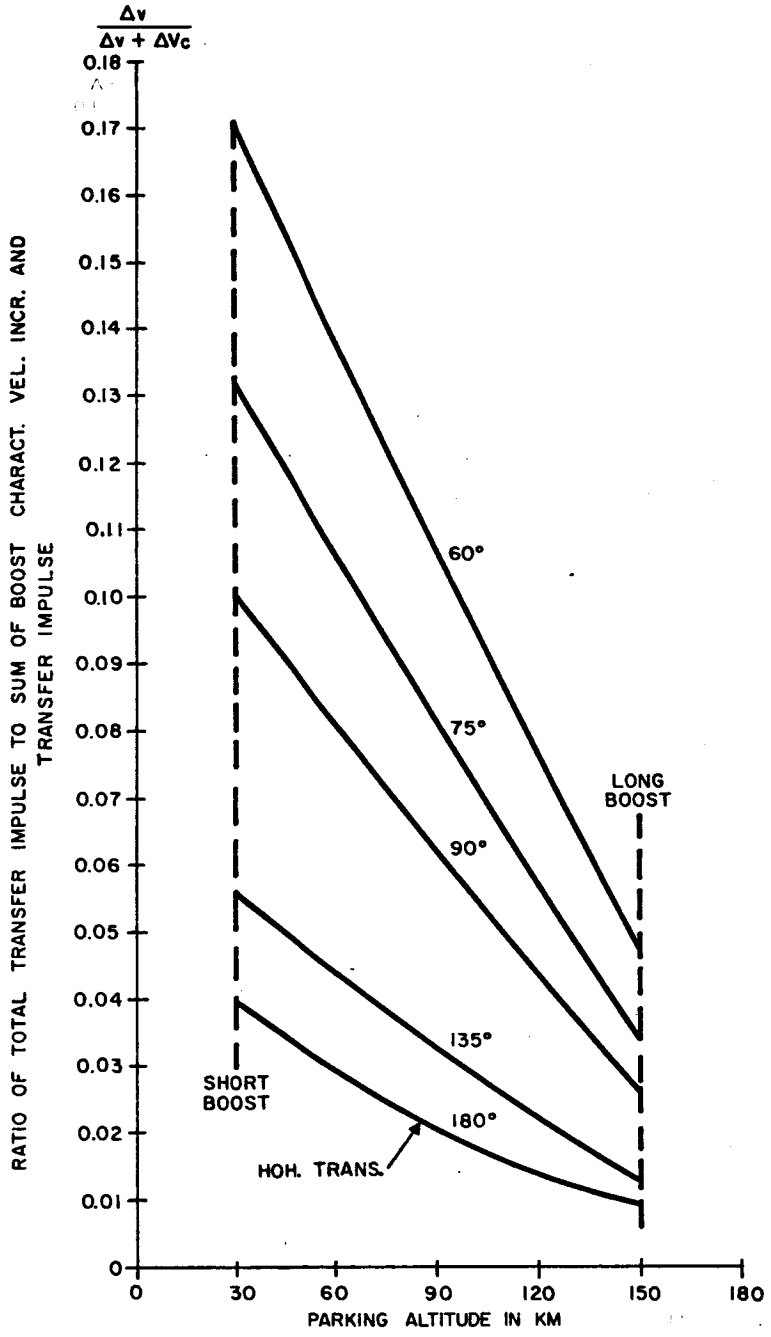

1316A-VB-41

FIGURE 8.5-5: Percentage of Fuel Required for Transfer vs. Parking Altitude for Various Central Transfer Angles (200 km Target Orbit)

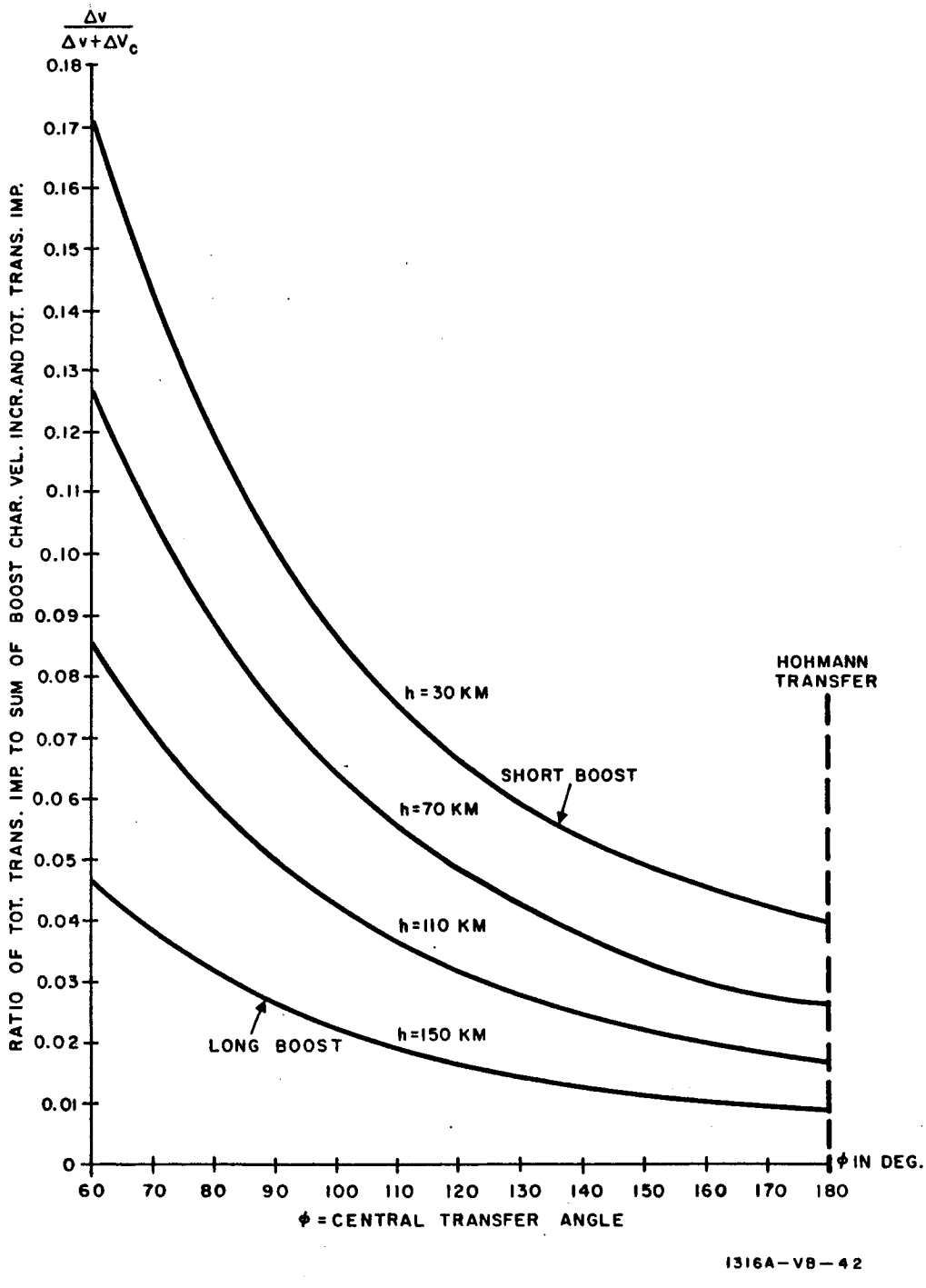

FIGURE 8.5-6: Percentage of Fuel Required for Transfer vs. Central Transfer Angle for Various Parking Altitudes (200 km Target Orbit)

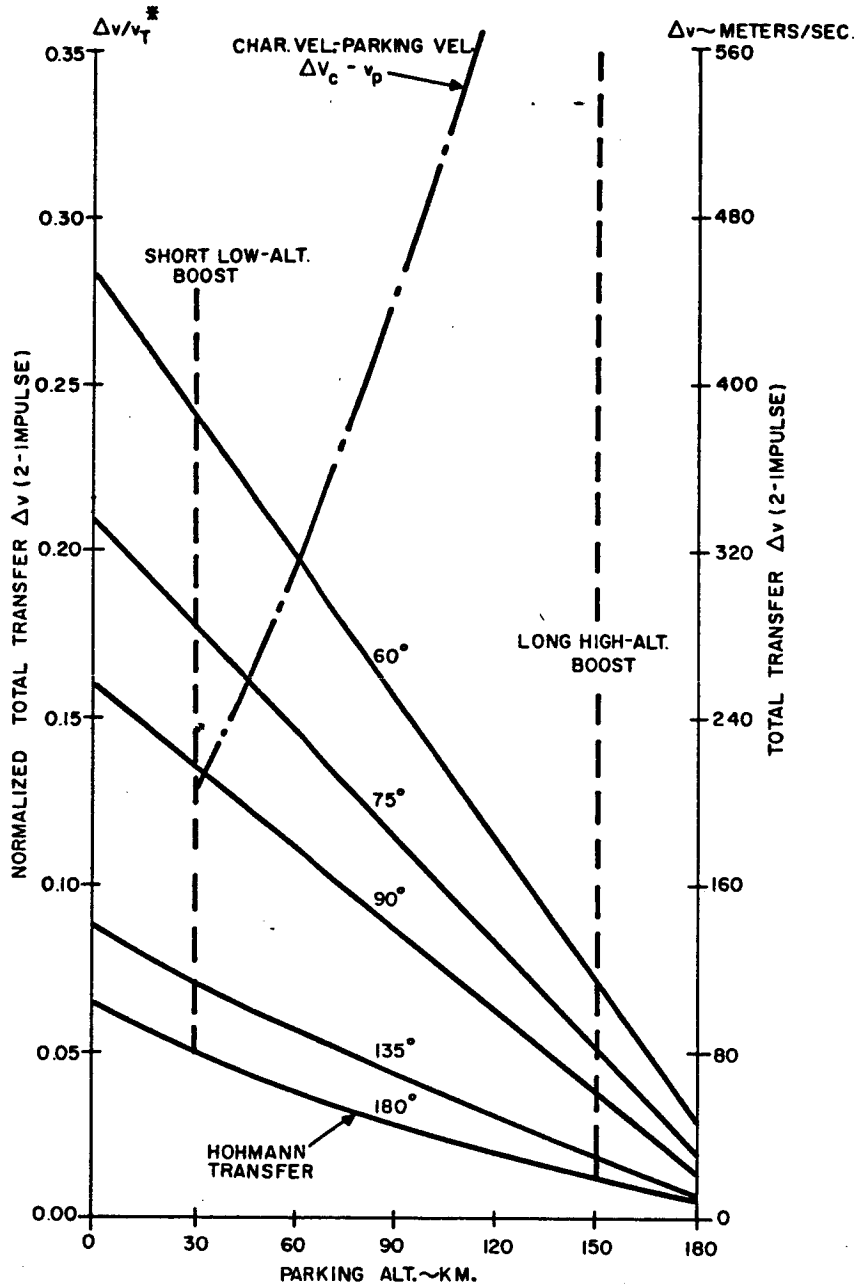

1316A-VB-43

FIGURE 8.5-7: Total Required Transfer Velocity Increment vs. Parking Altitude for Various Central Transfer Angles (200 km* Target Orbit)

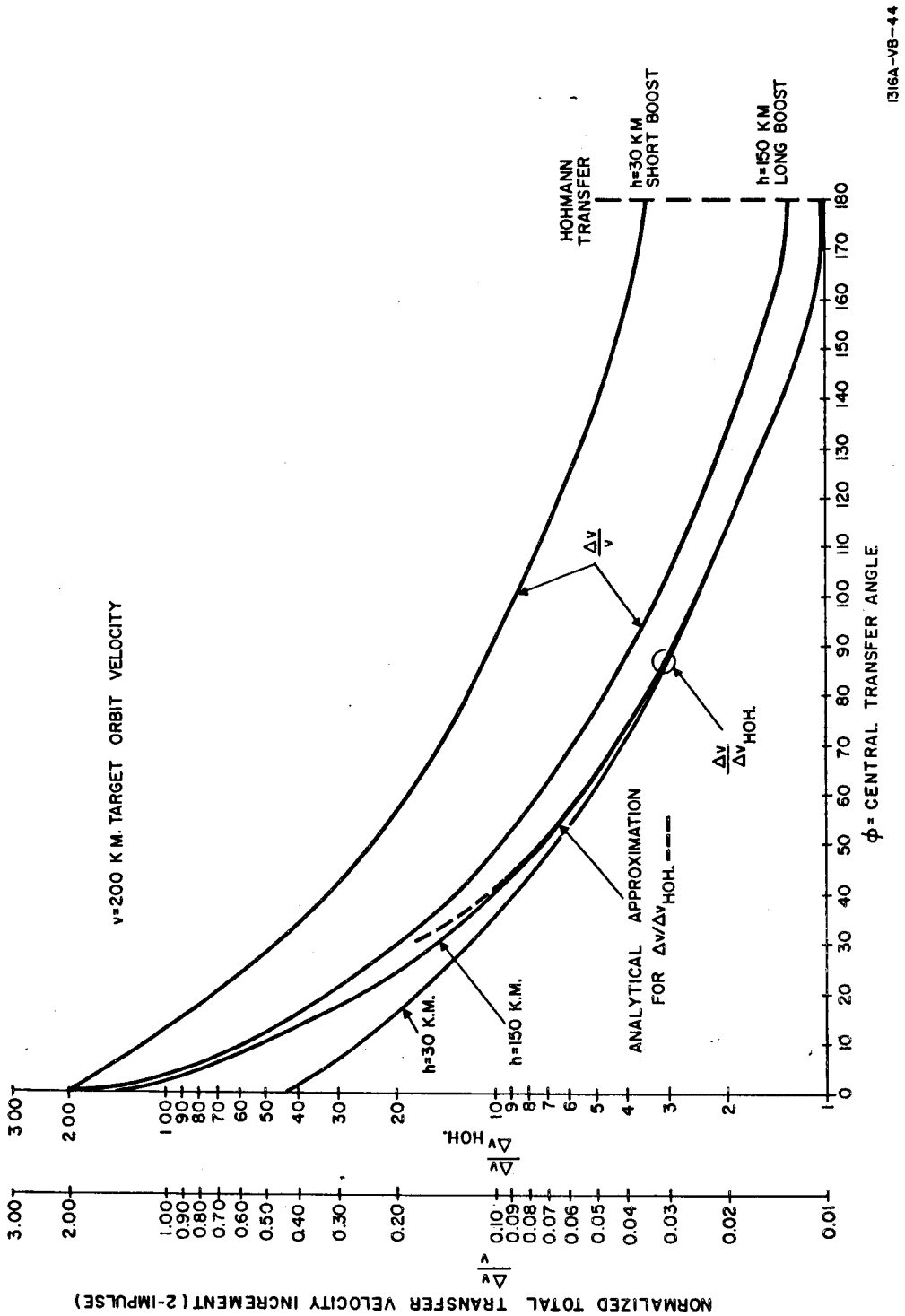

FIGURE 8.5-8: Total Required Transfer Velocity Increment for Minimum Energy Circle-to-Circle Transfer

This page intentionally left blank

8.6 Interpretation of Results

The results will be considered from three aspects: fuel, time and sensor requirements. The first two will be discussed simultaneously.

Referring to Fig. 8.5-4 which provides a measure of the total ascent and transfer fuel requirements, Δv^* is defined as the total velocity impulse required for the minimum fuel ascent and transfer trajectory. This trajectory insures terrain avoidance during parking at 30 km. and is followed by a 180° Hohmann transfer to 200 km. For a similar transfer but with an initial boost to 150 km, 21% more fuel is required; for a 90° transfer from 30 km. to 200 km. the fuel penalty is 7%, but the time saving is roughly equivalent to one-fourth the period of the target orbit, or 15 minutes. For faster transfers from 30 km. the fuel penalty becomes quite significant, i.e., a direct ascent is preferable.

For the high altitude boost, which takes only a few hundred more seconds than the 30 km. boost, it is evident that low transfer angles have a significantly lesser effect. The fuel penalty between a 75° and Hohmann transfer is only 3% for the high altitude, long boost.

For a very quick ascent, time savings close to 25 min. can be achieved at a fuel penalty of less than 30% compared with the minimum fuel ascent. This fuel difference is equivalent to a Δv of roughly 1/2 km./sec.

Referring to Fig. 8.5-5 which gives the ratio of transfer fuel to the total fuel required, a 6% penalty is paid for a 90° transfer compared to the Hohmann from 30 km. This penalty is reduced to 1-1/2% for the 150 km. parking orbit. Obviously, fast transfers from low altitudes may place requirements on the rendezvous scheme which are too stringent, i.e., fuel is wasted in obtaining injection velocity. Figure 8.5-6 also substantiates this conclusion.

Fig. 8.5-7 simply provides the magnitude of the total transfer

impulse for various parking orbits and transfer angles. In addition it is relevant to indicate a close approximation to the efficiency of the boost phase by itself. Thus, the difference between the characteristic velocity increment and the parking velocity is plotted vs. altitude.

Fig. 8.5-8 is an expanded plot indicating the inefficiency of small transfer angles for circle-to-circle transfer. Note that $\Delta v / \Delta v_{HOH.}$ is practically independent of the altitude of the parking orbit for transfers above 40°. This provides obvious justification for limiting the parking orbit to the lowest possible altitude, if fuel is the only criteria.

Interpretation of the sensor error analysis is considered from four aspects:

1. System-sensor error propagation
2. Propagation of initial condition uncertainties
3. Propagation of errors during parking
4. Integration of boost, parking, and transfer

The first two items are discussed comparatively; discussion of the latter two provides the method and criteria used to determine sensor requirements.

Referring to Table 8.5-3, it is evident that for the short boost, inaccurate launch site location contributes errors at least ten times that of the internal system errors. For this reason r.m.s. sums were not given. The situation is much the same for the longer boost. These results are expected since the system was assumed to have no up-dated position monitoring. Anomalies in the local vertical which do not exceed 30 sec. of arc on each axis contribute relatively sizeable errors, but far less than those discussed above.

Since velocity errors (Table 8.5-2) are grossly unaffected by launch site location, system-sensor errors should have the same order of magnitude as those errors caused by initial verticality anomalies. Note that for both

boosts, the r.m.s. magnitudes are nearly equal and do not exceed 0.3 m/sec. at thrust cut-off. As expected (Table 8.5-1) the primary error sources are accelerometer bias along the input axes and platform alignment. If requirements on the non-g-sensitive drift of the gyros are relaxed, larger errors would result.

The significance of the cut-off errors is primarily determined by the type of ascent and capabilities of the rendezvous scheme. Difficulties during rendezvous are characterized by limited fuel capability and the uncertanties with which the injection conditions are known. Therefore, any criteria for evaluation of the boost sensors necessitates an integrated approach.

It is obvious that the establishment of <u>any</u> parking orbit not imposing severe fuel constraints on the rendezvous scheme is the first requirement to be met. Since partial or total control exercised by the target on the interceptor is not assumed, the accuracy in achieving a pre-selected orbit is essentially independent of the target vehicle, although a better estimate of launch-site radius may be attained by pre-launch tracking procedures. It is emphasized that relative measurements primarily function in the <u>selection</u> of a nominal parking orbit, but in no way guarantees the accuracy with which the orbit is established. Should a situation arise in which the interceptor must leave the surface of a planet when the target is on the other side, a given orbit must still be attained without the help of communication or tracking. For these reasons, it is assumed that the accuracy in achieving the parking orbit is independent of tracking or communication between the vehicles.

For the lunar ascent, the accuracy attained at thrust cut-off yields parking parameters resulting in an orbit more than adequate for transfer. In fact, requirements on the boost sensors need not be as stringent as those

initially selected on the basis of normal present-day capability.

As an example, consider half a parking orbit. Referring to Fig. 8.5-2, for 180° of parking, the initial tangential velocity and altitude errors multiply their effects on altitude by 3 and 4 respectively. The boost to 30 km. yields a normalized velocity error of 390×10^{-6} and normalized radial error of approximately 72×10^{-6}. A normalized value of 500×10^{-6} magnified 5 times is equivalent to $\frac{\Delta r}{r} = 2500 \times 10^{-6}$. Taking $r = Ro + 30$ km., Δr is then 4.3 km. If the datum of the moon were known no better than we know now, i.e., 1 km., multiplication by 4 at 180° then yields an altitude error of 4 km.

Since velocity errors have the most significant effect on the geometry of the parking orbit, it is relevant to determine which error source is the primary contributor. This was done previously in the discussion and seems to be surface alignment at the launch site. Alignment procedures can be relaxed by a factor of 2 or 3 before the errors at 180° become anywhere near significant.

The previous discussion indicated that good state-of-the-art inertial platforms are more than adequate to establish a lunar parking orbit. The question of using the boost sensors to partially establish the injection conditions from the parking orbit to rendezvous will now be considered.

Once the interceptor is in the parking phase, position and velocity of both vehicles with respect to the center of the planet must be established. The magnitude and direction of the impulse applied at the initiation of transfer depends on target ephemeris prediction as well as determination of the kinematic state of the interceptor just prior to injection. Both conditions may be determined by one of the following methods:

1. Interceptor trajectory determination plus vehicle-to-vehicle measurements.

2. Target trajectory determination plus vehicle-to-vehicle

measurements.

3. Independent interceptor and target trajectory determination.

Measurements of the above may be attained by either or both vehicles with or without vehicle-to-vehicle communication. The boost sensors at best can provide only part of the necessary measurements. Therefore, it is impossible to specify requirements without considering tracking procedures and target ephemeris prediction. This is a fringe area requiring additional investigation.

For a direct ascent in which the cut-off conditions yield the transfer orbit immediately, boost sensor accuracy is extremely critical. In essence, the launch window is a minimum. A scheme which accurately forces the interceptor to a given location with a given velocity at a preselected time is required. For the parking ascent, conventional long-range ballistic missile guidance is perfectly adequate as orbit-to-orbit synchronization is of little consequence during boost.

In summary, it is a foregone conclusion that good state-of-the-art inertial platforms are more than adequate for the type of lunar rendezvous considered. Requirements should certainly be relaxed if the reliability of any selected high-accuracy platform is questionable. Note that insight predicts results of this nature, i.e., since the lunar gravitational attraction is roughly 1/6 that of the earth, any vertical g-sensitive error propagation should be reduced roughly by 1/6 and g^2-sensitivity by 1/36. The same rule of thumb could be used for other planetary rendezvous, but should only provide a direction to be taken for subsequent boost guidance and navigation analysis.

The use of unmonitored inertial platforms for prediction of instantaneous position and velocity just prior to transfer injection

requires additional investigation. A study in which rendezvous capabilities and target prediction are integrated with the boost and parking phase would of necessity provide sensor requirements for the entire initial-to-terminal maneuvers.

8.7 Sensor Requirements

The discussion in the previous section concluded that state-of-the-art capability is more than adequate for achieving any lunar parking orbit which may be desired for a rendezvous with a low altitude target. The following chart simply summarizes those sensor accuracies which were used to prove the above statement.

TABLE 8.7-1: Sensor Requirements for Lunar Parking Ascent

Device	Accuracy (1 σ Uncompensated value)
A. Integrating Accelerometers (1-1/2 g range)	
1. Input axis	
Bias	2×10^{-5} g
Scale Factor	2×10^{-5} g/g
2. Cross-axis sensitivity	
Bias	1×10^{-5} g/cross-g
Scale Factor	1×10^{-5} g/g/cross-g
B. S.D.F. Gyros	
1. Fixed Drift	0.02°/hr.
2. Mass Unbalance	0.02°/hr./g
3. Anisoelasticity	0.02°/hr./g^2
C. Platform	
1. Factory Misalignment	10 sec. of arc
2. Servo Bias	10 sec. of arc

NOTE: Above accelerations in earth g's

8.8 Recommendations

The following recommendations apply mainly to extra-terrestrial ascents:

1. The accuracy in achieving a given parking orbit with inertial sensors is primarily limited by pre-launch uncertainties, i.e., verticality and position anomalies at the launch site. Since the uncertainty in the magnitude of the position vector may be reduced by subtracting the launch site-to-target altitude from the target radius, effort should be made to establish a predictable error in tracking range measurements and instantaneous radius prediction. Anomalies in the local vertical are very difficult to compensate unless knowledge of such variables as shape, mass distribution, local ore deposits, etc. are available.
2. If inertial boost sensors are used to predict instantaneous position and velocity at any point in the parking phase, a computer program would be desirable. Inputs variations would include sensor errors, initial condition uncertainties, and variation in trajectory coefficients. By utilizing error sensitivity coefficients for near-circular orbits, the results could be given as miss distances and velocities at any point during parking. Provisions could be made in such a program for external monitoring (stellar, horizon scanning, etc.). Thus, rendezvous sensor specification could be integrated with the previous two phases.
3. A general study of guidance schemes which integrate rendezvous and boost in a direct ascent is recommended. Such a study is necessary for emergency situations in which flight time is minimal. The analysis would necessarily present fuel, launch delays, and flight time trade-offs.

9.0 LUNAR RENDEZVOUS, MANNED

9.1 Introduction

The rendezvous area of interest commences with the establishment of the ascent trajectory and covers the active maneuvering required to effect a rendezvous with a lunar orbiting target vehicle.

The basic purpose of this study is to determine sensor requirements which will make rendezvous possible. For the purposes of this study a rendezvous model was selected which is not only practicable but representative of a number of typical systems being proposed for lunar missions. The lunar orbital rendezvous model, illustrated by Fig. 9-1, presumes the target vehicle to be in a 500 km circular lunar orbit, while the chaser vehicle is initially in a nominal 30 km circular parking orbit substantially coplanar with the target orbit. When the chaser, on the basis or prior or present lunar and target measurements, determines that it is correctly phased with the target, it imparts a computed incremental velocity vector by means of rocket propulsion. The effect of this velocity maneuver is to establish an ascending transfer ellipse which is nominally cotangential to the target orbit at the anticipated interception point. Much of the ascent is a pure coasting phase, but finally at a relatively short range the active phase of rendezvous commences. On the basis of rendezvous sensor measurements to the target, the chaser executes a series of propulsion maneuvers to smoothly and safely close with the target. Since the chaser vehicle is considered to be manned, the actual docking including the final phase of rendezvous, is presumed to be accomplished with manual control using visual observations. The study area of interest terminates when the automatic rendezvous system brings the chaser to a preset standoff range from the target with essentially zero relative velocity.

9.2 Background and Approach

The general problem of rendezvousing with a satellite vehicle is

presented in Ref. 9-1 which covers not only the launch phase as well as direct and indirect ascents, but also reviews four of the more general schemes for effecting final closure with the target. The rendezvous systems considered include a variety of guidance equations, sensing elements, and propulsion means.

Velocity maneuvers are executed by a variety of propulsion, attitude, and control combinations, such as:

a. variable thrust or fixed thrust rocket engines

b. single-firing or re-startable engines

c. gimballed rocket engines or rockets aligned to the body axes

d. with fixed rockets, the vehicle may be attitude stabilized or may be pointed in the desired direction whenever a rocket impulse is to be made

e. with variable-thrust engines, the thrust level is varied as a function of range and range rate

f. restartable engines are fired and cut off within firing regions defined by phase-plane firing lines or are operated only once or twice for an "optimistic" approach. Firing normal to the nominal velocity vector is generally controlled to null the line-of-sight rates.

g. Velocity cutoff is controlled by:

   1. switching signal from control

   2. timing

   3. integrating accelerometers

Rendezvous sensors take the form of:

a. a tracking radar mounted on the vehicle with a gimballed antenna.

   1. range and range rate are measured directly

   2. angular line-of-sight rates are computed from signals taken from the gimbals and the inertial platform

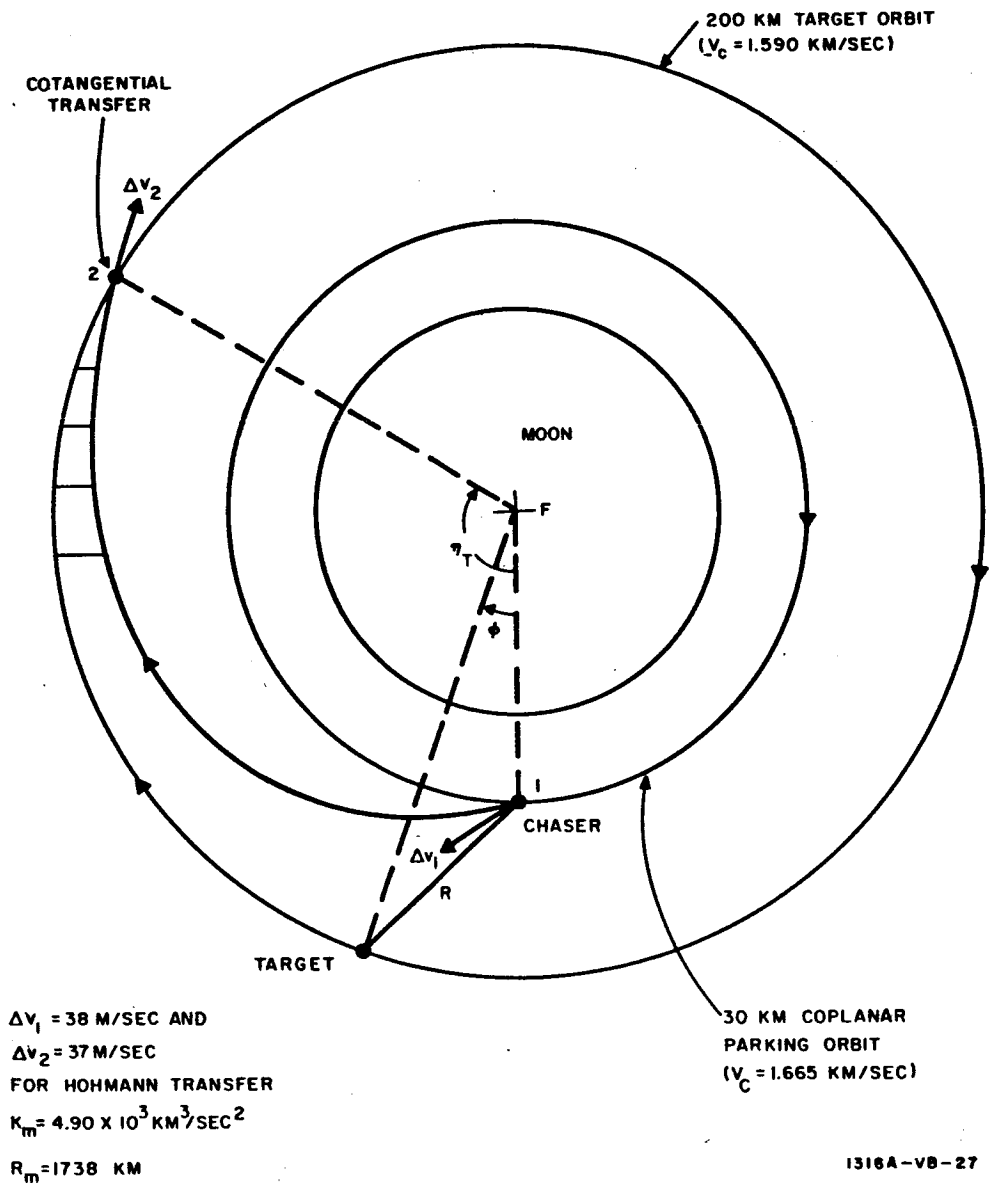

FIGURE 9-1. Lunar Orbital Rendezvous

This page intentionally left blank

3. range, range rate and angular rate of the line-of-sight may be divided into orthogonal components for control purposes

b. integrating accelerometers whether mounted on the vehicle or the inertial platform measure incremental velocities produced by rocket impulses.

The approach taken for this portion of the study involves, first, the selection of a suitable rendezvous model. This model, briefly described in paragraph 9-1, is programmed on the IBM 7094 digital computer and the nominal trajectories are determined for 90- and 180-degree transfers. Velocity requirements are also determined in general for transfer angles from zero to 180 degrees. Injection errors are then introduced in position, velocity vector, and time to simulate errors in measurement or in knowledge of chaser or target orbit data. The miss distance sensitivity coefficients are finally established.

A rendezvous guidance method is selected--as described in some detail in paragraph 9-4--since it is believed that a physical mechanization is necessary for evaluating the effects of injection errors and sensor inaccuracies during rendezvous. This guidance method reflects a compromise with the various systems that have been proposed using different guidance laws, propulsion, sensors, attitude references, and data processing methods. The guidance system is programmed into the computer in conjunection with the rendezvous model. Appropriate measurement errors are introduced into the rendezvous simulation program.

The effects of injection errors on propellant consumption are determined and, as a consequence, sensible levels of injection errors are established and translated into injection attitude and sensor requirements for initiating the ascent trajectory from the parking orbit.

All subsequent active rendezvous runs are made with a nominal injection error (-0.3 m/sec in velocity). Random rendezvous sensor errors are then intro-

duced at several levels and with two ratios. Ten sample runs are made at each level and ratio. The results, based on this limited sampling, are then used to determine the following: first, whether or not the rendezvous is successfully completed; and, second, the relative amount of propellant consumed during the transfer from the parking orbit to the point of actual rendezvous. Based on the information obtained, a decision is then made about the rendezvous sensor requirements.

9.3 Problem Definition

The sensors required for the overall rendezvous phase may be divided into two separate and distinct categories.

9.3.1 Injection Conditions

When a velocity maneuver is made to inject a vehicle from a parking orbit into an ascent trajectory to intercept the target orbit at a time when the target is in the vicinity, injection errors develop as a consequence of inaccuracies in measurement and execution. Injection errors may be introduced in position, velocity vector, and time.

Position errors may be split up into three components:

1. The radial error reflects as a lack of precision in knowing the radius from the center of the lunar force field. Prior to making manned lunar flights it is to be hoped that the radius of the local lunar surface will be known to considerably greater precision than the present one km or so. With this assumption and with an assist from the human navigator who will know his subpoint position, an equivalent measure of the radius vector will be local altitude as measured by an altimeter.
2. Lateral displacement reflects as an out-of-plane condition which must be corrected--preferably when the chaser enters the orbital

plane of the target vehicle. The parking orbit will normally be essentially coplanar with the target orbit.

3. Down-range errors are equivalent to phasing errors which will be considered later.

Velocity vector errors may develop in one of the following forms:

1. The magnitude of the incremental velocity imparted may be in error because of improper command due to poor orbital information or because of improper execution due to an error in velocity cutoff as a consequence of an integrating accelerometer error or incorrect thrust termination of the rocket itself.
2. The direction of the velocity maneuver may have an angular error in elevation (in the orbital plane) or in azimuth (out of the orbital plane). These directional errors may result from improper velocity vector commands, vehicle attitude errors during firing, or a rocket thrust misalignment.

Phasing errors develop when the chaser fails to inject into the desired transfer trajectory at the correct time, either because of inaccurate orbital or target data or because of an error in execution. It is assumed here that target range measurements form the criteria for the correct injection time.

Various levels of injection errors were inserted into the computer program for the following injection parameters.

a. altitude--the chaser basing the velocity maneuver on the measured altitude.

b. magnitude of the incremental velocity vector maneuver.

c. direction of the velocity vector maneuver.

d. central angle--corresponding to a phasing or timing error or to an equivalent range measurement error.

The allowable magnitudes of the errors are derived in Section 9.7.1.

9.3.2 Active Rendezvous

The active phase of rendezvous commences at relatively short range and requires the following types of sensor information:

a. range to the target. It is assumed that the range measurement inaccuracies are random in nature and follow a Gaussian distribution about the actual range. The noise level is further assumed to be either a percentage of total range or the same percentage of a 10 km range, whichever is greater.

b. the angular orientation of the LOS vector relative to an inertial reference. It is intended that the elevation and azimuth angles correspond to equivalent gimbal angles of the target ranging device. It is assumed that the angular inaccuracies are random in nature and follow a normal distribution about the actual LOS angles. The angular noise is considered to be uncorrelated to the range noise. The angular noise is assumed to be at a level independent of the actual angles.

c. The inertial platform forms the attitude reference to which the LOS angles are measured. Although the platform may have an attitude error, the platform is presumed to be heavily filtered by Schuler tuning so that the angular rate error is essentially negligible.

d. The range and angular information is combined to form the range components which are first smoothed and then differentiated to form range rate components. The basic information required, however, of the rendezvous sensor includes only range and two angles; the remaining required information is derived from this.

9.3.3 Propellant Consumption

The amount of propellant expended in executing an orbital transfer and

rendezvous is of great importance to a space mission because of the equivalent vehicle mass penalty. All the analysis in this phase of the study considers an equivalent incremental velocity, ΔV, applied during the rendezvous phase as the non dimensional measure of propellant consumption, independent of I_{sp} and vehicle masses. The equivalent mass of propellant consumed may be determined by the relation:

$$M_p = M_o\left[1 - \exp(-\Delta V/g I_{sp})\right] \quad (kg)$$

(assuming constant thrust)

where

M_o = initial vehicle mass (kg)

$g = 9.81$ m/sec^2

I_{sp} = specific impulse (sec)

Next to the requirements for mission safety, the cost in incremental velocity is the primary consideration in evaluating the effects of injection errors and rendezvous sensor errors.

9.4 Analytical Description

The moon is presumed to develop an ideal central force field with a gravitational parameter of:

$$K_m = 4.90 \times 10^3 \text{ km}^3/\text{sec}^2$$

The mean lunar surface radius is assumed to be:

$$R_m = 1738 \text{ km}$$

As previously mentioned, the rendezvous model selected for the manned lunar case involves a target vehicle considered to be in a 200 km circular orbit about the moon as indicated in Fig. 9-1. The manned chaser vehicle is presumed to be in a 30 km circular parking orbit coplanar with the target orbit. It is not essential for this sensor study that either orbit be circular or even coplanar but for convenience the computer program was so arranged. When the

chaser obtains information that it is correctly phased to the target by angle, ϕ, or by measured range, R, it imparts a computed incremental velocity vector at point 1. The application of this velocity maneuver places the chaser into an ascending transfer ellipse which is designed to intercept the target orbit cotangentially at point 2, at which time a posigrade tangential velocity increase of the correct magnitude would theoretically bring the two vehicles together with zero final relative velocity. Practically, as further described, a series of active rendezvous maneuvers commences at short range and continues until the two vehicles are in the same orbit but displaced by a preset standoff range. The computer program is designed to accommodate any desired transfer angle, η_T, and to modify the velocity maneuvers and ascent ellipse accordingly. Some runs were made with a 90 degree transfer angle, but the majority of runs were taken with the full 180 degrees--nominally the Hohmann transfer, which is more conservative of propellant.

For the nominal 180 degree case, the chaser vehicle fires a posigrade tangential velocity increment of 37.75 m/sec at point 1, where the range is 414.2 km at an elevation angle of 18.2 degrees, and the range rate is -203.6 m/sec.

The guidance method employed for the lunar rendezvous is illustrated by Fig. 9-2. As the chaser rises toward the target it approaches ahead of the target but its velocity decreases and the target tends to overtake the chaser vehicle. The chaser is stabilized to the local selenocentric vertical and to the orbital plane as established by the inertial platform with its associated sensors. The platform defines a reference coordinate system which rotates at orbital rate and the LOS angles are referenced to it. Vehicle attitude errors are thus of little consequence except during the occasional rocket firing periods when cross-coupling may develop if the rockets are fired off the intended axis. The propulsion rockets are assumed to have a multiple restart capability with fixed thrust levels

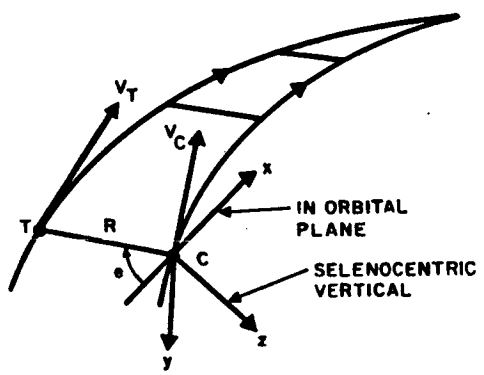

1. CHASER VEHICLE STABILIZED TO SELENOCENTRIC VERTICAL AND TO ORBITAL PLANE.
2. RESTARTABLE FIXED-THRUST ROCKETS ARE FIRED ALONG BODY AXES.

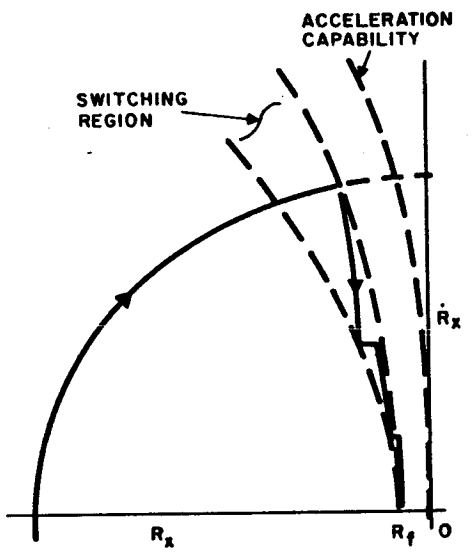

HORIZONTAL CONTROL

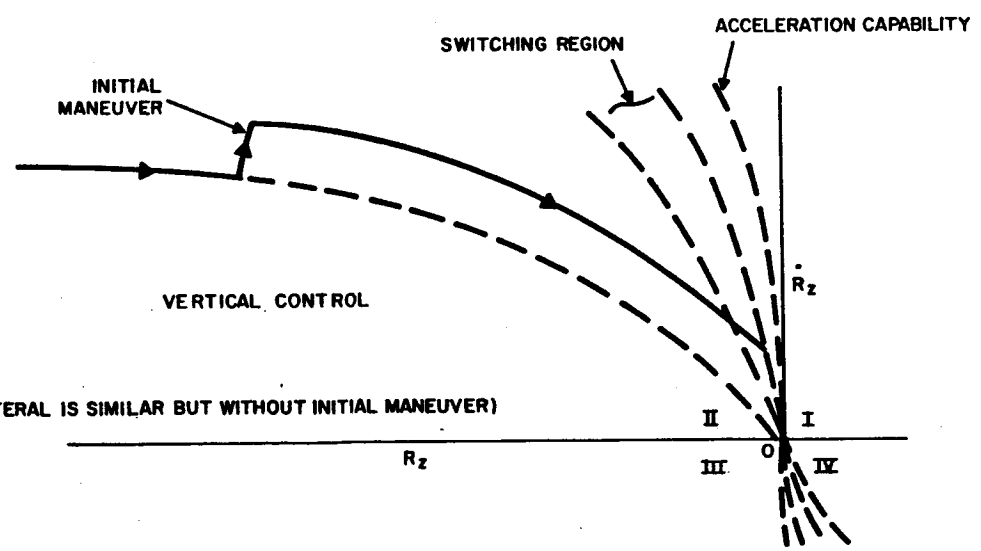

1316A-VB-50

FIGURE 9-2. Rendezvous Guidance (Lunar Orbit)

This page intentionally left blank

and aligned along the body axes. Rockets are fired orthogonally--the chaser does not change attitude for a velocity maneuver. This avoids the severe attitude control problems and disturbances that develop when the vehicles are controlled at short range where the firing is done at rather short intervals. With this type of transfer, there is little to be gained in propellant conversation with the alternative use of thrust vector control.

9.4.1 Vertical Control

As shown in Fig. 9-2 control in the vertical axis commences with an initial bias maneuver executed when:

$$R_z \geq -15 \text{ km}$$

The firing time is computed to be:

$$t_F = \frac{|44 - \dot{R}_z|}{|a_z|} \qquad (\text{sec})$$

where: $\dot{R}_z$ = vertical range rate (m/sec)

and $|a_z| = 0.5 \text{ m/sec}^2$

Since the total ΔU is small, constant thrust produces essentially constant acceleration.

The applied vertical acceleration is then:

$$a_z = -|a_z| \operatorname{sgn}(44 - \dot{R}) \qquad (\text{m/sec}^2)$$

This initial maneuver drives $\dot{R}_z$ to 44 m/sec, thereby expediting the vertical rendezvous and ensuring a terminal rendezvous along the horizontal axis. The maneuver also allows for moderately large injection errors by reducing the vertical dispersion that normally occurs.

The rocket firing philosophy in both axes is to, first, compute the firing time required for a specific rocket to develop a desired equivalent velocity increment, and, second, to fire that particular rocket for that computed firing time in an open-loop fashion to alleviate the control problems associated

with controlling to the regulated velocity change.

After the initial maneuver, the chaser coasts until either:

1. $$\dot{R}_z \geq \sqrt{K_2 \, |R_z|} \qquad \text{(m/sec)}$$

where: $K_2 = 0.75 \text{ m/sec}^2$

or 2. $$R_x > -3 \text{ km}$$

The latter condition only applies for certain large types of injection errors. From this point on the vertical control system acts to drive the vertical range to zero and thereafter maintain both range and range rate around zero.

The system first determines which phase plane quadrant of the vertical plane it is in by observing the sign of R_z and $\dot{R}_z$ as follows:

sign		Quadrant
R_z	$\dot{R}_z$	
+	+	I
-	+	II
-	-	III
+	-	IV

The system then attempts to keep itself within the phase plane switching regions to expeditiously drive toward a null while yet preserving an acceleration safety margin. The switching regions are bounded by pairs of parabolic switching curves.

1. If in quadrant I, compute a firing time:

$$t_F = \frac{\sqrt{K_1 |R_z| + \dot{R}_z}}{|a_z|} \qquad \text{(sec)}$$

where: $k_1 = 0.5$ m/sec^2

and fire with an acceleration of:

$$a_z = + |a_z| \qquad \text{(m/sec}^2\text{)}$$

2. If in quadrant II

a. If $\dot{R}_z > \sqrt{K_2 |R_z|}$ (m/sec)

compute a firing time:

$$t_F = \frac{2(-\sqrt{K_1 |R_z|} + \dot{R}_z)}{|a_z|} \qquad \text{(sec)}$$

and accelerate as follows:

$$a_z = + |a_z| \qquad \text{(m/sec}^2\text{)}$$

b. If $\dot{R}_z < \sqrt{K_1 |R_z|}$ (m/sec)

compute the firing time:

$$t_F = \frac{(\sqrt{K_1 |R_z|} - \dot{R}_z)}{|a_z|} \qquad \text{(sec)}$$

and fire with an acceleration of:

$$a_z = - |a_z| \qquad \text{(m/sec}^2\text{)}$$

3. If in quadrant III, compute the firing time:

$$t_F \frac{(\sqrt{K_1 |R_z|} - \dot{R}_z)}{|a_z|} \qquad \text{(sec)}$$

and accelerate as follows:

$$a_z = -|a_z| \qquad (\text{m/sec}^2)$$

4. If in quadrant IV

a. If $\dot{R}_z < -\sqrt{K_2 |R_z|}$ (m/sec)

the firing time is computed:

$$t_F = \frac{-2\left(\sqrt{K_1 |R_z|} + \dot{R}_z\right)}{|a_z|} \qquad (\text{sec})$$

and the vehicle is accelerated:

$$a_z = -|a_z| \qquad (\text{m/sec}^2)$$

b. If $\dot{R}_z > \sqrt{K_1 |R_z|}$ (m/sec)

then compute the firing time:

$$t_F = \frac{\left(\sqrt{K_1 |R_z|} + \dot{R}_z\right)}{|a_z|} \qquad (\text{sec})$$

and fire as follows:

$$a_z = +|a_z| \qquad (\text{m/sec}^2)$$

To avoid nuisance firings which waste propellant particularly in the presence of noise:

a. A rocket is not fired if the computed firing time is less than 3 sec (equivalent to a 1.5 m/sec velocity change)

b. A minimum coast time of 2 sec is required between firings.

9.4.2 Lateral Control

Control in the lateral (out-of-plane) axis is similar to that described above for vertical except that no initial bias maneuver is undertaken. The computer program was actually developed only for the planar case and consequently lateral control was not included in the program.

9.4.3 Horizontal Control

Control along the horizontal axis becomes possible after

$$R_z \geq -15 \text{ km},$$

the condition for initiating the vertical bias maneuver.

The chaser vehicle coasts in the horizontal mode until it enters the phase plane switching region bounded by the pair of parabolic firing curves. When the horizontal range rate satisfies the relation:

$$\dot{R}_x \geq \sqrt{K_2 \, |R_x - R_f|} \qquad \text{(m/sec)}$$

where: $K_2 = 0.75 \text{ m/sec}^2$

and R_f = desired standoff range

$= 0.1$ km

The firing time is computed:

$$t_F = \frac{2\left(\sqrt{K_1 \, |R_x - R_f|} - \dot{R}_x\right)}{|a_x|} \qquad \text{(sec)}$$

where: $K_1 = 0.5 \text{ m/sec}^2$

and $|a_x| = 0.5 \text{ m/sec}^2$

This level of acceleration provides positive and definite velocity control without being too sensitive. The appropriate rocket is then fired to produce an acceleration of:

$$a_x = + \, |a_x| \qquad \text{(m/sec}^2\text{)}$$

This increases chaser velocity to more closely match target velocity. As in the vertical control case, a minimum coast time of two seconds is provided between rocket firings and no firing is attempted when the computed firing time is less than three seconds.

Horizontal firing for the nominal case commences when R_x equals -2 km. Firing is repeated as necessary until the chaser ends up at the standoff range with essentially zero velocity. At this point the problem is considered to be completed. In an actual case the crew would then normally assume manual control for the final approach and docking phase using visual observations and employing lower thrust level maneuvering rockets.

9.4.4 Data Processing

Rendezvous sensor inaccuracies are simulated in the digital program by the inclusion of white noise developed by uncorrelated random number generating routines. Because of the noise appearing on range and angle measurements it is necessary to smooth the raw data before attempting to use these data for control purposes. A digital data smoother, illustrated in Fig. 9-3, is included in the system to process and smooth the data for the control system, thereby permitting operation at higher noise levels. The on-board computer (B) accepts the noisy range and angle inputs, R_N and e_N, which are directly equivalent to actual sensor signals and computes the range components:

$$R_{xn} = R_n \cos e_n \cos a_n$$

and

$$R_{zn} = R_n \sin e_n \cos a_n$$

$$(a_n = 0 \text{ for this program})$$

These components are then fed into the appropriate digital data smoother at a rate of one sample, b, each data storage interval, Δt_i--taken as one second for this program. An adjustable smoothing time, t_s, is provided in the program

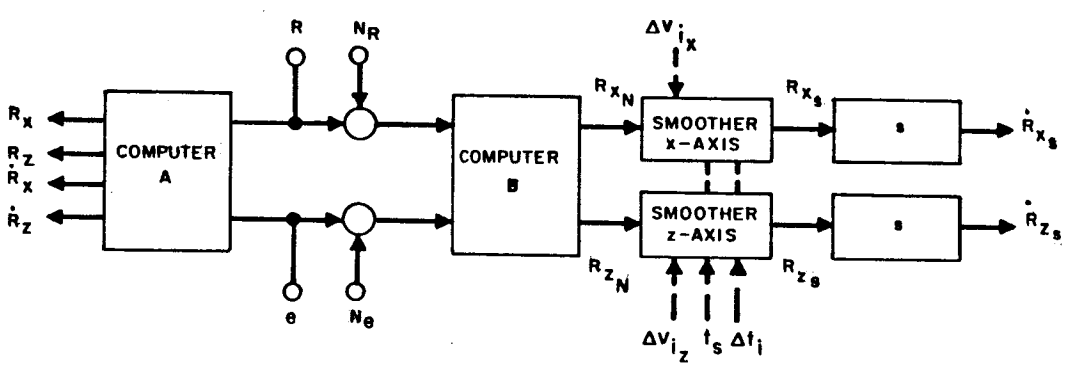

N_R = NOISE ON RANGE, R (% OF R OR OF 10 KM)

N_e = NOISE ON ANGLE, e (mr)

CONTROL SIGNALS: $R_{x_s}, R_{z_s}, \dot{R}_{x_s}, \dot{R}_{z_s}$

1316A— VB-47

FIGURE 9-3. Digital Smoother
(Range Components)

This page intentionally left blank

although a fixed 15-second smoothing time was used throughout this study. Over this smoothing time, the number of stored data samples is:

$$m = \left(\frac{t_s}{\Delta t_i} + 1 \right)$$

or 16 samples for the runs actually made. Thus at each interval of Δt_i (1 sec) the most recent value is stored and the oldest value is rejected. Velocity compensation is included to permit smoothing to continue without appreciable error during actual rocket firing periods. The Δv provided during the last storage interval is determined:

$$\Delta v_{ix} = a_x \Delta t_{Fx}$$

or $$\Delta v_{iz} = a_z \Delta t_{Fz}$$

where: Δt_F is amount of firing time within the storage interval.

Each stored data sample is updated each storage interval and a weighted velocity correction is also applied when applicable as follows:

$$b_0|_t = \text{most recent value of } R_x \text{ (or } R_z)$$
$$b_1|_t = b_0|_{t-1} + 0.5 \Delta v_i$$
$$b_2|_t = b_1|_{t-1} + 1.5 \Delta v_i$$
$$b_3|_t = b_3|_{t-1} + 2.5 \Delta v_i$$

etc.

Using the method of least squares the smoother determines the best linear fit of the updated, compensated stored data samples. The smoothed range component, R_{xs} (or R_{zs}) is then obtained by extrapolating the smoothed line over one storage interval. The present slope of the smoothed line produces the smoothed range rate component, $\dot{R}_{xs}$ (or $\dot{R}_{zs}$). The actual rendezvous control signals are all smoothed values, i.e., R_{xs}, R_{zs}, $\dot{R}_{xs}$, and $\dot{R}_{zs}$.

9.5 Digital Program

A digital computer program to simulate a method of lunar rendezvous was prepared for the IBM 7094. The program simulates the radar measurements, data conditioning, computations and maneuvering of a chaser in achieving a rendezvous with a non-maneuvering target.

Inputs to the program have been designed so that the effects of a number of different parameters can easily be studied. Among the inputs to the program are four quantities which represent errors in the injection of the chaser into its parking orbit and ascent ellipse. Other inputs include the specification of standard deviations of noise quantities, the order of smoothing to be used on the simulated radar readings and the number of points to be smoothed.

The main computational problem encountered in this study was a loss of accuracy in the computation of orbital elements from position and velocity vectors. This problem became noticeable near the end of the maneuver when the orbit of the chaser began to approach a circle. It was found that the method described in Section 22.7, Part B similarly suffers from a loss of accuracy as the orbit approaches a circle. This problem was sufficiently reduced by performing all the computations of that particular method in double precision.

For a much more detailed description of the program see Section 22.

9.6 Program Results

9.6.1 Transfer Angle

In considering the consequences of varying the transfer angle of the ascent ellipse, it was assumed that the transfer is always made cotangential to the target orbit for two reasons.

1. It is the minimum energy transfer
2. It establishes the smoothest rendezvous approach, requiring no abrupt maneuvers.

The eccentricity of the transfer ellipse varies as a function of transfer angle, as illustrated by the curve of Fig. 9-4, which is based on the relation:

$$e = \frac{\frac{r_a}{r_1} - 1}{\cos \eta_1 + \frac{r_a}{r_1}} \qquad (1)$$

where:

r_a = apo-asis

= target orbit radius

r_1 = initial radius from the lunar center

η_1 = initial eccentric anomaly

Next the incremental velocities required to initiate (at point 1) and terminate (at point 2) the transfer orbit are calculated by the relations:

$$\overline{\Delta v_1} = \frac{e \sin \eta_1 (v_{ca})}{\sqrt{1-e}} + i v_{c1}\left(\sqrt{\frac{r_a}{r_1}}\sqrt{1-e} - 1\right) \qquad (2)$$

$$\overline{\Delta v_2} = i\, v_{ca}\left(1 - \sqrt{1-e}\right) \qquad (3)$$

The total incremental velocity required to transfer from the parking orbit to the target orbit is:

$$\Delta V_T = \Delta V_1 + \Delta V_2 \qquad (4)$$

The magnitudes of these incremental velocities are presented as a function of transfer angle by the curves of Fig. 9-5. It may be noted that the requirement increases from 75 m/sec for the 180 degree transfer case to 217 m/sec for the 90 degree transfer—a significant increase.

9.6.2 Injection Errors

At the moment of insertion into the ascent ellipse from the parking orbit at point 1, errors in position, velocity and time cause the ascent trajectory to deviate from the nominal case.

9.6.2.1 Effects on Miss Distance

The introduction of injection errors will result in a miss distance to the target if the ascent is passive (without active rendezvous corrections). For comparison purposes the miss distance is pessimistically considered as occuring when the nominal transfer angle has been traversed. The minimum range will frequently be considerably smaller. The following table indicates the miss distance sensitivity coefficients for the 90-and 180-degree transfers.

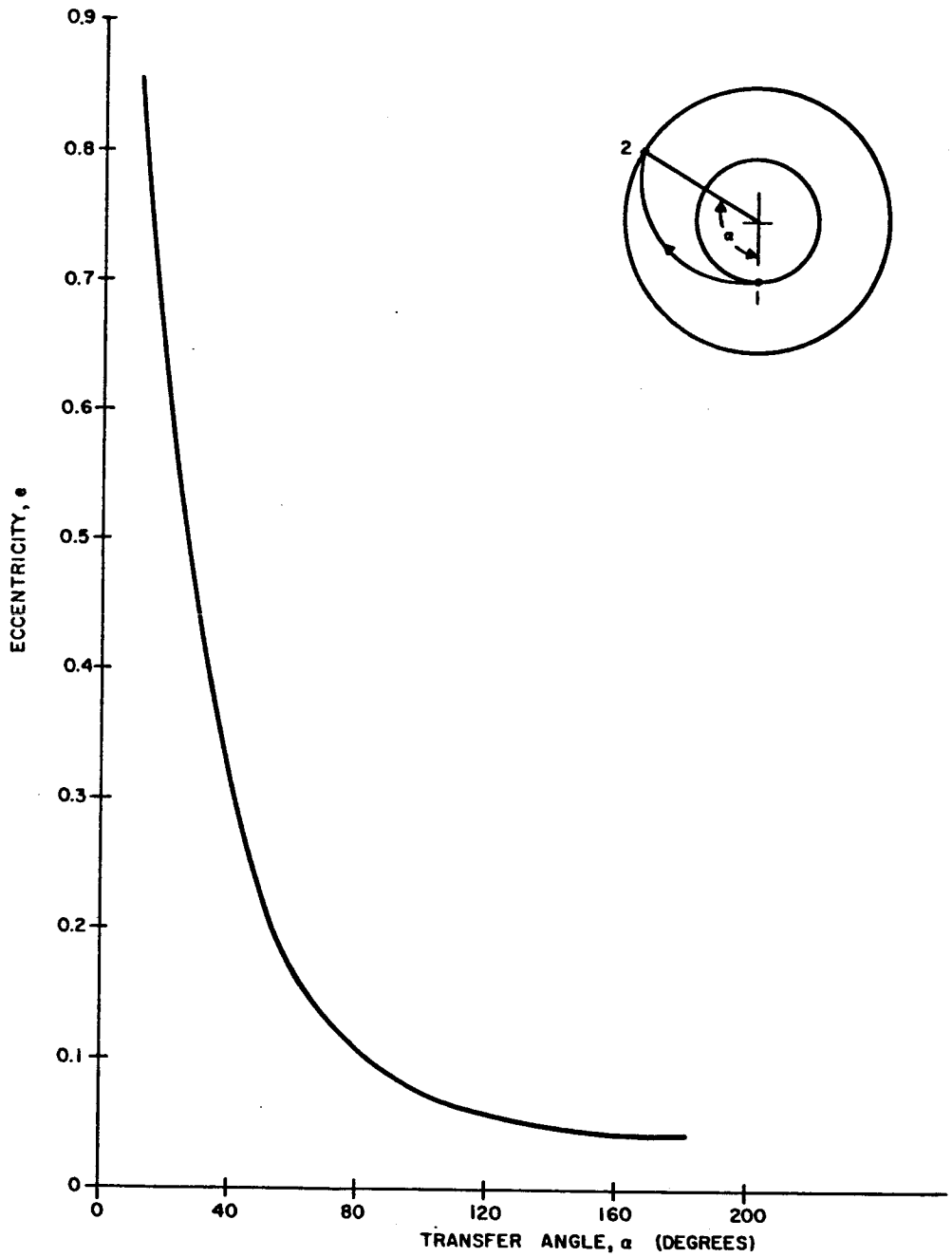

1316A-VB-2

FIGURE 9-4 Effect of Transfer Angle on Eccentricity of Cotangential Transfer Orbit (From 30 KM Lunar Parking Orbit to 200 KM Circular Target Orbit)

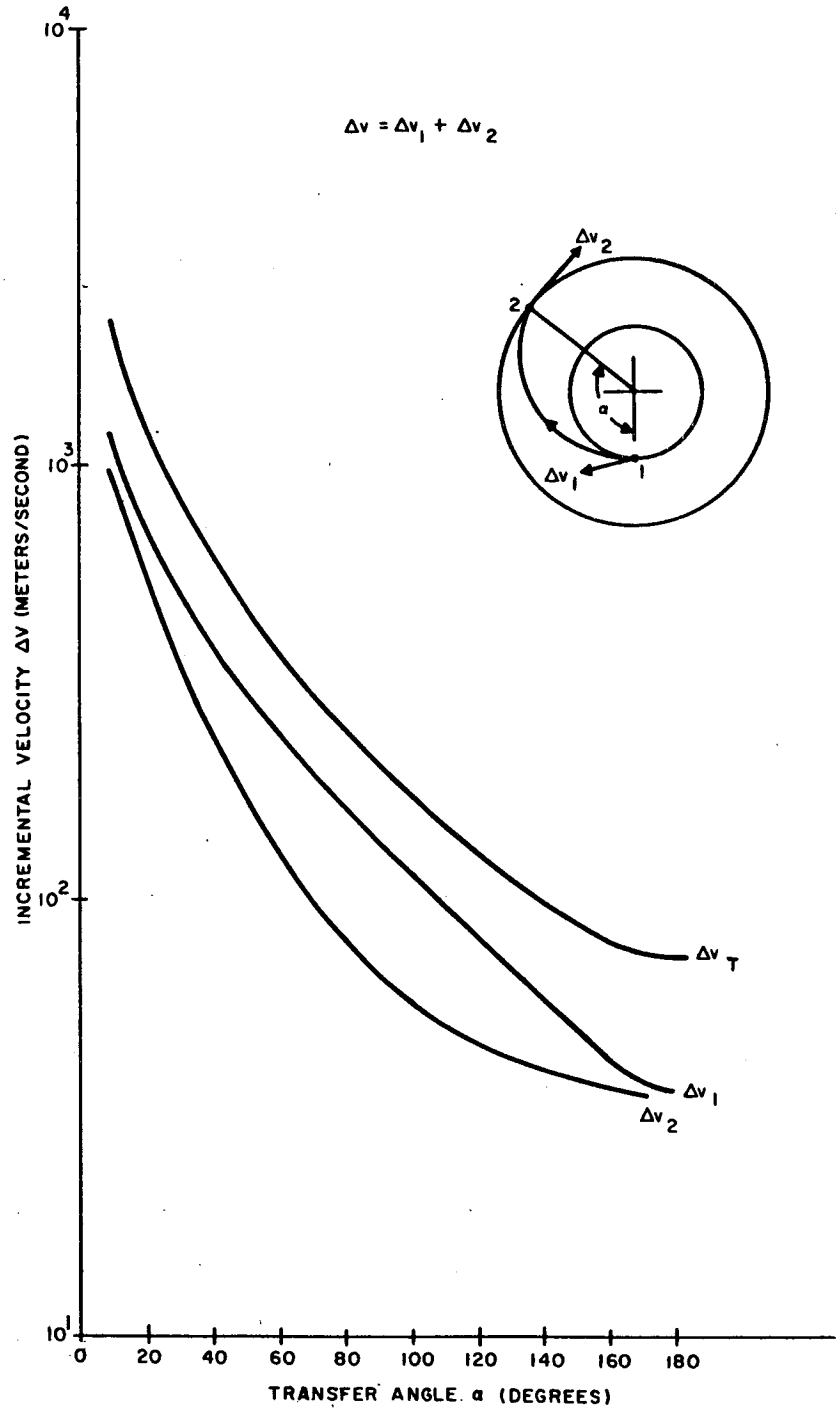

1316A-VB-3

FIGURE 9-5 Effect of Transfer Angle on Incremental Velocities of Cotangential Transfer Orbit (From 30 KM Lunar Parking Orbit to 200 KM Circular Target Orbit)

TABLE 9.6-1

Miss Distance Sensitivity Coefficients

(for 30/200 km Lunar Orbit Cotangential Transfer)

Horizontal Coefficients	η_T 180°	η_T 90°	Units	Vertical Coefficients	η_T 180°	η_T 90°	Error
$\partial M_x / \partial r_1$	4.94	2.63	$\frac{km}{km}$	$\partial M_z / \partial r_1$	1.14	1.15	altitude
$\partial M_x / \partial v_1$	11.0	2.52	$\frac{km}{m/sec}$	$\partial M_z / \partial v_1$	4.77	1.28	velocity
$\partial M_x / \partial \gamma_1$	-2.94	-2.38	$\frac{km}{deg}$	$\partial M_z / \partial \gamma_1$	0	-6.22	attitude
$\partial M_x / \partial t_1$	0.274	0.233	$\frac{km}{sec}$	$\partial M_z / \partial t_1$	0	0	target lead

The miss effects of several simultaneous injection errors may be combined by the equation:

$$\begin{bmatrix} M_x \\ M_z \end{bmatrix} = \begin{bmatrix} \frac{\partial M_x}{\partial r_1} & \frac{\partial M_x}{\partial v_1} & \frac{\partial M_x}{\partial \gamma_1} & \frac{\partial M_x}{\partial t_1} \\ \frac{\partial M_z}{\partial r_1} & \frac{\partial M_z}{\partial v_1} & \frac{\partial M_z}{\partial \gamma_1} & \frac{\partial M_z}{\partial t_1} \end{bmatrix} \begin{bmatrix} \delta r_1 \\ \delta v_1 \\ \delta \gamma_1 \\ \delta t_1 \end{bmatrix} \qquad (5)$$

In the lateral axis, if the chaser was initially in the orbital plane of the target, lateral range is approximated by the relation:

$$R_y \doteq a \sin \Delta i \sin \eta \qquad (6)$$

For the 180 degree transfer (η_T= 180 deg.),

$$R_y = 0$$

$$\therefore \frac{\partial M_y}{\partial \psi} = 0$$

For the 90 degree case:

$$R_y \doteq a \sin \Delta i$$

$$\doteq a \frac{\Delta U_1}{U_1} \sin \psi$$

$$\frac{\partial M_y}{\partial \psi} \doteq a \frac{\Delta U_1}{U_1}$$

$$= 2.73 \ \frac{\text{km}}{\text{deg}}$$

9.6.2.2 Effects on Propellant Consumption

The effects of various initial conditions on consumption of propellant is displayed in the four separate curves of Fig. 9-6 which represent the results of a series of computer runs with an active rendezvous system operating. It may be noted that the non-linear guidance and control system reacts in occasionally rough fashion with certain injection error levels. The reference ΔU_T level, ΔU_{NOM}, is based on the total ΔU consumed by the nominal trajectory (perfect injection) during a normal active rendezvous.

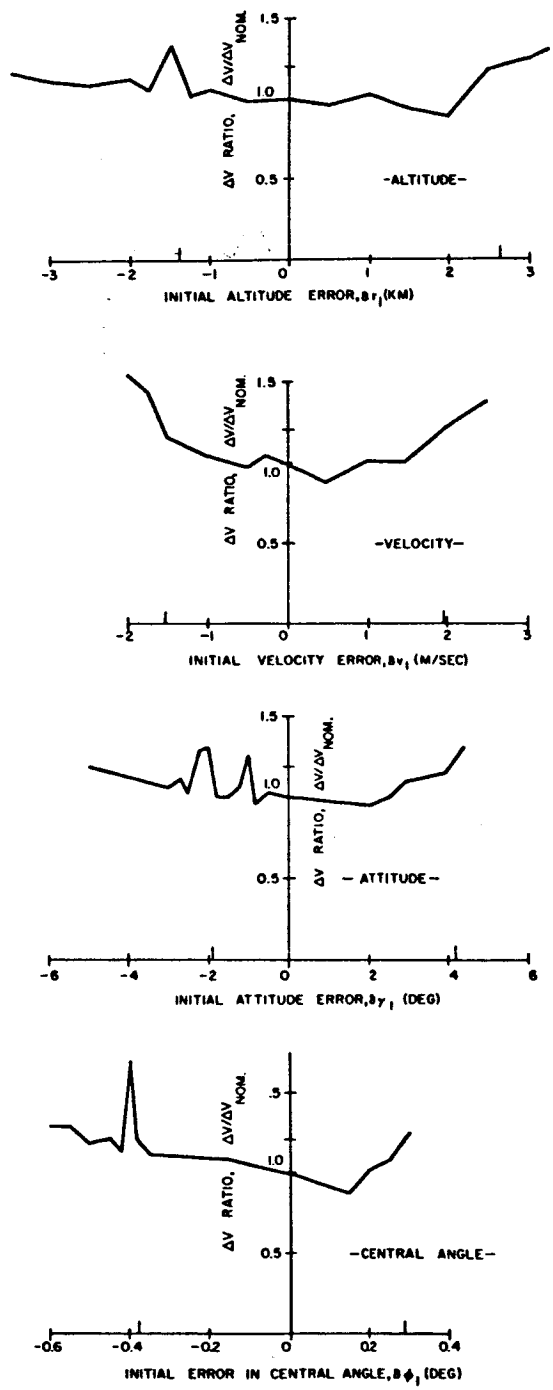

FIGURE 9-6 Effects of Initial Conditions on Propellant Consumption (Lunar Orbit)

This page intentionally left blank

9.6.2.3 Effects on Accuracy

The consequences of injection errors on trajectory variations during normal rendezvous runs is demonstrated in the following three figures. In each figure the nominal trajectory is shown together with the dispersion from the nominal that develops with 3σ injection errors.

The vertical phase plane diagram of Fig. 9-7 indicates the dramatic reduction in dispersion as a consequence of the initial bias maneuver. The humped area at the shorter range appears at certain high levels of injection errors to ensure vertical closure prior to horizontal rendezvous. The horizontal phase plane diagram of Fig. 9-8 demonstrates how the dispersed trajectories are constrained to follow the switching region right down to the standoff range, R_f.

The range diagram of Fig. 9-9 clearly depicts the large dispersion introduced by the various 3σ levels of injection errors. Rendezvous may be considered satisfactorily consummated for the cases shown.

9.6.3 Rendezvous Sensor Errors

A series of computer runs were made of the rendezvous mission with various levels of rendezvous sensor noise included. All runs were made with the identical injection error (-0.3 m/sec in velocity) for comparison purposes. The reference magnitude of incremental velocity, ΔU_N, coincides with the ΔU obtained for the identical run without noise, i.e., perfect sensors. The ΔU consumed during each individual run is compared with ΔU_N. Each set of runs consists of ten runs all with ostensibly the same rendezvous sensor noise level but each with an unique pair of uncorrelated random number routines to simulate the random noise present in an actual system.

The velocity requirements for a group of these runs at various levels is shown in Fig. 9-10 for the case where:

$$\sigma_e = 30\,\sigma_R$$

where: σ_e = standard deviation of noise on angle (mr)

σ_R = standard deviation of noise on range (% of range)

The limited number of ten samples for each noise run is not sufficient for a good distribution, but is adequate for preliminary work of this sort. While the results are jumpy a definite trend may be established. All runs shown had sufficient rendezvous accuracy to be considered usable.

Another series of runs was made in like fashion but with a different error ratio:

$$\sigma_e(mr) = \sigma_R\,(\%\text{ of } R)$$

The results of these runs are shown in Fig. 9-11. Some of the runs with σ levels of 1.2 and 1.5 were unsatisfactory from an accuracy standpoint and therefore cannot be considered acceptable for rendezvous usage.

9.7 Discussion and Interpretation of Results

The development of sensor requirements falls naturally into two separate categories.

9.7.1 Injection Sensors

In developing acceptable error levels for establishing the ascent trajectory, the four curves of Fig. 9-6 are employed. The assumption is arbitrarily made that a 3σ error in any one injection parameter shall not result in more than a 20% increase in energy consumption over the nominal case utilizing the 180 degree orbital transfer.

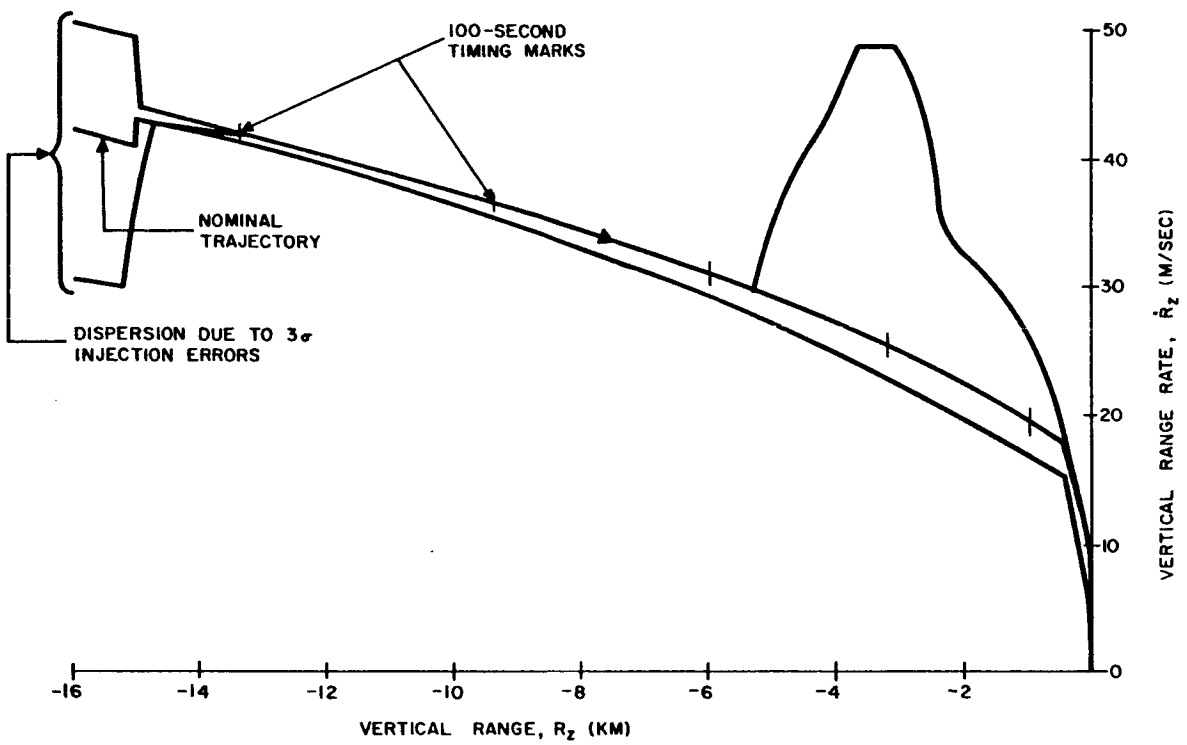

1316A-V8-52

FIGURE 9-7 Vertical Phase Plane
(Lunar Orbit)

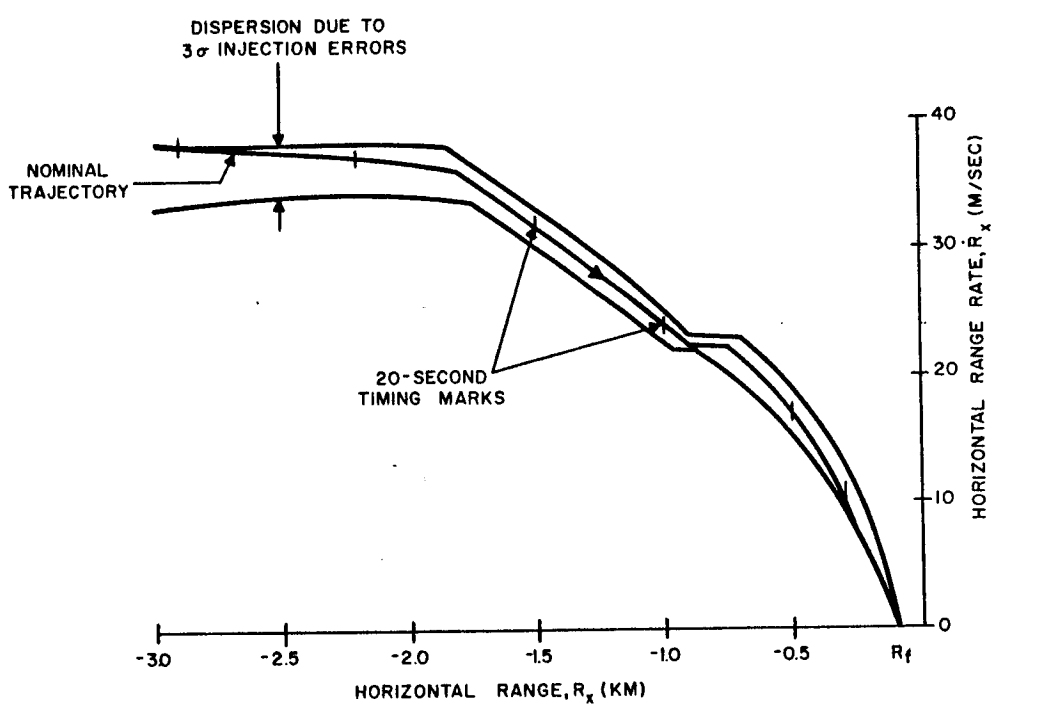

FIGURE 9-8 Horizontal Phase Plane
(Lunar Orbit)

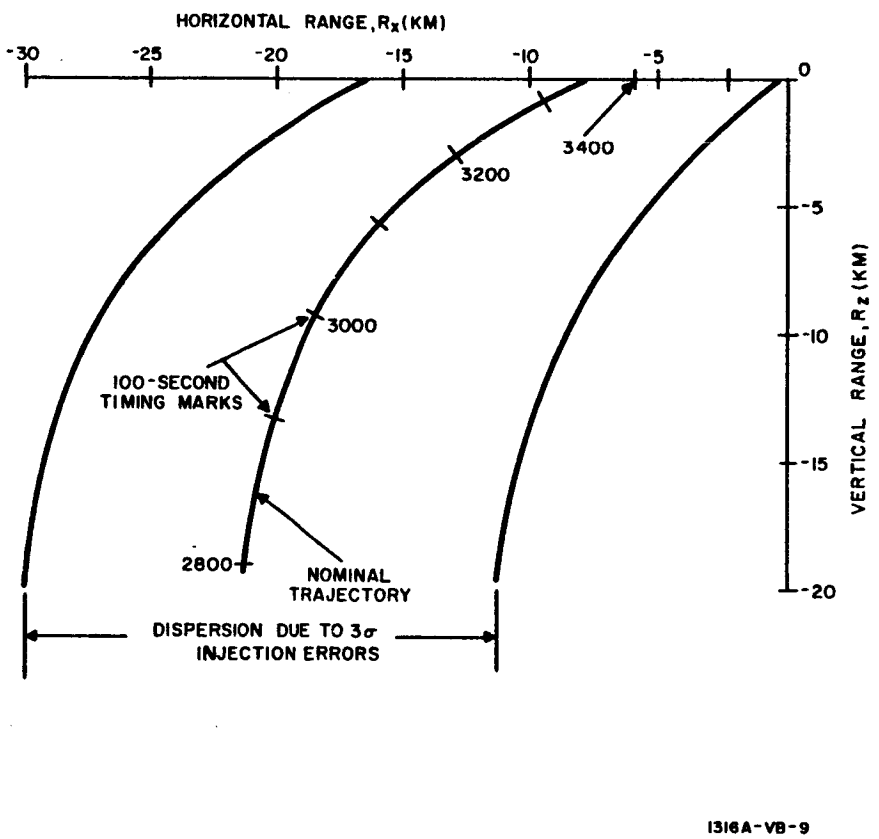

FIGURE 9-9 Range Diagram (Lunar Orbit)

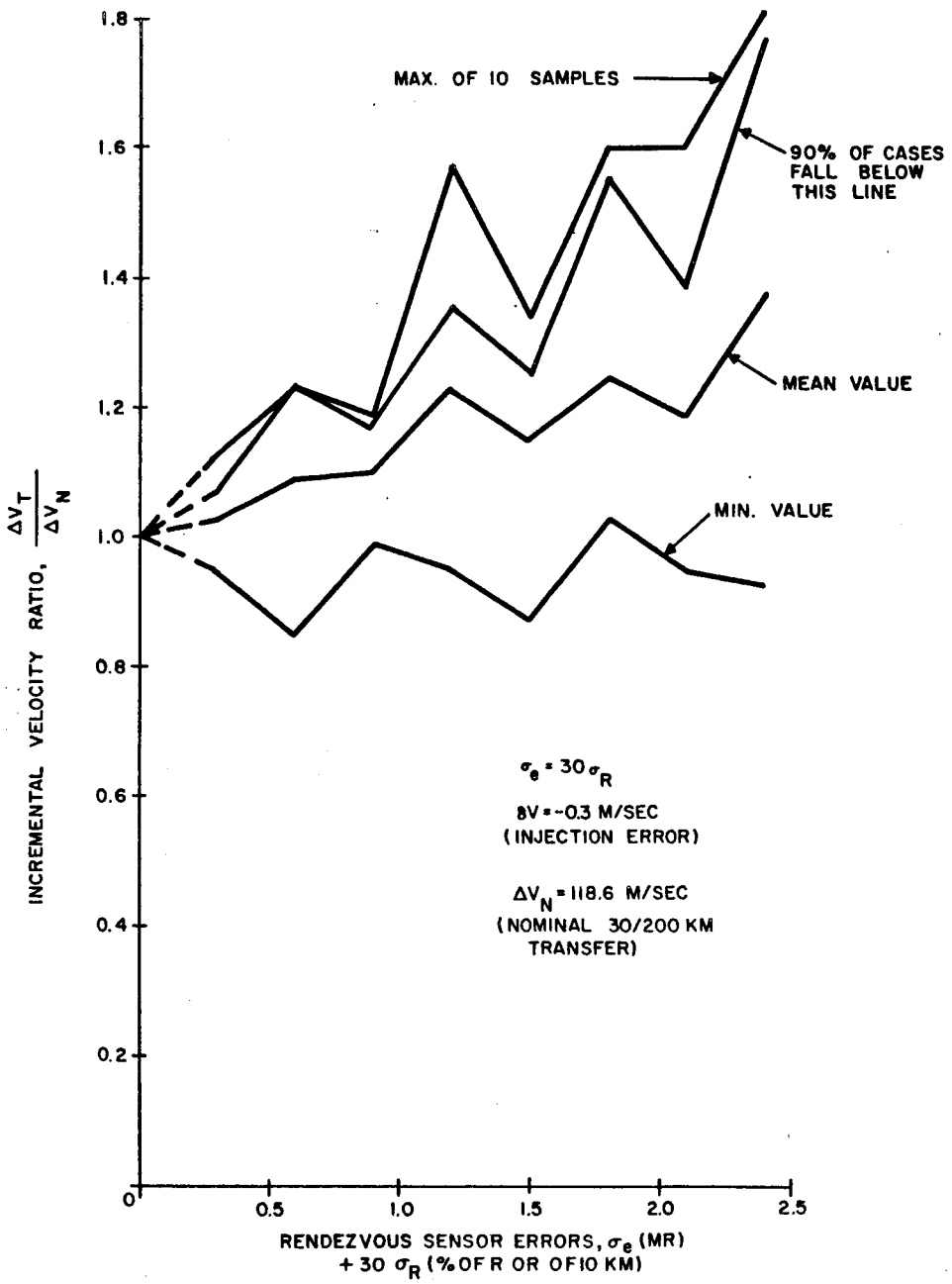

1316A—VB—55

FIGURE 9-10 Effect of Rendezvous Sensor Errors on Propellant Consumption (Lunar Orbit)

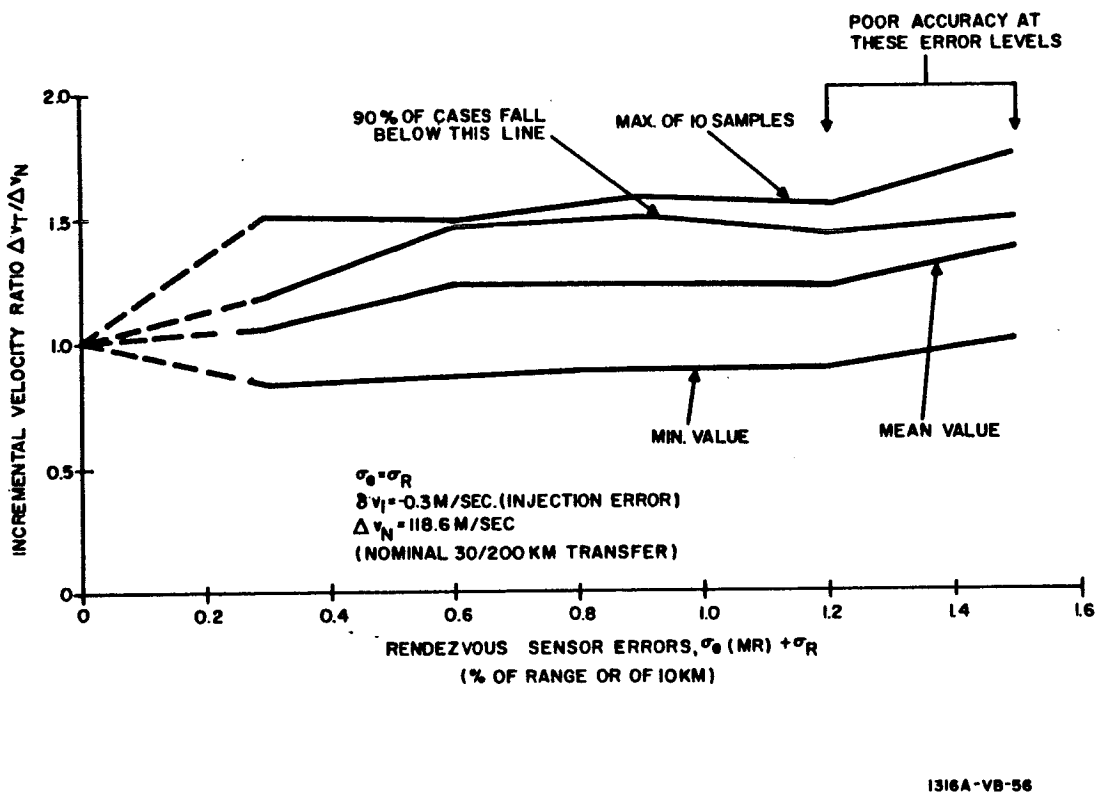

FIGURE 9-11 Effect of Rendezvous Sensor Errors on Propellant Consumption (Lunar Orbit)

This page intentionally left blank

The lead angle error, $\delta\phi$, may be converted into either an equivalent range error, δR, or a timing error, δt. From the program results we have:

$$\frac{dR}{d\phi} = 29.5 \text{ km/deg.}$$

$$\frac{d\phi}{dt} = 0.0069 \text{ deg/sec.}$$

and $R_1 = 414.2$ km (for the nominal case)

The equivalent range error is then:

$$\delta R = \delta\phi \frac{dR}{d\phi}$$

$$= 29.5 \times 0.28$$

$$= 8.25 \text{ km} \qquad (3\sigma)$$

$$\text{or: } \delta R = \frac{8.25}{414.2}$$

$$= 1.996 \% \text{ of R}$$

The equivalent timing error is similarly obtained:

$$\delta t = \frac{\delta\phi}{d\phi/dt}$$

$$= \frac{0.28}{0.0069}$$

$$= 40.6 \text{ sec} \qquad (3\sigma)$$

The lateral velocity error due to azimuth misalignment is:

$$\dot{R}_y \doteq \Delta V_1 \sin \psi$$

or: $$\delta\psi \doteq \sin^{-1}\left(\frac{0.2\,\Delta V_{NOM}}{\Delta V_1}\right)$$

$$\doteq \sin^{-1}\left(\frac{0.2 \times 113.1}{37.8}\right)$$

$$= 22.2 \text{ deg} \quad (3\sigma)$$

The differential inclination between chaser and target orbits requires an out-of-plane correction to bring the chaser orbit coplanar with the target orbit.

$$i \doteq \sin^{-1}\left(\frac{\Delta V}{V_2}\right) \qquad \text{(for the worst case)}$$

$$\delta i = \sin^{-1}\left(\frac{0.2 \times 113.1}{1590}\right) = 0.82 \text{ deg} \quad (3\sigma)$$

The required injection sensor accuracies are summarized in the following table along with reasonable state-of-the-art equivalents.

TABLE 9.7-1

Injection Sensor Errors

Symbol	Quantity	Sensor Accuracy (3σ)	State-of-the-art Accuracy (3σ)
δr	altitude	1.4 km(4.7% of R)	30 m (0.1% of R)*
δv	velocity	1.5 m/sec.	0.3 m/sec.
$\delta \gamma$	pitch attitude	2.0 deg.	0.3 deg.
$\delta \psi$	yaw attitude	22.2 deg.	0.3 deg.
$\delta \phi$	central angle	0.28 deg.	-
δR	range	2.0 % of R	0.1 % of R
δt	timing	40.6 sec.	3 sec.
δi	inclination	0.8 deg.	0.1 deg.

* While a radar altimeter can measure relative altitude this accurately, the absolute altitude could not be determined to this degree of precision.

Attitude and range measurements may be made using radar to the state-of-the-art accuracy indicated. Integrating accelerometers form a ready means of measuring incremental velocity. Pitch (and roll) attitude references may be measured with infrared horizon scanners, while the yaw reference angle may be determined by gyrocompassing techniques. Inclination may be determined by lunar navigation methods.

It should be observed that in every case the state-of-the-art accuracies for the injection sensors are significantly better than required for the rendezvous mission.

9.7.2 Rendezvous Sensors

The rendezvous sensor requirements are based on an interpretation of the results shown in Figs. 9-10 and 9-11. Considering first the case where $\sigma_e(mr) = 30\,\sigma_R$ (% of R) as displayed in Fig. 9-10 and realizing the roughness of the data is principally due to the limited number of samples taken, it was decided to arbitrarily specify that where the 90% line equaled a 1.5 velocity ratio, the corresponding error would be the level of acceptability, with this criterion:

$$\sigma_e = 1.75\,mr \text{ and } \sigma_R = 0.058\% \text{ of R.}$$

Comparing these error values with state-of-the-art accuracies we have:

Quantity	Sensor Accuracy (3σ)	State-of-the-art* Accuracy (3σ)
Range	0.174% of R or 17.4 m	0.1% of R or 10 m
Angle	5.25 mr	3 mr

* Gemini rendezvous radar.

These results would seem to indicate that the state-of-the-art rendezvous sensor accuracies are satisfactory for the rendezvous mission although some energy penalty is incurred as a consequence of these inaccuracies.

Applying the same criterion to the results shown on Fig. 9-11 where the error ratio is very different:

$$\sigma_e (mr) = \sigma_R (\% \text{ of } R)$$

we cannot justify a sensor error level in excess of:

$$\sigma_e = 0.9 \text{ mr and } \sigma_R = 0.9\% \text{ of R}$$

because of inferior accuracy at higher levels. If we compare these sensor errors with those associated with the state-of-the-art equipment:

Quantity	Sensor Accuracy (3σ)	State-of-the-art Accuracy (3σ)
Range	2.7% of R or 0.27 km	0.1% of R or 10 m
Angle	2.7 mr	3 mr

It is seen that the required angular accuracy is a bit shy of that available while on the other hand the range accuracy requirements are very crude by comparison.

9.8 Sensor Requirements

For the lunar orbital rendezvous phase of the mission, several types of sensing devices are necessary. Certain minimum levels of accuracy are required of each sensor for successful completion of the mission while also considering the important factor of propellant conservation.

9.8.1 Injection Sensor Requirements

The injection sensor dynamic ranges and accuracy requirements are tabulated below.

TABLE 9.8-1

Injection Sensor Requirements

Quantity Measured	Dynamic Range		Max. Allowable RMS Sensor Error
	Max.	Min.	
altitude	+40 km	0	0.5 km (1.6% of R)
incremental velocity*	+50 m/sec	0	0.5 m/sec
pitch angle*	+90 deg	-90 deg	0.7 deg
yaw angle*	+180 deg	-180 deg	7.4 deg
range	+500 km	0	2.7 km (0.7% of R)
inclination angle	+5 deg	-5 deg	0.3 deg

* With the quantities so indicated the listed error is the total error permitted in that particular quantity, including both measurement and control system inaccuracies.

While sensors with the above accuracy levels will produce a satisfactory rendezvous ascent, it should be emphasized that the use of more accurate sensors will normally conserve propellant--a precious commodity at the moon.

9.8.2 Rendezvous Sensor Requirements

The bandwidth and accuracy requirements of rendezvous sensors necessary to complete a satisfactory rendezvous mission without serious propellant expenditure are presented in the table below.

TABLE 9.8-2

Rendezvous Sensor Requirements

Quantity Measured	Dynamic Range		Max. Allowable RMS (1σ) Sensor Error
	Max.	Min.	
range	30 km*	0	0.06 % of R or 6 m
LOS angles (azimuth & elevation)	+20 deg	-20 deg	1.7 mr
vehicle attitude	+180 deg-Y	-180 deg-Y	0.2 deg during firing period (to reduce cross-coupling)
(pitch, roll & yaw)	+90 deg-R&P	-90 deg-R&P	5 deg during tracking (vehicle may change attitude to accomodate LOS angle limits)

* The maximum range of the ranging device is that required for the active phase of rendezvous. Actually this device should probably be the same sensor that measures target range prior to injection and which may also occasionally monitor the target during the coasting period of the rendezvous ascent.

Although the above sensor requirements will afford a satisfactory rendezvous it should be stressed that greater accuracy will generally reduce the energy expended during the rendezvous phase.

9.9 Recommendations

The guidance method utilized for the earth space station rendezvous in Section 11 appears to be definitely superior to that used for the lunar orbital rendezvous case. It is believed that if the other guidance system were used here, a significant reduction in fuel consumption would result as well as making it possible to specify less stringent lunar sensor requirements. It is recommended that the other guidance system be adapted to the lunar rendezvous model and the sensor requirements be re-evaluated accordingly.

Further development is definitely indicated in the area of smoothing the raw rendezvous sensor data, including such items as variable smoothing time, number of stored data samples, and second order compared with first order fits. In future analyses, the data should be obtained more accurately by using a large enough number of computer runs to obtain smoother error curves than those obtained in this preliminary study.

It is recommended that effort also be applied to the unmanned rendezvous case, covering the specialized short range sensor requirements of the final rendezvous approach as well as the docking phase.

10.0 MIDCOURSE RETURN, MANNED

10.1 Introduction

Since the problems involved in a manned moon-earth flight are similar in many ways to the earth-moon flight discussed in Section 4.0, this section will be primarily concerned with the differences between the outbound and return of a lunar flight, and the effect of these differences on sensor requirements. A similar navigation-guidance model that was analyzed in Section 4.0 is assumed and it will be shown that this model is sufficient for the return trip.

The primary differences between the outbound and return phases of a lunar mission are as follows:

1) Higher approach velocities are encountered in the return phase than in the outbound flight
2) There may be a ballistic atmospheric re-entry into the earth's atmosphere rather than thrust into a circular orbit
3) The target area may be less precise since the earth's atmosphere affords the possibility of maneuvering after re-entry. The mission may be safely completed even if the vehicle is required to land at other than the pre-assigned touchdown location
4) The possibility exists that the return flight may not be made at a pre-assigned time due to difficulties encountered on or near moon.

The effect of these differences on sensor requirements will be considered in a semi-qualitative way in the following section.

10.2 Discussion of the Effect of Differences Between Earth-Moon and Moon-Earth Flights on Sensor Requirements

The factor of most immediate concern in the return phase of a

lunar flight is the fact that the velocities encountered as the vehicle nears Earth are much larger than for the Moon approach and as a result the position and velocity deviations are greater.

An analysis of return flights was not conducted in this study. However, from Refs. 4-2, 4-3, and 4-4 some indication of the difference in position deviation from an outbound flight may be obtained.

In Ref. 4-4, the return flight from a lunar orbit of 100 km was analyzed, assuming a theodolite and standard parameters similar to those in Table 4-3. For a 74.1 hour return flight with 45 measurements and 3 corrections the rms miss distance at Earth perigee was 69.3 km (5.3 km in altitude). For similar conditions on an outbound flight of 70.7 hours, the miss was 18.7 km (3.0 km in altitude). From this limited data, one might assume that although the total rms position deviation at the Earth is 4 or 5 times as large as at the Moon, the altitude component of this miss distance is only doubled. Since for re-entry conditions, the altitude miss is the primary consideration, the results of this analysis show that the same sensors and number of operations on the return as on the outbound phase will give adequate results. Other results in Refs. 4-2, 4-3, and 4-4 indicated similar conclusions. In fact, in Ref. 4-4, the <u>minimum</u> number of sextant observations on a return flight to achieve a safe re-entry (where safe re-entry was defined as $r_{alt} = 10$ km) was 15-19 observations for a 78.7 hour flight. Although extrapolation of these results is a hazardous process, the indications are that the sensor requirements for the return to earth phase of a lunar mission are less stringent than for the outbound flight, primarily due to the larger miss distance allowed.

The other difference in return flight is that the flight may not be made at the pre-assigned time. This difference will require that the scheduling of operations be done on-board (or on the moon), since adherence

to some preassigned schedule may not be possible. However, this capability for onboard rescheduling would be required of the outbound flight also, in case of mission abort.

This page intentionally left blank

11.0 RENDEZVOUS WITH ORBITING SPACE STATION

11.1 Introduction

This portion of the study is concerned with the rendezvous of a manned spacecraft with a cooperative and manned earth space station.

For comparison and computational purposes a specific rendezvous model was selected as being both practicable and representative of proposed space station missions. A specific rendezvous mechanization method is applied to the chaser or ferry vehicle as it attempts to rendezvous with the space station.

The space station is assumed to be in a posigrade circular orbit about the earth at an altitude of 500 km as shown in Figure 11-1. The chaser (ferry) vehicle is considered to be in a 200 km circular parking orbit coplanar with the orbital plane of the target. When correctly phased the chaser injects into an ascending transfer orbit—nominally the Hohmann transfer. Near the end of the ascent, the chaser commences the active phase of rendezvous with the space station.

The effects of injection errors are determined and requirements are established for both injection and rendezvous sensors considering such factors as mission success and energy conservation.

11.2 Background and Approach

The background for the rendezvous problem has been previously discussed in Section 9.2.

The approach taken for this portion of the study requires the selection of a suitable rendezvous model—briefly described in Section 11-1. A representative rendezvous guidance method is developed and is described in some detail in Section 11-4. These models and guidance methods are programmed on

the IBM 7094 computer. Variable injection errors and sensor inaccuracies are introduced into the program to demonstrate the consequences of such errors and to aid in determining reasonable sensor requirements based on mission safety and propellant consumption.

All computer runs used to develop rendezvous sensor requirements were made with a -0.3 m/sec. injection error in velocity. Ten samples of each run were made at each sensor noise level in an effort to establish propellant consumptions consistent with each noise level.

11.3 Definition Problem

The sensors to be considered in this phase of the study, as well as for the lunar mission of Section 9, cover several types of injection and attitude sensors as well as sensors suitable for measuring the quantities needed during the active phase of rendezvous.

The amount of propellant consumed by the ascent and rendezvous maneuvers is of considerable importance and is given corresponding significance in establishing sensor requirements. All the analysis in this portion of the study refers the required incremental velocity to that of the ideal Hohmann transfer, thereby providing for each run a non-dimensional measure of effectiveness in consumed propellant.

11.4 Analytical Description

For the purposes of this study the earth is considered to be an ideal central force field with a gravitational parameter of:

$$K_e = 3.986 \times 10^5 \text{ km}^3/\text{sec.}^2$$

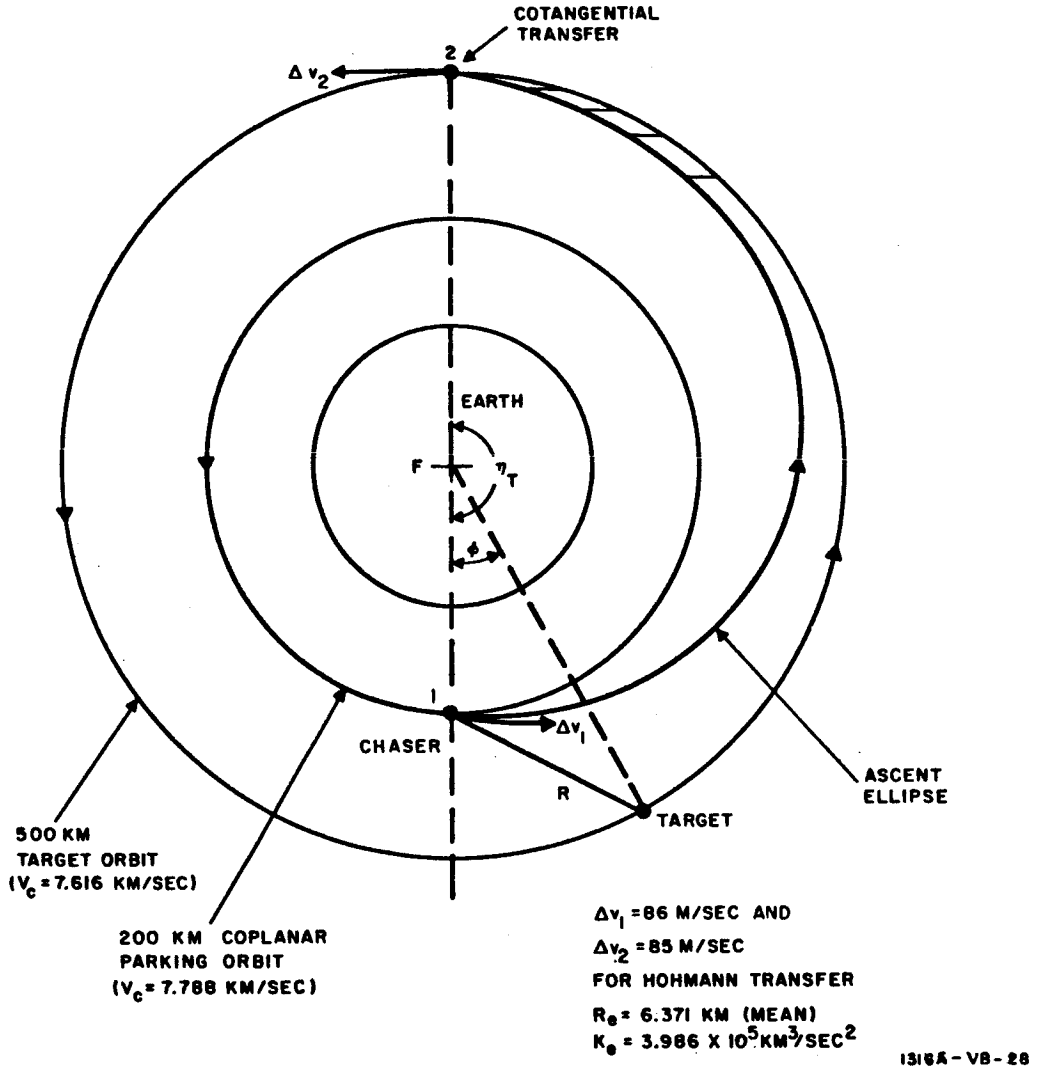

FIGURE 11-1 Earth Orbital Rendezvous

This page intentionally left blank

The earth is presumed to be spherical with a mean surface radius of:

$$R_e = 6371 \text{ km}$$

Although the effects of the earth's oblateness are thereby disregarded, this is not serious because of the short problem flight time (about 2800 sec.).

As briefly mentioned in section 11.1 and as illustrated by Fig. 11-1, the rendezvous model selected for this manned earth space station case includes the space station orbiting the earth in a circular 500 km posigrade orbit while the ferry vehicle is in a lower-energy 200 km parking orbit essentially coplanar to the orbital plane of the space station. When on the basis of measurements the chaser (ferry) determines that it is correctly phased for a good intercept, the chaser fires a posigrade rocket impulse to establish the requisite ascent and orbit which is designed to intercept the superior orbit co-tangentially at the correct time for a successful rendezvous. Actually, as the chaser nears the target, it commences a series of rendezvous maneuvers which place the chaser ahead of the space station at a desired stand-off range and with essentially zero relative velocity.

Although the IBM 7094 computer program was able to accommodate 90 and 180 degree transfer angles, all runs were limited to the 180 degree case primarily because it involves a considerably smaller expenditure of propellant.

For the nominal case, the chaser vehicle injects from the parking orbit into the ascent ellipse by applying a tangential posigrade velocity increment of 86.4 m/sec at point 1, where the range to the space station is 749.8 km at an elevation angle of 20.6 deg., while the range rate is -472.2 m/sec.

The guidance method employed for the space station rendezvous differs considerably from that used for lunar orbit rendezvous in Section 9. The rendezvous guidance method is illustrated by Fig. 11-2. As the chaser approaches the target, it moves ahead, but is gradually being overtaken by the target. At a range of 25 km the inertial reference of the chaser is aligned, as indicated, to the range vector and to the geocentric vertical, and thereafter it is space-stabilized to this space reference. The chaser vehicle is then attitude-stabilized to this space reference for the duration of the approach. Fixed thrust-level rockets with a multiple-restart capability are aligned to the body axes, so that an incremental velocity may be established along any body axis without altering the attitude of the chaser, permitting rapid velocity maneuvering without the necessity for changing vehicle attitude.

11.4.1 Vertical Control

Rendezvous control in the vertical axis (normal to LOS) is initiated when the range:

$$R < R_i = 25 \text{ km}$$

at which time the inertial platform is set to the corresponding space reference, to which all LOS angles are referred.

When the LOS rate subsequently exceeds a threshold value for two consecutive seconds:

$$|\dot{e}| > \epsilon = 0.3 \text{ mr/sec.}$$

a firing time is then computed:

$$t_F = \frac{C\,|R\,\dot{e}|}{|a_z|} \quad \text{(sec)}$$

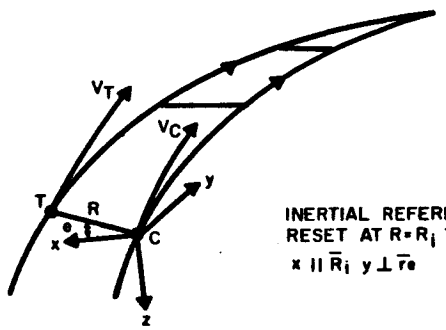

INERTIAL REFERENCE RESET AT $R = R_i$ TO:
$x \parallel \bar{R}_i \quad y \perp \bar{r}_e$

1. CHASER VEHICLE STABILIZED TO FIXED INERTIAL REFERENCE WHEN $R \leq R_i$.
2. RESTARTABLE FIXED-THRUST ROCKETS ALIGNED TO BODY AXES.

VERTICAL CONTROL:

IF $|e| > \epsilon$ COMPUTE FIRING TIME:
$t_F = CR|\dot{e}| / |a_z|$

IF $t_F \geq 2$ SEC, FIRE ROCKET TO REDUCE $\dot{e}$:
$a_z = -|a_z| \, SGN(\dot{e})$

LATERAL CONTROL IS SIMILAR TO VERTICAL

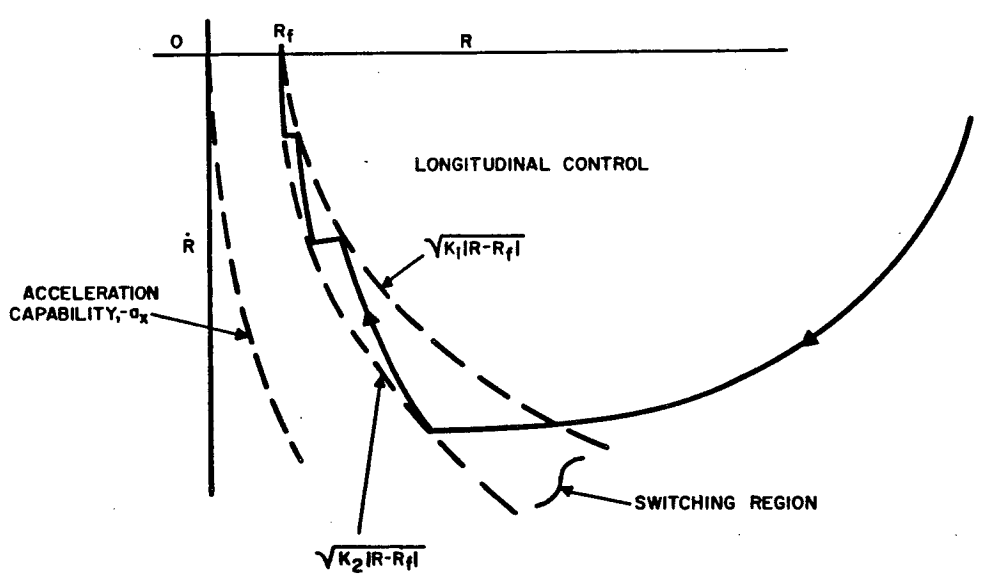

1316A-VB-49

FIGURE 11-2 Rendezvous Guidance (Earth Space Station)

where:

$C = 0.9$ (included to provide a deliberate undershoot to prevent wasteful over-shooting in the presence of noise)

$|a_z|$ = acceleration level of vertical rockets

= 1.0 m/sec^2 (0.5 m/sec^2 would have been ample)

A vertical rocket is then fired for this computed firing time with the following acceleration:

$$a_z = - |a_z| \ \text{sgn}(\dot{e}) \qquad (\text{m/sec}^2)$$

This maneuver is repeated as necessary and serves to severely restrict any rotation of the LOS. Two limitations are applied to firing the vertical rockets to minimize nuisance firings and to curtail firings resulting from noise modulation:

1. A rocket is not fired if $t_F < 2$ sec.
2. A coasting period of at least 5 sec. is mandatory between rocket firings.

11.4.2 Lateral Control

Although lateral control is not implemented by the computer since the computer program is limited to the planar case, it employs firing logic virtually identical to the vertical axis.

11.4.3 Longitudinal Control

The firing logic employed in the longitudinal control mode is to coast until the switching region bounded by a pair of parabolic curves is entered (see Fig. 11-2) at a nominal 3.5 km range.

The chaser alternately fires and coasts to remain within this switching region, driving itself to the desired standoff range at zero closing rate. When

the range rate intercepts the switching boundary, i.e., if

$$\dot{R} < \sqrt{K_2 \left| R - R_f \right|} \quad \text{(m/sec)}$$

where:

$$K_2 = 2.25 \text{ m/sec}^2$$

and:

$$R_f = \text{standoff range}$$
$$= 200 \text{ m}$$

compute a firing time:

$$t_F = \frac{2 \left| -\sqrt{K_1 \left| R - R_f \right|} - \dot{R} \right|}{\left| a_x \right|} \quad \text{(sec)}$$

where:

$$K_1 = 1.5 \text{ m/sec}^2$$

$$\left| a_x \right| = \text{acceleration level developed by longitudinal rocket}$$

$$= 1.5 \text{ m/sec}^2$$

The longitudinal rocket is then fired posigrade using the following acceleration:

$$a_x = - \left| a_x \right| \quad (\text{m/sec}^2)$$

To minimize nuisance firings and overshoots, the following control limitations are provided:

1. The longitudinal rocket will not fire if $t_F < 2$ sec.
2. A mandatory coast period of at least 2 sec. is provided between periods of rocket firing.

11.4.4 Data Processing

The inaccuracies of the rendezvous sensors in the digital computer program are simulated by adding noise to the pure range and angle inputs. Because of the necessity for operating in the presence of noise, it is necessary to smooth the raw data before attempting to use these data for control purposes. A digital data smoother, shown in block diagram form in Fig. 11-3, provides the requisite range and angle smoothing. Velocity compensation is afforded during periods of rocket firing to permit smoothing to continue during these periods without a significant decrease in accuracy. The smoother operation is generally as described in Section 9.4.4 except that the vertical corrections are elements of $\Delta U_i/R$ to provide an equivalent angular correction.

A 15-sec. smoothing time utilizing 16 stored data samples was employed for all runs together with a least squares linear fit. Range rate and angular rate are derived by taking the present slope of the smoothed lines of updated stored data points. The actual rendezvous control signals are all smoothed values:

$$R_s,\ \dot{R}_s,\ \text{and}\ \dot{e}_s.$$

11.5 Digital Program

The digital computer program for the lunar rendezvous simulation was modified to simulate an earth rendezvous technique. Since this model used a different guidance law than the lunar rendezvous described in Section 22, the section of the program which made the firing decisions had to be modified extensively. Other sections of the program required less extensive modifications in order to simulate the new system. A more detailed description of the modifications is given in Section 22.8.

The program is designed to simulate the rendezvous maneuvering of a chaser from an initial parking orbit until the rendezvous is completed. At each observation point simulated radar measurements are taken and fed to a smoother. The output of the smoother from the previous observation is examined by the firing laws and all necessary corrections to the orbit due to firing are made. This process is repeated from observation to observation until the rendezvous is completed.

11.6 Program Results

11.6.1 Nominal Trajectory

With the nominal trajectory and without injection errors, the curve of range as a function of transit time is shown in Figure 11-4. Figure 11-5 illustrates the variation in elevation angle with transit time where the elevation angle is referred to an inertial reference at perigee (and apogee). Of particular interest is the small angle at ranges below 25 km. This indicates a very small LOS angular change up to rendezvous even without corrective control—fitting in nicely with the control scheme actually used.

11.6.2 Injection Errors

11.6.2.1 Effects on Miss Distance

When the transfer angle has been traversed without any active rendezvous maneuvers, the errors at injection will result in subsequent miss distances. These miss distances are pessimistic in that they are not generally minimum range cases. The following table presents the miss distance sensitivity coefficients for the 180 degree transfer.

TABLE 11.6-1

Miss Distance Sensitivity Coefficients

(200/500 km Earth Orbit Cotangential Transfer)

Horizontal Coefficients		Units	Vertical Components		Error
$\frac{\partial M_x}{\partial r}$	+4.83	$\frac{km}{km}$	$\frac{\partial M_z}{\partial r}$	+1.07	Altitude
$\frac{\partial M_x}{\partial v}$	+8.32	$\frac{km}{m/sec}$	$\frac{\partial M_z}{\partial v}$	+3.57	Velocity
$\frac{\partial M_x}{\partial \gamma}$	+5.21	$\frac{km}{deg}$	$\frac{\partial M_z}{\partial \gamma}$	0	Attitude
$\frac{\partial M_x}{\partial t}$	+0.53	$\frac{km}{sec}$	$\frac{\partial M_z}{\partial t}$	0	Phasing

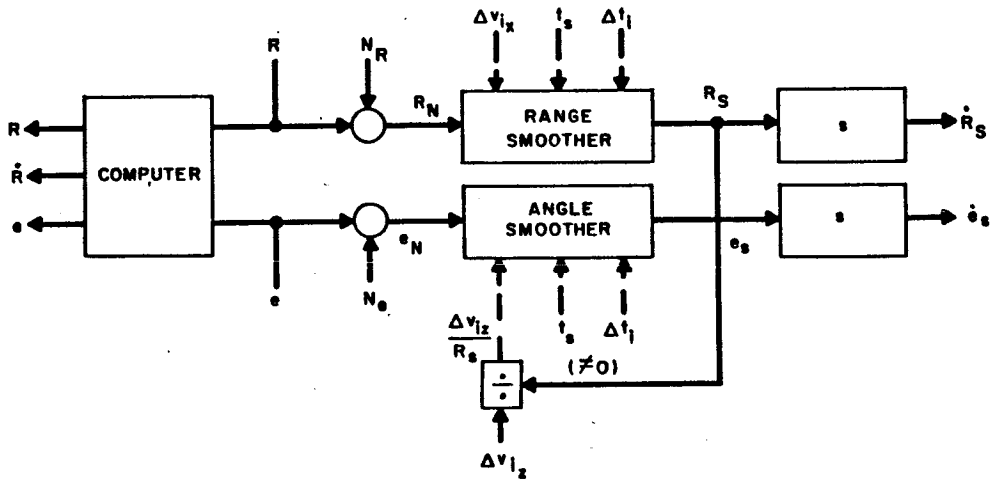

N_R = NOISE ON RANGE, R (% OF R OR OF 10 KM)

N_e = NOISE ON ANGLE, e (mr)

CONTROL SIGNALS: $R_s, \dot{R}_s, \dot{e}_s$

1316A-VB-48

FIGURE 11-3 Digital Smoother (Range and Angle)

This page intentionally left blank

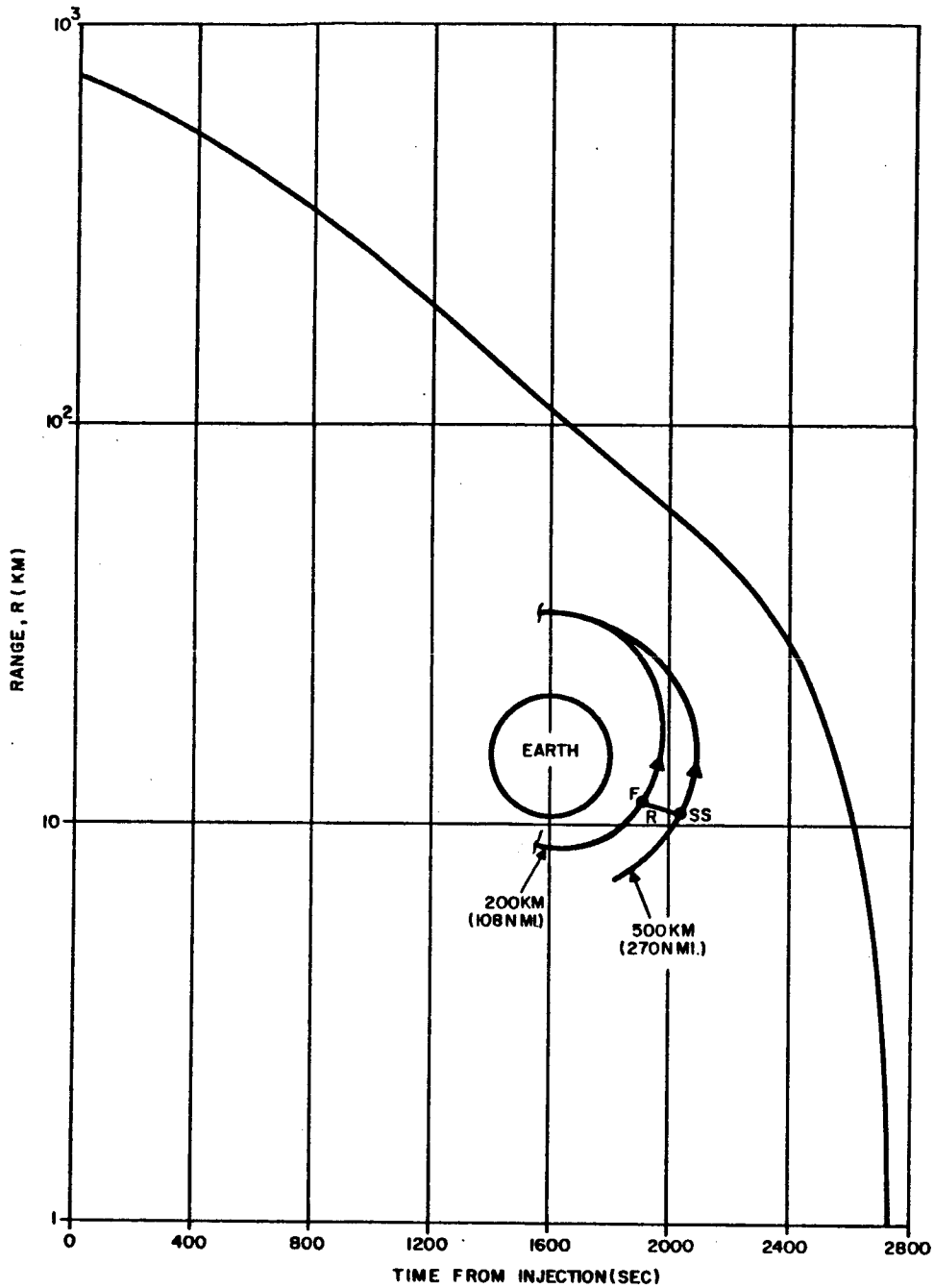

FIGURE 11-4 Range vs. Transit Time

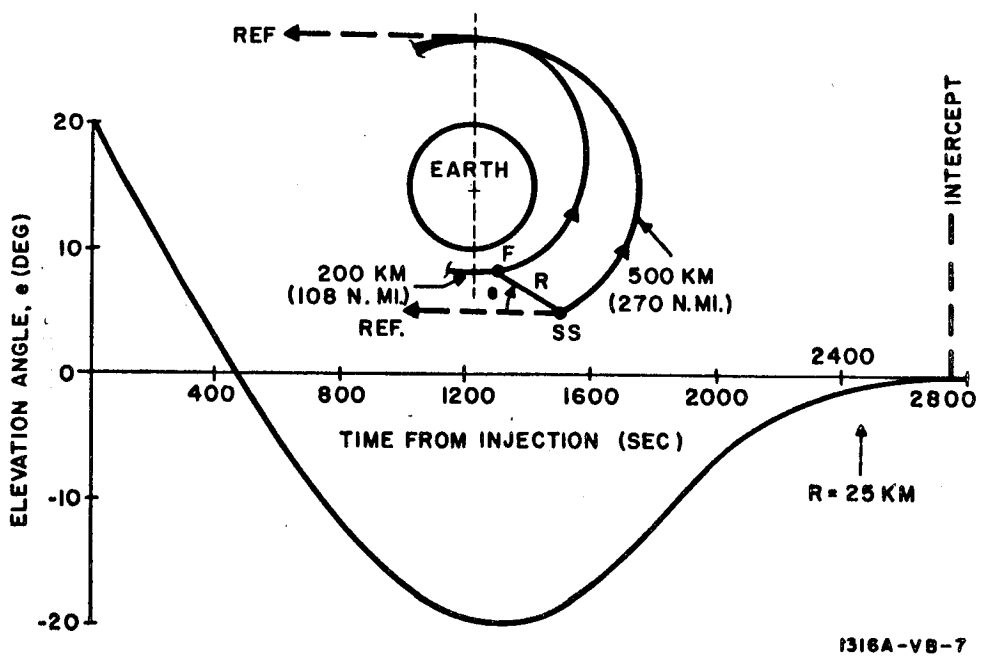

FIGURE 11-5 Elevation Angle vs, Transit Time

In the lateral axis, if the chaser was initially in the target plane:

$$\frac{\partial M_y}{\partial \psi} = 0 \qquad \text{(yaw attitude)}$$

11.6.2.2 Effects on Propellant Consumption

The effects of various levels of four types of injection errors are illustrated by the four curves of Figure 11-6, based on a series of runs made on the computer with an active rendezvous system in operation. The actual ΔV used in each case is compared with that required for the equivalent Hohmann transfer, ΔV_H, to yield a non-dimensional comparison of incremental velocity. It may be observed that these curves are considerably smoother than the corresponding curves of Section 9.

The incremental velocity profiles for a nominal trajectory are shown in Figure 11-7, pointing out that essentially no vertical correction was necessary and also demonstrating the proportional reduction in firing duration as range closes.

11.6.2.3 Effects on Accuracy

The consequences of injection errors on the accuracy and dispersion of active rendezvous trajectories is displayed by the phase plane diagram of Figure 11-8, which clearly shows how the various dispersed trajectories are trapped within the switched region and end up essentially at the standoff range, R_f, with substantially zero velocity. Figure 11-9 shows the dispersion in elevation angle that develops as the range closes to zero.

11.6.3 Rendezvous Sensor Errors

A series of computer runs were made of the rendezvous mission with various levels of rendezvous sensor noise included. All runs were made with the same injection error (-0.3 m/sec. in velocity) for comparison purposes.

The ΔV consumed during each run was compared with ΔV_H, the perfect Hohmann ΔV. Ten runs were made at each noise level, but with a different random number routine for each case. The ratio of angular noise to range noise is taken as:

$$\sigma_e \text{ (mr)} = 30\ \sigma_R \quad (\% \text{ of R})$$

The results of these runs are shown by Figure 11-10. The roughness of the curves indicates the inadequacy of the number of noise samples taken for each run. All runs shown had acceptable levels of accuracy and a successful rendezvous.

11.7 Discussion and Interpretation of Results

11.7.1 Injection Sensors

In developing acceptable error levels for establishing the ascent trajectory, the four curves of Fig. 11-6 are employed. The criterion is arbitrarily made that a 3 σ error in any one injection parameter shall not result in more than a 20% increase in propellant consumption compared with the perfect Hohmann transfer.

From the program results we obtain:

$$\frac{dR}{d\phi} = 107\ \frac{\text{km}}{\text{deg}}$$

$$\frac{d\phi}{dt} = -0.0044\ \frac{\text{deg}}{\text{sec}}$$

and:

$$R_1 = 749.8 \text{ km}$$

Converting the lead angle error, $\delta\phi$, to an equivalent range error:

$$\delta R = \delta\phi\ \frac{dR}{d\phi}$$

$$= 0.19 \times 107 \qquad (3\sigma)$$

$$= 20.4 \text{ km}$$

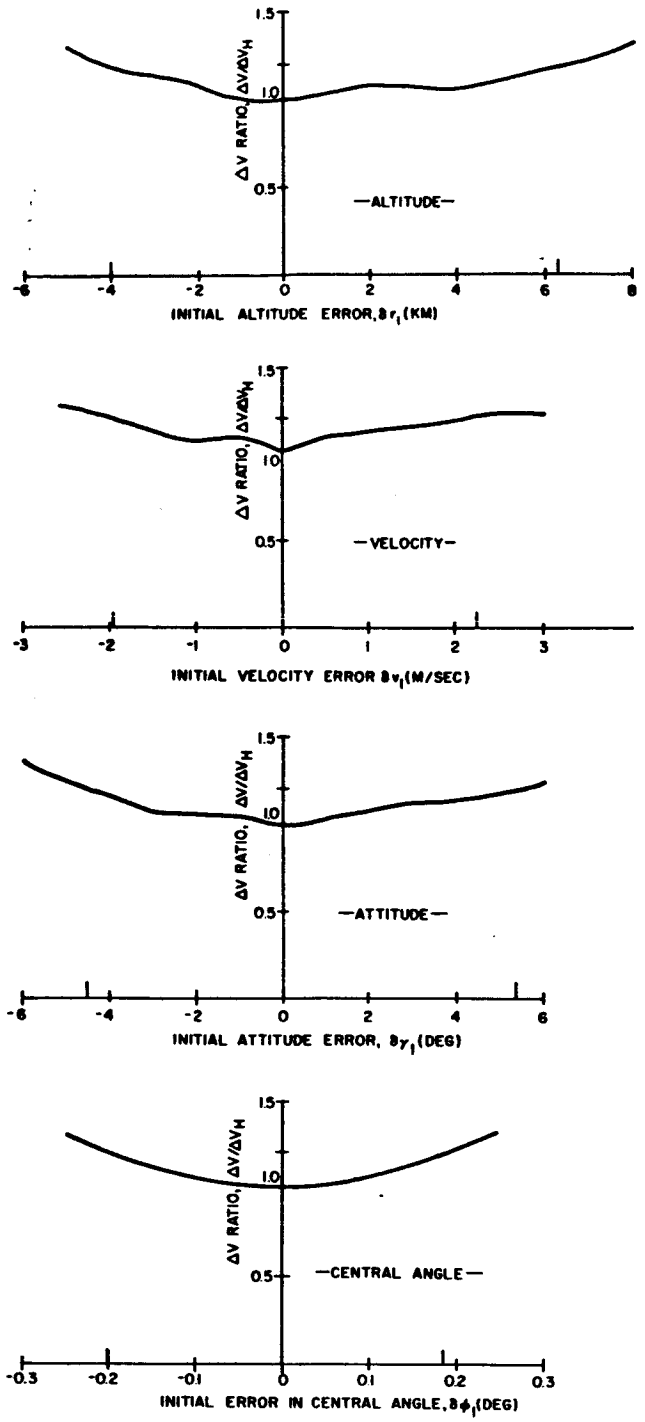

1316A-VC-5

FIGURE 11-6 Effects of Initial Conditions on Propellant Consumption (Earth Space Station)

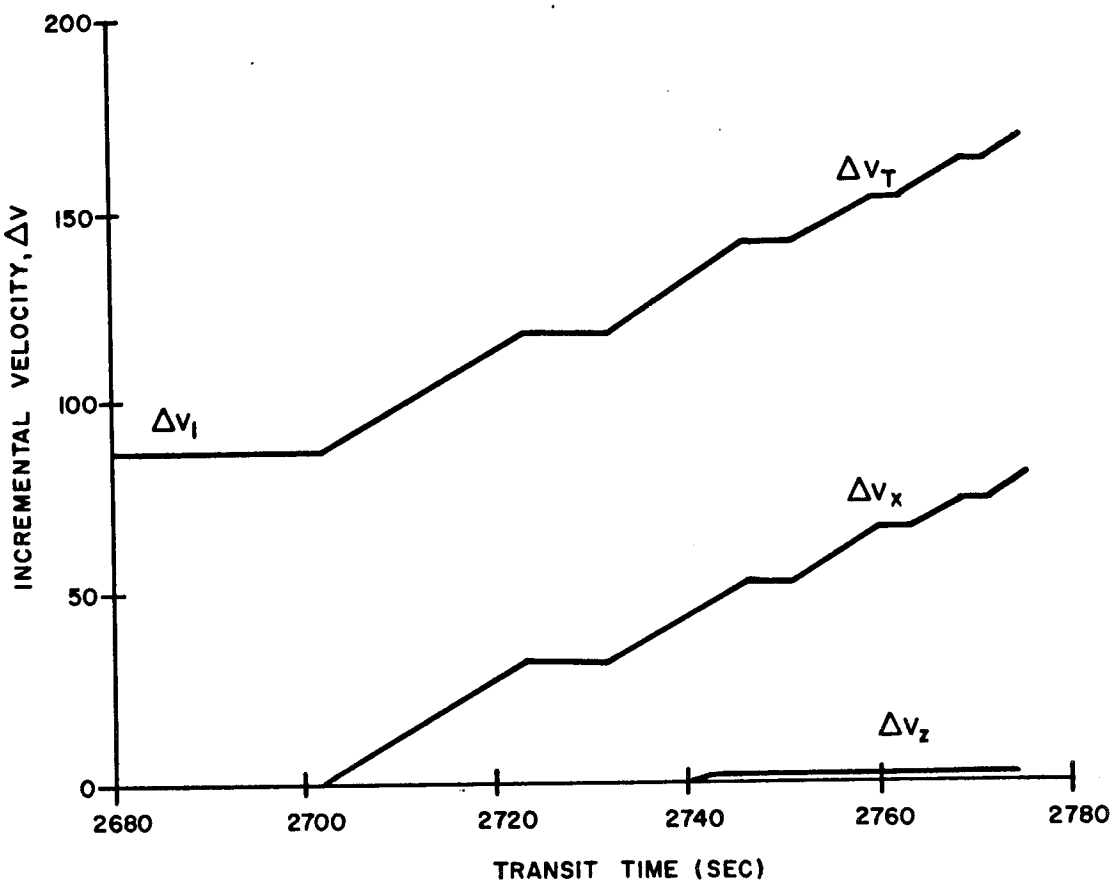

1316A-VB-4

FIGURE 11-7 Velocity Applications for a Nominal Trajectory (Earth Space Station)

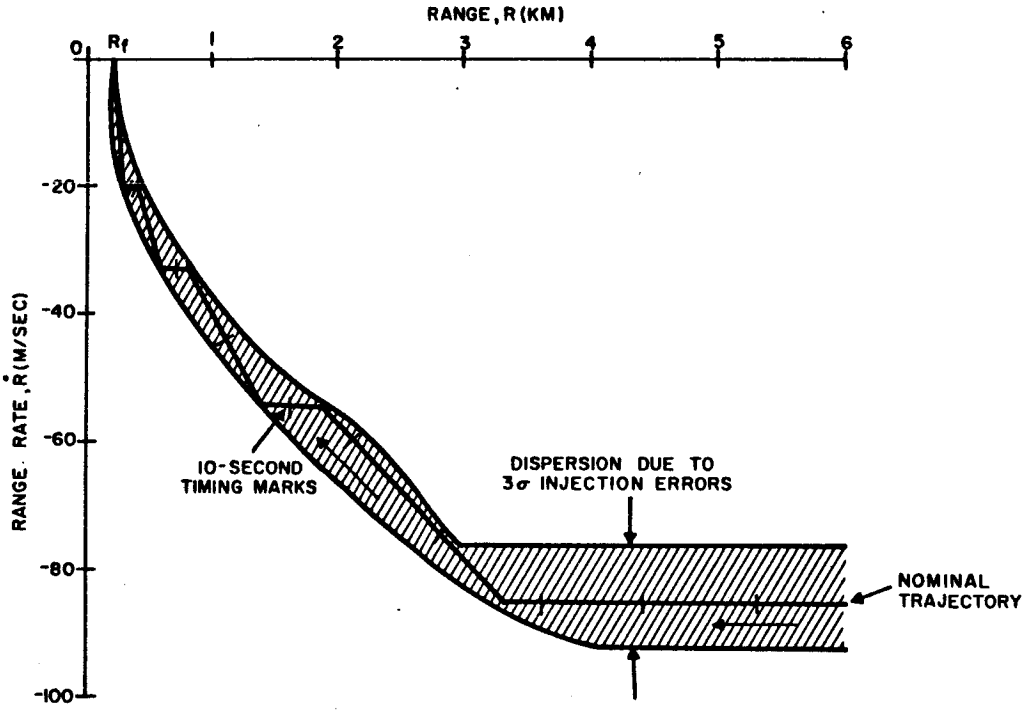

1316A-VB-8

FIGURE 11-8 Phase Plane of Active Rendezvous (Earth Space Station)

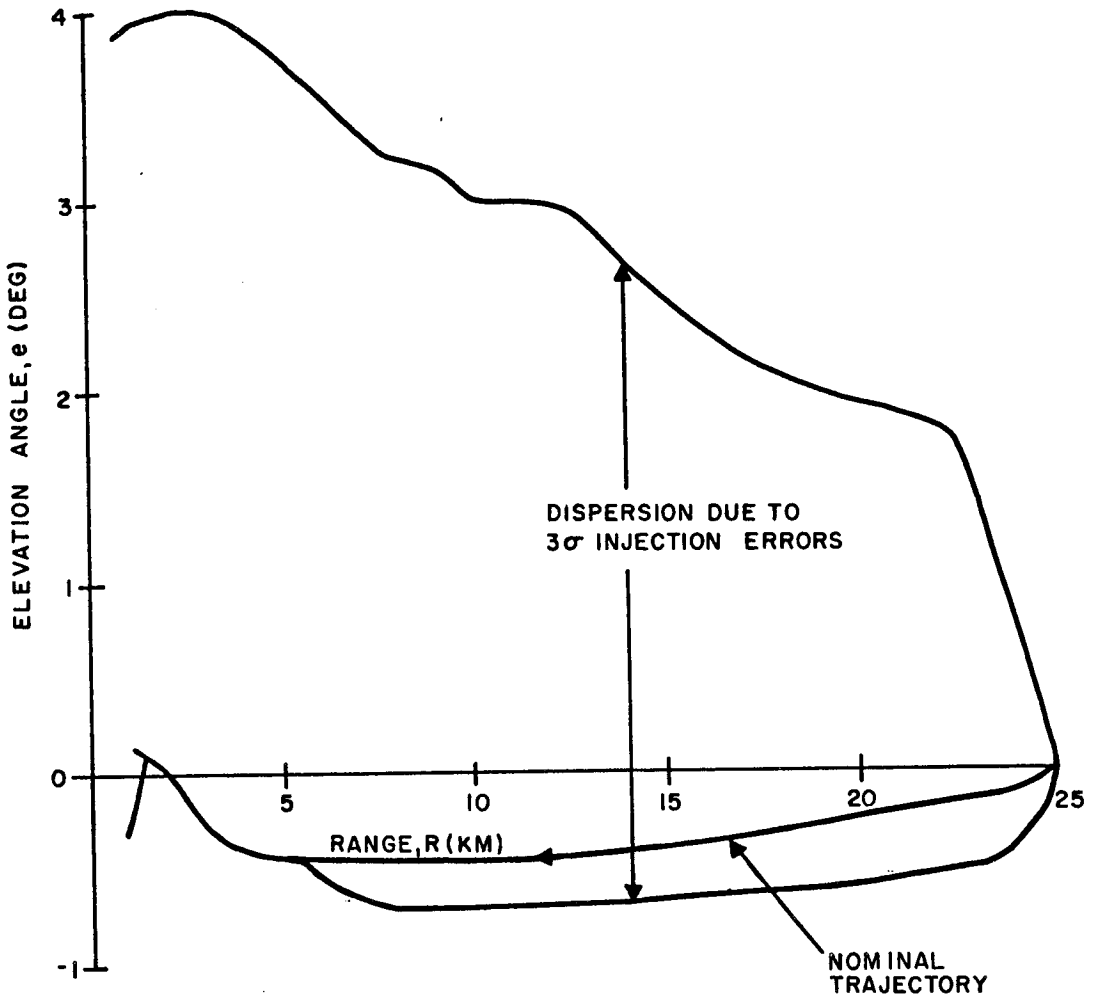

1316A-VB-10

FIGURE 11-9 Variation in Elevation Angle with Range (Earth Space Station)

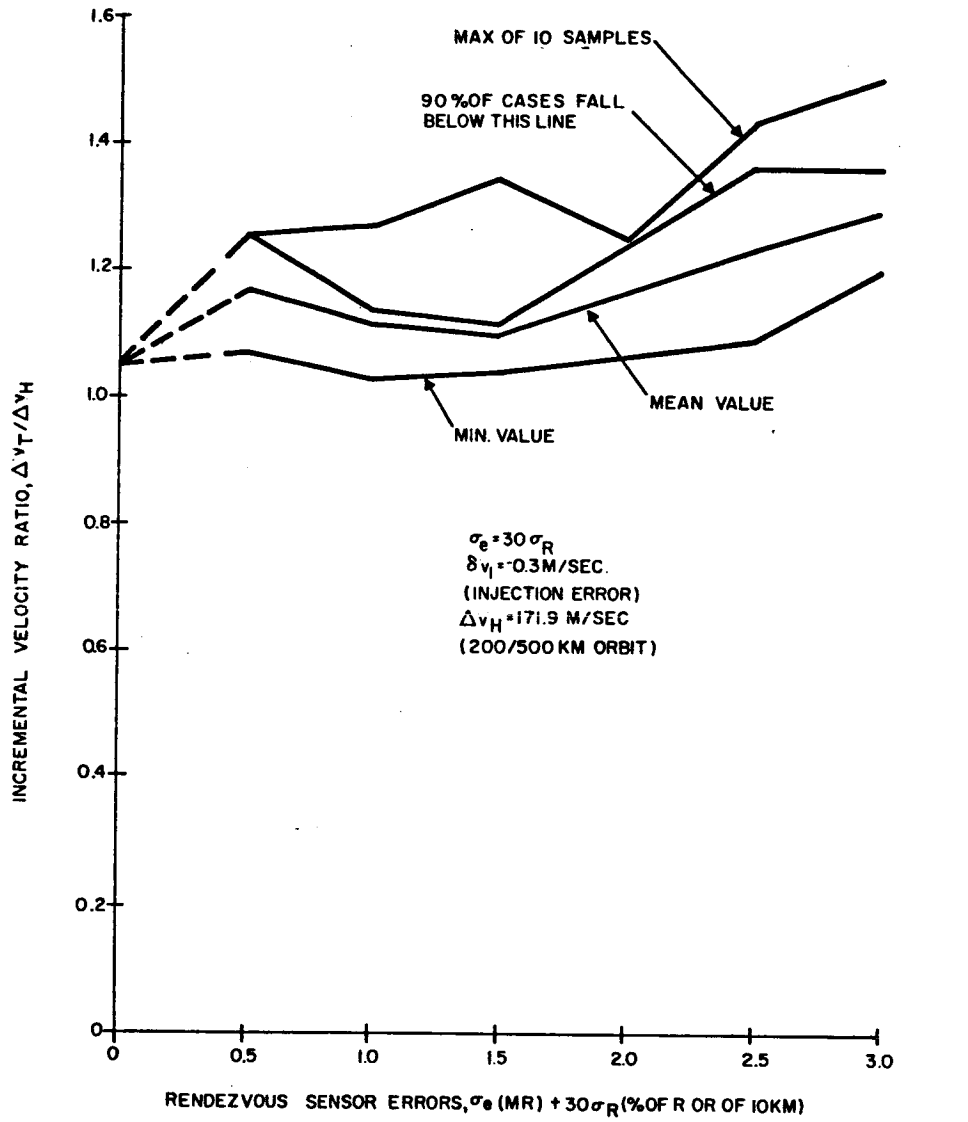

FIGURE 11-10 Effect of Rendezvous Sensor Errors on Propellant Consumption (Earth Space Station)

This page intentionally left blank

where the value for $\delta\phi$ is obtained from Fig. 11-6,

or:

$$\delta R = \frac{20.4}{750}$$

$$= 2.72\% \text{ of } R \qquad (3\sigma)$$

Converting the lead angle error, $\delta\phi$, to an equivalent error in phasing time:

$$\delta t = \frac{\delta\phi}{d\phi/dt}$$

$$= \frac{0.19}{0.0044}$$

$$= 43.2 \text{ sec} \qquad (3\sigma)$$

The lateral velocity error due to azimuth misalignment is:

$$\delta\psi \doteq \sin^{-1}\left(\frac{0.2\,\Delta v_H}{\Delta v_1}\right)$$

$$= \sin^{-1}\left(\frac{0.2 \times 171.9}{86.4}\right)$$

$$= 26.6 \text{ deg.} \qquad (3\sigma)$$

The differential inclination between chaser and target orbital planes requires a lateral out-of-plane correction to bring the chaser orbit coplanar to the target orbit:

$$\delta i \doteq \sin^{-1}\left(\frac{\Delta v}{v_2}\right) \qquad \text{(worst case)}$$

$$\doteq \sin^{-1}\left(\frac{0.2 \times 171.9}{7616}\right)$$

$$\doteq 0.26 \text{ deg} \qquad (3\sigma)$$

The required injection sensor accuracies are summarized in the following table along with reasonable state-of-the-art equivalents.

TABLE 11.7-1

Injection Sesnor Accuracy Requirements

Symbol	Quantity	Sensor Accuracy (3σ)	State-of-the-art Accuracy (3σ)
δr	Altitude	4.0 km (2% of R)	200 m (0.1% of R)*
δv	Velocity	2.0 m/sec	0.3 m/sec
$\delta \gamma$	Pitch Attitude	4.5 deg	0.3 deg
$\delta \psi$	Yaw Attitude	26.6 deg	0.3 deg
$\delta \phi$	Central Angle	0.19 deg	- - -
δR	Range	2.7% of R	0.1% of R
δt	Timing	43.2 sec	3 sec
δi	Inclination	0.26 deg	0.1 deg

*A radar altimeter can measure terrain altitude to this accuracy, but it cannot measure absolute altitude to this degree of precision.

In every case, the state-of-the-art injection sensor accuracies are significantly better than those required for the rendezvous mission.

11.7.2 Rendezvous Sensors

The rendezvous sensor requirements are based on an interpretation of the results shown in Figure 11-10. In view of the small sampling it was decided to arbitrarily specify that where the 100% line (max. of 10 samples) used a velocity ratio of 1.5 would constitute a reasonable level of accuracy. Using this criterion we have in the following table the results compared with a state-of-the-art rendezvous radar system.

Quantity	Sensor Accuracy (3σ)	State-of-the-art Accuracy (3σ)
Range	0.3% or 30 m	0.1% of R or 10 m
Angle	9 mr	3 mr

This indicates that a state-of-the-art rendezvous sensor is more than adequate for the rendezvous mission. Use of higher-accuracy sensors will, however, be beneficial in conserving propellant.

11.8 Sensor Requirements

For the earth space station rendezvous mission phase, various types of sensing devices are necessary. Minimum levels of accuracy are required of each sensor for successful completion of the mission, but another important factor is the conservation of propellant.

11.8.1 Injection Sensor Requirements

The injection sensor range and accuracy requirements are tabulated below:

TABLE 11.8-1

Injection Sensor Requirements

Quantity Measured	Dynamic Range Max.	Min.	Max. Allowable RMS (1σ) Sensor Error
Altitude	+250 km	0	1.3 km (0.7% of R)
Incremental Velocity*	+100 m/sec	0	0.7 m/sec
Pitch Angle*	+90 deg	-90 deg	1.5 deg
Yaw Angle*	+180 deg	-180 deg	8.9 deg
Range	1000 km	0	0.9% of R
Inclination Angle	+5 deg	-5 deg	0.09 deg

*These quantities include the total error permitted in that particular quantity, covering both measurement and control system inaccuracies.

While injection sensors with the above accuracy levels will produce a satisfactory rendezvous ascent, it should be stressed that the use of more accurate sensors will permit a more efficient rendezvous, thereby conserving propellant.

11.8.2 Rendezvous Sensor Requirements

The dynamic range and accuracy requirements of rendezvous sensors necessary to satisfactorily complete a rendezvous mission without an excessive expenditure of propellant is presented in the table below.

TABLE 11.8-2

Rendezvous Sensor Requirements

Quantity Measured	Dynamic Range		Max. Allowable RMS (1σ) Sensor Error
	Max.	Min.	
Range	30 km*	0	0.1% of R or 10 m
LOS angles (azimuth & elevation)	+20 deg	-20 deg	3 mr
Vehicle Attitude	+90 deg - P& R	-90 deg -P & R	0.2 deg during firing periods (to reduce cross coupling)
(pitch, roll & yaw)	+180 deg -Y	-180 deg -Y	5 deg during tracking

*The maximum range of the ranging device is that required solely for the active phase of rendezvous. If this device is the identical instrument that measures target range prior to injection and occasionally monitors the target during the coasting position of the ascent, its dynamic range should then be extended to 1000 km.

Although rendezvous sensors with the above accuracies will provide a satisfactory rendezvous, it should be borne in mind that better accuracy will result in lower propellant consumption.

All the above sensor accuracy requirements provided sufficiently accurate rendezvous approaches, so that the deciding factor in each and every case was solely an energy consideration.

11.9 Recommendations

It is evident that the rendezvous guidance method employed in this section is definitely superior to the system used for the lunar orbit case discussed in Section 9. While the energy consumption of the space station rendezvous system is quite reasonable, it is believed that a significant improvement can be subsequently made by further development of the data smoother in such areas as velocity compensation and variable smoothing time. In addition, more computer runs for a given set of conditions, should be made to produce smoother sets of data than that needed for the preliminary study.

12.0 UNMANNED MIDCOURSE GUIDANCE

For unmanned midcourse guidance, it will be assumed that an earth-command system based on information from the DSIF tracking facilities will be used. In the analysis of onboard midcourse guidance, the quantity of data employed was such that the major source of miss distance at the Moon was the uncertainty in the position and velocity estimates at the time of each correction, rather than the uncertainties in applying the corrective thrust. However, the high data rate normally employed in ground-tracking (1 point/minute) results in a more refined orbit determination, so that the errors made in applying the corrections are more significant.

12.1 Analysis

Analysis of a 73-hour flight to a perilune of 186 km using radio-command midcourse guidance was done in Reference 12-1. A summary of the results is presented in Table 12-1. The mission under consideration employs two velocity corrections, one at 12 hours and one at 48 hours. System performance is described by the miss quantities $\bar{B}\cdot\bar{T}$ and $\bar{B}\cdot\bar{R}$*. The position error at the beginning of main deboost may be obtained by multiplying $\bar{B}\cdot\bar{T}$ and $\bar{B}\cdot\bar{R}$ by 0.6 to include the focusing effect of lunar gravity on the trajectory. The error in hyperbolic excess velocity, V_∞, and the required correction accuracy, Δv, for a few of the cases are also given.

The results of this study show that system performance is primarily a function of the data rate and that correction errors on the order of those assumed have little effect on the miss distance. In other words, the assumed

* $\bar{B}$ is the vector from the center of the moon perpendicular to the asymtote of the lunar approach hyperbola. The T-component, $\bar{B}\cdot\bar{T}$ is parallel to the earth equatorial plane and the R component forms an orthogonal coordinate with T and a line parallel to the asymtote of the hyperbola.

Ground Command Midcourse Guidance

TABLE 12-1

System Characteristics:

1) Trajectory - parking orbit, 91 degree launch azimuth, 186-km circular orbit, flight time to moon = 73 hours. Injection accuracy comparable to Centaur system.

2) Tracking - DSIF, 3 stations, σ_{angles} = 0.04 degrees, $\sigma_{\dot{R}}$ = 0.15 m/s (no range data), data rate = 1 pt/min.

3) Correction Errors - Orientation angles: 2 mils (1 σ)
Accelerometer constant: 0.4 (10^{-4}) (1 σ)
Thrust cutoff: 0.003 m/s (1 σ)

After First Δv at 12 Hours: (3 σ values):

	$\bar{B}\cdot\bar{T}$, km	$\bar{B}\cdot\bar{R}$ (km)	V_∞ (m/s)	ΔV (m/s)
Standard case	27.9	20.5	.49	34
Correction magnitude errors (x5)	27.9	20.5	.49	
Correction angle errors (x5)	76.2	91.1	.55	
Tracking rate 1/10 min	76.2	38.4	1.52	
Tracking rate 6/min	16.7	18.6	.21	33

After Second Midcourse at 48 Hours: (3 σ values)

	$\bar{B}\cdot\bar{T}$, km	$\bar{B}\cdot\bar{R}$, km	V_∞ (m/s)	ΔV (m/s)
Standard case	10.8	6.1	.24	.55
Correction magnitude errors (x5)	10.8	6.1	.24	
Correction angle errors (x5)	10.8	6.1	.24	
Tracking rate (1/10 min)	33.6	18.6	.73	
Tracking rate (6/min)	4.5	2.6	.09	.27

Systematic Errors (3 values)	Landing Position
μ_e and distance to moon	5.6 km
Tracking station location uncertainties	6.9 km

accuracies in the execution of correction commands (0.015 m/s in magnitude and 10 mils pointing are sufficient, but not necessarily required. Since this was the case, a preliminary analysis was conducted for this study to determine whether or not these requirements could be lessened, assuming a standard data rate of 1 point/min.

Since in Table 12-1, there was no difference between the standard correction accuracies and a degradation of these accuracies by a factor of 5, it may be assumed that all the predicted error which results after the first correction is due to the uncertainties in position and velocity at the time of the first correction. Therefore, the predicted miss distance at the time of application of the first correction may be represented by

$$r_p = \sqrt{\left[\left(\frac{\partial M}{\partial \Delta V_1}\right)\sigma_{\Delta V_1}\right]^2 + \left[\left(\frac{\partial M}{\partial \Delta \alpha}\right)\sigma_{\Delta \alpha}\right]^2 + 27.9^2 + 20.5^2 + 2.8^2 + 3.5^2}$$

where $\partial M / \partial \Delta V_1$, and $\partial M / \partial \Delta \alpha$ are the miss-distance coefficients due to errors in the magnitude and angle of the applied thrust. The error components 2.8 and 3.5 are due to systematic errors which were considered reduced (from the values shown in Table 12-1) by a factor of 2 due to the expected improvements in the post-Apollo time period.

For this analysis, it was assumed that the correction accuracy required is that which would assure that the miss distance was not degraded by correction errors by more than 10%. In addition, it was arbitrarily assumed that the miss distances due to the correction errors would be equally divided between the two sources (angle and magnitude).

Miss distance coefficients of $\partial M / \partial \Delta V_1$ = 92.7 km/(m/s), and $\partial M / \partial \Delta \alpha$ = 62.7 km/deg, were obtained from Reference 12-2. Using these values and the 10% error criterion, the required sensor accuracies were obtained from the following relationship:

$$1.1\, r_p = \sqrt{2E + 27.9^2 + 20.5^2 + 2.8^2 + 3.5^2}$$

where $$E = \left[\left(\partial M / \partial \Delta V_1\right) \Delta V_1\right]^2 = \left[\left(\partial M / \partial \Delta \alpha\right) \Delta \alpha\right]^2$$

$$E = .105\left(1228\ km^2\right) = 129\ km^2$$

Therefore, $$\Delta V_1 = \frac{\sqrt{129\ km^2}}{92.7\ km/(m/s)} = .122\ m/s\ (3\sigma)$$

$$\Delta \alpha = \frac{\sqrt{129\ km^2}}{62.7\ km/deg} = .181\ degrees\ (3\sigma)$$

Thus, the rms values of correction magnitude accuracy may be relaxed to .041 m/s (from .015 m/s). The rms value of the pointing error obtained above, however, is 1 mil. This indicates, then, that a greater pointing error will result in an increase in Δv required at the second correction, although not necessarily a degradation of target accuracy due to the lack of critical dependence of target errors on pointing errors at the second correction. (This last effect has been shown in Reference 12-3).

12.2 Sensor Requirements

Requirements for correction accuracy on an unmanned, Earth-controlled vehicle on a 73 hour flight to a 186 km perilune are as follows:

Magnitude:	.041 m/s, rms
Pointing:	1 milliradian, rms
Data rate required:	1 pt/min
Corrections required:	2

13.0 Parking Orbit, Unmanned

Much of the discussion in Section 5 can be applied quantitatively to the unmanned lunar mission and, in a qualitative sense, to unmanned lunar and interplanetary missions. The observations described in Section 5 could be replaced by angle measurements between a beacon and an inertial reference. Presumably, the on-board navigation system would include altitude measurements also.

For unmanned missions, on-board navigation will probably be augmented by earth communication in this phase, as well as the midcourse phase of the mission. The facilities for earth tracking of satellites are summarized in the Part I document.

This page intentionally left blank

14.0 LUNAR DESCENT TRAJECTORY, UNMANNED

14.1 Introduction

The lunar descent trajectory for an unmanned vehicle can be initiated with the vehicle in an orbital condition, or directly at the end of the Earth-Moon transfer. The lunar orbit is completely by-passed in the latter approach. This section discusses the descent trajectory from initiation down to a hovering state above the lunar surface.

It has been assumed that unmanned vehicles are guided by radio command from the Earth in all phases up to an including the mid-course corrections. The accuracy of terminal approach guidance and landing guidance using radio control are seriously impaired by imperfect knowledge of astronomical constants, such as the Earth-Moon distance, to the extent that an on-board guidance system is indicated for these terminal maneuvers.

14.2 Problem Approach and Results

The analytical approach to the unmanned landing problem is identical to that taken in Section 6.0 when discussing manned missions. The guidance system, trajectory, and sensors discussed there are in no way restricted to manned vehicles. In fact, the analyses and results of Section 6.0 with the exception of paragraph 6.7.2.9, are directly applicable to unmanned descent trajectories.

14.3 Recommendations

It is stated above that the lunar orbital phase can be omitted from unmanned lunar missions. It is also possible that unmanned landing will be made directly from a high parking orbit, omitting the descent orbit which is generally included in manned mission planning. There are thus three distinct sets of initial conditions which can exist for unmanned descent trajectories.

Of these, only one is analyzed in Section 6.0. It is recommended that the techniques and digital programs developed in the course of the aforementioned analysis be extended to provide results for descent trajectories initiated from a high parking orbit and directly from the midcourse trajectory; in addition to the results already obtained for a descent trajectory initiated from a descent orbit. The recommendations of Section 6.0 are also applicable to the unmanned mission.

15.0 LUNAR LANDING TRAJECTORY, UNMANNED

The general discussion of Section 7.0 applies here, and this phase is not covered. A possible method of analysis would assume a Schuler tuned inertial reference and an altitude sensor. The approximate analysis is performed in reference 3-1.

This page intentionally left blank

16.0 INTEGRATION BETWEEN PHASES (Manned Lunar Mission)

In the Part I document, space missions were sub-divided into standard phases. It is possible to treat these missions phases as being independent of one another when studying the effects of sensor inaccuracies on space vehicle performance. Two measures of guidance and control system performance are the miss parameters at termination of the mission phase, and the accuracy of position and velocity information at phase termination. Both of these quantities are functions of sensor and control system accuracy, and as such, can only be described satistically. By treating the mission phases independently, the analyst is able to develop trade-offs between a sensor accuracy, and guidance and navigation system performance. This flexibility to analyze the effects of variation in the nominal flight path, which might not be considered if an integrated mission is assumed, must necessarily be included if mission phases are analyzed independently. This is the only way to assure that the separate analyses will be able to cover the integrated missions which will actually be flown. All of the trade-offs developed provide information which will be useful when determining the optimum phase interfaces for an integrated mission.

Throughout this study, a manned lunar mission profile has been used for analysis wherever a model is required to produce useful information. Within certain of the phases nominal initial and final conditions were used that are compatible with interface conditions of adjacent mission phases. For example, all phases which take place entirely in the vicinity of the moon were analyzed using integrated interfaces. These include: lunar parking orbit, lunar descent orbit, lunar descent trajectory, lunar hover to touchdown, lunar ascent, second lunar parking orbit, and lunar orbit rendezvous. However, the nominal interface conditions that were selected are used only as a sample

and all can readily be changed to analyze other integrated mission profiles simply by changing inputs to the computer programs.

Generally, to achieve an analysis applicable to other integrated missions the only modifications to the analyses performed will be alterations of the nominal flight paths. With this change, the effects of sensor inaccuracies at each interface will be available using the results and/or programs of this study. Then, specification of maximum allowable miss parameters and/or maximum allowable position and velocity uncertainties at interfaces will allow specification of sensor requirements for the integrated mission.

17.0 Conclusions and Recommendations

The analysis technique employed in this report has been to select as basic, as simple, and as representative a system as possible to study with regard to sensor requirements. As a result, the sensor accuracies derived may, in general, be considered to be fundamental to the mission phase considered, rather than dependent upon the idiosyncracies of a particular detailed mechanization assumed. As an example, for lunar midcourse with local navigation and control, the results indicate that angular accuracies of the order of 10 or 20 seconds of arc are needed to obtain the terminal errors assumed. It is believed that the work presented in this Part II document proves the feasibility and usefulness of this approach. While the results obtained are subject to qualification, further work using essentially the programs already established in this study could be used to reduce the qualifications imposed. It is felt that this should be done. Sensor accuracy requirements are presented in sections of this report for a variety of initial and terminal conditions. In the lunar descent trajectory phase, results are presented in the form of error coefficients, relating sensor accuracy to terminal errors. For this phase a particular set of sensor accuracies may be assumed, and an approximation to the terminal errors obtained by multiplying the assumed sensor errors by the appropriate coefficients and adding in rms fashion, the results for each component of terminal error.

Detailed conclusions and recommendations are included at the end of various sections of this report.

This page intentionally left blank

18.0 APPROACH TO PART III

In terms of the guidelines furnished by MIL-D-8684A paragraph 3.4.3, the next step following the completion of the Part II "Analytical Solution" study would be the "Mechanization", Part III. This study would convert the general requirements for the sensors considered in Part II into an explicit definition of physical equipment. The observable measured, its required accuracy of measurement, and the sensor scheme employed, all taken from the Part II and supplementing studies, would be used as the basis for the mechanization study.

This page intentionally left blank

19.0 Appendix I: Lunar Midcourse Trajectory

19.1 Appendix I-A: Analytical Development of Estimation and Correction Equations

Trajectory Estimation

The estimation problem may be stated as follows: given a nominal trajectory, and some observations on the actual trajectory, make the "best" estimate of the actual trajectory.

The equation of motion of a vehicle in space under the influence of n gravitational fields is as follows:

$$\ddot{R}_{vR} = -\frac{\mu_r R_{vr}}{|R_{vr}|^3} - \sum_{\substack{i=1 \\ i \neq r}}^{n} \mu_i \left[\frac{R_{vi}}{|R_{vi}|^3} - \frac{R_{ri}}{|R_{ri}|^3} \right]$$

where R is the position vector, u_i is the gravitational effect of the ith planet, and the subscripts v and r refer to vehicle and the planet at which the coordinate reference is located. The gravitational pull of the vehicle is neglected.

For a vehicle in earth-moon space, the equations of motion in an earth-centered non-rotating Cartesian coordinate system may be written.

$$\text{(A-1)} \quad \begin{aligned} \ddot{x} &= -\frac{\mu_e x}{R_e^3} - \frac{\mu_m}{R_{vm}^3}(x - x_m) - \frac{\mu_m x_m}{R_m^3} \\ \ddot{y} &= -\frac{\mu_e y}{R_e^3} - \frac{\mu_m (y - y_m)}{R_{vm}^3} - \frac{\mu_m y_m}{R_m^3} \\ \ddot{z} &= -\frac{\mu_e z}{R_e^3} - \frac{\mu_m (z - z_m)}{R_{vm}^3} - \frac{\mu_m z_m}{R_m^3} \end{aligned}$$

where $R_e = \sqrt{x^2 + y^2 + z^2}$

$$R_m = \sqrt{x_m^2 + y_m^2 + z_m^2}$$

$$R_{vm} = \sqrt{(x - x_m)^2 + (y - y_m)^2 + (z - z_m)^2}$$

and u_e, u_m are the gravitational constants of the earth and moon. The coordinate system is illustrated in the sketch:

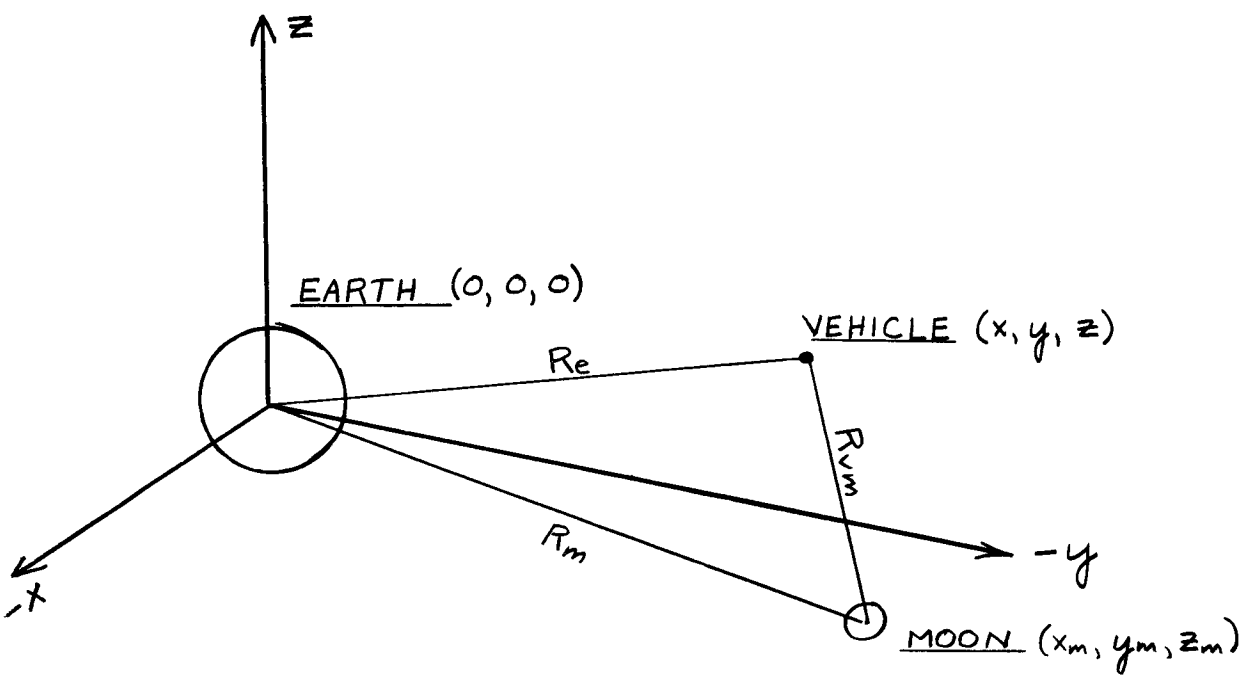

It was assumed that the only gravitational forces present are those due to a spherical earth and moon. Although at least the sun's g-field and the first harmonic term in the earth's oblateness must be considered on an actual mission, they are not required for a parametric analysis of this type.

The equations of motion, (1), are nonlinear and can be solved only by numerical integration. In order to apply linear filtering techniques for estimation purposes, the equations of motion are linearized about the nominal (desired)

trajectory. Re-writing (1) as:

$$
\text{(A-2)} \qquad
\begin{aligned}
\ddot{x} &= f_1(x, y, z, t) \\
\ddot{y} &= f_2(x, y, z, t) \\
\ddot{z} &= f_3(x, y, z, t)
\end{aligned}
$$

Expanding in a Taylor series at some time t_k:

$$
\text{(A-3)} \qquad \delta\ddot{x} \doteq \left.\frac{\partial f_1}{\partial x}\right|_{t_k} \delta x + \left.\frac{\partial f_1}{\partial y}\right|_{t_k} \delta y + \left.\frac{\partial f_1}{\partial z}\right|_{t_k} \delta z
$$

where higher order partial derivatives have been dropped and the equations for $\delta\ddot{y}$ and $\delta\ddot{z}$ are of similar form. The quantities $\delta x = (x - x_N)$, $\delta y = (y - y_N)$, $\delta z = (z - z_N)$ represent the deviations from the nominal trajectory at t_k and the equations (3) are now linear in the deviation quantities.

Letting $x_1 = \delta x$, $x_2 = \delta y$, $x_3 = \delta z$, $x_4 = \delta\dot{x}$, $x_5 = \delta\dot{y}$, $x_6 = \delta\dot{z}$ the linearized equations of motion may now be written in the form:

$$
\text{(A-4)} \qquad
\begin{aligned}
\dot{x}_1 &= x_4 \\
\dot{x}_2 &= x_5 \\
\dot{x}_3 &= x_6 \\
\dot{x}_4 &= \left(\frac{\partial f_1}{\partial x}\right) x_1 + \left(\frac{\partial f_1}{\partial y}\right) x_2 + \left(\frac{\partial f_1}{\partial z}\right) x_3 \\
\dot{x}_5 &= \left(\frac{\partial f_2}{\partial x}\right) x_1 + \left(\frac{\partial f_2}{\partial y}\right) x_2 + \left(\frac{\partial f_2}{\partial z}\right) x_3 \\
\dot{x}_6 &= \left(\frac{\partial f_3}{\partial x}\right) x_1 + \left(\frac{\partial f_3}{\partial y}\right) x_2 + \left(\frac{\partial f_3}{\partial z}\right) x_3
\end{aligned}
$$

Using these equations, it is possible to derive linear relationships between deviations from the nominal trajectory at t_k, and deviations at some later time t_{k+1}. Defining $[x]$ as a column vector whose 6 components are x_1, x_2, - - -, x_6, then the 6 x 6 matrix $\Phi(t_{k+1}, t_k)$ is defined by the following matrix equation:

$$\text{(A-5)} \qquad [x](t_{k+1}) = \Phi(t_{k+1}, t_k)[x](t_k)$$

In other words, $\Phi(t_{k+1}, t_k)$ is a matrix which relates deviations from the nominal at t_{k+1} to deviations at t_k. The matrix Φ may be calculated numerically by evaluating the partial derivatives $\partial f_1/\partial x$, etc. along the nominal trajectory and solving the equations (4) 6 times, each time using an initial condition of 1 on one of the unknowns and zero on the other five. The Φ matrix is then of the form:

$$\Phi(t_{k+1}, t_k) = \begin{bmatrix} \varphi_{11} & \varphi_{12} & - & - & - & \varphi_{16} \\ \varphi_{21} & & & & & - \\ - & & & & & - \\ - & & & & & - \\ - & & & & & - \\ \varphi_{61} & - & - & - & - & \varphi_{66} \end{bmatrix}$$

where φ_{11} is the effect of a unit deviation in x_1 at t_k on the deviation x_1 at t_{k+1}, φ_{21} is the effect of a unit deviation in x_1 at t_k on the deviation x_2 at t_{k+1} and so on.

Equation 5 then can be used to find the deviations from nominal at any time t from knowledge of the deviations in the injection conditions by the relation:

$$\text{(A-6)} \qquad [x](t) = \Phi(t, t_0)[x](t_0)$$

where t_o is time of injection into the midcourse trajectory.

Of course, the injection conditions are not known exactly. It will be assumed, however, that they can be described probabilistically at least up to second-order statistics. Regarding the injection deviations from nominal as a vector whose components are random variables with zero mean, the covariance matrix of injection conditions is defined as:

$$\text{(A-7)} \qquad \mathrm{cov}\left\{[x](t_o)\right\} \equiv E\left\{[x](t_o)\,[x]^T(t_o)\right\} \equiv P(t_o)$$

where E means expected value, and T indicates a transpose.

By equations (6) and (7), the covariance matrix of trajectory deviations is then given by:

$$\text{(A-8)} \qquad R(t) \equiv E\left\{[x](t)\,[x]^T(t)\right\} = \Phi(t, t_o)\,P(t_o)\,\Phi^T(t, t_o)$$

Thus, the statistics of the trajectory deviations are expressed in terms of the injection statistics and the linearized transition (Φ) matrices.

In order to estimate the trajectory deviations from noisy observations, the relationship between the observations and the state deviation vector $[x](t_k)$ must be developed. By state deviation vector is meant the 6-row column vector whose components x_1 - - - - x_6 are the deviations from the nominal trajectory at some time. For the system being considered here, the observations are simply measurements of the deviation of the angle from the value which would be obtained if the vehicle were on the nominal

trajectory. This is illustrated in the sketch:

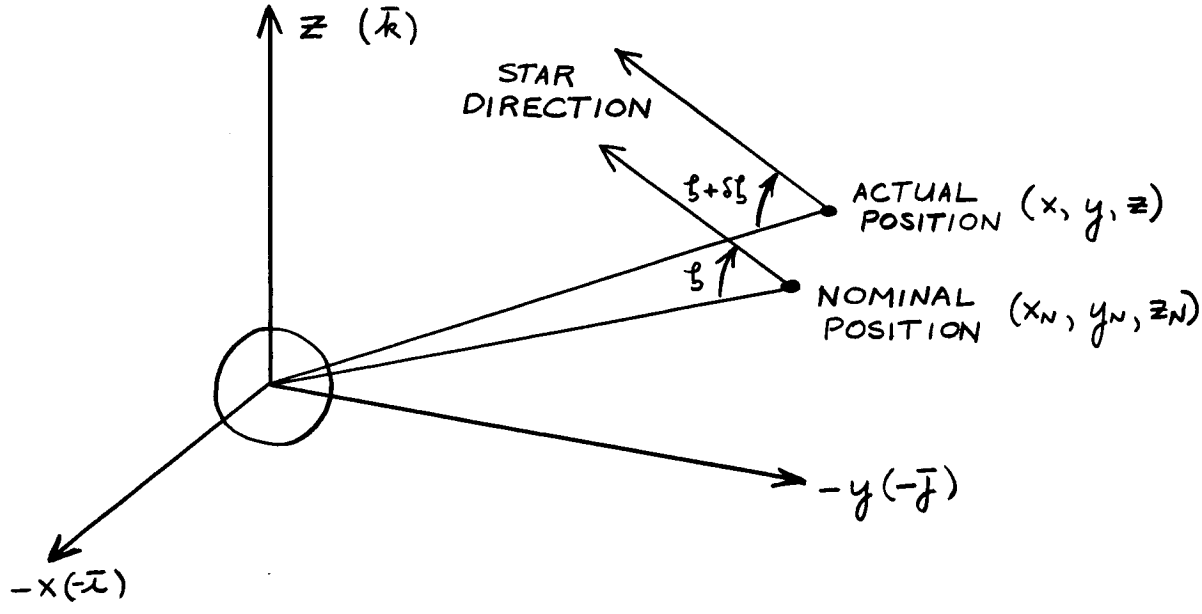

Letting the star direction have the vector value $a\bar{i} + b\bar{j} + c\bar{k}$, then;

$$\zeta = \cos^{-1}\left[-\frac{(ax_N + by_N + cz_N)}{\sqrt{x_N^2 + y_N^2 + z_N^2}}\right] \tag{A-9}$$

Linearizing the deviation $\delta\zeta$ of the angle ζ from its nominal value,

$$\delta\zeta_{t_k} = \left(\frac{\partial\zeta}{\partial x}\right)_{t_k}\delta x_{t_k} + \left(\frac{\partial\zeta}{\partial y}\right)_{t_k}\delta y_{t_k} + \left(\frac{\partial\zeta}{\partial z}\right)_{t_k}\delta z_{t_k} \tag{A-10}$$

Writing this equation in matrix form,

$$\delta\zeta_{t_k} = H_1(t_k)[x](t_k) = [H_1 \quad 0_{33}][x](t_k) \tag{A-11}$$

where $$H_1(t_k) = \left[\left.\frac{\partial\zeta}{\partial x}\right|_{t_k} \quad \left.\frac{\partial\zeta}{\partial y}\right|_{t_k} \quad \left.\frac{\partial\zeta}{\partial z}\right|_{t_k}\right]$$

For errorless observations, the simultaneous solution of equation (11) taken at 3 different times points would determine a position fix, and 2 position fixes (a total of 6 observations) would completely determine the free-flight trajectory.

For the estimation process under consideration, however, the measurements of $\delta\zeta$ will be assumed to be noisy, with errors having known gaussian distribution about zero mean. It is assumed that the measurement variance, Q, is known. (Q need not be constant in general, but will be assumed so in this analysis).

In order to include the effects of instrument noise in the estimate, the assumption is made that these errors can be represented as the output, n(t) of a dynamic system excited by an independent (vector-valued) Gaussian random process, $u_n(t)$, where $u_n(t)$ is "white noise".

$$\text{(A-12)} \qquad n(t_{k+1}) = \Phi_n(t_{k+1}, t_k)\, n(t_k) + \int_{t_k}^{t_{k+1}} \Phi_n(t_{k+1}, t_k)\, u_n(\tau)\, d\tau$$

Adding equations (12) and (5) there is;

$$\text{(A-13)} \qquad [x^*](t_{k+1}) = \Phi^*(t_{k+1}, t_k)[x^*](t_k) + \int_{t_k}^{t_{k+1}} \Phi_n(t_{k+1}, t_k)\, u_n(\tau)\, d\tau$$

where $[x^*](t_k)$ is an augmented state vector composed of $[x](t_k)$ plus the components of $n(t_k)$ and $\Phi^*(t_{k+1}, t_k)$ is the transition matrix defined by

$$\Phi^*(t_{k+1}, t_k) = \left[\begin{array}{c|c} \Phi(t_{k+1}, t_k) & 0 \\ \hline 0 & \Phi_n(t_{k+1}, t_k) \end{array}\right]$$

Assuming additive errors on the observation process, then the observations y are given by:

$$y(t_k) = \delta\rho_{t_k} + n(t_k) = H[x](t_k) + n(t_k)$$

by substitution of eq. (11). This may be written:

$$\text{(A-14)} \qquad y(t_k) = M(t_k)[x^*](t_k)$$

where M is the row matrix $\left[\frac{\partial\rho}{\partial x} \quad \frac{\partial\rho}{\partial y} \quad \frac{\partial\rho}{\partial z} \quad 0 \quad 0 \quad 0 \quad 1\right]$

Letting $\int_{t_k}^{t_{k+1}} \Phi_n(t_{k+1}, t_k) u_n(\tau)\, d\tau = u(t_{k+1}, t_k)$ in eq. (12) for convenience and re-writing equations (13) and (14), the equations describing the random processes $\{[x^*](t_k)\}$ and $\{[y^*](t_k)\}$ are:

$$\text{(A-15)} \qquad [x^*](t_{k+1}) = \Phi^*(t_{k+1}, t_k)[x^*](t_k) + u(t_{k+1}, t_k)$$

$$\text{(A-16)} \qquad y(t_k) = M(t_k)[x^*](t_k)$$

The problem of determining the optimum linear estimate of $[x^*](t_k)$, given $y(t_o)$, - - - $y(t_k)$, for a norm-squared error criterion has been solved by Kalman in ref. 4-5. It is shown that $[\hat{x}^*](t_k)$, where the $\wedge$ indicates the optimum linear estimate may be generated by the following linear relationships:

$$[\hat{x}^*](t_k) = \Phi^*(t_k, t_{k-1})[\hat{x}^*](t_{k-1}) + K^*(t_k)\left[y(t_k) - M(t_k)\Phi^*(t_k, t_{k-1})[\hat{x}^*](t_{k-1})\right]$$

$$K^*(t_k) = P^*(t_k) M^T(t_k)\left[M(t_k) P^*(t_k) M^T(t_k)\right]^{-1}$$

$$P^*(t_{k+1}) = \Phi(t_{k+1}, t_k)\left[P^*(t_k) - K^*(t_k)M(t_k)P^*(t_k)\right]\Phi^T(t_{k+1}, t_k) + Q^*(t_{k+1}, t_k)$$

where $P^*(t_k)$ is the covariance matrix of the error in estimation at t_k, and $Q^*(t_k + 1, t_k)$.

When considering observation errors which are uncorrelated from one observation to the next, these equations may be simplified, as shown in ref. 4-1 to:

$$\text{(A-17)} \quad [\hat{x}](t_k) = \Phi(t_k, t_{k-1})[\hat{x}](t_{k-1}) + K(t_k)\left[y(t_k) - H(t_k)\Phi(t_k, t_{k-1})[\hat{x}](t_{k-1})\right]$$

$$\text{(A-18)} \quad K(t_k) = P(t_k)H^T(t_k)\left[H(t_k)P(t_k)H^T(t_k) + Q(t_k)\right]^{-1}$$

$$\text{(A-19)} \quad P(t_{k+1}) = \Phi(t_{k+1}, t_k)\left[P(t_k) - K(t_k)H(t_k)P(t_k)\right]\Phi^T(t_{k+1}, t_k)$$

For the case of single angle measurements per observation, the equations may be further simplified. The P matrix may be calculated recursively by:

$$P(t_{k+1}) = \Phi(t_{k+1}, t_k)P'(t_k)\Phi^T(t_{k+1}, t_k)$$
$$P'(t_k) = P(t_k) - K(t_k)H(t_k)P(t_k)$$

Letting

$$P = \begin{bmatrix} P_1 & P_2^T \\ P_2 & P_3 \end{bmatrix}$$

where the submatrices P_1, etc. are 3 x 3's,

and

$$H = \begin{bmatrix} \frac{\partial f}{\partial x} & \frac{\partial f}{\partial y} & \frac{\partial f}{\partial z} & 0 & 0 & 0 \end{bmatrix} = \begin{bmatrix} H_1 & 0_{13} \end{bmatrix}$$

then equation (18) becomes

$$K = \begin{bmatrix} P_1 \\ P_2 \end{bmatrix} H_1^T \left[H_1 P_1 H_1^T + Q \right]^{-1}$$

where the time arguments (t_k) have been omitted for simplicity. Since the quantity $\left[H_1 P_1 H_1^T + Q \right]$ is a scaler, matrix inversion is not required to compute K.

The estimation equations are grouped here for convenience in discussion, omitting time arguments where possible:

(A-20) $$[\hat{x}] = \Phi [\hat{x}]_{k-1} + K \left[y - H \Phi [\hat{x}]_{k-1} \right]$$

(A-21) $$K = \begin{bmatrix} P_1 \\ P_2 \end{bmatrix} H_1^T \left[H_1 P_1 H_1^T + Q \right]^{-1}$$

(A-22) $$P_{k+1} = \Phi_{k+1} \left[P - KHP \right]$$

It can be seen that the estimation procedure is a recursive operation employing the following steps;

(1) P (t_o), Q, H, and Φ are inputs with H and Φ being computed from the reference trajectory.

(2) At each observation time, t_k, the estimate of the deviation quantity $[x]$, based on k - 1 observations, is computed as $\Phi[\hat{x}]_{k-1}$ where $[\hat{x}]_{k-1}$ is the estimate of the deviations at t_{k-1}. As mentioned previously, Φ (t_k, t_{k-1}) is a matrix relating deviations from the reference trajectory at t_{k-1} to deviations at t_k. The estimate of the deviation at t_k based on k-1 observations is then $\Phi[\hat{x}]_{k-1}$.

(3) The quantity $H\Phi[\hat{x}]_{k-1}$, where H is a geometry matrix previously described, is the predicted measurement of the angle α based on k-1 measurements. y is the actual measurement. When y is measured at t_k, the difference between the predicted and actually measured angles are multiplied by the weighting vector K and the result is added to $\Phi[\hat{x}]_{k-1}$ to obtain $[\hat{x}]$, the updated estimate of the deviations based on k measurements.

(4) The weighting vector K, is seen to be a function of Q, the instrument variance W, H, the relation of the measured angle to the deviations W, and P.

(5) Starting with $P(t_o)$, the covariance matrix of injection errors (assumed known), the P matrix, which is the covariance matrix of the errors in estimate is also generated recursively. The quantity in brackets in Eq. 22, (P - KHP) represents the decrease in P due to the observation. The multiplication of this quantity by $\Phi[\quad]\Phi^T$ is the change in P from 1 observation to another.

The matrices Φ and H are calculated from some "reference" trajectory. For an unbiased estimate, this reference trajectory should be the estimated trajectory, since in general, the reference trajectory should be closerto the true state than the nominal trajectory. However, if the deviations from the nominal trajectory are relatively small, the matrices Φ and

H could be precomputed from the nominal trajectory with little change in the numerical results.

Velocity Corrections

The previous section describes a process which may be used to estimate the trajectory, based on optical measurements of the star-planet angles. Since, in general, injection accuracy attainable by present-day equipment is not sufficient for precise lunar missions, corrective thrusts will be required during the flight. Data for the computation of the required ΔV will be obtained from the up-dated estimate of trajectory deviations described previously.

For this analysis, it will be assumed that a fixed-time-of-arrival, fixed correction time guidance law is being used. Though not necessarily an "optimum" scheme, this guidance law is convenient for mechanization and analysis.

Calling t_A, the time of arrival at perilune on the nominal trajectory, then the predicted deviation at t_A based on the deviation at t_k is:

$$[x](t_A) = \Phi(t_A, t_k)[x](t_k) \tag{A-23}$$

Letting $\Phi(t_A, t_k) = A$, and writing (1) in partitioned form:

$$\begin{bmatrix} r_A \\ V_A \end{bmatrix} = \begin{bmatrix} A_1 & A_2 \\ A_3 & A_4 \end{bmatrix} \begin{bmatrix} r_k \\ V_k \end{bmatrix} \tag{A-24}$$

where A_1, A_2, etc. are 3 x 3 submatrices of A, and r and v are 3 x 1 vectors of position and velocity deviations.

Since a single impulsive thrust can correct only 3 components of the predicted deviation at t_A, it will be assumed that the ΔV will be applied in such a way as to null out predicted position errors at t_A.

This is a sensible way to apply midcourse corrections for the manned lunar mission, since mission safety depends most strongly on position errors and velocity deviations from nominal at t_A will be wiped out by the large thrust required to inject into a lunar orbit.

If a ΔV is applied to null out the indicated position error, r_A, then from equation (24) there is:

$$\text{(A-25)} \qquad \begin{bmatrix} O_{13} \\ V_A' \end{bmatrix} = \begin{bmatrix} A_1 & A_2 \\ A_3 & A_4 \end{bmatrix} \begin{bmatrix} r_k \\ V_k + \Delta V \end{bmatrix}$$

where V_A is the new predicted velocity deviation as a result of the applied ΔV. Expanding (25) and solving for ΔV:

$$\text{(A-26)} \qquad O_{33} = A_1 r_k + A_2 (V_k + \Delta V)$$

$$\text{(A-27)} \qquad \Delta V = -A_2^{-1} A_1 r_k - V_k$$

$$\text{(A-28)} \qquad \Delta V = -\begin{bmatrix} A_2^{-1} A_1 & I_{33} \end{bmatrix} \begin{bmatrix} r_k \\ V_k \end{bmatrix}$$

$$\text{(A-29)} \qquad \Delta V = G_k' [x] (t_k)$$

where $G_k = -\left[A_2^{-1} A_1 \quad I_{33}\right]$. Thus, the indicated velocity correction at any t_k is computed as a function of the deviation at that time.

After a velocity correction has been made, P (t_k), the covariance matrix of estimation errors must be incremented because of the increased uncertainty of the deviations due to the error in the measurement of the applied ΔV. Letting the ΔV measurement error be represented by the 3 x 3 covariance matrix C, and partitioning P such that

$$P = \begin{bmatrix} P_1 & P_2 \\ P_3 & P_4 \end{bmatrix} \tag{A-30}$$

then after a correction

$$P_c = \begin{bmatrix} P_1 & P_2 \\ P_3 & (P_4 + C) \end{bmatrix} \tag{A-31}$$

The estimate of the deviation from nominal after a velocity correction is simply:

$$[\hat{X}]_c(t_k) = [\hat{X}](t_k) + [\Delta V_m] \tag{A-32}$$

where $[\Delta V_m]$ is the measured velocity impulse applied. When P and $[\hat{X}]$ have been incremented in this manner, the estimation process described in Section 4.3.1 continues on as before.

19.2 Appendix I-B. Computation of Statistical Information

Statistical information about the performance of the estimation and guidance system described in Appendix IA may be developed by computation of the R and P matrices developed along the nominal trajectory.

Since $R = E\left[[X][X]^T\right]$ as shown in eq. (8), section 4.3.1, then

$$(B\text{-}1) \qquad R = \begin{bmatrix} \sigma_{\delta x}^2 & \rho_{xy}\sigma_{\delta x}\sigma_{\delta y} & - & - & - & - \\ - & \sigma_{\delta y}^2 & - & - & - & - \\ - & - & \sigma_{\delta z}^2 & - & - & - \\ - & - & - & \sigma_{\delta \dot{x}}^2 & - & - \\ - & - & - & - & \sigma_{\delta \dot{y}}^2 & - \\ \rho_{x\dot{z}}\sigma_{\delta x}\sigma_{\delta \dot{z}} & - & - & - & - & \sigma_{\delta \dot{z}}^2 \end{bmatrix}$$

by the definition of the covariance matrix.

The variance of the position and velocity deviations from nominal in each coordinate are the components of the major diagonal of the R matrix. Since the rms position deviations, r are

$$r = \sqrt{\sigma_x^2 + \sigma_y^2 + \sigma_z^2}$$

and the rms velocity deviations, v are

$$v = \sqrt{\sigma_{\dot{x}}^2 + \sigma_{\dot{y}}^2 + \sigma_{\dot{z}}^2}$$

then, by partitioning R such that

$$R = \begin{bmatrix} R_1 & R_2 \\ R_3 & R_4 \end{bmatrix}$$

where the submatrices are 3 x 3's, then

$$r = \sqrt{Tr(R_1)}$$

(B-2)

$$v = \sqrt{Tr(R_4)}$$

where the notation Tr (trace) is the sum of the terms along the major diagonal of the matrix.

The errors in estimation may be treated similarly, and

$$\tilde{r} = \sqrt{Tr(P_1)}$$

(B-3)

$$\tilde{v} = \sqrt{Tr(P_4)}$$

where $\tilde{r}$ and $\tilde{v}$ are the rms values of the error in position and velocity estimate, respectively.

The above shows how the rms deviations and estimation may be obtained from the P and R matrices. What follows is the process by which these matrices, are developed for an ensemble of trajectories which include corrections. In addition, the development of u, which is required for propellant consumption considerations, is shown.

If no corrective maneuvers have been made over the interval (t_o, t_k), then R (t_k) as shown in eq. (8), section 4.3.1 is simply:

(B-4) $$R(t_k) = \Phi(t_k, t_o) P(t_o) \Phi^T(t_k, t_o)$$

From eq. (22), the P matrix over the same interval is calculated recursively as:

$$P(t_{k+1}) = \Phi(t_{k+1}, t_k)\left[P(t_k) - K(t_k)H(t_k)P(t_k)\right]\Phi^T(t_{k+1}, t_k) \tag{B-5}$$

where $K(t_k) = P(t_k)H^T(t_k)\left[H(t_k)P(t_k)H^T(t_k) + Q\right]^{-1}$

and $H(t_k) = \left[\frac{\partial f}{\partial x} \quad \frac{\partial f}{\partial y} \quad \frac{\partial f}{\partial z} \quad 0 \quad 0 \quad 0\right]$

These quantities are functions of P (t_o), Q and the reference trajectory from which the matrices Φ and H are developed. It was assumed in section 4.3.1, that on an actual flight this reference trajectory would be the estimated trajectory as calculated during the flight. Since this trajectory is random, it is not convenient to use as a reference for parametric analyses. Instead, the nominal trajectory will be used as a reference. Thus, integration of an actual trajectory need be performed only once. It has been shown that use of the nominal has little effect on the numerical calculations for deviations close to the nominal trajectory. In general, however, the calculation of the P matrices by this method will be slightly pessimistic.

When a correction has been made, the P matrix changes as shown in eq. (8) section 4.3.2:

$$P_c = \begin{bmatrix} P_1 & P_2 \\ P_3 & (P_4 + C) \end{bmatrix}$$

where P_1, P_2, etc. are 3 x 3 submatrices of P before the correction and C is the covariance matrix of the errors in measuring the ΔV applied.

The change in R when a correction is made is a little more complicated. It is shown in ref. 4-2 that after a correction has been made,

$$R_c = \left[I_{66} + G\right](R - P)\left[I_{66} + G\right]^T + P + S \tag{B-6}$$

where:

$$G = -\begin{bmatrix} O_{33} & O_{33} \\ A_2^{-1}A_1 & I_{33} \end{bmatrix} = \begin{bmatrix} O_{36} \\ G' \end{bmatrix} \tag{B-7}$$

and S is the covariance matrix of the errors in making the correction, e.g.

$$S = \begin{bmatrix} O_{33} & O_{33} \\ O_{33} & S' \end{bmatrix} \tag{B-8}$$

where:

$$S' = \frac{1}{4}\begin{bmatrix} \left[u^2(\sigma_\theta^2 + \sigma_\psi^2) + \sigma_u^2\right] & 0 & 0 \\ 0 & \left[u^2(\sigma_\theta^2 + \sigma_\psi^2) + \sigma_u^2\right] & 0 \\ 0 & 0 & 2\left[u(\sigma_\theta^2) + \sigma_u^2\right] \end{bmatrix} \tag{B-9}$$

where u^2 is the mean-squared value of the expected velocity correction:

$$u^2 = Tr\left[G'(R - P)G'^T\right] \tag{B-10}$$

and σ_θ, σ_ψ, and σ_u are the variances in the errors made in applying a thrust correction using azimuth, elevation and thrust magnitude.

The above formulation is not entirely adequate from a theoretical standpoint. For one thing, the derivation of S' assumes that corrections in any direction are equally likely which is not necessarily true. In addition, the derivation of R_c assumes that the correction errors are uncorrelated with the deviations from the nominal trajectory, but are functions of the correction magnitude. Since the correction magnitude is a function of the trajectory deviations, the above assumption is not necessarily valid.

However, since the only objection is to the deletion of certain small cross-correlation effects, and will have little effect on the overall system performance, the above formulation was used to calculate the change in the R matrix due to corrections and the quanitity u, the rms of the ΔV applied. For this study, it was assumed that there is no difference between the error in making the correction and the error in measuring it. A 3 x 3 diagonal matrix C was assumed to represent the errors in making the correction.

The quantities $\tilde{r}$, $\tilde{v}$, r, v, and u were used to evaluate the effect of changing the parameters Q, the instrument variance, C, the control accuracy, $P(t_o)$, the injection accuracy and the observation and correction schedule.

19.3 Appendix I-C: Literature Survey

A brief review of some of the important papers dealing with the topic of spacecraft guidance is given in this appendix.

Ref. 4-1. G.L. Smith, et al., NASA TR R-135

In this paper, a procedure is developed for statistically combining angle measurements onboard a space vehicle to make an optimum estimation of position and velocity. The physical model assumed is a vehicle on a 78-hour (to 4258-km perilune) circumlunar trajectory, making measurements of the azimuth, elevation and subtended angle of the earth or moon with respect to a stabilized platform. The estimation scheme is based on measurement of deviations from a reference trajectory. It was shown that the reference trajectory could be updated after each observation to obtain a better estimate, especially in abort situations.

Statistical analyses and simulations were run out to t = 2.4 hours and the effects of varying the angle measurement accuracy and the number of measurements were investigated. It was shown that, for small injection errors and a schedule of 20 measurements having uncorrelated errors of 20 seconds of arc RMS, the position and velocity uncertainties were reduced by a factor of about 7. For 200 secs. of arc RMS, the reduction is uncertainty was by a factor of 2. It was also shown that doubling the observation rate (39 measurements instead of 20) yielded a reduction of only 20% in reducing the position and velocity estimation errors.

The statistical methods employed in the estimation were shown to be equivalent to the Bayes estimation procedure employed by JPL, and superior to least squares smoothing of the measured data itself. Another important result was that measurements of the angle subtended by a planet were evidently ineffective in reducing the estimation uncertainties.

Ref. 4-2, G.L. Smith, et al. NASA TN D-1208

This paper is a continuation of the work started in ref. 4-1, above, where the optimization procedure has been applied to the entire circumlunar mission including the effects of 6 corrections (3 out-bound).

Statistical data is developed for the ensembles of flights having the following things in common: injection errors, correction schedule and accuracy, observation schedule and accuracy. The standard case had rms injection errors of 1 km and 1 m/s in position and velocity respectively, rms measurement errors of 10 secs of arc and rms correction accuracy of .1 m/s in magnitude and 0.5° in angle, and a total of 844 observations for the circumlunar flight. This standard case gave results at perilune as follows: rms position and velocity deviations from the nominal trajectory at the predicted time of arrival were 4.8 km and 1.2 m/s and rms position and velocity estimation errors were 0.8 km and 0.08 m/s, and total ΔV (for corrections) = 9.9 m/s. The rms miss distance at the moon was 1.7 km.

In addition to the standard case above, variations in the parameters were made in order to determine their effects. These variations are summarized as follows:

(1) Making perfect velocity corrections resulted in some improvement of the miss distance (from 1.7 km to .7 km), but overall system performance is not greatly effected by errors of the magnitude assumed in the standard case.

(2) Increasing the measurement error by a factor of 5 resulted in an increase in position and velocity deviation from nominal by a factor of 3, and an increase in estimation errors by a factor of 5. As expected, measurement accuracy is a critical system parameter.

(3) Increasing the injection errors by a factor of 5 caused a significant increase only in the ΔV consumed, primarily due to the large first correction. Evidently then, injection errors are not a critical factor in determining midcourse sensor requirements.

(4) Decreasing the total observations from 844 to 77 (39 outbound) only doubles the deviations from nominal and trebles the estimation errors. Since the resulting deviations and estimation errors are still small, this indicates that the 77 observations is much closer to an "optimum" number when one considers the cost of making the observations.

The results at perigee (re-entry into the earth's atmosphere) are poorer than at perilune due to the much higher velocities approaching the earth. However, the accuracy requirements on earth re-entry are not as severe since the atmosphere affords the vehicle the possibility of maneuvering to a landing.

Although some assumptions made in this report would not be applicable to a manned lunar mission, the utility of this type of estimation and guidance system is demonstrated. In addition, the report presents a convenient method of performing statistical analyses on lunar trajectories without resorting to Monte Carlo methods. The method developed in this reference was the basis for the digital program used in this midcourse study at Air Arm.

Ref. 4-3, R.H. Battin, ARS 2461-62

In this paper, statistical methods are developed for estimating position and velocity onboard a spacecraft from measurement of angles between celestial objects. Although the methods used in this paper and Refs. 4-1 and 4-2 are similar, there are several important differences:

(1) In 4-2, a pre-set observation and correction schedule was employed. In this paper, a number of "decision points" were preset, at which it was determined whether to make a correction, observation or to do nothing. One set of decision rules, were that the ratio of the indicated velocity correction to the uncertainty in the estimate must be greater than some R_v^2 to make a correction, and that the ratio of the reduction in position uncertainty at the target with the best measurement to the uncertainty without this measurement be greater than some R_p^2. Computer runs employing several values of R_p and R_v were made.

(2) A mathematical derivation of cross-correlation effects between measurement errors was made. However, this effect was not incorporated in the numerical data.

(3) A mathematical derivation of the optimum plane in which to make a measurement was made.

(4) In Ref. 4-2, the observables employed consisted of elevation angle, azimuth angle and subtended angle to the earth or moon from some stabilized coordinate system. This suggests the use of a theodolite-type instrument. In Battin's work, each observation consisted of a single angle measurement such as would be obtained by a sextant-type device. Although comparison of the numerical results obtained in 4-2 and 4-3 is difficult due to the different nominal trajectories employed, it appears that the results obtained by measuring just one angle at a time are comparable with the results obtained in 4-2.

Ref. 4. Working Papers, Ames Research Center

During the course of this study, a group of working papers written at Ames Research Center were received. These papers report on the work done at Ames to use the methods described in ref. 4-2 to determine optimum measurements and correction schedules. Some of the important results are summarized here:

(1) The approach to optimum scheduling used in ref. 4-3 is not an optimum method of reducing target errors since that method made decisions (to observe or correct the trajectory) based only on what has taken place in the past. This was shown by employing a decision criterion similar to that used by Battin, developing a schedule, and then showing that the schedule could be improved by changing one of the observations. The conclusion is that any optimizing scheme must include the effects of the entire correction-observation schedule to correctly assess the worth of any single action.

(2) Since it seemed impractical to develop an analytical method of optimum scheduling, a cut-and-try technique was employed utilizing the criteria of (1) minimum number of operations, (2) minimum correction ΔV expenditure and (3) achievement of accuracy requirements. Schedules were written using these criteria and the primary improvement was in the correction ΔV consumed. In general, system accuracy performance was not greatly affected by scheduling but is essentially a function of the total number of observations made.

(3) Comparison of system performance for 3-angle, 2-angle (theodolite) and 1-angle (sextant) observations were made. The comparison of the 3-angle and 2-angle observation runs confirmed that measurement of the subtended angle of a planet contributes little information. This measurement is useful only in the immediate vicinity of the planet, where the measured angle is large. The single-angle runs were made using a ratio of 5 right ascension measurements to one declination angle measurement. Comparison of the theodolite and sextant-type observations shows only a slight gain in performance by using the theodolite, even though 2 angles are measured rather than one. Also, the choice of the stars from which the angles are measured has a definite effect on system performance.

(4) A comparison of the schedule chosen at Ames for a 100-nm perilune flight with that used by Battin in ref. 4-3 was made. The results were inconclusive due to differences in the trajectory and the assumptions on errors, but in general it was shown that the MIT schedule could be improved upon slightly.

Ref. 5. R. Kalman, Journal of Basic Engineering, 1960

In this paper, the Wiener filtering problem is solved, using state-transition concepts of modern control theory. The mathematical results obtained were used in Ref. 4-1 to solve the problem of making an optimal estimate of the position and velocity of a space vehicle from noisy measurement data.

This page intentionally left blank

20.0 Appendix II: Lunar Parking and Descent Orbits

The following is a set of derivations which form the mathematical basis of all numerical results, conclusions, and recommendations listed in Section 5. This presentation is divided into analysis of

- Nominal orbits
- On-board navigation
- Linear prediction
- Guidance logic
- Typical values of input errors

Throughout the analysis, the concept of a six dimensional state vector is used, in which the first three components represent x, y, and z position co-ordinates, and the last three components represent velocity.

20.1 Determination of Nominal Orbits

The following equations for an elliptical orbit were taken directly from Reference 5-5.

For position at time (t_k), $1 \leqslant j \leqslant 3$

$$X_{kj} = \left[1 - \frac{a}{r_o}(1 - \cos \nu_K)\right] X_{oj} + \left[(t_k - t_o) - \frac{a^{3/2}}{\sqrt{\mu}}(\nu_K - \sin \nu_K)\right] X_{o,\, j+3} \qquad (20\text{-}1)$$

and the magnitude of the radius vector is

$$r_k = a(1 - \cos \nu_K) + r_o \cos \nu_K + d_o \sqrt{\frac{a}{\mu}} \sin \nu_K \qquad (20\text{-}2)$$

For velocity, $4 \leqslant j \leqslant 6$

$$X_{kj} = \left[- \frac{\sqrt{\mu a}}{r_k \, r_o} \sin \nu_K \right] X_{o,\, j-3} + \left[1 - \frac{a}{r_k} \left(1 - \cos \nu_K\right) \right] X_{oj} \tag{20-3}$$

With the nominal parking orbit defined by two noncollinear vectors,

$$R_o = \begin{vmatrix} r_o \cos \lambda_o \cos \psi_o \\ r_o \cos \lambda_o \sin \psi_o \\ r_o \sin \lambda_o \end{vmatrix} \tag{20-4}$$

$$R_p = \begin{vmatrix} r_p \cos \lambda_p \cos \psi_p \\ r_p \cos \lambda_p \sin \psi_p \\ r_p \sin \lambda_p \end{vmatrix} \tag{20-5}$$

of equal magnitude,

$$r_o = r_p = a \tag{20-6}$$

The period of the circular orbit is

$$T = \frac{2\pi a^{3/2}}{\sqrt{\mu}} \tag{20-7}$$

With the vector (R_p) as the orbital plane reference,

$$E_p = 0 \tag{20-8}$$

and the eccentric anomaly at time (t_o) is

$$E_o = \theta_o = \left\{ \operatorname{sgn} (\theta_o) \right\} \operatorname{Arc} \cos \left\{ \frac{1}{a^2} \left(R_o \cdot R_p\right) \right\} \tag{20-9}$$

This defines the quadrant of the angle, when the inverse cosine function is defined as the principal value, less than (π) radians in absolute value.

It is seen from Figure 5-2 that (E_o) is, in this case, positive and equal to ($\pi - \psi_p$). With the injection point as the reference in the orbital plane,

$$\nu_o = 0 \tag{20-10}$$

the incremental eccentric anomaly separating (t_o) and (t_p) is

$$\nu_p = 2\pi - E_o \tag{20-11}$$

for a retrograde orbit.

The fraction of a period separating the two vectors is merely ($\nu_p / 2\pi$). Finally, the radius vector is always normal to the velocity vector in a circular orbit, so that

$$d_o = 0. \tag{20-12}$$

All of the necessary quantities are now available for computation of the initial velocity vector (V_o). This completes the geometric definition of the parking orbit.

In order to provide an automatic rendezvous capability in the event that no landing is made after descent, the descent orbit period is chosen equal to the period of the circular orbit. It follows that

$$a_d = a \tag{20-13}$$

The eccentricity of the descent orbit is

$$e_d = 1 - \frac{p}{a_d} \tag{20-14}$$

The eccentric anomaly of the descent arc (E_F) must be ninety degrees, in order for equation (20-13) to hold. From the well known relation

$$\sin \theta_F = \frac{\sqrt{1 - e_d^2} \sin E_F}{1 - e_d \cos E_F} \tag{20-15}$$

plus the fact that the true anomaly separating (t_F) and (t_L) of Figure 5-2 is the same for the circular and elliptical orbits,

$$\sin \theta_E = \sqrt{1 - e_d^2} \tag{20-16}$$

Since the true anomaly is never less than the corresponding eccentric anomaly, and (t_E) lags (t_L), the principal value of (θ_E) is negative and greater than ($\pi/2$) radians in absolute value. The eccentric anomaly of the descent arc, as measured on the circular orbit, is simply

$$E_E = \theta_E \tag{20-17}$$

Since descent is initiated on the second revolution, the incremental eccentric anomaly at descent time is

$$\nu_E = 2\pi + \left\{ \text{principal value of } (E_E - E_o) \right\}$$

In this case, E_E is negative and E_o is positive; the value of (ν_E) comes out to be

$$\nu_E = 4\pi - \left| E_E \right| - E_o \tag{20-19}$$

Since this is measured along the circular orbit, the time interval separating (t_o) and (t_E) is

$$t_E - t_o = \frac{\nu_E}{2\pi}(T) \tag{20-20}$$

By substituting the subscript (E) for (K) in equation (20-1) the position vector ($R_E = R_F$) at descent initiation can now be computed.

Now with (t_F) as the reference initial point of the descent orbit,

$$\nu_F = 0 \quad . \tag{20-21}$$

so that the incremental eccentric anomaly at time (t_L) is

$$\nu_L = - E_F \tag{20-22}$$

The descent time can be computed from Kepler's second law,

$$t_L - t_F = \frac{a_d^{3/2}}{\sqrt{\mu}} \left\{ \left| E_F \right| - e_d \sin \left| E_F \right| \right\} \tag{20-23}$$

Finally, with

$$r_F = a = a_d \tag{20-24}$$

the velocity vector at time (t_F) can be computed from equation (20-3):

$$X_{F,j+3} = \frac{X_{Lj} - (\cos \nu_L) \; X_{Fj}}{(t_L - t_F) - \frac{(a_d)^{3/2}}{\sqrt{\mu}} \; (\nu_L - \sin \nu_L)} \tag{20-25}$$

in which the position vector (R_L) is the nominal perilune radius vector,

$$\begin{vmatrix} X_{L1} \\ X_{L2} \\ X_{L3} \end{vmatrix} = \begin{vmatrix} r_L \cos \lambda_p \cos \psi_p \\ r_L \cos \lambda_p \sin \psi_p \\ r_L \sin \lambda_p \end{vmatrix} \tag{20-26}$$

For use in transition matrix computation, magnitudes of radius vectors, velocity vectors, and their dot products are always computed from the same simple expressions:

$$r_K = \sqrt{(X_{K1})^2 + (X_{K2})^2 + (X_{K3})^2} \tag{20-27}$$

$$v_K = \sqrt{(X_{K4})^2 + (X_{K5})^2 + (X_{K6})^2} \tag{20-28}$$

$$d_K = R_K \cdot V_K \tag{20-29}$$

The nominal perigee velocity vector is readily computed from equation (20-3) with the subscripts (K) and (O) replaced by (L) and (F), respectively, and (a) replaced by (a_d).

The nominal velocity impulses are merely the vector differences between velocities before and after thrust application. Since injection into the parking orbit is assumed impulsive and tangential,

$$X_{Aj} = X_{oj}, \qquad 1 \leqslant j \leqslant 3 \tag{20-30}$$

$$X_{Aj} = (v_{A/v_o})\ X_{oj}, \qquad 4 \leqslant j \leqslant 6 \tag{20-31}$$

A typical speed of 2400 meters/sec. is assumed for (v_A), and

$$F_{Aj} = X_{o,j+3} - X_{A,j+3} \tag{20-32}$$

Similarly,

$$F_{Ej} = X_{F,j+3} - X_{E,j+3} \tag{20-33}$$

in which the velocity vector at (t_F) is computed from equation (20-25) and the velocity vector at (t_E) follows from equation (20-3) with the subscript (K) replaced by (E).

20.2 On-Board Navigation Technique

As explained in the Part I (Problem Definition) document, the basic observable chosen for navigation is the angle between a known star and landmark. The measurement analysis is then associated with the computation of three vectors at each measurement time. With the moon center again taken as the coordinate

system reference, these are

- the instantaneous radius vector (R_m) to the vehicle at the time (t_m), of the (m^{th}) measurement,
- the vector L_m terminating on the (m^{th}) landmark,
- a vector Q_m of length (q) in the direction of the (m^{th}) star sightline.

The position vector (R_m) is computed at each measurement time from equation (20-1). The vectors L_m and Q_m are chosen by an error minimization technique to be described in Section 20.3.3.

The sightline vector from the vehicle to the landmark is simply ($L_m - R_m$); its magnitude follows from the cosine law,

$$\left| L_m - R_m \right| = \sqrt{l_m^2 + r_m^2 - 2\, L_m \bullet R_m} \tag{20-34}$$

With the measured angle labeled as ($\mathcal{X}$) it is clear that

$$Q_m \bullet (L_m - R_m) = q \sqrt{l_m^2 + r_m^2 - 2\, L_m \bullet R_m} \cos \mathcal{X}_m \tag{20-35}$$

or

$$\mathcal{X}_m = \text{Arc cos} \left\{ \frac{Q_m \bullet L_m - Q_m \bullet R_m}{q \sqrt{l_m^2 + r_m^2 - 2\, L_m \bullet R_m}} \right\} \tag{20-36}$$

Since the basic data reduction technique is differential correction, a quantity of fundamental importance is the partial derivative of this angle w.r.t. each component of the vehicle state. This is easily seen to be

$$\frac{\partial \mathcal{X}_m}{\partial X_{mi}} = h_{mi} = \tag{20-37}$$

$$\frac{\csc \mathcal{X}_m}{q} \left\{ \frac{(l_m^2 + r_m^2 - 2\, L_m \bullet R_m) q_{mi} + (Q_m \bullet L_m - Q_m \bullet R_m)(X_{mi} - l_{mi})}{(l_m^2 + r_m^2 - 2\, L_m \bullet R_m)^{3/2}} \right\},$$

$1 \leq i \leq 3$.

$$h_{mi} = 0, \qquad 4 \leqslant i \leqslant 6 \tag{20-38}$$

Inherent in the already mentioned differential correction computation is the assumption that, when the vehicle deviates from its reference state, the resulting angle deviation is

$$\xi_m = H_m \; x_m \tag{20-39}$$

in which (H_m) is the row vector composed of the six previously defined partial derivatives. In the on-board system, of course, it is the angles that are known, and the state vector deviation is to be computed. Thus it is necessary to invert* the linearized computation; there are, consequently, not one but two necessary conditions for successful navigation by the linear scheme. Qualitatively, these are:

- The vehicle must be sufficiently close to its reference state, so that equation (20-39) is accurate.
- It must be possible to obtain an accurate inversion.

Unfortunately, satisfaction of the first requirement does not at all guarantee the second. It is absolutely necessary, therefore, to condition the measurements** to whatever extent possible, for accurate reduction capability. A discussion of this technique must follow the description of the estimation scheme.

---

* The method of estimating the state vector deviation is discussed in Section 20.3

**Specification of measurements is less stringent when the reference is not a single star, but an on-board inertial coordinate system. The conditioning problem is not even mentioned in ref. 5-6. Therefore, the seemingly stringent demands made upon availability of stars is comparatively insignificant in the true mechanization. Availability of landmarks, however, will pose a problem if landmarks are the only observables - see section 5.9.

20.3 On-Board Linear Prediction

This section contains a resume of the statistical filter theory equations associated with the prescribed on-board data processor. Most of the equations have been extracted directly from the literature.

20.3.1 Linearized State Transition

Throughout the orbital flight, the on-board system operates on the assumption that deviations in state can be linearly translated in time, i.e.,

$$x_k = \Phi\,(t_k, t_o)\, x_o \tag{20-40}$$

This is also representative of a differential correction procedure, in which the general term in the state transition matrix,

$$\varphi_{kij} = \frac{\partial X_{ki}}{\partial X_{oj}} \tag{20-41}$$

can be found by differentiating a modified form of equations (20-1) - (20-3). Every symbol in these equations is first replaced by its equivalent, expressed in terms of the initial state vector components, e.g.,

$$r_o = \sqrt{(X_{01})^2 + (X_{02})^2 + (X_{03})^2}\ ; \tag{20-42}$$

$$d_o = X_{01}\,X_{04} + X_{02}\,X_{05} + X_{03}\,X_{06}\ ; \tag{20-43}$$

$$a = \frac{\sqrt{X_{01}^2 + X_{02}^2 + X_{03}^2}\ \mu}{2\mu - (X_{04}^2 + X_{05}^2 + X_{06}^2)\sqrt{X_{01}^2 + X_{02}^2 + X_{03}^2}} \tag{20-44}$$

By the method suggested here, derivation of the state transition matrix is perhaps tedious but perfectly straightforward.

20.3.2 Statistical Filter Equations

The equations in this section were taken from references 5-2 and 5-3.

A combination of equations (20-39) and (20-40) provides a method for predicting the deviation (ξ_m) of a measured angle ($\hat{\mathcal{X}}_m$) from its nominal value ($\mathcal{X}_m$), by using its estimated state deviation ($\hat{x}$) at some previous time (t_{m-1}):

$$\xi_m \doteq H_m \Phi (t_m, t_{m-1}) \hat{x}_{m-1} = B_m \hat{x}_{m-1} \qquad (20\text{-}45)$$

If then, the observed deviation from the nominal angle is

$$(\mathcal{X}'_m - \mathcal{X}_m) - \tilde{\xi}_m \qquad (20\text{-}46)$$

then the deviation of the observation from its predicted value is

$$\hat{\xi}_m = \left[(\mathcal{X}'_m - \mathcal{X}_m) - \tilde{\xi}_m\right] - \left[B_m \hat{x}_{m-1}\right] \qquad (20\text{-}47)$$

This is weighted by Kalman's optimum weighting factor, K_m (ref. 5-1), to produce a revised state estimate after each measurement,

$$\hat{x}_m = \Phi (t_m, t_{m-1}) \hat{x}_{m-1} + K_m \hat{\xi}_m \qquad (20\text{-}48)$$

The error in this estimate,

$$\tilde{x}_m = x_m - \hat{x}_m \qquad (20\text{-}49)$$

has a covariance matrix given by

$$P_m = \Phi (t_m, t_{m-1}) \left[P_{m-1} - K_{m-1} H_{m-1} P_{m-1}\right] \Phi^T (t_m, t_{m-1}) \qquad (20\text{-}50)$$

and the optimum weighting factor is computed as,

$$K_m = P_m H_m^T \left[H_m P_m H_m^T + \Gamma\right]^{-1} \qquad (20\text{-}51)$$

Although (Γ) is defined as a covariance matrix, in this analysis it is a constant scalar, i.e., the variance of the measurement error. The H-matrix is merely a row vector, and it is seen that the bracketed quantity in equation (20-51) is merely a scalar. The weighting factor, of course, is a six-dimensional column vector.

A starter for the recursive (P) matrix computation is provided by the covariance matrices of initial uncertainties:

$$P_o = \begin{vmatrix} \Gamma_3 & 0 \\ 0 & \Gamma_4 + \Gamma_6 \end{vmatrix} \qquad (20\text{-}52)$$

Since no measurement is taken exactly at injection time, the initial weighting vector is

$$K_o = 0 \qquad (20\text{-}53)$$

20.3.3 Data Conditioning

The weighting vector (K) may be though of loosely as an "error distributor" which attributes the measurement deviation to each possible cause, according to (1) the a priori sensitivity of the measurement to that cause, and (2) the theoretical capability of the weighted increment (equation 20-48) to reduce the rms uncertainty in the estimate. In the star-landmark observation considered here, for example, the angle is independent of position deviations parallel to the vehicle-landmark sightline. It is most sensitive to errors in the direction of the star, and comparatively insensitive to errors normal to the plane of the angle.* It follows that a measurement would be futile if

* If the star sightline is perpendicular to the vehicle-landmark sightline, the angle is independent of errors in this direction also.

the star were in the direction of the smallest error and the landmark were chosen so that its sightline were parallel to the largest error.

The ideal measurement for minimization of position uncertainty (reference 5-4) can now be made clear. With the covariance matrix of the estimation error partitioned into (3 x 3) submatrices,

$$\begin{vmatrix} P_m^{(1)} & P_m^{(2)} \\ P_m^{(3)} & P_m^{(4)} \end{vmatrix}$$

the optimum measurement at time (t_m) is found as follows:

- Diagonalize the upper left submatrix $P_m^{(1)}$ and extract the unit eigenvector (U_m) corresponding to the largest eigenvalue.
- Choose the star sightline parallel to (U_m).
- Choose the vehicle-landmark sightline normal to (U_m)*

Unfortunately, it is not always possible to fulfill the above requirements (e.g., if U_m is radial, the landmark would have to lie in a horizontal direction). Furthermore, it becomes increasingly more difficult to fulfil the requirements as the landmark is chosen closer to the vertical. It is desirable, therefore, to choose the landmark as close to the horizon as possible, without impairing its visibility. At a 200 KM altitude, a downlook angle of 30° off horizontal was chosen for this analysis. This corresponds to a radial angle (α_L) of 15° at the moon center (see section 5.3.2.2.).

The desired landmark vector is found from the solution of the vector equations which arise from the optimization criteria, its angle off vertical, and

*This is the geometric equivalent to Battin's statement that the "measurement geometry vector" should coincide with the eigenvector.

its known length:

$$(L_m - R_m) \cdot U_m = 0 \tag{20-54}$$

$$L_m \cdot \rho_m = \ell_m \cos \alpha_L \tag{20-55}$$

$$L_m \cdot L_m = \ell_m^2 \tag{20-56}$$

or

$$L_m \cdot U_m = \beta_1 \ell_m \tag{20-57}$$

$$L_m \cdot \rho_m = \beta_2 \ell_m \tag{20-58}$$

a solution exists if the quantity*

$$y^2 = 1 - (\beta_1^2 + \beta_2^2 + \beta_3^2) + 2\,\beta_1 \beta_2 \beta_3 \tag{20-59}$$

is positive; when this is the case,

$$L_m = \ell_m \left\{ \frac{(\beta_1 - \beta_2 \beta_3) U_m + (\beta_2 - \beta_1 \beta_3) \rho_m \pm y (U_m \times \rho_m)}{1 - \beta_3^2} \right\} \tag{20-60}$$

When (y^2) is negative, a test is made to see whether the second largest eigenvalue of $P_m^{(1)}$ is half as large as the first. If so, the original eignevector is replaced by the second. If this fails, a landmark is chosen as close as possible to the desired position, with its angle off vertical held fixed:

$$L_m = \ell_m \left\{ \left(\beta_2 - \beta_3 \sqrt{\frac{1-\beta_2^2}{1-\beta_3^2}} \right) \rho_m + \sqrt{\frac{1-\beta_2^2}{1-\beta_3^2}}\, U_m \right\} \tag{20-61}$$

* β_3 is defined as the dot product $U_m \cdot \rho_m$.

With the above optimization included in the analysis, computation of the navigation quantities must be carried out in the following order:

- P_o and Γ are given (Section 20.3.2).
- P_1 can be computed from equation (20-50) with (K_o) set to zero.
- With P_1 known, L_1 and Q_1 can be determined as previously explained.
- $\mathcal{X}_1$, H_1, and B_1 follow in order.
- K_1 is computed from equation (20-51).
- P_2 is determined from equation (20-50). This begins the second set of navigation quantities; the computation continues in the same order.

20.4 Linearized Dynamic Equations

The fixed time-of-arrival, end point guidance law described in references 5-2 and 5-3 has been adopted for this study. The equations presented here can be found in these references also.

20.4.1 The Guidance Law

With a state deviation of (x_o) at injection, equation (20-40) gives the estimated deviation at time (t_E):

$$x_E = \Phi\,(t_E,\, t_o)\, x_o \tag{20-62}$$

which can be partitioned as

$$\begin{vmatrix} \Delta r_E \\ \Delta V_E \end{vmatrix} = \begin{vmatrix} \Phi_E^{(1)} & \Phi_E^{(2)} \\ \Phi_E^{(3)} & \Phi_E^{(4)} \end{vmatrix} \begin{vmatrix} \Delta r_o \\ \Delta V_o \end{vmatrix} \tag{20-63}$$

The position deviation at time (t_E) can be brought to zero by supplying an impulse (f_o) such that

$$\begin{vmatrix} 0 \\ \Delta V_E \end{vmatrix} \quad \begin{vmatrix} \Phi_E^{(1)} & \Phi_E^{(2)} \\ \Phi_E^{(3)} & \Phi_E^{(4)} \end{vmatrix} \begin{vmatrix} \Delta r_0 \\ \Delta V_0 + f_0 \end{vmatrix} \tag{20-64}$$

or

$$\Phi_E^{(1)} \Delta r_0 + \Phi_E^{(2)} (\Delta V_0 + f_0) = 0 \quad ; \tag{20-65}$$

$$f_0 = -\left[\Phi_E^{(2)}\right]^{-1} \Phi_E^{(1)} \Delta r_0 - \Delta V_0 \quad . \tag{20-66}$$

This last equation is partitioned as

$$f_0 = -\left(\left[\Phi_E^{(2)}\right]^{-1} \Phi_E^{(1)} \quad I\right) \chi_0 = G_A \chi_0 . \tag{20-67}$$

It follows that, for an observed state deviation of $\hat{x}_A$ at arrival from midcourse, the deviation from the nominal injection command as indicated by the on-board computer will be

$$\hat{f}_A = G_A \hat{\chi}_A \tag{20-68}$$

Similarly, the indicated deviation from nominal descent impulse will be

$$\hat{f}_E = G_E \hat{x}_E \tag{20-69}$$

in which (G_E) is constructed from the state transition matrix $\left[\Phi(t_L, t_F)\right]$, exactly in the manner described above.

20.4.2 Computation of Extrapolated Covariance Matrices

The error in the estimated state after injection was already given in equation (20-52). The same reasoning applies to the covariance matrix of the estimation error at time (t_F):

The matrix (P_M), computed recursively from equation (20-50) is readily transformed to the end of the circular orbit by

$$P_E = \Phi\,(t_E,\ t_M)\ \ P_M\ \Phi^T(t_E,\ t_M), \qquad (20\text{-}70)$$

and the uncertainty after descent initiation is found simply by adding the appropriate thrust measurement error,

$$P_F = P_E + \begin{vmatrix} 0 & 0 \\ 0 & \Gamma_8 \end{vmatrix} \qquad (20\text{-}71)$$

The actual deviation in state after injection is simply

$$x_o = x_A + G_A\,\hat{x}_A - C_A \qquad (20\text{-}72)$$

where (C_A) is the random error in velocity impulse application. Equation (20-72) is more conveniently written as

$$\begin{aligned} x_o &= x_A + G_A\,(x_A - \tilde{x}_A) - C_A\ ; \\ x_o &= (G_A + I)\ x_A - G_A\,\tilde{x}_A - C_A \end{aligned} \qquad (20\text{-}73)$$

The equivalent covariance quality is

$$\begin{aligned} N_o = {} & (G_A + I)\ N_A\ (G_A + I)^T - (G_A + I)\ \mathrm{cov}\ (x_A,\ \tilde{x}_A)\ G_A^T \\ & - G_A\ \mathrm{cov}\ (x_A,\ \tilde{x}_A)\ (G_A + I)^T + G_A\ P_A\ G_A^T + S_A \end{aligned} \qquad (20\text{-}74)$$

Since*

$$\text{cov}\,(x_A, \tilde{x}_A) = \text{cov}\left\{ (\hat{x}_A + \tilde{x}_A), \tilde{x}_A \right\} = 0 + P_A, \tag{20-75}$$

equation (20-74) can be rearranged to read

$$N_o = (G_A + I)\ (N_A - P_A)\ (G_A + I)^T + P_A + S_A \tag{20-76}$$

The covariance matrix (S_A) consists only of error in the applied velocity impulse;

$$S_A = \begin{vmatrix} 0 & 0 \\ 0 & \Gamma_5 \end{vmatrix} \tag{20-77}$$

By an identical derivation

$$N_F = (G_E + I)\ (N_E - P_E)\ (G_E + I)^T + P_E + \begin{vmatrix} 0 & 0 \\ 0 & \Gamma_7 \end{vmatrix} \tag{20-78}$$

As always, the covariance matrices of the deviations (N_F) and uncertainties (P_F) are transformed into corresponding perilune errors through premultiplication by the transition matrix $\left[\Phi\ (t_L, t_F)\right]$ and postmultiplication by its transpose. The resulting matrices are partitioned,

$$N_L = \begin{vmatrix} N_L^{(1)} & N_L^{(2)} \\ N_L^{(3)} & N_L^{(4)} \end{vmatrix} \tag{20-79}$$

$$P_L = \begin{vmatrix} P_L^{(1)} & P_L^{(2)} \\ P_L^{(3)} & P_L^{(4)} \end{vmatrix} \tag{20-80}$$

* It is a basic characteristic of the optimum linear system that the error in the estimated state is uncorrelated with the estimated state deviation.

and the perilune errors are transformed into a coordinate system of three orthogonal vectors in the directions of

- nominal perilune radius vector
- nominal perilune velocity vector
- transverse perilune vector

by means of the matrix

$$W = \begin{vmatrix} \frac{1}{v_L} X_{L4} & \frac{1}{v_L} X_{L5} & \frac{1}{v_L} X_{L6} \\ \frac{1}{r_L} X_{L1} & \frac{1}{r_L} X_{L2} & \frac{1}{r_L} X_{L3} \\ \frac{1}{r_L v_L} (I \times V_L \cdot R_L) & \frac{1}{r_L v_L} (J \times V_L \cdot R_L) & \frac{1}{r_L v_L} (K \times V_L \cdot R_L) \end{vmatrix} \qquad (20\text{-}81)$$

where I, J, and K represent unit vectors in the x, y, and z directions, respectively.

20.5 Typical Input Error Magnitudes

20.5.1 Thrust Tolerances

With three independent and orthogonal thrust error components of zero mean and equal variance, the total rms thrust error is:

$$\sqrt{3}\ \sigma_T \qquad (20\text{-}82)$$

where σ_T is the rms thrust error in each axis. This applies to both thrust application and thrust measurement.

Although the velocity increments are assumed impulsive for the analysis, typical error figures should be derived on the basis of finite pulse width. At injection, the total impulse is;

$$v_A - \sqrt{\frac{\mu}{a}} = 2400 - 1589 = 811 \text{ meters/sec.} \qquad (20\text{-}83)$$

This is equivalent to a time-acceleration product of (82.8) earth g's, corresponding to (13.8) g's for 6 seconds in the allowable acceleration limit (ref. 5-11). At half thrust for twice as long an interval, the acceleration is essentially 7 g's for 12 seconds. The linearity error in an accelerometer is the predominant factor at this g-level; a reasonable estimate of total thrust measurement error at injection is

$$\frac{10^{-5}\ \text{g's}}{\text{g}} \times 7\text{g} \times 12\ \text{sec.} = 0.00825\ \text{meters/sec.} \qquad (20\text{-}84)$$

or an rms error in each axis of

$$\frac{0.00825}{\sqrt{3}} \doteq 0.005\ \text{meter/sec.} \qquad (20\text{-}85)$$

Descent thrust pulse width is not as readily fixed by obvious considerations, and no detailed attention has been devoted to descent mechanization. As an expedient, the rms impulse measurement errors have been assumed equal for descent and injection into the parking orbit.

For control of applied thrust, the errors are not expected to be so small. One per cent of the applied impulse is a reasonable estimate of rms application error. For injection, then, the rms error in each axis is typically

$$\frac{(0.01)\ (811)}{\sqrt{3}} \doteq 5\ \text{meters/sec.} \qquad (20\text{-}86)$$

For descent, the total nominal impulse is 150 meters per second; rms error for each axis in applying the descent impulse is typically

$$\frac{(0.01)\ (150)}{\sqrt{3}} \doteq 1\ \text{meter/sec.} \qquad (20\text{-}87)$$

20.5.2 Measurement Errors

The two sources of error considered are landmark uncertainties and instrument readability. They can be lumped together for analysis.

It is convenient to consider the landmark uncertainty as a vector with independent components in the following three directions:

- along the sightline from the vehicle to the landmark
- along the star sightline vector.
- along the vector cross product of the above vectors.

The first component cannot contribute any error, since it does not affect the angle to be measured. It is also readily shown that, when the star sightline is normal to the sightline from the vehicle to the landmark, the last component cannot contribute any error to the measurement. It was explained in Section 20.3.3. that these sightlines are chosen perpendicular for optimum data conditioning. Therefore, only one component of the landmark uncertainty vector affects the measurement; if the total rms landmark uncertainty is (σ_s) kilometers, the rms error introduced into the measurement is

$$\left(\frac{\sigma_s}{\sqrt{3}}\right) \div \text{(distance from vehicle to landmark)}$$

For an altitude of 200 KM, and a value of fifteen degrees for (α_L), this corresponds to roughly one milliradian per kilometer uncertainty. Since the instrument error is independent of landmark error, the total rms error per measurement is

$$\sqrt{(0.001\ \sigma_s)^2 + \sigma_m^2}$$

where (σ_m) is the standard deviation of the instrument error.

20.5.3 Initial Conditions

The following rms errors at midcourse termination were taken from the NASA standard trajectory of Reference 5-3.

- Position deviation 4.8 KM
- Position uncertainty 0.8 KM
- Velocity deviation 1.2 m/sec.
- Velocity uncertainty 0.08 m/sec.

Actually, rms errors of these magnitudes were assumed for each axis in this study, due to the larger errors found in the higher energy trajectory of Section 4, of this report.

This page intentionally left blank

21.0 Appendix III: Lunar Descent Trajectory

21.1 Appendix III-A: Guidance Law Derivation

The guidance terms are derived by following the procedure of reference 21-1. As discussed in the text of this report, (Section 6.3.1), time is retained as the independent variable. The following presentation carries through to completion the derivation of guidance terms S_1 through S_8 with time as the independent variable. In the Ames report used as a basis for this work, time has been dropped in favor of a velocity dependent system. The nomenclature of reference 21-1 has been retained for the most part.

The applicable equations of motion are:

$$\dot{h} = V \sin \gamma \tag{21-1a}$$

$$\dot{\theta} = \frac{-V \cos \gamma}{r_o + h} \tag{21-1b}$$

$$\dot{\gamma} = \frac{V \cos \gamma}{r_o + h} - \frac{T \sin \alpha}{m V} - \frac{\mu \cos \gamma}{V(r_o + h)^2} \tag{21-1c}$$

$$\dot{V} = -\frac{T \cos \alpha}{m} - \frac{\mu \sin \gamma}{(r_o + h)^2} \tag{21-1d}$$

Where:

$V \equiv$ magnitude of the velocity vector

$r_o \equiv$ radius of reference sphere

$T \equiv$ magnitude of applied thrust vector

$m \equiv$ mass of landing vehicle

$\mu \equiv$ lunar gravitational constant

and the remaining parameters are defined by figure 21-1. For a constant thrust, gravity turn trajectory,

$$T = To = \text{a constant}$$

and

$$\alpha = 0$$

on the nominal trajectory.

The perturbation equations relating deviations in the dynamic state variable derivatives to deviations in state variables and thrust control quantities, in matrix form, are:

$$\left[\delta \dot{\xi}\right] \doteq \left[\frac{\partial \dot{\xi}_i}{\partial \xi_j}\right]\left[\delta \xi_j\right] + \left[\frac{\partial \dot{\xi}_i}{\partial \nu_j}\right]\left[\delta \nu_j\right] \qquad (21\text{-}2)$$

For ease of handling, the state variables and control quantities have been redefined:

$$\dot{\xi}_i \equiv (\dot{h})_{i=1} \quad ; \quad (\dot{\theta})_{i=2} \quad ; \quad (\dot{\gamma})_{i=3} \quad ; \quad (\dot{V})_{i=4}$$

$$\xi_j \equiv (h)_{j=1} \quad ; \quad (\theta)_{j=2} \quad ; \quad (\gamma)_{j=3} \quad ; \quad (V)_{j=4}$$

$$\nu_j = (T)_{j=1} \quad ; \quad (\alpha)_{j=2}$$

For example:

$$\frac{\partial \dot{\xi}_3}{\partial \xi_2} = \frac{\partial \dot{\gamma}}{\partial \theta}$$

and

$$\frac{\partial \dot{\xi}_2}{\partial \nu_2} = \frac{\partial \dot{\theta}}{\partial \alpha}$$

The operator, δ, indicates a deviation from the nominal value.

The equations adjoint the perturbation equations (21-2) are:

$$\left[\dot{\lambda}_i\right] = -\left[\frac{\partial \dot{\xi}_i}{\partial \xi_j}\right]^T \left[\lambda_j\right] \qquad (21\text{-}3)$$

for

$$i = 1, 2, 3, 4$$
$$j = 1, 2, 3, 4$$

Superscript T indicates transpose

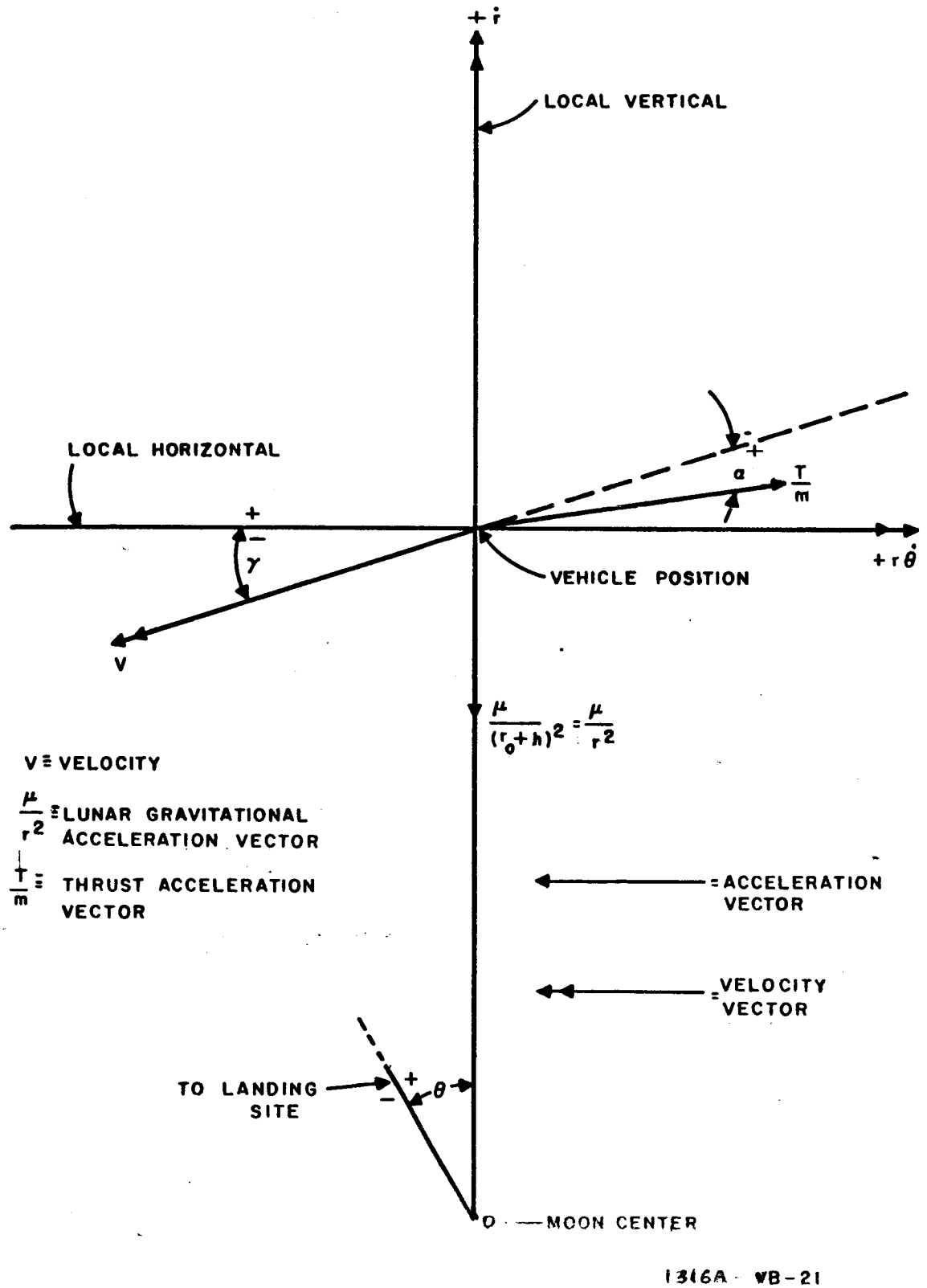

1316A - VB-21

FIGURE 21-1: Velocity-Acceleration Diagram of Landing Maneuver

This page intentionally left blank

The two resulting sets of equations are:

$$\left[\delta \dot{\xi}_i\right] \doteq \left[\frac{\partial \dot{\xi}_i}{\partial \xi_j}\right]\left[\delta \xi_j\right] + \left[\frac{\partial \dot{\xi}_i}{\partial \nu_j}\right]\left[\delta \nu_j\right] \tag{21-4a}$$

$$\left[\dot{\lambda}_i\right] = -\left[\frac{\partial \dot{\xi}_i}{\partial \xi_j}\right]^T\left[\lambda_j\right] \tag{21-4b}$$

Pre-multiply 21-4a by $\left[\lambda_j\right]^T$ and 21-4b by $\left[\delta \xi_j\right]^T$:

$$\left[\lambda_j\right]^T\left[\delta \dot{\xi}_i\right] \doteq \left[\lambda_j\right]^T\left[\frac{\partial \dot{\xi}_i}{\partial \xi_j}\right]\left[\delta \xi_j\right] + \left[\lambda_j\right]^T\left[\frac{\partial \dot{\xi}_i}{\partial \nu_j}\right]\left[\delta \nu_j\right] \tag{21-5a}$$

$$\left[\delta \xi_j\right]^T\left[\dot{\lambda}_i\right] = -\left[\delta \xi_j\right]^T\left[\frac{\partial \dot{\xi}_i}{\partial \xi_j}\right]^T\left[\lambda_j\right] \tag{21-5b}$$

Adding 21-5a and 21-5b yields:

$$\left[\lambda_j\right]^T\left[\delta \dot{\xi}_i\right] + \left[\delta \xi_j\right]^T\left[\dot{\lambda}_i\right] = \left[\lambda_j\right]^T\left[\frac{\partial \dot{\xi}_i}{\partial \nu_j}\right]\left[\delta \nu_j\right] \tag{21-6}$$

Note that the matrix formed by the product $\left[\lambda_j\right]^T\left[\frac{\partial \dot{\xi}_i}{\partial \xi_j}\right]\left[\delta \xi_j\right]$ is identically equal to the transpose of the matrix formed by $\left[\delta \xi_j\right]^T\left[\frac{\partial \dot{\xi}_i}{\partial \xi_j}\right]^T\left[\lambda_j\right]$. However, since both of these multiplications produce a matrix containing only a single element (first row, first column), the products are equal and their difference is zero.

Equation 21-6 can now be rewritten in the long form.

$$\lambda_1 \delta \dot{h} + \lambda_2 \delta \dot{\theta} + \lambda_3 \delta \dot{\gamma} + \lambda_4 \delta \dot{V} + \dot{\lambda}_1 \delta h + \dot{\lambda}_2 \delta \theta + \dot{\lambda}_3 \delta \gamma + \dot{\lambda}_4 \delta V = \lambda_3 \frac{\partial \dot{\gamma}}{\partial \alpha} \delta \alpha + \lambda_4 \frac{\partial \dot{V}}{\partial T} \delta T \quad (21\text{-}7)$$

For a constant thrust gravity turn, all elements of $\left[\frac{\partial \dot{\xi}_i}{\partial \nu_j}\right]$ except $\frac{\partial \dot{\gamma}}{\partial \alpha}$ and $\frac{\partial \dot{V}}{\partial T}$ are zero.

Regrouping the expressions on the left side of equation 21-7, and integrating with respect to time from $t = t_1$ to $t = t_f$ yields:

$$\int_{t_1}^{t_f} \left[(\lambda_1 \delta \dot{h} + \dot{\lambda}_1 \delta h) + (\lambda_2 \delta \dot{\theta} + \dot{\lambda}_2 \delta \theta) + (\lambda_3 \delta \dot{\gamma} + \dot{\lambda}_3 \delta \gamma) + (\lambda_4 \delta \dot{V} + \dot{\lambda}_4 \delta V) \right] dt = \int_{t_1}^{t_f} \left[\lambda_3 \frac{\partial \dot{\gamma}}{\partial \alpha} \delta \alpha + \lambda_4 \frac{\partial \dot{V}}{\partial T} \delta T \right] dt \quad (21\text{-}8)$$

$$0 \leq t_1 \leq t_f$$

Since the δ operator and the differentiation indicated by the dot are commutative, each pair of products enclosed within parentheses forms a perfect differential such that the left hand integral can be evaluated as a function of end point values.

$$\begin{aligned} \int_{t_1}^{t_f} \left[\lambda_3 \frac{\partial \dot{\gamma}}{\partial \alpha} \delta \alpha + \lambda_4 \frac{\partial \dot{V}}{\partial T} \delta T \right] dt = & \left[\lambda_1(t_f) \delta h(t_f) - \lambda_1(t_1) \delta h(t_1) \right] \\ & + \left[\lambda_2(t_f) \delta \theta(t_f) - \lambda_2(t_1) \delta \theta(t_1) \right] \quad (21\text{-}9) \\ & + \left[\lambda_3(t_f) \delta \gamma(t_f) - \lambda_3(t_1) \delta \gamma(t_1) \right] \\ & + \left[\lambda_4(t_f) \delta V(t_f) - \lambda_4(t_1) \delta V(t_1) \right] \end{aligned}$$

Equation 21-9 can be re-arranged to form:

$$\left[\lambda_1 \delta h + \lambda_2 \delta \theta + \lambda_3 \delta \gamma + \lambda_4 \delta V \right]_{t=t_f} = \left[\lambda_1 \delta h + \lambda_2 \delta \theta + \lambda_3 \delta \gamma + \lambda_4 \delta V \right]_{t=t_1} + \int_{t_1}^{t_f} \left[\lambda_3 \frac{\partial \dot{\gamma}}{\partial \alpha} \delta \alpha + \lambda_4 \frac{\partial \dot{V}}{\partial T} \delta T \right] dt \quad (21\text{-}10)$$

To solve equation 21-10 for the final position deviations, which are δh and $\delta\theta$ evaluated at $t = t_f$, proceed as follows. Integrate the set of adjoint equations (21-3) backward in time from $t = t_f$ to determine the values of λ_1, λ_2, λ_3, and λ_4 at $t = t_1$. This backward integration is performed twice, using two different sets of values for $[\lambda_j(t_f)]$. The first set is denoted $[{}_h\lambda_j(t_f)]$, and yields a solution for $\delta h(t_f)$. The second set, $[{}_\theta\lambda_j(t_f)]$, yields a solution for $\delta\theta(t_f)$. In particular

$$\left[{}_h\lambda_j(t_f)\right] = \begin{bmatrix} {}_h\lambda_1(t_f) \\ {}_h\lambda_2(t_f) \\ {}_h\lambda_3(t_f) \\ {}_h\lambda_4(t_f) \end{bmatrix} = \begin{bmatrix} 1 \\ 0 \\ 0 \\ 0 \end{bmatrix} \tag{21-11a}$$

and

$$\left[{}_\theta\lambda_j(t_f)\right] \quad \begin{bmatrix} {}_\theta\lambda_1(t_f) \\ {}_\theta\lambda_2(t_f) \\ {}_\theta\lambda_3(t_f) \\ {}_\theta\lambda_4(t_f) \end{bmatrix} \quad \begin{bmatrix} 0 \\ 1 \\ 0 \\ 0 \end{bmatrix} \tag{21-11b}$$

Applying equation 21-11a and 21-11b to equation 21-10 results in:

$$\begin{aligned}(\delta h)_{t=t_f} = {} & \left({}_h\lambda_1\delta h + {}_h\lambda_2\delta\theta + {}_h\lambda_3\delta\gamma + {}_h\lambda_4\delta V\right)_{t=t_1} \\ & + \int_{t_1}^{t_f}\left({}_h\lambda_3\frac{\partial\dot{\gamma}}{\partial\alpha}\delta\alpha + {}_h\lambda_4\frac{\partial\dot{V}}{\partial T}\delta T\right)dt\end{aligned} \tag{21-12a}$$

and,

$$(\delta\theta)_{t=t_f} = \left({}_{\theta}\lambda_1 \delta h + {}_{\theta}\lambda_2 \delta\theta + {}_{\theta}\lambda_3 \delta\gamma + {}_{\theta}\lambda_4 \delta V\right)_{t=t_1} + \int_{t_1}^{t_f} \left({}_{\theta}\lambda_3 \frac{\partial\dot{\gamma}}{\partial\alpha}\delta\alpha + {}_{\theta}\lambda_4 \frac{\partial\dot{V}}{\partial T}\delta T\right) dt \qquad (21\text{-}12b)$$

The symbols ${}_h\lambda_j$ and ${}_\theta\lambda_j$ refer to values of λ_j computed from backward integration using the final conditions ${}_h\lambda_j(t_f)$ and ${}_\theta\lambda_j(t_f)$ respectively. Final deviation in the remaining two state variables, γ and V, can be found by performing backward integration of equations 21-3 for two more sets of $\lambda_j(t_f)$ conditions. Namely:

$$\begin{bmatrix} {}_\gamma\lambda_1(t_f) \\ {}_\gamma\lambda_2(t_f) \\ {}_\gamma\lambda_3(t_f) \\ {}_\gamma\lambda_4(t_f) \end{bmatrix} = \begin{bmatrix} 0 \\ 0 \\ 1 \\ 0 \end{bmatrix} \qquad \text{for } \delta\gamma(t_f)$$

and

$$\begin{bmatrix} {}_V\lambda_1(t_f) \\ {}_V\lambda_2(t_f) \\ {}_V\lambda_3(t_f) \\ {}_V\lambda_4(t_f) \end{bmatrix} = \begin{bmatrix} 0 \\ 0 \\ 0 \\ 1 \end{bmatrix} \qquad \text{for } \delta V(t_f)$$

The control errors δT and $\delta\alpha$ are considered constants over the trajectory and can therefore be removed from the integrals. This step, along with the following substitutions allow equations 21-12 to be expressed in a more convenient form. Let:

$$E_{Sh} \equiv \left({}_h\lambda_1 \, \delta h + {}_h\lambda_2 \, \delta\theta + {}_h\lambda_3 \, \delta\gamma + {}_h\lambda_4 \, \delta V\right)_{t=t_1}$$

$$E_{S\theta} \equiv \left({}_\theta\lambda_1 \, \delta h + {}_\theta\lambda_2 \, \delta\theta + {}_\theta\lambda_3 \, \delta\gamma + {}_\theta\lambda_4 \, \delta V\right)_{t=t_1}$$

$$I_{Th} \equiv \int_{t_1}^{t_f} {}_h\lambda_4 \, \frac{\partial \dot{V}}{\partial T} \, dt$$

$$I_{T\theta} \equiv \int_{t_1}^{t_f} {}_\theta\lambda_4 \, \frac{\partial \dot{V}}{\partial T} \, dt$$

$$I_{\alpha h} \equiv \int_{t_1}^{t_f} {}_h\lambda_3 \, \frac{\partial \dot{\gamma}}{\partial \alpha} \, dt$$

$$I_{\alpha\theta} \equiv \int_{t_1}^{t_f} {}_\theta\lambda_3 \, \frac{\partial \dot{\gamma}}{\partial \alpha} \, dt$$

Then:

$$\delta h\,(t_f) = E_{Sh} + I_{Th}\,\delta T + I_{\alpha h}\,\delta\alpha \qquad (21\text{-}13a)$$

$$\delta\theta\,(t_f) = E_{S\theta} + I_{T\theta}\,\delta T + I_{\alpha\theta}\,\delta\alpha \qquad (21\text{-}13b)$$

It is desired to find the value of δT and $\delta\alpha$ that will reduce the final position errors to zero. These are found by solving the following set of simultaneous equations:

$$0 = E_{Sh} + I_{Th}\,\delta T + I_{\alpha h}\,\delta\alpha \qquad (21\text{-}14a)$$

$$0 = E_{S\theta} + I_{T\theta}\,\delta T + I_{\alpha\theta}\,\delta\alpha \qquad (21\text{-}14b)$$

The solutions are:

$$\delta T = \frac{E_{S\theta}\, I_{\alpha h} - E_{Sh}\, I_{\alpha\theta}}{I_{Th}\, I_{\alpha\theta} - I_{T\theta}\, I_{\alpha h}} \qquad (21\text{-}15a)$$

$$\delta\alpha = \frac{E_{sh} I_{T\theta} - E_{s\theta} I_{\alpha h}}{I_{Th} I_{\alpha\theta} - I_{T\theta} I_{\alpha h}} \tag{21-15b}$$

Expanding the quantities $E_{S\theta}$ and E_{Sh} produces,

$$\delta T = \frac{\left[(I_{\alpha h})(_{\theta}\lambda_1) - (I_{\alpha\theta})(_{h}\lambda_1)\right]_{t=t_1} \delta h(t_1) + \left[(I_{\alpha h})(_{\theta}\lambda_2) - (I_{\alpha\theta})(_{h}\lambda_2)\right]_{t=t_1} \delta\theta(t_1)}{D(t_1)} \tag{21-16a}$$

$$+ \frac{\left[(I_{\alpha h})(_{\theta}\lambda_3) - (I_{\alpha\theta})(_{h}\lambda_3)\right]_{t=t_1} \delta\gamma(t_1) + \left[(I_{\alpha h})(_{\theta}\lambda_4) - (I_{\alpha\theta})(_{h}\lambda_4)\right]_{t=t_1} \delta V(t_1)}{D(t_1)}$$

and

$$\delta\alpha = \frac{\left[(I_{T\theta})(_{h}\lambda_1) - (I_{Th})(_{\theta}\lambda_1)\right]_{t=t_1} \delta h(t_1) + \left[(I_{T\theta})(_{h}\lambda_2) - (I_{Th})(_{\theta}\lambda_2)\right]_{t=t_1} \delta\theta(t_1)}{D(t_1)} \tag{21-16b}$$

$$+ \frac{\left[(I_{T\theta})(_{h}\lambda_3) - (I_{Th})(_{\theta}\lambda_3)\right]_{t=t_1} \delta\gamma(t_1) + \left[(I_{T\theta})(_{h}\lambda_4) - (I_{Th})(_{\theta}\lambda_4)\right]_{t=t_1} \delta V(t_1)}{D(t_1)}$$

Where:

$$D(t_1) \equiv \left[I_{Th} I_{\alpha\theta} - I_{T\theta} I_{\alpha h}\right]_{t=t_1}$$

The guidance terms are defined from this pair of equations.

$$S_1(t_1) \equiv \frac{\left[I_{\alpha h}\, {}_{\theta}\lambda_1 - I_{\alpha\theta}\, {}_{h}\lambda_1\right]_{t=t_1}}{D(t_1)}$$

$$S_2(t_1) \equiv \frac{\left[I_{\alpha h}\, {}_{\theta}\lambda_2 - I_{\alpha\theta}\, {}_{h}\lambda_2\right]_{t=t_1}}{D(t_1)}$$

$$S_3(t_1) \equiv \frac{\left[I_{\alpha h}\,{}_{\theta}\lambda_3 - I_{\alpha\theta}\,{}_{h}\lambda_3\right]_{t=t_1}}{D(t_1)}$$

$$S_4(t_1) \equiv \frac{\left[I_{\alpha h}\,{}_{\theta}\lambda_4 - I_{\alpha\theta}\,{}_{h}\lambda_4\right]_{t=t_1}}{D(t_1)}$$

$$S_5(t_1) \equiv \frac{\left[I_{T\theta}\,{}_{h}\lambda_1 - I_{Th}\,{}_{\theta}\lambda_1\right]_{t=t_1}}{D(t_1)}$$

$$S_6(t_1) \equiv \frac{\left[I_{T\theta}\,{}_{h}\lambda_2 - I_{Th}\,{}_{\theta}\lambda_2\right]_{t=t_1}}{D(t_1)}$$

$$S_7(t_1) \equiv \frac{\left[I_{T\theta}\,{}_{h}\lambda_3 - I_{Th}\,{}_{\theta}\lambda_3\right]_{t=t_1}}{D(t_1)}$$

$$S_8(t_1) \equiv \frac{\left[I_{T\theta}\,{}_{h}\lambda_4 - I_{Th}\,{}_{\theta}\lambda_4\right]_{t=t_1}}{D(t_1)}$$

Equations 21-16a and 21-16b then become:

$$\delta T(t_1) = \left[S_1\,\delta h + S_2\,\delta\theta + S_3\,\delta\gamma + S_4\,\delta V\right]_{t=t_1} \qquad (21\text{-}17a)$$

$$\delta\alpha(t_1) = \left[S_5\,\delta h + S_6\,\delta\theta + S_7\,\delta\gamma + S_8\,\delta V\right]_{t=t_1} \qquad (21\text{-}17b)$$

The guidance terms are computed along the nominal trajectory and stored in the guidance computer along with the reference state variables.

21.2 Appendix III-B: Equations Relating Observables to Dynamic State Variables

Figure 6-7 illustrates the geometrical situation existing for the descent phase. The symbols that will be used are defined as follows:

$\gamma \equiv$ The angle between the velocity vector and the local horizontal plane. (Measured in the plane of motion).

$h \equiv$ Altitude of vehicle above reference sphere of radius r_o

$\phi \equiv$ Angle between local vertical and line-of-sight to point A.

$R \equiv$ Line-of-sight range from vehicle to point A.

$r_o \equiv$ radius of moon to point A.

$\dot{R} \equiv$ Range rate from vehicle to point A.

$\theta \equiv$ Angular displacement of vehicle from landing site in moon centered coordinates. (Measured in the plane of motion).

$V \equiv$ Velocity vector of landing vehicles.

The landing site at point A, is allowed to be in the plane formed by the velocity vector and local vertical.

To derive expressions relating the state variables h, θ, γ, and V to the observables R, $\dot{R}$, ϕ, and $\dot{\phi}$ proceed as follows. The known quantities are R, $\dot{R}$, ϕ, $\dot{\phi}$, and r_o. The angle θ can be computed by applying the law of sines to triangle AOB.

$$\frac{\sin \theta}{R} = \frac{\sin \phi}{r_o}$$

$$\therefore \theta = \sin^{-1} \left[\frac{R \sin \phi}{r_o} \right]$$

Then the quantity h is available from the law of sines.

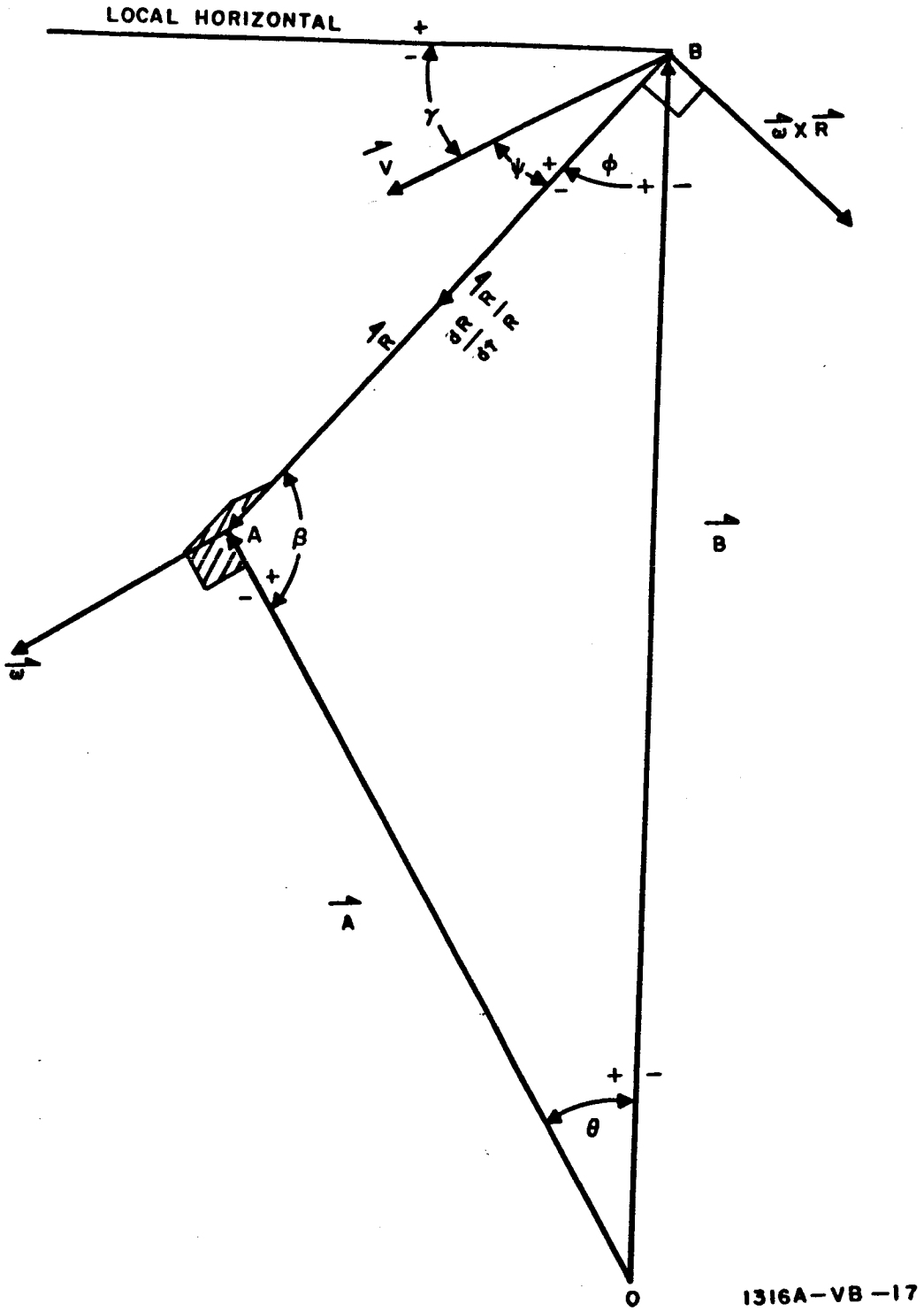

FIGURE 21-2: Vector Diagram of Landing Maneuver

This page intentionally left blank

$$\frac{r_o + h}{\sin\left[\pi - (\phi + \theta)\right]} = \frac{r_o}{\sin \phi}$$

$$r_o + h = \frac{r_o \sin(\phi + \theta)}{\sin \phi}$$

$$h = r_o \frac{\left[\sin \phi \cos \theta + \cos \phi \sin \theta\right]}{\sin \phi} - r_o$$

$$h = r_o \cos \theta + \frac{r_o \sin \theta}{\tan \phi} - r_o$$

$$h = R \cos \phi + \left[r_o^2 - R^2 \sin^2 \phi\right]^{\frac{1}{2}} - r_o$$

Functions relating γ and V to the observables are most conveniently derived through vector analysis. In the following analysis an arrow over a quantity refers to a vector and the quantity alone is the vector magnitude. For example, $\vec{V}$ is the velocity vector and $V = |\vec{V}|$.

The following definitions refer to figure 21-2.

$\vec{A}$ = A vector from point O to point A.

$\vec{B}$ = A vector from point O to point B.

$\vec{R}$ = A vector from point B to point A.

$\vec{V}$ = The landing vehicle velocity vector.

In vector notation,

$$\vec{R} = \vec{A} - \vec{B}$$

and

$$\dot{\vec{R}} = \dot{\vec{A}} - \dot{\vec{B}}$$

Since $\vec{A}$ is a constant vector, $\dot{\vec{A}}$ is zero, and

$$\dot{\vec{R}} = -\dot{\vec{B}} = -\vec{V}$$

Vector differentiation results in the expression

$$\overset{\circ}{\vec{R}} = \frac{dR}{dt}\,\frac{\vec{R}}{R} + \vec{\omega} \times \vec{R}$$

$\frac{\vec{R}}{R}$ is a unit vector in the direction of $\vec{R}$

The vector $\vec{\omega}$ is perpendicular to the plane formed by $\vec{A}$ and $\vec{R}$ and equal in magnitude to $\dot{\beta}$. For the geometry of figure 21-2, $\vec{\omega}$ is positive toward the reader. The quantity $\vec{\omega} \times \vec{R}$ is perpendicular to $\vec{R}$ and in the plane formed by $\vec{A}$ and $\vec{R}$. The positive senses of all vector quantities are illustrated in Figure 21.2. The following statements can be made:

$$\frac{dR}{dt} = \overset{\circ}{R} = \text{ an observable}$$

$$\beta = \pi - (\phi + \theta)$$

$$\omega = \dot{\beta} = -\overset{\circ}{\phi} - \overset{\circ}{\theta}$$

where $\overset{\circ}{\phi}$ is an observable and $\overset{\circ}{\theta}$ as a function of observables can be obtained by differentiation of the expression obtained earlier for θ.

$$\theta = \sin^{-1}\left[\frac{R}{r_o}\sin\phi\right]$$

$$\dot{\theta} = \frac{d\theta}{dt} = \frac{R\dot{\phi}\cos\phi + \overset{\circ}{R}\sin\phi}{\left[r_o^2 - R^2\sin^2\phi\right]^{\frac{1}{2}}}$$

Therefore, if

$$\overset{\circ}{\vec{R}} = \overset{\circ}{R}\,\frac{\vec{R}}{R} + \vec{\omega} \times \vec{R}$$

then

$$\vec{V} = -\overset{\circ}{\vec{R}} = -\overset{\circ}{R}\,\frac{\vec{R}}{R} - \vec{\omega} \times \vec{R}$$

$$V^2 = (\overset{\circ}{R})^2 + R^2\,(\overset{\circ}{\phi} + \overset{\circ}{\theta})^2$$

$$V = \left[(\overset{\circ}{R})^2 + R^2\,(\overset{\circ}{\phi} + \overset{\circ}{\theta})\right]^{\frac{1}{2}}$$

and

$$\tan \Psi = \tan\left[-\tan^{-1}\frac{\omega R}{\dot{R}}\right] = -\frac{\omega R}{\dot{R}}$$

$$\tan \Psi = \frac{R\,(\dot{\phi} + \dot{\theta})}{\dot{R}}$$

From figure 21-2 it can be shown that

$$\phi + \Psi - \gamma = \pi/2$$

$$\therefore\ \gamma = \phi + \Psi - \pi/2$$

$$\gamma = \phi - \pi/2 + \tan^{-1}\left[\frac{R(\dot{\phi} + \dot{\theta})}{\dot{R}}\right]$$

The four resulting transformation equations are:

$$\theta = \sin^{-1}\left[\frac{R}{r_o}\ \sin\phi\right]$$

$$h = R\cos\phi + \left[r_o^{\,2} - R^2\sin^2\phi\right]^{\frac{1}{2}} - r_o$$

$$\gamma = \phi - \frac{\pi}{2} + \tan^{-1}\left[\frac{R\,(\dot{\phi} + \dot{\theta})}{\dot{R}}\right]$$

$$V = \left[(\dot{R})^2 + R^2\,(\dot{\phi} + \dot{\theta})^2\right]^{1/2}$$

where

$$\dot{\theta} = \frac{R\,\dot{\phi}\cos\phi + \dot{R}\sin\phi}{\left[r_o^{\,2} - R^2\sin^2\phi\right]^{1/2}}$$

The term $\dot{\theta}$ appearing in the expressions for γ and V appreciably complicates the partial derivative equations required for the linearized error analysis. However, over the range of parameter values covered by the landing maneuver, $\dot{\theta}$ is very much smaller than $\dot{\phi}$ so that the approximation $\dot{\phi} + \dot{\theta} = \dot{\phi}$ is very accurate. The equations from which the partial derivatives were derived are then:

$$\Theta = \sin^{-1}\left[\frac{R}{r_o}\sin\phi\right]$$

$$h = R\cos\phi + \left[r_o^{\,2} - R^2\sin^2\phi\right]^{\frac{1}{2}} - r_o$$

$$\gamma = \phi - \pi/2 + \tan^{-1}\left[\frac{R\dot{\phi}}{\dot{R}}\right]$$

$$V = \left[(\dot{R})^2 + (R\dot{\phi})^2\right]^{1/2}$$

The resulting partial derivative expressions which are used in the analysis are:

$$\frac{\partial h}{\partial R} = \cos\phi - \frac{R\sin^2\phi}{\left[r_o^{\,2} - R^2\sin^2\phi\right]^{\frac{1}{2}}}$$

$$\frac{\partial \Theta}{\partial R} = \frac{\sin\phi}{\left[r_o^{\,2} - R^2\sin^2\phi\right]^{\frac{1}{2}}}$$

$$\frac{\partial \gamma}{\partial R} \doteq \frac{\dot{R}(\dot{\phi})}{\left[(\dot{R})^2 + (R\dot{\phi})^2\right]}$$

$$\frac{\partial V}{\partial R} \doteq \frac{R\,(\dot{\phi})^2}{\left[(\dot{R})^2 + (R\dot{\phi})^2\right]^{\frac{1}{2}}}$$

$$\frac{\partial h}{\partial \dot{R}} = 0$$

$$\frac{\partial \Theta}{\partial \dot{R}} = 0$$

$$\frac{\partial \gamma}{\partial \dot{R}} \doteq -\frac{1}{(\dot{R})^2 + (R\dot{\phi})^2}$$

$$\frac{\partial V}{\partial \dot{R}} \doteq \frac{\dot{R}}{\left[(\dot{R}) + (R\dot{\phi})^2\right]^{\frac{1}{2}}}$$

$$\frac{\partial h}{\partial \phi} = -R \sin \phi \left[1 + \frac{R \cos \phi}{\left(r_o^{\,2} - R^2 \sin^2 \phi\right)^{\frac{1}{2}}} \right]$$

$$\frac{\partial \theta}{\partial \phi} = \frac{R \cos \phi}{\left[r_o^{\,2} - R^2 \sin^2 \phi\right]^{\frac{1}{2}}}$$

$$\frac{\partial \gamma}{\partial \phi} \doteq 1$$

$$\frac{\partial V}{\partial \phi} \doteq 0$$

$$\frac{\partial h}{\partial \dot{\phi}} = 0$$

$$\frac{\partial \theta}{\partial \dot{\phi}} = 0$$

$$\frac{\partial \gamma}{\partial \dot{\phi}} \doteq \frac{R \dot{R}}{(\dot{R})^2 + (R\dot{\phi})^2}$$

$$\frac{\partial V}{\partial \dot{\phi}} \doteq \frac{R^2 \dot{\phi}}{\left[(\dot{R})^2 + (R\dot{\phi})^2\right]^{\frac{1}{2}}}$$

21.3 Appendix III-C: Computer Program

The linearized error analysis, is dependent upon the calculation of small components of the total error that occur in each of N time increments into which the landing trajectory has been divided. The following information is required to compute the error component attributed to the ith time interval.

$$\left.\begin{bmatrix} h(t_i) \\ \theta(t_i) \\ \gamma(t_i) \\ V(t_i) \end{bmatrix}\right\} \text{nominal trajectory values}$$

$$\left.\begin{bmatrix} {}_h\lambda_1(t_i) \\ {}_h\lambda_2(t_i) \\ {}_h\lambda_3(t_i) \\ {}_h\lambda_4(t_i) \end{bmatrix} \begin{bmatrix} {}_\theta\lambda_1(t_i) \\ {}_\theta\lambda_2(t_i) \\ {}_\theta\lambda_3(t_i) \\ {}_\theta\lambda_4(t_i) \end{bmatrix}\right\} \text{See Appendix III-A for definition}$$

9) $$\frac{\partial \dot{\xi}_3}{\partial \xi_1} = \frac{\partial \dot{\gamma}}{\partial h} = \frac{2\mu \cos\gamma}{V\,(r_o + h)^3} - \frac{V \cos\gamma}{(r_o + h)^2}$$

10) $$\frac{\partial \dot{\xi}_3}{\partial \xi_2} = \frac{\partial \dot{\gamma}}{\partial \theta} = 0$$

11) $$\frac{\partial \dot{\xi}_3}{\partial \xi_3} = \frac{\partial \dot{\gamma}}{\partial \gamma} = \frac{\mu \sin\gamma}{V\,(r_o + h)^2} - \frac{V \sin\gamma}{r_o + h}$$

12) $$\frac{\partial \dot{\xi}_3}{\partial \xi_4} = \frac{\partial \dot{\gamma}}{\partial V} = \frac{\cos\gamma}{r_o + h} + \frac{\mu \cos\gamma}{V^2 (r_o + h)^2}$$

13) $$\frac{\partial \dot{\xi}_4}{\partial \xi_1} = \frac{\partial \dot{V}}{\partial h} = \frac{2\mu \sin\gamma}{(r_o + h)^3}$$

14) $$\frac{\partial \dot{\xi}_4}{\partial \xi_2} = \frac{\partial \dot{V}}{\partial \theta} = 0$$

15) $$\frac{\partial \dot{\xi}_4}{\partial \xi_3} = \frac{\partial \dot{V}}{\partial \gamma} = -\frac{\mu \cos\gamma}{(r_o + h)^2}$$

16) $$\frac{\partial \dot{\xi}_4}{\partial \xi_4} = \frac{\partial \dot{V}}{\partial V} = 0$$

B) The matrix $\left[\frac{\partial \dot{\xi}_i}{\partial \nu_j}\right]$

1) $$\frac{\partial \dot{\xi}_1}{\partial \nu_1} = \frac{\partial \dot{\xi}_1}{\partial \nu_2} = \frac{\partial \dot{\xi}_2}{\partial \nu_1} = \frac{\partial \dot{\xi}_2}{\partial \nu_2} = \frac{\partial \dot{\xi}_3}{\partial \nu_1} = \frac{\partial \dot{\xi}_4}{\partial \nu_2} = 0$$

2) $$\frac{\partial \dot{\xi}_3}{\partial \nu_2} = \frac{\partial \dot{\gamma}}{\partial \alpha} = -\frac{T}{mV}$$

3) $$\frac{\partial \dot{\xi}_4}{\partial \nu_1} = \frac{\partial \dot{V}}{\partial T} = -\frac{1}{m}$$

C) Observables in terms of state variables

1) $$R = \left[r_o^2 + (r_o + h)^2 - 2\, r_o\, (r_o + h) \cos \theta\right]^{\frac{1}{2}}$$

$$= \left[h^2 + 4\left(1 + \frac{h}{r_o}\right) r_o^2 \sin^2 \left(\frac{\theta}{2}\right)\right]^{\frac{1}{2}}$$

2) $$\dot{R} = \frac{V\,(r_o + h) \sin \gamma - V\, r_o \sin(\gamma + \theta)}{R}$$

3) $$\phi = \sin^{-1}\left[\frac{r_o \sin \theta}{R}\right]$$

4) $$\dot{\phi} = \frac{V \cos \gamma}{r_o + h} - \frac{V \cos(\gamma - \phi)}{R}$$

D) Partial derivatives relating observation errors to the resulting errors in state variable estimates.*

1) $$\frac{\partial h}{\partial R} = \cos \phi - \frac{R \sin^2 \phi}{\left[r_o^2 - R^2 \sin^2 \phi\right]^{1/2}}$$

2) $$\frac{\partial \theta}{\partial R} = \frac{\sin \phi}{\left[r_o^2 - R^2 \sin^2 \phi\right]^{\frac{1}{2}}}$$

3) $$\frac{\partial \gamma}{\partial R} \doteq \frac{\dot{R}\,\dot{\phi}}{(\dot{R})^2 + (R\dot{\phi})^2}$$

4) $$\frac{\partial V}{\partial R} \doteq \frac{R\,(\dot{\phi})^2}{\left[\dot{R}^2 + (R\dot{\phi})^2\right]^{\frac{1}{2}}}$$

5) $$\frac{\partial \gamma}{\partial \dot{R}} \doteq - \frac{1}{(\dot{R})^2 + (R\,\dot{\phi})^2}$$

*See Appendix III-B for derivation of this group of equations.

$$\left.\begin{array}{l} I_{T\theta}(t_i) \\ I_{\alpha\theta}(t_i) \\ I_{Th}(t_i) \\ I_{\alpha h}(t_i) \end{array}\right\} \quad \text{See Appendix III-A for definition}$$

When these parameters have been evaluated at $t = t_i$, all the guidance terms and linearization partial derivatives can be evaluated because they are expressable in terms of the above quantities.

Both initial and final conditions of the reference trajectory are known, so that the equations of motion can be integrated in either forward or backward in time. To solve for the adjoint variables, backward time integration is required since only the final values are specified. The four integral expressions, of which $I_{T\theta}$ is typical, are handled as follows:

$$I_{T\theta} = \int_{t_i}^{t_f} {}_{\theta}\lambda_4(t) \frac{\partial \dot{V}}{\partial T}(t)\, dt \qquad 0 \leq t_i \leq t_f$$

By interchanging the limits,

$$I_{T\theta} = -\int_{t_f}^{t_i} {}_{\theta}\lambda_4(t) \frac{\partial \dot{V}}{\partial T}(t)\, dt$$

Differentiation with respect to time yields

$$\dot{I}_{T\theta} = -{}_{\theta}\lambda_4(t) \frac{\partial \dot{V}}{\partial T}(t)$$

The value of $\dot{I}_{T\theta}(t_f)$ is known since both ${}_{\theta}\lambda_4(t_f)$ and $\frac{\partial \dot{V}}{\partial T}(t_f)$ are known. The function $I_{T\theta}(t_i)$ can be obtained by integrating $\dot{I}_{T\theta}(t)$ backward in time from $t = t_f$ to $t = t_i$.

Therefore, all the required quanties can be obtained by integrating a set of inter-related differential equations backward in time from $t = t_f$ to

$t = t_i$. Then, at $t = t_i$ all the quantities required to evaluate the ith components of the final mean squared error transformation coefficients can be computed. The ith components are then added to the sum of components calculated in the intervals between the ith and the Nth so that a running summation is developed. (The process is backward in time so that components on the final error caused by errors in the Nth time interval are actually calculated first).

The equations used to compute the partial derivatives required for this analysis are listed below, along with the set of differential equations discussed above.

A) The matrix $\left[\dfrac{\partial \dot{\xi}_i}{\partial \xi_j}\right]$

1) $\dfrac{\partial \dot{\xi}_1}{\partial \xi_1} = \dfrac{\partial \dot{h}}{\partial h} = 0$

2) $\dfrac{\partial \dot{\xi}_1}{\partial \xi_2} = \dfrac{\partial \dot{h}}{\partial \theta} = 0$

3) $\dfrac{\partial \dot{\xi}_1}{\partial \xi_3} = \dfrac{\partial \dot{h}}{\partial \gamma} = V \cos \gamma$

4) $\dfrac{\partial \dot{\xi}_1}{\partial \xi_4} = \dfrac{\partial \dot{h}}{\partial V} = \sin \gamma$

5) $\dfrac{\partial \dot{\xi}_2}{\partial \xi_1} = \dfrac{\partial \dot{\theta}}{\partial h} = \dfrac{V \cos \gamma}{(r_o + h)^2}$

6) $\dfrac{\partial \dot{\xi}_2}{\partial \xi_2} = \dfrac{\partial \dot{\theta}}{\partial \theta} = 0$

7) $\dfrac{\partial \dot{\xi}_2}{\partial \xi_3} = \dfrac{\partial \dot{\theta}}{\partial \gamma} = \dfrac{V \sin \gamma}{r_o + h}$

8) $\dfrac{\partial \dot{\xi}_2}{\partial \xi_4} = \dfrac{\partial \dot{\theta}}{\partial V} = -\dfrac{\cos \gamma}{r_o + h}$

6) $$\frac{\partial V}{\partial \dot{R}} \doteq \frac{\dot{R}}{\left[(\dot{R})^2 + (R\dot{\phi})^2\right]^{\frac{1}{2}}}$$

7) $$\frac{\partial h}{\partial \phi} = -R \sin \phi \left[1 + \frac{R \cos \phi}{(r_o^2 - R^2 \sin^2 \phi)^{1/2}}\right]$$

8) $$\frac{\partial \theta}{\partial \phi} = \frac{R \cos \phi}{(r_o^2 - R^2 \sin^2 \phi)^{\frac{1}{2}}}$$

9) $$\frac{\partial \gamma}{\partial \dot{\phi}} \doteq 1$$

10) $$\frac{\partial \gamma}{\partial \dot{\phi}} \doteq \frac{R\dot{R}}{(\dot{R})^2 + (R\dot{\phi})^2}$$

11) $$\frac{\partial V}{\partial \dot{\phi}} \doteq \frac{R^2\dot{\phi}}{\left[(\dot{R})^2 + (R\dot{\phi})^2\right]^{\frac{1}{2}}}$$

E) Partial derivatives giving acceleration errors caused by thrust vector control errors.

1) $$\frac{\partial \dot{V}}{\partial T} = -\frac{\cos \alpha}{m}$$

2) $$\frac{\partial \dot{V}}{\partial \alpha} = \frac{T \sin \alpha}{m}$$

3) $$\frac{\partial \ddot{h}}{\partial T} = \frac{\sin (\gamma + \alpha)}{m}$$

4) $$\frac{\partial \ddot{h}}{\partial \alpha} = \frac{T \cos (\gamma + \alpha)}{m}$$

5) $$\frac{\partial \ddot{\theta}}{\partial T} = \frac{\cos (\gamma + \alpha)}{m(r_o + h)}$$

6) $$\frac{\partial \ddot{\theta}}{\partial \alpha} = \frac{T \sin (\gamma + \alpha)}{m\ (r_o + h)}$$

F) Guidance Terms

1) $D = I_{Th}\, I_{\alpha\theta} - I_{T\theta}\, I_{\alpha h}$

2) $S_1 = \dfrac{(I_{\alpha h})\,({}_{\theta}\lambda_1) - (I_{\alpha\theta})\,({}_{h}\lambda_1)}{D}$

3) $S_2 = \dfrac{(I_{\alpha h})\,({}_{\theta}\lambda_2) - (I_{\alpha\theta})\,({}_{h}\lambda_2)}{D}$

4) $S_3 = \dfrac{(I_{\alpha h})\,({}_{\theta}\lambda_3) - (I_{\alpha\theta})\,({}_{h}\lambda_3)}{D}$

5) $S_4 = \dfrac{(I_{\alpha h})\,({}_{\theta}\lambda_4) - (I_{\alpha\theta})\,({}_{h}\lambda_4)}{D}$

6) $S_5 = \dfrac{(I_{T\theta})\,({}_{h}\lambda_1) - (I_{Th})\,({}_{\theta}\lambda_1)}{D}$

7) $S_6 = \dfrac{(I_{T\theta})\,({}_{h}\lambda_2) - (I_{Th})\,({}_{\theta}\lambda_2)}{D}$

8) $S_7 = \dfrac{(I_{T\theta})\,({}_{h}\lambda_3) - (I_{Th})\,({}_{\theta}\lambda_3)}{D}$

9) $S_8 = \dfrac{(I_{T\theta})\,({}_{h}\lambda_4) - (I_{Th})\,({}_{\theta}\lambda_4)}{D}$

G) Set of differential equations

1) $\dot{h} = V \sin \gamma$

2) $\dot{\theta} = -\dfrac{V \cos \gamma}{r_o + h}$

3) $\dot{\gamma} = \dfrac{V \cos \gamma}{r_o + h} - \dfrac{\mu \cos \gamma}{V\,(r_o + h)^2}$

4) $\dot{V} = -\frac{T\cos\alpha}{m} - \frac{\mu\sin\gamma}{(r_o + h)^2}$

5) ${}_h\dot{\lambda}_1 = -\frac{\partial\dot{h}}{\partial h}\,{}_h\lambda_1 - \frac{\partial\dot{\theta}}{\partial h}\,{}_h\lambda_2 - \frac{\partial\dot{\gamma}}{\partial h}\,{}_h\lambda_3 - \frac{\partial\dot{V}}{\partial h}\,{}_h\lambda_4$

6) ${}_h\dot{\lambda}_2 = -\frac{\partial\dot{h}}{\partial\theta}\,{}_h\lambda_1 - \frac{\partial\dot{\theta}}{\partial\theta}\,{}_h\lambda_2 - \frac{\partial\dot{\gamma}}{\partial\theta}\,{}_h\lambda_3 - \frac{\partial\dot{V}}{\partial\theta}\,{}_h\lambda_4$

7) ${}_h\dot{\lambda}_3 = -\frac{\partial\dot{h}}{\partial\gamma}\,{}_h\lambda_1 - \frac{\partial\dot{\theta}}{\partial\gamma}\,{}_h\lambda_2 - \frac{\partial\dot{\gamma}}{\partial\gamma}\,{}_h\lambda_3 - \frac{\partial\dot{V}}{\partial\gamma}\,{}_h\lambda_4$

8) ${}_h\dot{\lambda}_4 = -\frac{\partial\dot{h}}{\partial V}\,{}_h\lambda_1 - \frac{\partial\dot{\theta}}{\partial V}\,{}_h\lambda_2 - \frac{\partial\dot{\gamma}}{\partial V}\,{}_h\lambda_3 - \frac{\partial\dot{V}}{\partial V}\,{}_h\lambda_4$

9) ${}_\theta\dot{\lambda}_1 = -\frac{\partial\dot{h}}{\partial h}\,{}_\theta\lambda_1 - \frac{\partial\dot{\theta}}{\partial h}\,{}_\theta\lambda_2 - \frac{\partial\dot{\gamma}}{\partial h}\,{}_\theta\lambda_3 - \frac{\partial\dot{V}}{\partial h}\,{}_\theta\lambda_4$

10) ${}_\theta\dot{\lambda}_2 = -\frac{\partial\dot{h}}{\partial\theta}\,{}_\theta\lambda_1 - \frac{\partial\dot{\theta}}{\partial\theta}\,{}_\theta\lambda_2 - \frac{\partial\dot{\gamma}}{\partial\theta}\,{}_\theta\lambda_3 - \frac{\partial\dot{V}}{\partial\theta}\,{}_\theta\lambda_4$

11) ${}_\theta\dot{\lambda}_3 = -\frac{\partial\dot{h}}{\partial\gamma}\,{}_\theta\lambda_1 - \frac{\partial\dot{\theta}}{\partial\gamma}\,{}_\theta\lambda_2 - \frac{\partial\dot{\gamma}}{\partial\gamma}\,{}_\theta\lambda_3 - \frac{\partial\dot{V}}{\partial\gamma}\,{}_\theta\lambda_4$

12) ${}_\theta\dot{\lambda}_4 = -\frac{\partial\dot{h}}{\partial V}\,{}_\theta\lambda_1 - \frac{\partial\dot{\theta}}{\partial V}\,{}_\theta\lambda_2 - \frac{\partial\dot{\gamma}}{\partial V}\,{}_\theta\lambda_3 - \frac{\partial\dot{V}}{\partial V}\,{}_\theta\lambda_4$

13) $\dot{I}_{Th} = -\frac{\partial\dot{V}}{\partial T}\,{}_h\lambda_4$

14) $\dot{I}_{T\theta} = -\frac{\partial\dot{V}}{\partial T}\,{}_\theta\lambda_4$

15) $\dot{I}_{\alpha h} = -\frac{\partial\dot{\gamma}}{\partial\alpha}\,{}_h\lambda_3$

16) $\dot{I}_{\alpha\theta} = -\frac{\partial\dot{\gamma}}{\partial\alpha}\,{}_\theta\lambda_3$

H) Initial conditions for integrations

1) $h(t_f) = 499.909782$ meters
2) $\theta(t_f) = 0.23058131 \times 10^{-6}$ rad.
3) $\gamma(t_f) = -1.46158768$ rad.
4) $V(t_f) = 0.69069945 \times 10^{-1}$ m/sec.
5) $t_f = 346.523438$ sec.
6) $T_o = 48{,}060.9375$ Newtons

Determined from nominal trajectory program.

7) $m(t_o) = 11{,}340.000$ kg.
8) $I_{sp} = 400$ sec.
9) ${}_h\lambda_1(t_f) = 1$
10) ${}_h\lambda_2(t_f) = {}_h\lambda_3(t_f) = {}_h\lambda_4(t_f) = 0$
11) ${}_\theta\lambda_2(t_f) = 1$
12) ${}_\theta\lambda_1(t_f) = {}_\theta\lambda_3(t_f) = {}_\theta\lambda_4(t_f) = 0$

I) Constraining equations implied by constant thrust, gravity turn trajectory.

1) $T = To = \text{constant}$
2) $\alpha = 0$
3) $m = m_o - \frac{dm}{dt} t$ where $\frac{dm}{dt}$ is a constant

$$\frac{dm}{dt} = \frac{To}{I_{sp} g_o}$$

I_{sp} = fuel specific impulse

g_o = earth gravitation = 9.80665 m/sec.^{2}

The evaluation of these quantities at $t = t_i$ provides sufficient information to compute the ith component of the final error mean squared value. For convenience in the computer program, all the (Δt_i) time intervals were allowed to be of equal length, however, the length is a variable parameter of the program.

This page intentionally left blank

22.0 Appendix IV: Computer Simulation of Rendezvous Techniques

A computer program has been developed to simulate a method of rendezvous for satellites in lunar orbit. This program is based on several assumptions about the orbits of the two vehicles. A non-maneuvering target vehicle is assumed to be in a circular retrograde orbit about the moon. A maneuverable chaser vehicle is assumed to be initially in a lower altitude circular retrograde parking orbit. The orbits of the two vehicles are assumed to be coplanar and no out of plane deviations have been considered thereby reducing the problem to a two dimensional model.

The nominal case has been defined to be the following. The altitudes of the target and chaser parking orbits are 200 and 30 km. respectively. The initial angle ϕ_0 (Figure 22-1) between the two vehicles is defined to be such that a horizontal nominal thrust applied to the chaser at its initial position will cause the chaser to collide with the target exactly 180 degrees later. The program has been arranged so that deviations from this nominal case can be studied. The deviations which have been considered are a deviation in the altitude of the chaser parking orbit, a deviation from a nominal incremental velocity vector in both magnitude and direction, and a deviation from the nominal central angle between the two vehicles.

22.1 Initial Positioning of Target and Chaser

The initial relative positioning of the target and chaser vehicles depends upon a set of deviations from nominal which are inputs to the program. The chaser vehicle has arbitrarily been placed on the positive x axis at the time when the injection into the ascent ellipse is made. The deviation from nominal thrust level is specified by an initial velocity increment Δv_0. Thus the position and velocity vectors defining the ascent ellipse of the chaser are:

$$x_e = x_p$$
$$y_e = 0$$
$$v_{xe} = \Delta v_0 \sin\gamma$$
$$v_{ye} = v_{yp} + \Delta v_n + \Delta v_0 \cos\gamma$$

where:

x_p, v_{yp} - position and velocity of chaser in parking orbit of specified altitude.

Δv_n - velocity increment due to nominal thrust

γ - deviation from nominal thrust angle (See Figure 22-1)

A set of orbital elements for the chaser is calculated from this position and velocity vector by the method described in Part B of Section 22.7. The target vehicle is placed in a 200 km. circular orbit and positioned initially with a specified deviation from the nominal angle ϕ_0 (Figure 22-1) between the two vehicles.

22.2 General Flow of the Program

The program increments time at a specified interval and performs calculations at each time point based on simulated sensor readings to determine when to make rendezvous achieving corrections to the orbit of the chaser vehicle. At each time point the program determines the selenocentric coordinates of both the target and chaser by applying the method described in Part A of Section 22.7 to the orbital elements of each vehicle. These selenocentric coordinates are then transformed into a local radar oriented $x'z'$ coordinate system with the origin located at the chaser. The positive x' axis lies horizontal to the surface of the moon in the direction of motion and the positive z' axis lies along the vertical in the direction of the moon. Thus the local coordinates of the target are

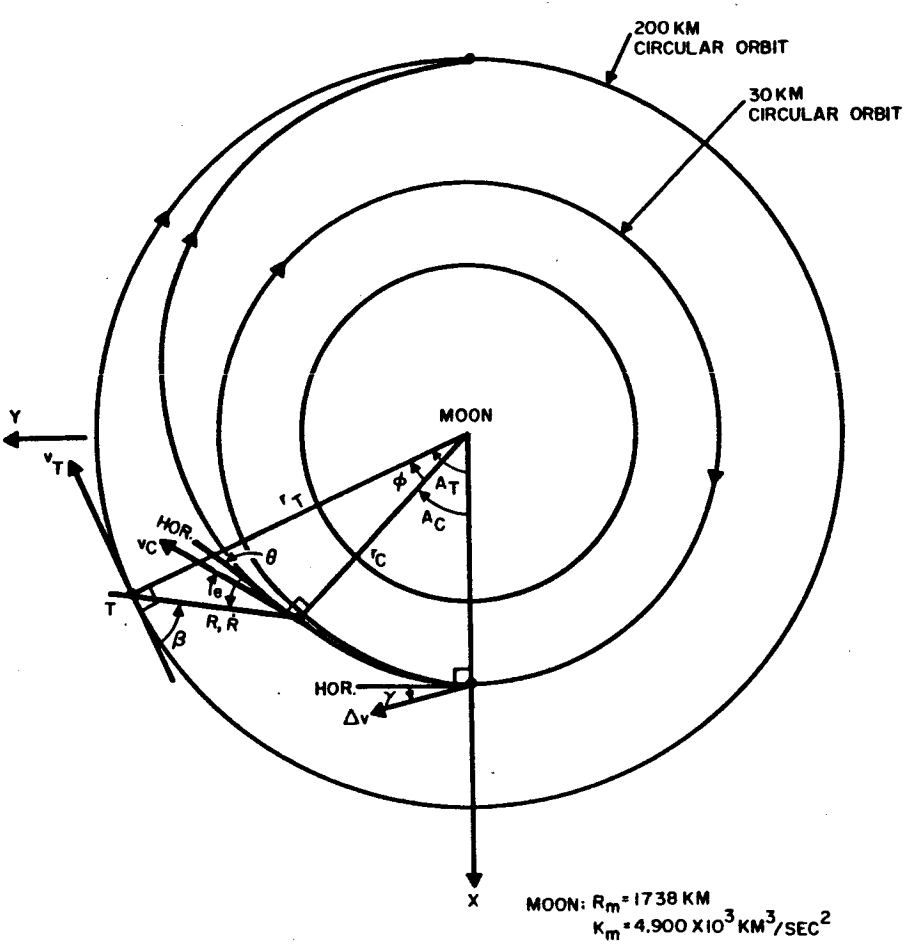

FIGURE 22-1, Orbit Diagram
(Lunar Orbit Rendezvous)

This page intentionally left blank

represented by a translation and rotation of the selenocentric coordinate system with the angle of rotation ψ being the angle the chaser makes with the x axis. Thus:

$$\psi = \tan^{-1} (y_c / x_c)$$

$$\begin{bmatrix} R_x & V_x \\ R_z & V_z \end{bmatrix} = \begin{bmatrix} \cos\psi & -\sin\psi \\ -\sin\psi & -\cos\psi \end{bmatrix} \cdot \begin{bmatrix} (y_T - y_c) & (v_{y_T} - v_{y_c}) \\ (x_T - x_c) & (v_{x_T} - v_{x_c}) \end{bmatrix}$$

where:

R_x, R_z, V_x, V_z - position and velocity of target relative to chaser in $x'z'$ coordinate system

$x_T, y_T, v_{x_T}, v_{y_T}$ - position and velocity of target in xy system.

$x_c, y_c, v_{x_c}, v_{y_c}$ - position and velocity of chaser in xy system.

However, due to the rotation of the $x'z'$ system from point to point, it was found that the relative velocity terms, V_x and V_z, were not truly representative of the closing rate between the vehicles. Thus it became necessary to define closing rates, $\dot{R}_x$ and $\dot{R}_z$, in the $x'z'$ system as the range difference divided by the time interval between two successive points.

The two quantities pertinent to sensor observations are range and elevation, defined as the angle between the positive x' axis (horizontal) and the line of sight from the chaser to the target (See Figure 22-1). Inaccuracies in the sensor measurements are simulated by superimposing random numbers of zero mean and specified standard deviation upon the actual values of range and elevation. These observations are resolved into x' and z' components of range and fed into a smoothing function. The smoothing function performs a least squares fit of a specified order on a specified number of points and extrapolates the solution to the next observation point where

the smoothed values of R_x, R_z, $\dot{R}_x$, and $\dot{R}_z$ will be used as the control variables in the firing laws.

22.3 Firing Laws

The firing laws described in this section serve to control the firing of the chaser rockets which are positioned along the x' and z' axis. The variables of control in these laws are the smoothed values of R_x, R_z, $\dot{R}_x$, and $\dot{R}_z$ which are obtained by the method described in sections 22.5 and 22.6.

The firing laws are designed to close the two vehicles on the z' axis and to hold them together on the z' axis until the vehicles can be brought together on the x' axis. No firing is made until the R_z range becomes less than 15 km. At this time the $\dot{R}_z$ term is driven to a preset value (44 m/sec) designed to prevent the possibility of missing the rendezvous. This is accomplished by calculating a firing time t_f and direction of acceleration as follows:

$$t_f = \frac{|44 - \dot{R}_z|}{|a_z|}$$

$$a_z = -a_{z_0} \frac{44 - \dot{R}_z}{|44 - \dot{R}_z|}$$

$$a_{z_0} = .5 \text{ m/sec}^2 \quad \text{(acceleration generated by thrusting rockets.)}$$

The following firing laws are designed to drive R_z and $\dot{R}_z$ to zero between the two curves defined by the equations:

$$\dot{R}_z = \pm\sqrt{K_2 |R_z|}$$

$$\dot{R}_z = \pm\sqrt{K_1 |R_z|}$$

where K_1 and K_2 have been defined to be .5 and .75 m/sec^2 respectively.

After the initial 15 km. firing all other firing is disabled and the chaser is allowed to coast until it has passed through the limiting curve determined when

$$\dot{R}_z \geq \sqrt{K_2 |R_z|}$$

At this time the general firing laws are enabled and the program will check these laws at every subsequent observation point unless a firing is already in progress. The firing laws for the z' axis corrections are expressed for each quadrant of the R_z, $\dot{R}_z$ system.

If the chaser is in either quadrant one ($R_z > 0, \dot{R}_z > 0$) or quadrant three ($R_z < 0, \dot{R}_z < 0$) of the R_z, $\dot{R}_z$ system, the firing time and direction of acceleration are expressed as follows:

$$t_F = \frac{\sqrt{K_1 |R_z|} + |\dot{R}_z|}{|a_z|}$$

$$a_z = a_{z_0} \frac{R_z}{|R_z|}$$

If the chaser is in either quadrant two ($R_z < 0, \dot{R}_z > 0$) or quadrant four ($R_z > 0, \dot{R}_z < 0$) and if

$$\sqrt{K_1 |R_z|} < |\dot{R}_z| < \sqrt{K_2 |R_z|}$$

then the chaser is following the desired trajectory and no correction is needed.

However, if

$$|\dot{R}_z| > \sqrt{K_2 |R_z|}$$

then a correction of duration and direction as follows is applied.

$$t_F = \frac{2\left(-\sqrt{K_1 |R_z|} + |\dot{R}_z|\right)}{|a_z|}$$

$$a_z = a_{z_0} \frac{\dot{R}_z}{|\dot{R}_z|}$$

In the same two quadrants if

$$|\dot{R}_z| < \sqrt{K_1 |R_z|}$$

then a correction of duration and direction as follows is applied:

$$t_f = \frac{\sqrt{K_1 |R_z|} - |\dot{R}_z|}{|a_z|}$$

$$a_z = a_{z_0} \frac{R_z}{|R_z|}$$

The firing laws controlling the x' axis corrections are designed very similarly to the z' firing laws. That is, they are designed to drive R_x and $\dot{R}_x$ to zero between the two curves defined by the equations:

$$\dot{R}_x = \sqrt{-K_2 (R_x - R_f)}$$

$$\dot{R}_x = \sqrt{-K_1 (R_x - R_f)}$$

where R_f is defined as a standoff range and has been set at 200 meters.

Firings on the x' axis are triggered when:

$$\dot{R}_x \geq \sqrt{-K_2 (R_x - R_f)}$$

Under these conditions a positive acceleration of .5 m/sec^2 is applied for the following duration of time.

$$t_f = \frac{-2 \left(\sqrt{-K_1 (R_x - R_f)} - \dot{R}_x \right)}{a_x}$$

Several additional restrictions are imposed on these firing laws. There must be at least a two second time delay between z' firings and a one second delay between x' firings. Any computed z' firing of less than six seconds or x' firing of less than 3 seconds will be suppressed. When the

term has been driven to less than one meter per second, the rendezvous maneuver is considered to be completed and the program is stopped.

22.4 Corrections to Chaser Orbit for Firing

During periods of firing, corrections must be made to the orbit of the chaser vehicle. These corrections are made by superimposing the effects of firing over a short time period (one second or less) on the position and velocity vectors of the chaser. The effects of firing must first be transformed back into the selenocentric coordinate system and then added to the chaser position and velocity vectors. This operation can be represented by the following matrix equation.

$$\begin{bmatrix} \hat{x}_c & \hat{v}_{xc} \\ \hat{y}_c & \hat{v}_{yc} \end{bmatrix} = \begin{bmatrix} x_c & v_{xc} \\ y_c & v_{yc} \end{bmatrix} + \begin{bmatrix} -\sin\psi & -\cos\psi \\ \cos\psi & -\sin\psi \end{bmatrix} \cdot \begin{bmatrix} \frac{1}{2} a_x \Delta t^2 & a_x \Delta t \\ \frac{1}{2} a_z \Delta t^2 & a_z \Delta t \end{bmatrix}$$

where:

$\hat{x}_c, \hat{y}_c, \hat{v}_{xc}, \hat{v}_{yc}$ - corrected position and velocity components of chaser.

Δt - time interval over which correction is made.

The corrected position and velocity vectors of the chaser are used to calculate a new set of orbital elements by the method described in Part B of Section 22.7. The new orbital elements are used for subsequent positioning of the chaser.

22.5 Noise Generation and Smoothing

The program has been planned to provide a specified order N, of least squares smoothing for a specified number of points, M . The noisy values of R_x and R_z are saved for the previous M time points. At each new time point (intervals of one second are taken when program is in noise generating mode) the blocks of noisy ranges are updated by adding the new values

and dropping the values associated with the oldest time point.

It is desired to fit a function of the following form to the observed data.

$$a_0 + a_1 t + a_2 t^2 + \ldots\ldots + a_N t^N = R$$

If we express the observed data at each of the M points in an equation of this form we obtain the matrix equation:

$$\begin{bmatrix} 1 & t_1 & t_1^2 \ldots\ldots & t_1^N \\ 1 & t_2 & t_2^2 \ldots\ldots & t_2^N \\ \vdots & & & \vdots \\ 1 & t_M & t_M^2 \ldots\ldots & t_M^N \end{bmatrix} \cdot \begin{bmatrix} a_0 \\ a_1 \\ a_2 \\ \vdots \\ a_N \end{bmatrix} = \begin{bmatrix} R_1 \\ R_2 \\ \vdots \\ R_M \end{bmatrix}$$

or in the matrix form:

$$[T] \cdot [A] = [R]$$

When the least squares technique is applied to this system of equations a solution for the coefficient matrix $[A]$ is obtained in the following form.

$$A = ([T]^T \cdot [T])^{-1} \cdot [T]^T \cdot [R]$$

The smoothed value of range and range rate can now be found at the next time point by substituting the time of the next observation into the general equation.

$$R_n = a_0 + a_1 t_n + a_2 t_n^2 + \ldots\ldots + a_N t_n^N$$
$$\dot{R}_n = a_1 + 2 a_2 t_n + \ldots\ldots\ldots + N a_N t_n^{N-1}$$

where:

t_n - time of the next observation

R_n - smoothed value of range at time t_n

$\dot{R}_n$ - smoothed value of range rate at time t_n

Since the on-board computer system cannot instantaneously perform the smoothing operation the smoothed values have been projected ahead to the next time point so that they can be used as the control variables in the firing laws while the present observations are being smoothed.

22.6 Corrections to Smoother Input for Firing

During periods when the control rockets of the chaser are firing, the acceleration of the chaser due to the firing is much greater than the acceleration due to orbital motion. This extra acceleration would normally tend to cause the smoother output to lag behind the actual values. However, since the firing laws allow the anticipation of firing from one time point to the next, the smoother input can be corrected to offset the effects of the added acceleration.

The noisy ranges can be adjusted by adding to each of the stored values an increment equal to the effects of the added acceleration applied over a time period from the projected time point to the time point associated with each stored value. Thus if the subscript 1 represented the oldest time point and the subscript M represented the most recent time point then the adjustment can be expressed as:

$$R_{ic} = R_i + (M - i + \tfrac{1}{2}) a \Delta t \qquad 1 \leq i \leq M$$

where:

R_{ic} - adjusted value of noisy range

R_i - uncorrected value of noisy range

a - acceleration due to rockets being fired

Δt - sample interval

These corrections are made to each of the components of range

whenever there is firing on that axis. The adjusted values of range are inputs to the smoother and serve to keep the smoothed values in phase with the actual values.

22.7 Transformations between Geocentric Coordinates and Orbital Elements[1]

Under the following subheadings methods are discussed for transforming geocentric coordinates to orbital elements and vice versa. Throughout this section a system of units is used in which the mean equatorial radius is set equal to one. The product of Newton's constant of gravitation and the mass of the earth, $K^2 M$, is also set equal to one. Symbols used in the following subheadings are defined as follows:

Z_1, Z_2, Z_3 - geocentric position components

$\dot{Z}_1, \dot{Z}_2, \dot{Z}_3$ - geocentric velocity components

The following six parameters are referred to as the orbital elements.

a - the length of the semi-major axis

e - the eccentricity of the ellipse

Ω - right ascension of ascending node (the ascending node is the point where the satellite crosses the $Z_1 - Z_2$ plane, equator, from south to north) $0 \leq \Omega < 2\pi$

i - inclination of the plane of the orbit to the $Z_1 - Z_2$ plane $0 \leq i \leq \pi$

W - argument of the perigee, the angle from the ascending node to the point of perigee $0 \leq W < 2\pi$

---

[1] Parts A, B and C of this section are extracted from Air Arm Report No. AA-2547-61 authored by Paul B. Davenport.

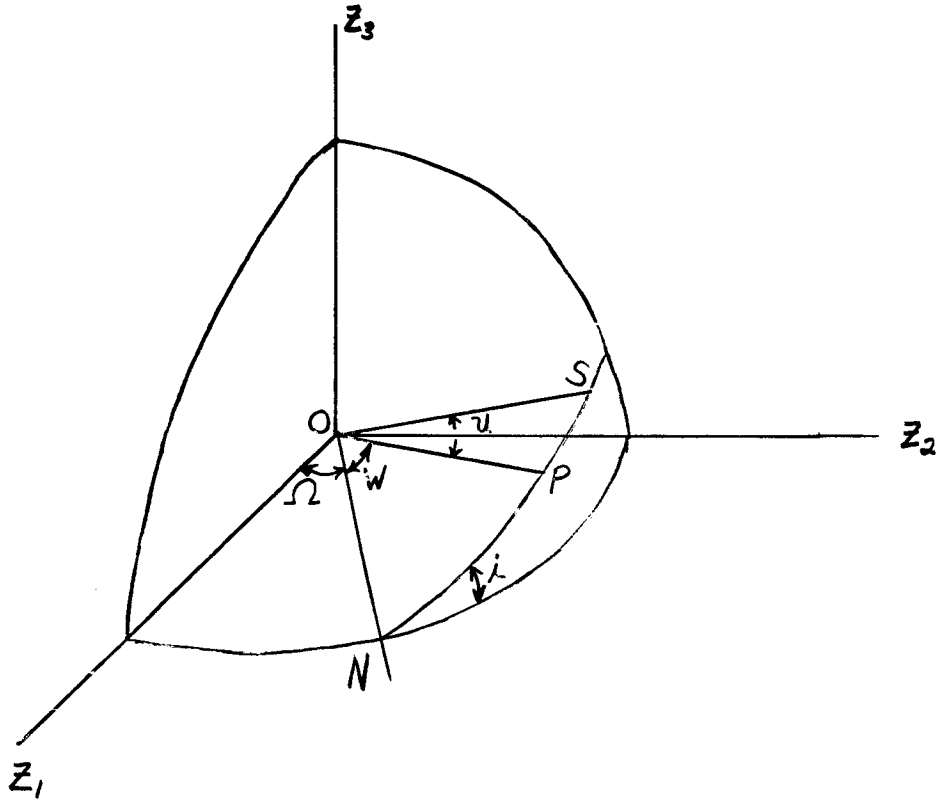

N - point of nodal crossing

P - point of perigee

S - satellite

w - NOP

u - POS

Figure 22-2

T_o - epoch for the coordinate system and the time perigee occurred.

The following auxiliary parameters are also often used.

P - period of the orbit

n - mean angular motion of the satellite in the plane of the orbit

T_n - Time of ascending node

A. Geocentric Rectangular Coordinates From Orbital Elements

The geocentric position, Z, and velocity $\dot{Z}$, are obtained from the elements a, e, Ω , i, w, and T_o (See Figure 22-2) at time t by the following:

$$n = a^{-3/2}$$

$$M = N\ (t - T_o)$$

the quantity M is known as the mean anomaly.

$$E = M + e \sin E$$

The equation above is Kepler's equation and must be solved for the eccentric anomaly E (See Part C). Once E has been obtained the sine and cosine of the true anomaly, u, (See Figure 22-3) and the length of radius vector r are given by

$$\sin u = \frac{\sqrt{1 - e^2} \sin E}{1 - e \cos E}$$

$$\cos u = \frac{\cos E - e}{1 - e \cos E}$$

$$r = a\ (1 - e \cos E)$$

Let

$$C_1 = \cos \Omega \cos (w + u) - \sin \Omega \cos i \sin (w + u)$$

S - satellite

C - center of ellipse

F - foci of ellipse (center of gravity)

E - eccentric anomaly

u - true anomaly

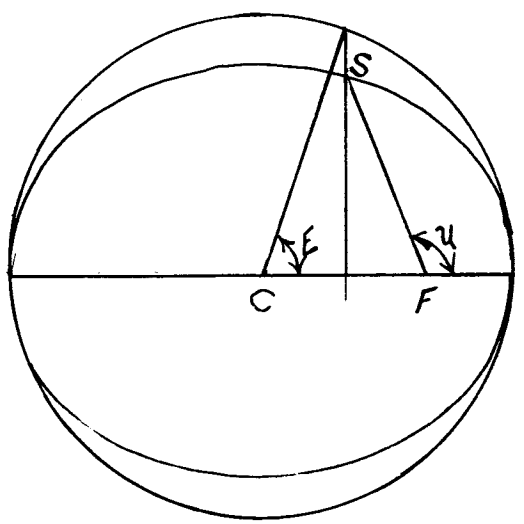

Figure 22-3

$$C_2 = \sin \Omega \cos(w + u) + \cos \Omega \cos i \sin (w + u)$$

$$C_3 = \sin i \sin(w + u)$$

(these are the direction consines of the satellite)

where

$$\sin(w + u) = \sin w \cos u + \cos w \sin u$$

$$\cos(w + u) = \cos w \cos u - \sin w \sin u$$

then

$$z_i = r\, c_i \qquad (i = 1, 2, 3)$$

$$b_1 = C_1 e \sin E - \sqrt{1 - e^2} \cos \Omega \sin(w + u) + \sin \Omega \cos i \cos(w + u)$$

$$b_2 = C_2 e \sin E - \sqrt{1 - e^2} \sin \Omega \sin(w + u) - \cos \Omega \cos i \cos(w + u)$$

$$b_3 = C_3 e \sin E + \sqrt{1 - e^2} \sin i \cos(w + u)$$

$$\dot{z}_i = \frac{\sqrt{a}}{r} b_i \qquad (i = 1, 2, 3)$$

Alternate expressions for the rates in terms of total velocity, V, but requiring further calculation are given below

$$V = \frac{\sqrt{a}}{r} \sqrt{1 - e^2 \cos^2 E}$$

$$s_i = \frac{b_i}{\sqrt{1 - e^2 \cos^2 E}} \qquad (i = 1, 2, 3)$$

(the s_i are direction cosines of the velocity vector)

$$\dot{z}_i = V s_i \qquad (i = 1, 2, 3)$$

In some instances the period, P, or mean motion, n, may be given

as an element instead of length of the semi-major axis, a. In either case a can be obtained by one or both of the following relationships:

$$n = \frac{2\pi}{P}$$

$$a = n^{-2/3}$$

The element T_n (time or ascending node) is often given rather than T_o (time of perigee). In this case T_o is obtained by the following relations:

$$E_w = \tan^{-1} \left(\frac{-\sin w \sqrt{1 - e^2}}{e + \cos w} \right)$$

$$\sin E_w = \frac{-\sin w \sqrt{1 - e^2}}{1 + e \cos w}$$

$$T_o = T_n - \left(\frac{E_w - e \sin E_w}{n} \right)$$

If E_w is in the third or fourth quadrant then it should be changed to a negative angle to make the time between T_n and T_o a minimum.

B. Orbital Elements From Geocentric Rectangular Coordinates

$$\Omega = \tan^{-1} \left[(z_2 \dot{z}_3 - z_3 \dot{z}_2)/(z_1 \dot{z}_3 - z_3 \dot{z}_1) \right]$$

$$i = \tan^{-1} \left[z_3/(z_2 \cos \Omega - z_1 \sin \Omega) \right]$$

$$\epsilon = w + u = \tan^{-1} \left[z_3/\sin i \, (z_1 \cos \Omega + z_2 \sin \Omega) \right]$$

$$r \dot{r} = z_1 \dot{z}_1 + z_2 \dot{z}_2 + z_3 \dot{z}_3$$

$$r^2 = z_1^2 + z_2^2 + z_3^2$$

$$V^2 = \dot{z}_1^2 + \dot{z}_2^2 + \dot{z}_3^2$$

$$a = \frac{1}{2/r - V^2}$$

$$e = 1/a \sqrt{a\,(r\dot{r})^2 + (a - r)^2}$$

If $e = 0$ then $w = 0$ and $M = E = u = \epsilon$

otherwise

$$E = \tan^{-1}\left[\sqrt{a}\, r\dot{r}/(a - r)\right]$$

$$u = \tan^{-1}\left[\sqrt{1 - e^2}\, \sin E \,/\, (\cos E - e)\right]$$

$$M = E - e \sin E$$

$$w = \epsilon - u$$

In either case T_o is found by the formulas

$$n = a^{-3/2}$$

$$T_o = t - \frac{M}{n}$$

Additional Relations

$$p = a(1 - e^2) \quad \text{(known as orbit parameter)}$$

$$r = \frac{p}{1 + e \cos u}$$

$$\dot{r} = \frac{\sqrt{a}\, e \sin E}{r} = \frac{a\, e\, n \sin E}{1 - e \cos E}$$

$$\sin u = \frac{\sqrt{a}\, \dot{r}\, (1 - e^2)^{3/2}}{e}$$

$$\cos u = \frac{p - r}{er}$$

$$\tan(u/2) = \sqrt{\frac{1+e}{1-e}}\,\tan(E/2) = \sqrt{\frac{1-\cos u}{1+\cos u}}$$

$$u = \tan^{-1}\left[\sqrt{1-e^2}\,\sin E/(\cos E - e)\right]$$

$$\dot{u} = \frac{\sqrt{a}\sqrt{1-e^2}}{r^2} = \frac{n\sqrt{1-e^2}}{(1-e\cos E)^2}$$

$$\sin E = \frac{\sqrt{1-e^2}\,\sin u}{1+e\cos u} = \frac{r\,\dot{r}}{\sqrt{a}\,e}$$

$$\cos E = \frac{e+\cos u}{1+e\cos u} = \frac{a-r}{a\,e}$$

$$\dot{E} = \frac{1}{r\sqrt{a}} = \frac{n}{1-e\cos E}$$

$$\frac{dr}{du} = \frac{r\,e\sin E}{\sqrt{1-e^2}}$$

$$V = \sqrt{r^2\,\dot{u}^2 + \dot{r}^2} = \sqrt{2/r - 1/a}$$

$$z_1\,\dot{z}_2 - z_2\,\dot{z}_1 = \sqrt{a}\,\sqrt{1-e^2}\,\cos i$$

$$z_2\,\dot{z}_3 - z_3\,\dot{z}_2 = \sqrt{a}\,\sqrt{1-e^2}\,\sin\Omega\,\sin i$$

$$z_1\,\dot{z}_3 - z_3\,\dot{z}_1 = \sqrt{a}\,\sqrt{1-e^2}\,\cos\Omega\,\sin i$$

$$e = \sqrt{\frac{a-p}{a}}$$

C. Solution of Kepler's Equation

$$E = M + e\sin E$$

Let

$$E_o = M + e\sin M\,(1 + e\cos M)$$

$$\Delta E = \frac{M - E_o + e\sin E_o}{1 - e\cos E_o}$$

$$E_1 = E_o + \Delta E$$

If E_1 and E_o agree to the accuracy wanted then E_1 is the desired approximation to E. If they do not agree then replace E_o by E_1 and compute a new E_1.

If the calculations are being done by hand the above process becomes more laborious as e approaches one. In this case a better value of E_o can be obtained by plotting the two curves:

$$y = \sin E$$

and

$$y = 1/e\ (E - M)$$

as a function of E. The abscissa of their point of intersection is the value of E satisfying the equation.

Another iteration which is simpler than the one above, but requiring more iterations for the same accuracy is

$$E_{i+1} = M + e \sin E_i$$

22.8 Modifications for Simulation of Earth Rendezvous

The digital computer program for the lunar rendezvous simulation was modified to simulate an earth rendezvous technique. All input and initialization procedures remained the same with the exception that the orbits of both vehicles were changed to posigrade and the nominal altitudes for the target and chaser parking orbits were set at 500 and 200 km. respectively.

The different firing laws being used in this system require the introduction of several different variables. The angle D (See Figure 22-4) is defined as the angle between the range vector from chaser to target and the positive x axis and can be expressed as:

$$D = \tan^{-1} \left(\frac{y_T - y_c}{x_T - x_c} \right)$$

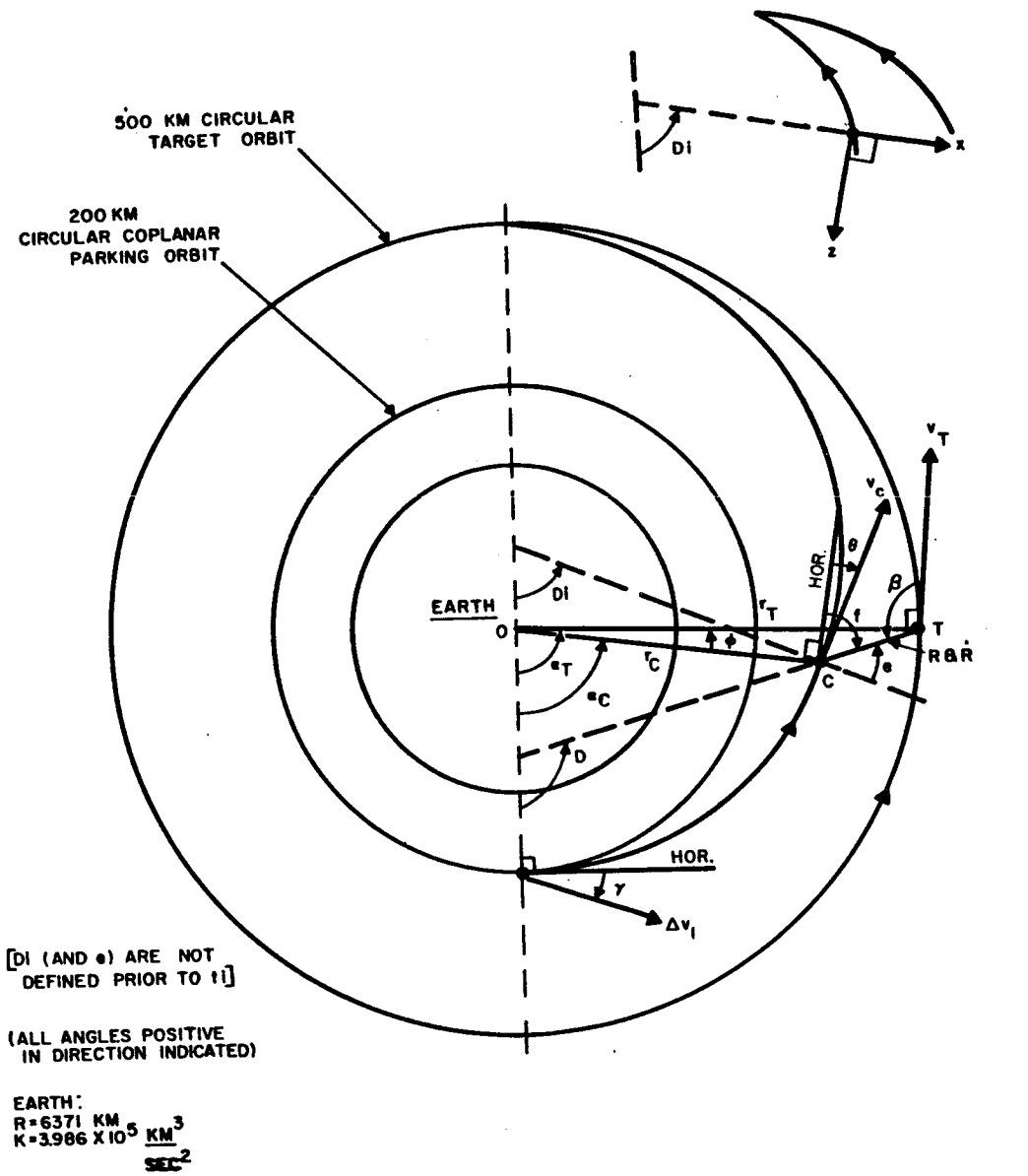

FIGURE 22-4. Orbit Diagram
(Earth Space Station Rendezvous)

This page intentionally left blank

where y_T, x_T, y_c, and x_c are the geocentric coordinates of the target and chaser.

When the target-chaser range has been reduced to 25 km., the angle D is used as a reference for locking the on-board coordinate system. Let the angle D_i be set equal to D at the time the target-chaser range is 25 km. Then the positive x' axis is locked in position at an angle D_i to the x axis. The positive Z' axis is perpendicular to the x' axis and is in the orbital plane opposite to the direction of motion. The elevation angle e (See Figure 22-4) is then defined as in the lunar case, that is, it is the angle between the positive x' axis and range vector from chaser to target.

The variables of control used in the firing laws are the range between the two vehicles R, the closing rate $\dot{R}$, and the rate of change of elevation angle $\dot{e}$. In simulating the firing laws the smoothed values of R, $\dot{R}$, and $\dot{e}$ are always used. The firing laws used in the simulation are designed to hold the elevation angle close to zero by firing along the Z' axis until the range and range rate can be driven to zero by firing along the x' axis.

If the rate of change of elevation angle becomes greater in magnitude than .3 milliradians per second, a z' acceleration of the following direction and duration will be applied.

$$t_F = .9 \; R \left| \frac{\dot{e}}{a_z} \right|$$

$$a_z = - a_{z_0} \frac{\dot{e}}{|\dot{e}|}$$

$a_{z_0} = 1$ m/sec^2 (acceleration due to thrust level of Z' rockets)

The x' axis firings are designed to drive R and $\dot{R}$ to zero between the two curves represented by the following inequality:

$$-\sqrt{K_2 \, |R - R_f|} \leq \dot{R} \leq -\sqrt{K_1 \, |R - R_f|}$$

where

$K_2 = 2.25 \text{ m/sec}^2$

$K_1 = 1.5 \text{ m/sec}^2$

R_f - standoff range (has been set to 200 meters)

Firings on the x' axis are triggered when:

$$\dot{R} \leq -\sqrt{K_2 \, |R - R_f|}$$

Under these conditions a negative acceleration, a_x, of -1.5 m/sec^2 is applied for the following duration of time.

$$t_f = \frac{2 \left| -\sqrt{K_1 \, |R - R_f|} - \dot{R} \right|}{|a_x|}$$

As in the lunar case several additional restrictions are superimposed on the firing laws. There must be at least a five second time delay between z' firings and at least a two second delay between x' firings . All computed firings of less than two seconds duration are suppressed. When the range rate has been driven to less than one meter per second the rendezvous maneuver is considered to be completed and the program is stopped.

The corrections to the orbit of the chaser are performed in a manner very similar to that described for the lunar rendezvous in Section 22.4. That is, the effects of the x' and z' firings are resolved back into the geocentric coordinate system and superimposed on the chaser position and velocity vectors. A new set of orbital elements for the chaser is then calculated using the method described in Section 22.7, Part B.

The noise generation and smoothing is also handled in a very similar manner to the method described in Section 22.5. White noise of a specified standard deviation is superimposed on the actual values of range and elevation and these noisy values are input to the smoother to obtain smoothed values of R, $\dot{R}$, and $\dot{e}$ which are used as the control variables in the firing laws.

The noisy range inputs to the smoother are adjusted for the effects of firing in the same manner as described in Section 22.6. However, the required adjustment to the noisy angle is slightly different. If the subscript 1 represents the oldest time point and the subscript M represents the most recent time point then the adjustment can be expressed as

$$e_{ic} = e_i + (M - i + \tfrac{1}{2}) \frac{a \Delta t^2}{R} \qquad 1 \leq i \leq M$$

where:

e_{ic} - adjusted value of noisy elevation

e_i - uncorrected value of noisy elevation

a - acceleration normal to the range vector

Δt - sample interval

These corrections are made whenever there is a component of acceleration normal to the range vector. Corrections are made to the noisy range inputs whenever there is a component of acceleration parallel to the range vector.

This page intentionally left blank

23.0 Appendix V: Lunar Ascent Trajectory

23.1 Appendix V-A: Velocity Requirements for Minimum Fuel Trajectories Between Two Circular Co-planar Orbits with Arbitrary Terminals

Problem definition consists of determining the minimum total velocity impulse for a theoretical 2-impulse transfer between co-planar circular orbits with arbitrary terminals. As stated in section 8.4.2.2, only two geometrical restrictions are implied: tangential capture (or apogee) at the target orbit, and intersection with the inner orbit.

In addition to the exact solution, an approximate solution is given for obtaining quick and accurate estimates for cases where the radii ratio is near unity and the central transfer angle is above 40°. For transfers below 40°, severe fuel requirements are imposed on the interceptor for cirlce-to-circle transfer.

Nomenclature:

V_T = circular target velocity

V_P = circular parking velocity

V_2 = elliptical velocity at apogee (point 2)

V_1 = elliptical velocity at injection (point 1)

$\Delta v_2 = v_T - v_2$ = velocity increment required at point 2.

$\Delta v_1 = |\underset{\sim}{v}_1 - \underset{\sim}{v}_P|$ = velocity increment required at point 1.

$\Delta v = \Delta v_1 + \Delta v_2$ = total velocity increment.

r_2 = target orbit radius

r_1 = parking orbit radius

ϕ = true anomaly between injection and target contact

μ = gravit. constant

a = semi-major axis of transfer ellipse

γ = flight path angle

$\rho = r_2 - r_1$

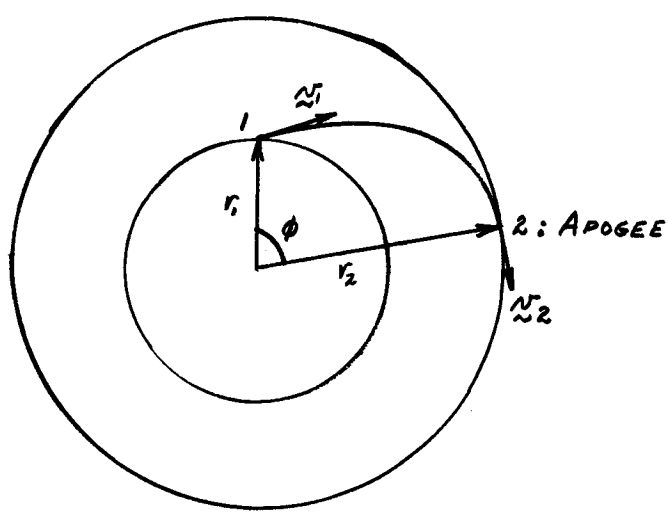

FIGURE 23.1-1: Tangential Capture for Transfer Between Circular Orbits

To obtain the total velocity increment, consider the following relationships available from orbital mechanics,

$$(1)\ v = \sqrt{\mu\left(\frac{2}{r} - \frac{1}{a}\right)} = \frac{\sqrt{\mu a\,(1 - e^2)}}{r \cos \gamma}$$

Substituting into the velocity increment required at point 2 and normalizing with respect to the target,

$$(2)\quad \frac{\Delta v_2}{v_T} = 1 - \frac{v_2}{v_T} = 1 - \sqrt{2 - \frac{r_2}{a}}$$

The cosine law yields $\frac{\Delta v_1}{v_T}$:

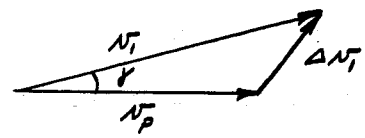

$$(3)\quad \frac{\Delta v_1}{v_T} = \sqrt{\left(\frac{v_1}{v_T}\right)^2 + \left(\frac{v_p}{v_T}\right)^2 - 2\cos\gamma\,\frac{v_1 v_p}{v_T^2}}$$

Substituting (1) in (3)

$$(4)\quad \frac{\Delta v_1}{v_T} = \sqrt{3\frac{r_2}{r_1} - \frac{r_2}{a} - 2\frac{r_2}{r_1}\sqrt{\frac{a}{r_1}(1-e^2)}}$$

To eliminate a and e and obtain ϕ as an independent variable, two additional equations for the ellipse are required. Imposing the minimum fuel constraint, i.e., target radius equalling transfer apogee,

$$r_2 = a\,(1 + e)$$

and at injection,

$$r = r_1 = \frac{r_2\,(1 - e)}{1 - e\cos\phi}$$

Substituting these two equations into (2) and (4), and summing to obtain the total required velocity increment,

$$(5)\quad \frac{\Delta v}{v_T} = 1 - x + \sqrt{3K - 2 + x^2 - 2K^{3/2}x}$$

$$\text{where } x = \frac{1 - \cos\phi}{K - \cos\phi}$$

$$K = \frac{r_2}{r_1}$$

The above differences under the radical are very small when the radii ratio is nearly unity and hence double precision on a digital computer was required to obtain graphical results appearing in Fig. 23.1-2. Comparison between Δv and the required total Hohmann increment $\Delta V_{HOH.}$ was obtained by simply normalizing the computer program yielding $\Delta v/\Delta V_{HOH.}$.

The following analysis provides a workable analytical approximation of $\Delta v/\Delta V_{HOH.}$, not requiring a digital computer program. The results are justified graphically by comparison with the above exact derivation.

The authors in ref.8-15 have provided a first-order linear approximation to the relationships between the initial and final state variations for low-eccentricity orbits. A discussion of their results and equations as well as similar work by other authors appears in Appendix V-C. Only the relevant equations in ref.8-15 will be used in this derivation. These are given as follows:

$$(6)\quad \Delta r = (2-\cos M)\Delta r_o + 2r\,(1-\cos M)\frac{\Delta v_x}{v} + r \sin M\,\frac{\Delta v_y}{v}$$

$$(7)\quad \Delta \dot{r} = 2\Delta v_x \sin M + \Delta v_y \cos M$$

where

r, v = initial circular parameters

Δr_o = initial radial variation

Δv_x = initial tangential velocity variation

Δv_y = initial radial velocity variation

M = mean anomaly between initial and final states

$\Delta r, \Delta \dot{r}$ = final state variations in radius and radial velocity

Note that all deviations are relative to a circular orbit. It is therefore expected that transfer trajectories of high eccentricity, obtained from a linear perturbation of a circular orbit should be very inaccurate, i.e., orbits requiring small transfer angles. Since the fuel penalty may be prohibitive at these angles, linearization is justified for the region under consideration.

To find the injection impulse, consider first a perturbation of the parking orbit. Since an initial altitude variation is not relevant $\Delta r_o = 0$, and, for tangential capture at the target orbit $\Delta \dot{r} = 0$. But Δr is constrained as the difference in radii between target and parking orbits, $\Delta r = r_2 - r_1 = \rho$. Substitution of the above into equations (6) and (7) yields,

$$(8) \quad \frac{\rho}{r_1} = 2\,(1 - \cos M)\,\frac{\Delta v_x}{v_p} + \sin M\,\frac{\Delta v_y}{v_p}$$

$$(9) \quad \frac{\Delta v_y}{\Delta v_x} = -2 \tan M$$

Elimination of Δv_x gives,

$$(10) \quad \frac{\Delta v_y}{v_p} = \frac{\rho}{2\,r_1}\,\frac{1}{1 - \sec M}$$

But, Δv_y is simply the normal component of the required injection impulse, $\Delta v_x = \Delta v_1 \cos \alpha_1$

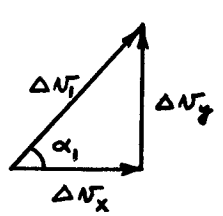

Also, from (9), $\dfrac{\Delta v_y}{\Delta v_x} = \tan \alpha_1 = -2 \tan M$

Solving (10) by eliminating α_1 and Δv_y, the initial required impulse is

$$(11) \quad \frac{\Delta v_1}{v_p} = \frac{\rho}{2\,r_1}\,\frac{\sqrt{4 - 3\cos^2 M}}{1 - \cos M}$$

The final impulse is found by simply reversing the logic, i.e., considering perturbations of the outer orbit. Since the only perturbed quantity is the tangential velocity, equation (6) takes the form,

$$(12) \quad \frac{\rho}{r_2} = 2\left[1 - \cos(-M)\right]\frac{\Delta v_2}{v_T}$$

where

$$\Delta v_y = 0 \quad \text{(orbital contact at apogee)}$$

$$\Delta v_2 = v_T - v_2$$

$$\Delta r_o = 0$$

$$\Delta r = -(r_1 - r_2) = \rho$$

$$(13) \quad \therefore \frac{\Delta v_2}{v_T} = \frac{\rho}{2r_2}\,\frac{1}{1 - \cos M}$$

Summing the two normalized impulses,

$$(14) \quad \frac{\Delta v}{v_T} = \frac{\rho}{2(1 - \cos M)}\left[\frac{1}{r_1}\,\frac{v_p}{v_T}\sqrt{4 - 3\cos^2 M} + \frac{1}{r_2}\right]$$

But, for circular orbits, $v = \sqrt{\frac{\mu}{r}}$

$$\therefore \frac{v_p}{v_T} = \frac{r_2}{r_1}$$

$$(15) \quad \therefore \frac{\Delta v}{v_T} = \frac{\rho}{2r_2(1 - \cos M)}\left[\left(\frac{r_2}{r_1}\right)^{3/2}\sqrt{4 - 3\cos^2 M} + 1\right]$$

Normalizing with respect to the Hohmann transfer M = 180°,

$$(16) \quad \frac{\Delta v}{\Delta v_{HOH.}} = \frac{2}{1 - \cos M}\left[\frac{\left(\frac{r_2}{r_1}\right)^{3/2}\sqrt{4 - 3\cos^2 M} + 1}{\left(\frac{r_2}{r_1}\right)^{3/2} + 1}\right]$$

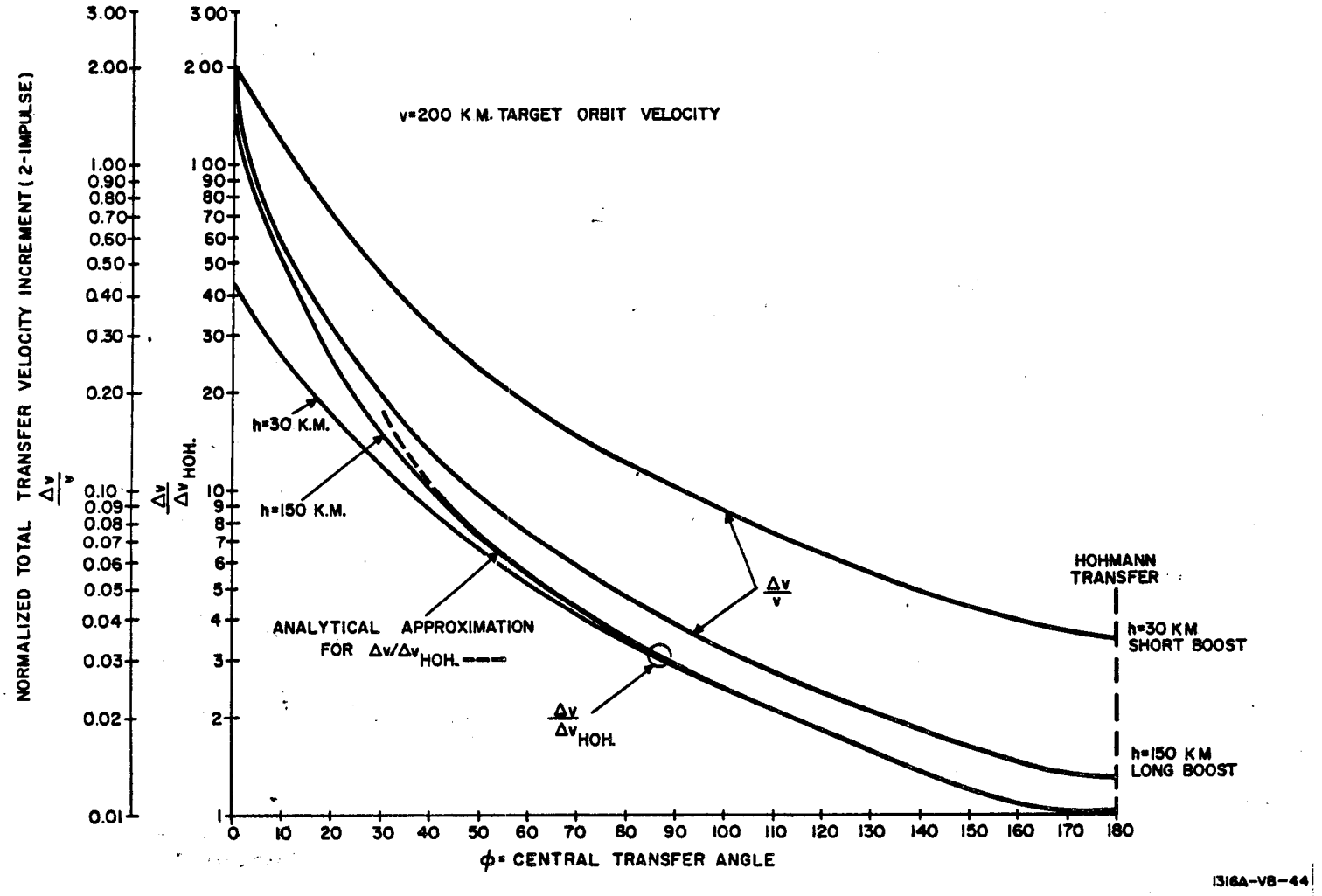

FIGURE 21.3-2: Total Required Velocity Increment for Minimum Energy Circle-to-Circle Transfer

As a first order approximation, let $r_1 \cong r_2$. Also, for low eccentricity orbits, take $M \cong \phi$. Hence,

$$(17)\quad \frac{\Delta V}{\Delta V_{HOH.}} = \frac{1 + \sqrt{4 - 3\cos^2\phi}}{1 - \cos\phi}$$

Although analytical justification for the above assumptions is not presumed, it is evident from a graphical comparison with the exact results (see Fig. 23.1-2) that the approximate equation is more than adequate in the region under consideration, i.e., transfers over 40°. Since it is a simple matter to calculate ΔV for a Hohmann transfer, equation (17) is extremely useful for quick and accurate estimates of the fuel penalty for various central transfer angles.

23.2 Appendix V-B: Determination of Thrust Acceleration Components

Referring to Figure 8.4-1 and Section 8.4.2.4, the thrust components, A_x and A_z are determined as follows:

$$A_x = g_\ell \frac{T}{W_\ell} \cos\psi \qquad A_z = g_\ell \frac{T}{W_\ell} \sin\psi$$

where

T = constant thrust

$W = W_o - \dot{W} t$

$\dot{W}$ = constant weight flow rate

$$\bar{t} = \frac{W_o}{\dot{W}} = \frac{g_\oplus}{g_\ell} \frac{I_{sp}}{T/W_{o_\ell}}$$

$\tan\psi = a - b\,(t - t_1)$ for $t \geq t_1$

$\psi = 90°$ for $0 \leq t < t_1$

t_1 = initial vertical flight time

Substituting into the above thrust components,

$$A_x = \frac{T}{W_{o_\ell}} \frac{g_\ell}{g_\oplus} \left[\frac{\cos\psi}{1 - t/\bar{t}}\right] \text{ in earth g's}$$

$$A_z = \frac{T}{W_{o_\ell}} \frac{g_\ell}{g_\oplus} \left[\frac{\sin\psi}{1 - t/\bar{t}}\right] \text{ in earth g's}$$

Using the trajectory constants given in Table 8.4-1, $\sin\psi$ and $\cos\psi$ were computed for 30 second increments in time for both trajectories. The thrust components were then computed and graphed, see Figure 8.4-4.

23.3 Appendix V-C: Error Sensitivity for Near-Circular Orbits

Since miss distances and velocities at boost cut-off are given in rectangular coordinates, it is preferable to use the results of an analysis in which the initial state variations are also expressed in rectangular coordinates. Such an analysis is found in reference 8-15.

Referring to Figure 23.3-1 for parameter definition, the in-plane analysis could begin with the functional relation,

$$r = r\,(r_o,\ V_{T_o},\ V_{r_o})$$

$$\phi = \phi\,(r_o,\ V_{T_o},\ V_{r_o})$$

Differentiation then yields the error functions,

$$\Delta r = \frac{\partial r}{\partial r_o}\Delta r_o + \frac{\partial r}{\partial V_{T_o}}\Delta V_{T_o} + \frac{\partial r}{\partial V_{r_o}}\Delta V_{r_o}$$

$$\frac{\Delta s}{r} = \Delta\phi = \frac{\partial \phi}{\partial r_o}\Delta r_o + \frac{\partial \phi}{\partial V_{T_o}}\Delta V_{T_o} + \frac{\partial \phi}{\partial V_{r_o}}\Delta V_{r_o}$$

Velocity error equations could be obtained by differentiating the above coefficients with respect to time,

$$\Delta \dot{r} = \Delta V_r = \Delta r_o \frac{\partial}{\partial t}\left[\frac{\partial r}{\partial r_o}\right] + \Delta V_{T_o}\frac{\partial}{\partial t}\left[\frac{\partial r}{\partial V_{T_o}}\right] + \Delta V_{r_o}\frac{\partial}{\partial t}\left[\frac{\partial r}{\partial V_{r_o}}\right]$$

$$r\Delta\dot{\phi} = \Delta V_T = r\Delta r_o \frac{\partial}{\partial t}\left[\frac{\partial \phi}{\partial r_o}\right] + r\Delta V_{T_o}\frac{\partial}{\partial t}\left[\frac{\partial \phi}{\partial V_{T_o}}\right] + r\Delta V_{r_o}\frac{\partial}{\partial t}\left[\frac{\partial \phi}{\partial V_{r_o}}\right]$$

The errors perpendicular to the nominal trajectory plane could be obtained similarly:

$$y = y\,(y_o,\ V_{N_o})$$

$$\Delta y = \frac{\partial y}{\partial y_o}\,\Delta y_o + \frac{\partial y}{\partial V_{N_o}}\,\Delta V_{N_o}$$

$$\Delta \dot{y} = \Delta V_N = \Delta y_o \frac{\partial}{\partial t}\left[\frac{\partial y}{\partial y_o}\right] + \Delta V_{N_o} \frac{\partial}{\partial t}\left[\frac{\partial y}{\partial V_{N_o}}\right]$$

In matrix form, the results of an equivalent analysis are (Ref. 8-15).

$$\begin{bmatrix} \Delta r/r \\ \Delta s/r \\ \Delta y/r \\ \Delta V_r/V \\ \Delta V_T/V \\ \Delta V_N/V \end{bmatrix} = \begin{bmatrix} 2-\cos\phi & 0 & 0 & \sin\phi & 2(1-\cos\phi) & 0 \\ 2\sin\phi - 3\phi & 1 & 0 & -2(1-\cos\phi) & -3(\phi-4\sin\phi) & 0 \\ 0 & 0 & \cos\phi & 0 & 0 & \sin\phi \\ \sin\phi & 0 & 0 & \cos\phi & 2\sin\phi & 0 \\ 2\cos\phi - 3 & 0 & 0 & -2\sin\phi & -3+4\sin\phi & 0 \\ 0 & 0 & -\sin\phi & 0 & 0 & \cos\phi \end{bmatrix} \begin{bmatrix} \Delta r_o/r \\ \Delta s_o/r \\ \Delta y_o/r \\ \Delta V_{r_o}/V \\ \Delta V_{T_o}/V \\ \Delta V_{N_o}/V \end{bmatrix}$$

In the above matrix, it was assumed that the mean anomaly may be replaced by the true anomaly. Curiously, the error coefficients given in refs. 8-4, 16, and 15 take similar forms, but in the first two, the coefficients are functions of the true anomaly. The true anomaly is, of course, easier to illustrate. For purposes of this study, the errors in using the above assumption should be negligible in terms of boost sensor and total fuel requirements. Results are graphed in Figures 8.5-2 and 8.5-3.

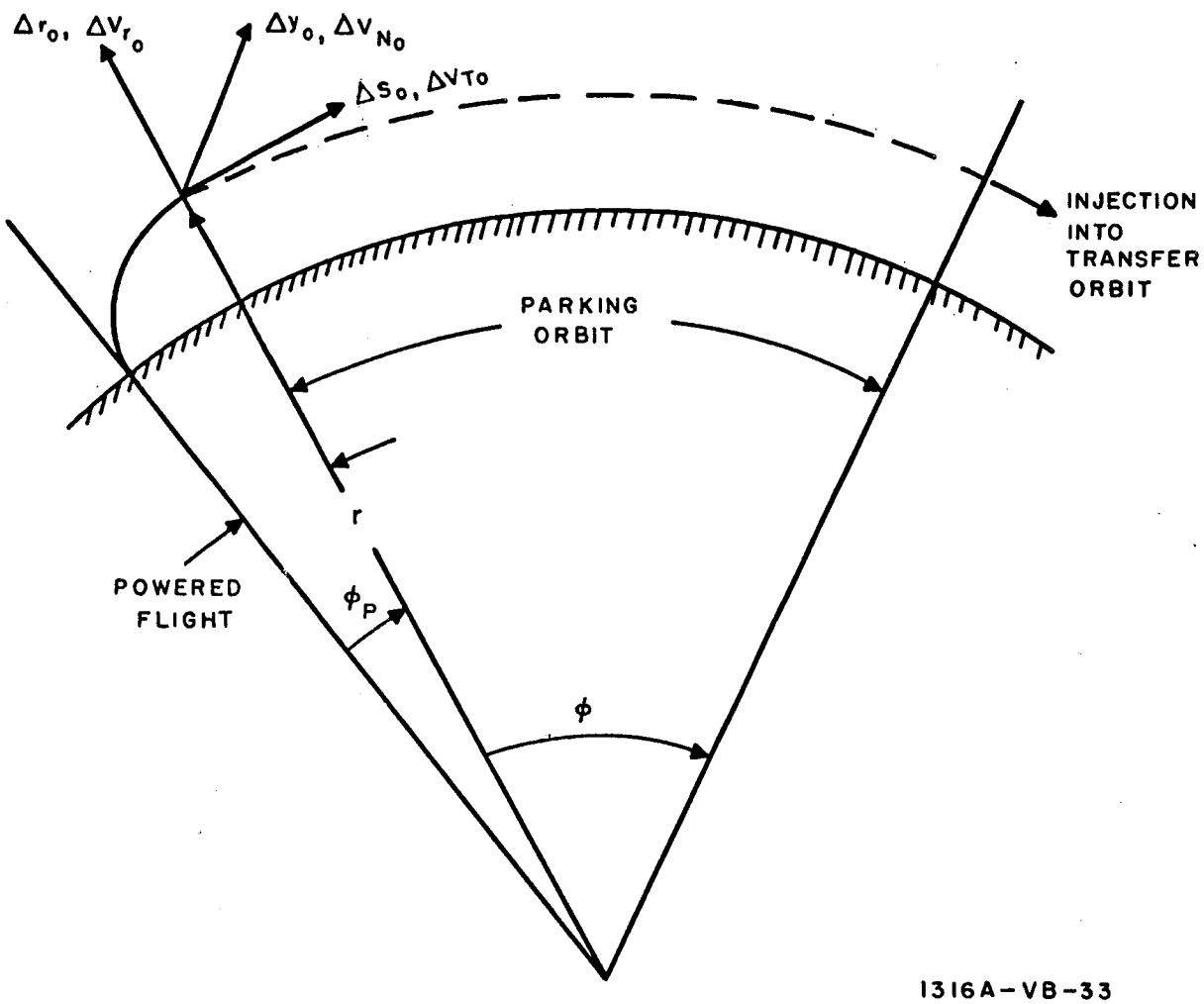

FIGURE 23.3-1: Coordinate System for Small Perturbations of Circular Orbits

23.4 Appendix V-D: Error Analysis for Space-Stabilized Inertial Navigation System

Figure 23.4-1 illustrates the system and defines the coordinate frame to which the system is referenced. This frame is the same as that given for the boost trajectory definition (Fig 8 4-2).

The following is a description of the mechanism of error propagation of each individual component within the system. The most significant error sources are given in Table 23.4-1. Much of the notation and description is taken directly from Pitman, ref. 8-6. A more detailed description is, of course, presented in his text.

A. Accelerometer:

It is possible to represent the errors associated with a typical integrating accelerometer as illustrated in Fig. 23.4-1 of a polynominal expansion of the actual thrust acceleration and other linear and non-linear functions of acceleration, time, and velocity, e.g.,

$$\Delta A_i = a_{0i} + a_{1i} A_i + a_{2i} A_j + a_{3i} A_i A_j + a_{4i} A_k + a_{5i} A_i A_k + a_{6i} A_i^2 + a_{7i} A_i^3$$

where i, j, k take on only cyclic permutations of x, y, and z.

The coefficients a_{0i}.... are defined in Table 23 4-1. Integration provides velocity and position errors, or

$$\Delta V_i = \int_0^t \Delta A_i \, dt$$

$$\Delta S_i = \int_0^t \Delta V_i \, dt$$

By neglecting the non-linear acceleration products (the last two terms), the following results are immediately available if the coefficients are assumed to

TABLE 23.4-1

Inertial Measurement Error Sources

Error Source	Symbol	Units
A. Accelerometers	X_A, Y_A, Z_Z	
1. Bias (along input axis, i)	a_o	g
2. Scale factor(along input axis, i)	a_1	g/g
3. Cross-Axis sensitivity		
a. Along perpendicular axis, j		
Bias	a_2	g/cross g
Scale factor	a_3	g/g/cross g
b. Along perpendicular axis, k		
Bias	a_4	g/cross g
Scale factor	a_5	g/g/cross g
B. Gyro	X_G, Y_G, Z_G	
1. Fixed Drift (about input axis)	b_o	deg./hr.
2. Mass Unbalance	b_1, b_2	deg/hr./g
3. Anisoelasticity	b_3	deg/hr./g^2
C. Platform		
1. Initial Misalignment	ϕ (o)	arc-sec.
2. Servo Error	e	arc-sec.

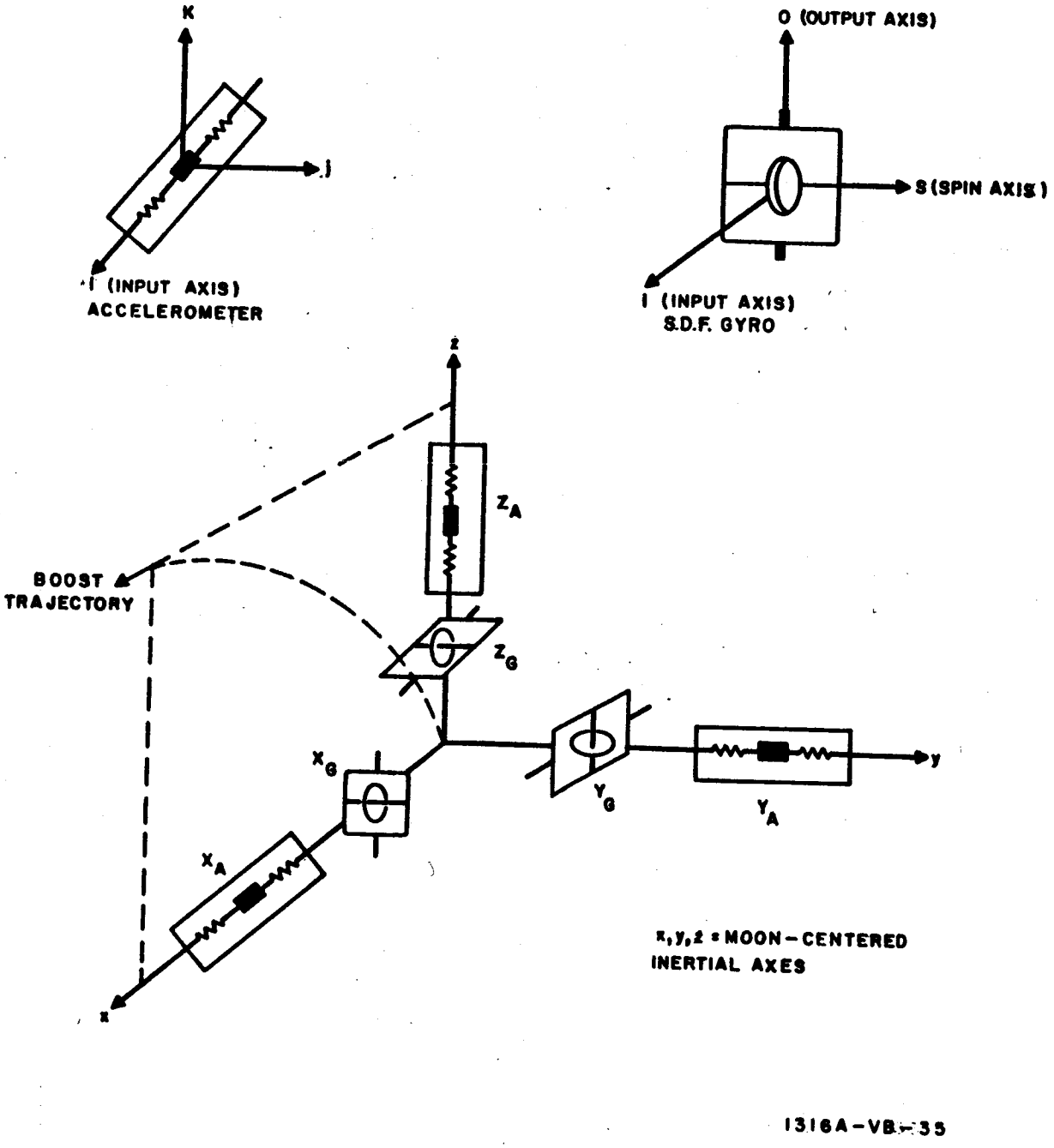

FIGURE 23.4-1: Orientation and Axes Definition of Inertial Sensors and Space Stabilized Platform

have constant average values:

$$\Delta V_x = a_{0x} t + a_{1x}\int_0^t A_x\,dt + a_{2x}\int_0^t A_y\,dt + a_{3x}\int_0^t A_x A_y\,dt + a_{4x}\int_0^t A_z\,dt + a_{5x}\int_0^t A_x A_z\,dt$$

$$\Delta V_y = a_{0y} t + a_{1y}\int_0^t A_y\,dt + a_{2y}\int_0^t A_z\,dt + a_{3y}\int_0^t A_y A_z\,dt + a_{4y}\int_0^t A_x\,dt + a_{5y}\int_0^t A_y A_x\,dt$$

ΔV_z is found similarly. Position errors are found by a second integration:

$$\Delta S_x = a_{0x}\frac{t^2}{2} + a_{1x}\int_0^t V_x\,dt + a_{2x}\int_0^t V_y\,dt + a_{3x}\int_0^t\left[\int_0^t A_x A_y\,dt\right]dt + a_{4x}\int_0^t V_z\,dt + a_{5x}\int_0^t\left[\int_0^t A_x A_z\,dt\right]dt$$

and similarly for ΔS_y and ΔS_z.

It is evident that each of the trajectory dependent coefficients may be tabulated in integral form. Referring to Table 23.4-2, the general results with $A_y = 0$ are:

$$\Delta V_x = a_{0x} t + a_{1x} I_1 + a_{4x} I_3 + a_{5x} I_{11}$$

$$\Delta V_y = a_{0y} t + a_{2y} I_3 + a_{4y} I_1$$

$$\Delta V_z = a_{0z} t + a_{1z} I_3 + a_{2z} I_1 + a_{3z} I_{11}$$

VELOCITY COEFF. INTEGRALS *					POSITION COEFF. INTEGRALS *				
SYMBOL	INTEGRAL	VALUE SHORT BOOST	VALUE LONG BOOST	UNITS	SYMBOL	INTEGRAL	VALUE SHORT BOOST	VALUE LONG BOOST	UNITS
I_1	$\int_0^t Axdt = Vx$	124.1	152.6	g-SEC	${}_1I_1$	$\int_0^t I_1\,dt$	12.5×10^3	23.5×10^3	g-SEC^2
I_2	$\int_0^t Aydt = Vy$	0	0	g-SEC	${}_2I_2$	$\int_0^t I_2 dt$	0	0	g-SEC^2
I_3	$\int_0^t Azdt = Vz$	38.5	61.9	g-SEC	${}_3I_3$	$\int_0^t I_3 dt$	4.39×10^3	26.57×10^3	g-SEC^2
I_4	$\int_0^t Axtdt$	21.9×10^3	47.0×10^3	g-SEC^2	${}_4I_4$	$\int_0^t I_4 dt$	14.2×10^5	54.3×10^5	g-SEC^3
I_5	$\int_0^t Aytdt$	0	0	g-SEC^2	${}_5I_5$	$\int_0^t I_5 dt$	0	0	g-SEC^3
I_6	$\int_0^t Aztdt$	2.44×10^3	2.05×10^3	g-SEC^2	${}_6I_6$	$\int_0^t I_6\,dt$	3.50×10^5	32.77×10^5	g-SEC^3
I_7	$\int_0^t VxAzdt$	2.71×10^3	-1.67×10^3	g^2-SEC^2	${}_7I_7$	$\int_0^t I_7 dt$	3.55×10^5	3.54×10^5	g^2-SEC^3
I_8	$\int_0^t VzAxdt$	4.08×10^3	11.13×10^3	g^2-SEC^2	${}_8I_8$	$\int_0^t I_8 dt$	3.37×10^5	14.76×10^5	g^2-SEC^3
I_9	$\int_0^t VzAzdt$	12.9×10^3	45.5×10^3	g^2-SEC^2	${}_9I_9$	$\int_0^t I_9\,dt$	8.56×10^5	9.55×10^5	g^2-SEC^3
I_{10}	$\int_0^t AxAydt$	0	0	g^2-SEC	${}_{10}I_{10}$	$\int_0^t I_{10} dt$	0	0	g^2-SEC^2
I_{11}	$\int_0^t AxAzdt$	24.58	2.94	g^2-SEC	${}_{11}I_{11}$	$\int_0^t I_{11} dt$	1.99×10^3	4.69×10^3	g^2-SEC^2
I_{12}	$\int_0^t AyAzdt$	0	0	g^2-SEC	${}_{12}I_{12}$	$\int_0^t I_{12} dt$	0	0	g^2-SEC^2

* EVALUATED BETWEEN LAUNCH AND THRUST CUT-OFF.

TABLE 23.4-2: MISS COEFFICIENT INTEGRAL SET FOR SENSOR AND PLATFORM ERROR-FORCING FUNCTIONS

1316A-VB-30

and for position errors,

$$\Delta S_x = a_{0x}\frac{t^2}{2} + a_{1x\,1}I_1 + a_{4x\,3}I_3 + a_{5x\,11}I_{11}$$

$$\Delta S_y = a_{0y}\frac{t^2}{2} + a_{2y\,3}I_3 + a_{4y\,1}I_1$$

$$\Delta S_z = a_{0z}\frac{t^2}{2} + a_{1z\,3}I_3 + a_{2z\,1}I_1 + a_{3z\,11}I_{11}$$

B. Gyros:

A S.D.F. gyro error model may be represented by the following equation, see Fig. 23.4-1,

$$\dot{\phi}_i = b_{oi} + b_{1i}^{s} A_i + b_{2i}^{i} A_S + b_{3i} A_i A_S$$

where:

$\dot{\phi}_i$ = drift rate about the input axis

b_{1i}^{s}, b_{2i}^{i} = g-sensitive drift rate coefficients about the spin and input axes respectively

b_{3i} = g^2- sensitive drift rate coefficient as caused by anisoelastic effects

To treat the misalignment effects independently that each gyro has on each axis, the following error angles are defined in accordance with Fig. 23.4-2:

x-axis: $\phi_{xy} = \int_0^t \dot{\phi}_z \, dt$ $\qquad$ $\phi_{xz} = \int_0^t \dot{\phi}_y \, dt$

y-axis: $\phi_{yx} = \int_0^t \dot{\phi}_z \, dt$ $\qquad$ $\phi_{yz} = \int_0^t \dot{\phi}_x \, dt$

z-axis: $\phi_{zx} = \int_0^t \dot{\phi}_y \, dt$ $\qquad$ $\phi_{zy} = \int_0^t \dot{\phi}_x \, dt$

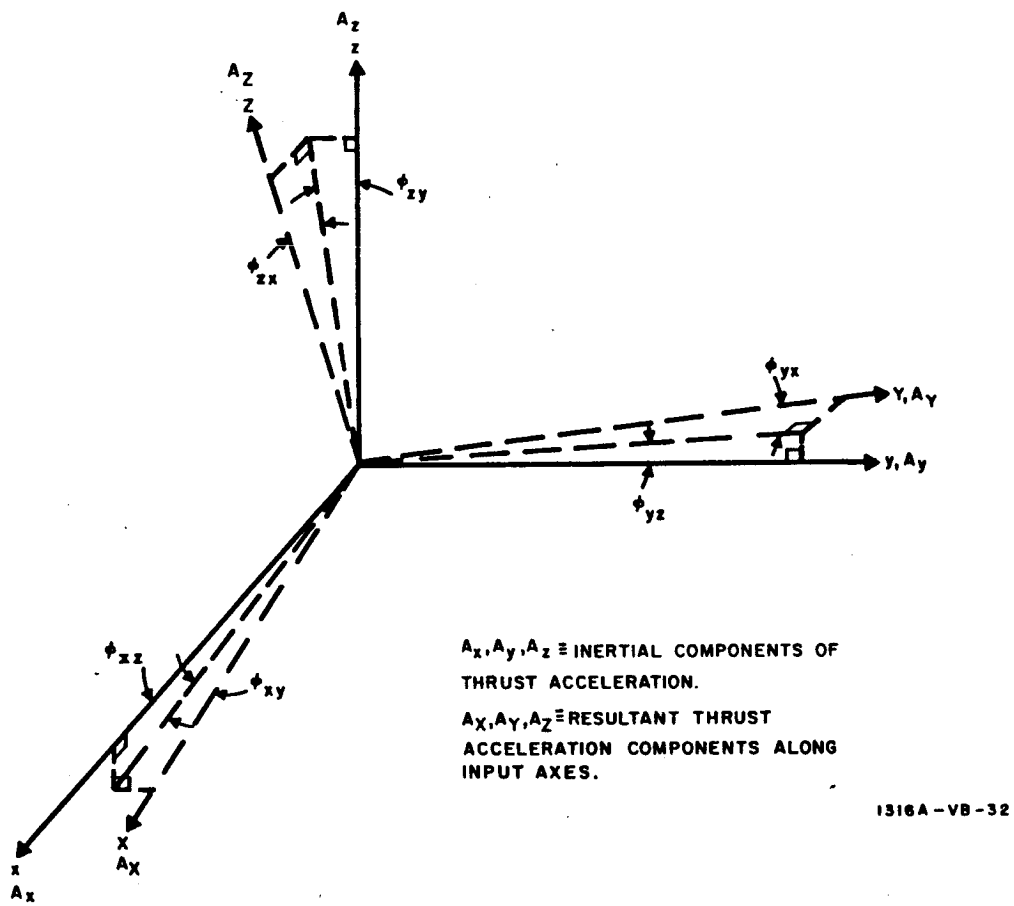

FIGURE 23.4-2: Misalignment Angles of Accelerometer Input Axes

where the drift rates for each gyro in the selected configuration are:

$$X_G: \quad \dot{\phi}_x = b_{ox} + b_{1x}^{y} A_x + b_{2x}^{x} A_y + b_{3x} A_x A_y$$

$$Y_G: \quad \dot{\phi}_y = b_{oy} + b_{1y}^{z} A_y + b_{2y}^{y} A_z + b_{3y} A_y A_z$$

$$Z_G: \quad \dot{\phi}_z = b_{oz} + b_{1z}^{y} A_z + b_{2z}^{z} A_y + b_{3z} A_z A_y$$

Since the accelerometer input axes displace by the amount designated by each misalignment angle, it is necessary to obtain the sensed accelerations A_X, A_Y, A_Z as functions of the actual thrust accelerations A_x, A_y, A_z. Referring to Fig. 23.4-2,

$$A_X = A_x \cos \phi_{xy} \cos \phi_{xz} + A_y \sin \phi_{xy} - A_z \sin \phi_{xy}$$

$$A_Y = A_y \cos \phi_{yx} \cos \phi_{yz} + A_z \sin \phi_{yz} - A_x \sin \phi_{yx}$$

$$A_Z = A_z \cos \phi_{zx} \cos \phi_{zy} + A_x \sin \phi_{zx} - A_y \sin \phi_{zy}$$

or, $A_I = A_i \cos \phi_{ij} \cos \phi_{ik} + A_j \sin \phi_{ik} - A_k \sin \phi_{ij}$

where i, j, k are cyclic permutations only of x, y, and z. For small misalignments,

$$A_I = A_i + A_j \phi_{ik} - A_k \phi_{ij}$$

The error in sensed acceleration is then,

$$\Delta A_i = A_j \phi_{ik} - A_k \phi_{ij}$$

Substitution of the drift rate equations yield,

$$\Delta A_i = A_j \int_o^t \dot{\phi}_k \, dt - A_k \int_o^t \dot{\phi}_j \, dt$$

Integration then provides velocity and position errors.

$$\Delta V_i = \int_o^t \Delta A_i dt \qquad \Delta S_i = \int_o^t \Delta V_i dt$$

The results for constant average error coefficients are (in terms of the tabulated integrals and $A_y = 0$),

$$\Delta V_x = - b_{oy} I_6 + b_{2y}^{y} I_9$$

$$\Delta V_y = b_{ox} I_6 + b_{1x} I_7 - b_{oz} I_4 - b_{1z}^{y} I_8$$

$$\Delta V_z = b_{oy} I_4 + b_{2y}^{y} I_8$$

Position error equations are simply found by replacing each integral I_i by ${}_iI_i$.

C. <u>Platform</u>:

The platform error model suggested in Pitman is,

$$\phi_{ij} = \phi_{ij}(0) + e_k + p_{ij} A_i + q_{ij} A_j$$

where ϕ_{ij} = same misalignment angles defined previously, see Fig. 23.4-2

e_k = servo stabilization error

p_{ij}, q_{ij} = platform g-sensitive deformation coefficients

Neglecting the effects of platform deformation, the error equations take a form identical to that obtained for the gyro equations, i.e.,

$$\Delta A_i = A_j \phi_{ij} - A_k \phi_{ik}$$

$$\therefore \quad \Delta V_i = \int_0^t A_j \left[\phi_{ij}(0) + e_k \right] dt - \int_0^t A_k \left[\phi_{ik}(0) + e_j \right] dt$$

Again assuming $A_y = 0$ and constant error coefficients, the results are,

$$\Delta V_x = -\left[\phi_{xy}(0) + e_y \right] I_3$$

$$\Delta V_y = \left[\phi_{yz}(0) + e_x \right] I_3 - \left[\phi_{yx}(0) + e_z \right] I_1$$

$$\Delta V_z = \left[\phi_{zx}(0) + e_y \right] I_1$$

For initial angular misalignments components $\phi_i(0)$ of the platform about each inertial axis i, the equations take a more obvious form,

$$\Delta V_x = -\left[\phi_y(0) + e_y \right] I_3$$

$$\Delta V_y = \left[\phi_x(0) + e_x \right] I_3 - \left[\phi_z(0) + e_z \right] I_1$$

$$\Delta V_z = \left[\phi_y(0) + e_y \right] I_1$$

Again, position errors are found by replacing I_i by ${}_iI_i$.

D. Navigation Computer:

For an analog computer, drift, bias, and compensation errors are relevant; for a digital computer, pickoff, roundoff, and truncation errors are relevant. If digital computations are used, the error magnitudes

are very small. In this study, computer errors hace been neglected.

E. Guidance Computer:

The following errors would be relevant in a mechanization study. However, their effects on position and velocity prediction are generally second order and therefore neglected.

1. Timing and thrust termination errors
2. Velocity resolution
3. Guidance and control equation errors
4. Physical planetary data uncertainties

F. Pre-Launch Uncertainties:

(discussed in section 8.4.3.4)

G. Summary:

The computational problem is now reduced to selecting a method for evaluating the tabulated integrals. As previously mentioned, digital, hand, or graphical procedures provide numerical results. Since only two representative trajectories are considered, the numerical values of each integral were obtained by a combination of graphical and polynominal expansion approximations. Note that integration is over the limits of the entire trajectory so that errors will be expressed as miss distances and velocities at thrust cut-off.

23.5 Appendix V-E: Development of a Computer Program for Evaluating the Differential Error Equations for an Inertial Navigation System

Since the generalized error differential equations are developed in almost every text on inertial guidance, only the results will be given. The

three component equations take the form,

$$\Delta \ddot{S}_i + g_o \frac{R_o^2}{R^3} \Delta S_i - 3 g_o \frac{R_o^2}{R^5} S_i (S_i \Delta S_i + S_j \Delta S_j + S_k \Delta S_k) = \Delta A_i$$

where i, j, k represent the 3 inertial axes and ΔA_i is the sensed acceleration error caused by the error forcing functions developed in the previous section.

ΔA_i may be further broken down into errors resulting from imperfections within the accelerometer and the measurement of false accelerations as a result of platform misalignment. The form for these errors is given by,

$$\Delta A_i = E_i - \phi_j \left(\ddot{S}_k + g_o \frac{R_o^2}{R^3} S_k \right) + \phi_k \left(\ddot{S}_j + g_o \frac{R_o^2}{R^3} S_j \right)$$

where E_i = accelerometer imperfections and the terms within the parentheses represent the trajectory coefficients for the error forcing functions.

Thus, three linear differential equations may be programmed to obtain three position errors ΔS_i and three velocity errors $\Delta \dot{S}_i$, as a function of the sensor errors E_i and ϕ_i. The required inputs are the trajectory parameters, S_i and $\ddot{S}_i$. Again, it is useful to type out the results at thrust cut-off which provides miss distances and miss velocities as initial condition perturbations for the orbital flight.

As an analytical example, let $R = R_o$ = const. and consider vertical flight only. Hence, $S_x = S_y = \ddot{S}_x = \ddot{S}_y = 0$. The error equations reduced to

$$\Delta \ddot{x} + \frac{g_o}{R_o} \Delta x = E_x - \phi_y \left(\ddot{z} + \frac{g_o}{R_o} z \right) = E_x - \phi_y A_z = F_x(t)$$

$$\Delta \ddot{y} + \frac{g_o}{R_o} \Delta y = E_y + \phi_x \left(\ddot{z} + \frac{g_o}{R_o} z \right) = E_y + \phi_x A_z = F_y(t)$$

$$\Delta \ddot{z} + \frac{g_o}{R_o} \Delta z = E_z \qquad = E_z \qquad = F_z(t)$$

The general solution with $\omega_o^2 = \frac{g_o}{r_o}$ is,

$$\Delta x = \Delta x_o \cos \omega_o t + \frac{V_{xo}}{\omega_o} \sin \omega_o t + \frac{1}{\omega_o} \int_o^t \sin \omega_o (t-\tau) F_x(\tau)\, d\tau$$

$$\Delta y = \Delta y_o \cos \omega_o t + \frac{V_{yo}}{\omega_o} \sin \omega_o t + \frac{1}{\omega_o} \int_o^t \sin \omega_o (t-\tau) F_y(\tau)\, d\tau$$

$$\Delta z = \Delta z_o \cos \omega_o t + \frac{V_{zo}}{\omega_o} \sin \omega_o t + \frac{1}{\omega_o} \int_o^t \sin \omega_o (t-\tau) F_z(\tau)\, d\tau$$

By assuming a small burning period, $\sin \omega_o(t-\tau) \cong \omega_o (t-\tau)$, the integrals may be readily evaluated. Also assume that the accelerometer and gyro errors are simple bias errors, so that E_i = const. and $\phi_i = b_i t + \phi_i(0)$. Substitution of the thrust components obtained in Appendix V-B yields,

$$F_x(t) = E_x - \frac{T}{W_{oc}} \frac{g_c}{g_o} \left[\frac{1}{1 - t/\bar{t}} \right] \left[b_y t + \phi_y(0) \right]$$

$$F_y(t) = E_y + \frac{T}{W_{oc}} \frac{g_c}{g_o} \left[\frac{\quad}{1 - t/\bar{t}} \right] \left[b_x t + \phi_x(0) \right]$$

$$F_z(t) = E_z$$

The integrals can now be evaluated and a simple analytical time solution is available.

The reason this approach was not used for hand computation of sensor requirements is now somewhat apparent. For the linear-tangent thrust program, the acceleration components, A_x and A_z provided results after integration which were much too cumbersome to work with. Fortunately, there is little

need for such a presentation.

The above equations also indicate the propogation of initial position and velocity errors. For small burning periods initial position errors propagate unaffected. However, initial velocity errors are integrated so that their effect on position prediction increases linearly with time.

In summary, the computer program could be very useful for a large variety of nominal optimized trajectories. Gravity feedback is included as part of the three differential error equations. This effect is usually negligible and therefore does not appear in the previous approach of evaluating the set of trajectory-dependent integrals, see Appendix 23.4.

24.0 References and Bibliography

Earth Launch to Injection

3-1 "A Report on the Guidance System For The Lunar Logistics Vehicle", Westinghouse Electric Corp., Air Arm Division, Balt. 3, Md., Report # 2-75214, March 15, 1963.

Midcourse Trajectory

4-1 G. L. Smith, S. F. Schmidt, L. A. McGee, "Application of Statistical Filter Theory to The Optimal Estimation of Position and Velocity on Board a Circumlunar Vehicle" - NASA TR R-135, 1962, Ames Research Center, Calif.

4-2 J. D. McLean, S. F. Schmidt, L.A. McGee, "Optimal Filtering and Linear Prediction Applied to a Midcourse Navigation System for the Circumlunar Mission" - NASA TN D-1208, March, 1962.

4-3 R. H. Battin, "A Statistical Optimizing Navigation Procedure For Space Flight" - ARS 2461-62, July, 1962.

4-4 G. L. Smith, J. S. White, "Working Papers", Ames Research Center, 1962.

4-5 R. E. Kalman, "A New Approach to Linear Filtering and Prediction Problems", Journal of Basic Engineering, March 1960.

4-6 R. H. Tolson, "Effect of Some Typical Geometrical Constraints on Lunar Trajectories". NASA TN D-938, August, 1961.

4-7 H. A. Hamer, C. R. Huss, J. P. Mayer, "Statistical Studies of Effects of Insertion Errors on Ascent Trajectories for Lunar Missions", NASA TN D-1262, May, 1962.

4-8 R. J. Weber, W. M. Pauson, R. R. Burley, "Lunar Trajectories", NASA TN D-866, August, 1961.

Lunar Parking Orbit

5-1 R. E. Kalman, "A New Approach to Linear Filtering and Prediction Problems", Trans ASME, Series D, Jour. Basic Engr., V 82 N 1, March 1960, pp. 35-45.

5-2 G. L. Smith, S. F. Schmidt, and L. A. McGee, "Application of Statistical Filter Theory to the Optimal Estimation of Position and Velocity on Board a Circumlunar Vehicle", NASA TR R-135, 1962.

5-3 J. D. McLean, S. F. Schmidt, and L. A. McGee, "Optimal Filtering and Linear Prediction Applied to a Midcourse Navigation System for the Circumlunar Mission", NASA TN D-1208, 1961.

5-4 R. H. Battin, "A Statistical Optimizing Navigation Procedure for Space Flight", ARSJ V32 n 11 Nov. 1962, pp. 1681-1696.

5-5 S. Pines, H. Wolf, D. Woolston and R. Squires, "Goddard Minimum Variance Orbit Determination Program", Goddard Space Flight Center Report No. X-640-62-191.

5-6 G. M. Levine, "Application of Midcourse Guidance Technique to Orbit Determination", IAS Paper No. 63-16; IAS 31st Annual Meeting, January 21-23, 1963, New York.

5-7 G. L. Smith and L. A. McGee, "Midcourse Navigation Scheme", NASA Inter-center Technical Conference on Control, Guidance, and Navigation Research for Manned Lunar Missions, July 24-25, 1962.

5-8 IBM Reference Manual #C20-8011 Random Number Generation and Testing.

5-9 P. G. Hoel, "Introduction to Mathematical Statistics", New York, Wiley, 1947.

5-10 C. J. Cohen and E. C. Hubbard, "A Nonsingular Set of Orbit Elements", NWL Report No. 1756.

5-11 A. E. Bryson, K. Mikami, and C. T. Battle, "Optimum Lateral Turns for a Re-Entry Glider", Aerospace Engineering V 21, n 3, March, 1963, p. 21.

Lunar Descent

6-1 Tunnell, P. J., and Lessing, H. C., Guidance Techniques for Lunar Approach and Letdown of the Apollo Spacecraft; Intercenter Technical Conference on Control, Guidance and Navigation Research For Manned Lunar Missions; Ames Research Center, July 24 and 25, 1962, pp. 320-331.

Lunar Ascent

8-1 Ting, Lu, "Optimum Orbital Transfer by Impulses," ARS Journal, Vol. 30, No. 11, Nov., 1960, pp 1013-1018.

8-2 Horner, J. M., "Optimum Impulsive Orbital Transfer Between Coplanar Orbits", ARS Journal, Vol 32, No. 7, July, 1963, pp 1082-1089.

8-3 Ehricke, K., "Space Flight, Vol II, Dynamics, "Principles of Guided Missile Design, D. Van Nostrand Co., 1962.

8-4 Duke, W. M., Goldberg, E. A., and Pfeffer, I., "Error Analysis Considerations for a Satellite Rendezvous," ARS Journal, Vol. 31, No. 4, April, 1961, pp 505-513.

8-5 Fernandel, M. and Macomber, G., "Inertial Guidance Engineering", Prentice-Hall, Inc., 1962.

8-6 Pitman, G. R., (Edit.), "Inertial Guidance", John Wiley & Sons, 1962.

8-7 Parvin, R. H., "Inertial Navigation", Principles of Guided Missile Design, D. Van Nostrand Co., 1962.

8-8 Zee, Chong-Hung, "Effect of Finite Thrusting Time in Orbital Maneuvers", AIAA J., Vol. 1, No. 1, Jan., 1963, pp 60-64.

8-9 Bryson, A. E., Mikami, K., and Battle, C. T., "Optimum Lateral Turns for a Re-entry", Aerospace Eng., Vol. 21, No. 3. March, 1962, p. 21.

8-10 De Bra, D. B., and Gundel, B. H., "Circularization of Elliptic Orbits", Advances in the Astronautical Sciences, 6th Annual Mtg. Proc., Jan. 18-21, 1960. Macmillan Co., pp. 556-570.

8-11 Thomson, W. T., "Introduction to Space Dynamics", John Wiley & Sons, 1961.

8-12 MacKay, J. S., "Approximate Solution for Rocket Flight with Linear-Tangent Thrust Attitude Control," ARS Journal, Vol. 30, No. 11, Nov., 1960, pp. 1091-1093.

8-13 Burley, R. R., and Weber, R. J., "Lunar Takeoff", ARS Journal, Vol. 32, No. 8, Aug. 1962, p. 1296.

8-14 Burns, R. E., and Singleton, L. G., "Ascent from the Lunar Surface", Marshall Space Flight Center, NASA Doc. MTP-P & VE-F-62-7, Rev. Dec. 7, 1962.

8-15 Jensen, J., Lock, J. Kraft, D., and Townsend, G., "Design Guide to Orbital Flight", McGraw Hill, 1962.

8-16 Gretz, R. W., "Error Sensitivities in Satellite Ascent and Orbital Transfer", ARS Journal, Vol. 32, No. 12, Dec., 1962, pp 1860-1866.

Lunar Rendezvous

9-1 Jensen, J., Townsend G., Kork, J., and Kraft, D., "Design Guide to Orbital Flight", McGraw-Hill Book Co., 1962.

Unmanned Midcourse

12-1 Final Report Analysis of Systems for Accurate Lunar Landings. Space Technology Laboratories, Inc. 9990-6022-RL-000. 4 January, 1962. Confidential.

12-2 Analysis of Radio-command Midcourse Guidance A.R.M. Noton, E. Cutting, F. L. Barnes, Report No. 32-28, JPL, Sept. 8, 1960.

12-3 A Report on the Guidance System for the Lunar Logistics Vehicle. Westinghouse Air Arm Division, 15 March, 1963.

Unmanned Lunar Landing

15-1 "A Report on the Guidance System For The Lunar Logistics Vehicle", Westinghouse Electric Corp., Air Arm Division, Balt. 3, Md., Report # 2-75214, March 15, 1963.

Computer Program for Descent Trajectory

21-1 Tunnell, P. J. and Lessing, H. C.; Guidance Techniques for Lunar Approach and Letdown of the Apollo Spacecraft. Working paper obtained from Ames Research Center; July 24, 1962.